UNIVERSITY OF SOUTHAMPTON

FACULTY OF ENGINEERING AND THE ENVIRONMENT

Aeronautics, Astronautics and Computational Engineering

Value Driven Design of Additive Manufactured Unmanned Aircraft

by

Mario Ferraro

Thesis for the degree of Doctor of Philosophy

March 2017

UNIVERSITY OF SOUTHAMPTON

ABSTRACT

FACULTY OF ENGINEERING AND THE ENVIRONMENT

Aeronautics, Astronautics and Computational Engineering

Thesis for the degree of Doctor of Philosophy

VALUE DRIVEN DESIGN OF ADDITIVE MANUFACTURED UNMANNED AIRCRAFT

By Mario Ferraro

This thesis introduces a novel value driven design methodology for mission-specific rapid-manufactured Unmanned Aerial Vehicles (UAVs). It is based on a holistic design environment that integrates a multi-disciplinary aircraft design tool, an agent-based operational simulation, and a life-cycle cost-benefit model. The definitions of the stakeholders' value drivers, the concept of operations, and the operating environment are used to create a detailed simulation capable of evaluating the mission effectiveness of the system and its life-cycle cost as well as, remarkably, the impact of the system performance on the operation of the other agents participating in the mission. This enhances the understanding of the design space and allows the designer to elicit the system characteristics that lead to the best value for the stakeholders.

This methodology is applied to the design of an unmanned aircraft to support search and rescue in cooperation with lifeboats. This case study demonstrates that counterintuitive effects can arise from the operation of the UAV in a complex environment. The holistic design environment can unveil these emergent behaviours and provide quantitative relationships between the technical characteristics of the system and the overall mission value, therefore improving design decision making. This study also highlights the importance of providing the decision maker with a comprehensive set of simulation outputs in order to facilitate the understanding of the factors and dynamics that contribute to the value generation.

This thesis also discusses the impact of additive manufacturing on the design of UAVs with a focus on selective laser sintering of plastic. The merits and limitation of this technology are discussed through the analysis of a number of case studies, including the design and test of the first entirely 3D printed UAV. Additive manufacturing decreases the product development time, increases its

adaptability, and facilitates the continuous system development. The absence of penalties associated with the production of complex geometries generates opportunities for mass and cost savings through multi-functionality and structural integration. Additionally, this research offers a principle to guide the architectural design of partly 3D printed UAVs. The principle is based on a measure of the manufacturing complexity, engineering judgment and network analysis of the product architecture and can identify the parts that would benefit the most from the adoption of additive manufacturing as well as highlight the opportunity for components integration and modularisation of the assembly.

Table of Contents

List of Tables ..... **xi**

List of Figures ..... **xiii**

Author's Publications ..... **xxi**

DECLARATION OF AUTHORSHIP ..... **xxiii**

Acknowledgements ..... **xxv**

Definitions and Abbreviations ..... **xxvii**

1 Introduction **1**

1.1 Unmanned Aerial Vehicles, Rapid Manufacturing and the Future of Aircraft Design 1

1.2 Research Questions and Hypotheses 5

1.2.1 Design for Additive Manufacturing of UAV Airframes 6

1.2.2 Development of a Value Driven Design Framework for the Design of Search and Rescue Unmanned Aerial Vehicles 6

1.3 Original Contribution to Knowledge 7

1.4 Thesis Structure 8

2 Aircraft Design and Systems Engineering **9**

2.1 Introduction: Engineering Design as a Decision Making Process 9

2.2 Aircraft Design 11

2.2.1 Design Optimisation 13

2.2.2 Multidisciplinary Design Optimisation and Aircraft Sizing Tools 14

2.3 Systems Engineering 16

2.3.1 Reductionist and Holistic System Models 18

2.3.2 Waterfall, Spiral and Agile Product Development Models 19

2.3.3 Concurrent Engineering and Integrated Product and Process Development 21

2.4 System Requirements, Concept of Operation and Mission Simulation 21

2.5 Summary 23

3 System Value Models and Value Driven Design Methodologies 25

3.1 Introduction 25

3.2 Value-Driven Design 25

3.2.1 What is Value-Driven Design? 25

3.2.2 How is VDD Different from Traditional Systems Engineering? 26

3.2.3 How is VDD Implemented? 26

3.3 Stakeholders Analysis 27

3.4 How to Define and Measure Value 28

3.4.1 Decision Under Uncertainty: Value and Utility 28

3.5 Decision with multiple objectives 31

3.5.1 Trade Space Exploration 31

3.5.2 Pareto Front 32

3.5.3 Technique for Order of Preference by Similarity to Ideal Solution 33

3.5.4 Analytic Hierarchy Process 33

3.5.5 Multi-Attribute Utility Theory 34

3.5.6 Decisions with Multiple Objectives: “Stanford School approach” 35

3.6 Monetising Value: Worth Models 35

3.6.1 Implications of Monetising Value: Risk Attitude and Discount Rate 36

3.7 Metrics for Worth Based Value Models 37

3.7.1 Return On Investment 38

3.7.2 Net Present Value 38

3.7.3 Surplus Value 39

3.7.4 Real Options 39

3.8 Cost and Operational Effectiveness Analysis 39

3.9 Some Applications of VDD to Aerospace Systems 40

3.10 Summary 42

4 Rapid Manufacturing and Additive Manufacturing 44

4.1 Introduction 44

4.2 What is Additive Manufacturing? 44

4.3 Additive Manufacturing Compared to Injection Moulding and High Pressure Die Casting 45
4.4 Selective Laser Sintering of Polyamide 46
4.5 Direct Metal Laser Sintering 49
4.6 Fused Deposition Modelling 50
4.7 Other Rapid Manufacturing Technologies for Low-Cost UAVs 51
4.7.1 CNC Foam Cutting 51
4.7.2 CNC Subtractive Manufacturing 52
4.8 Summary 52

5 The Impact of Additive Manufacturing on Aircraft Design 53

5.1 Introduction 53
5.2 Concept Generation 53
5.3 Process Flexibility and Product Delivery Time 53
5.4 Manufacture of Geometrically Complex Structures 54
5.5 Structural and Aerodynamic Optimisation 56
5.6 Non-Monetary Cost of Geometrical Complexity 58
5.7 Case Studies 59
5.7.1 Southampton University Laser Sintered Aircraft – The World's First Entirely 3D Printed Airframe 59
5.7.2 Integral Fuel Tank 66
5.8 Design for 3D Printing: the Implication on the System Architecture 70
5.8.1 System Architecture and Product Modularity 71
5.8.2 The Principle of Confined Complexity 73
5.8.3 Case study: The Network Analysis of the Empennage Assembly of two UAVs 76
5.9 Summary 81

6 Development of a Value-Driven Design Environment for Unnamed Aerial Vehicles 83

6.1 Introduction 83
6.2 Design Principles 84

6.3 DUADE Workflow 85
6.4 Problem Definition 86
6.4.1 Case Study: Design of a UAV for Search and Rescue Missions 87
6.4.2 Problem Definition and Assumptions 88
6.5 System Design Loop 89
6.6 Aircraft Sizing Tool 90
6.6.1 Design Philosophy and Manufacturing Processes 93
6.6.2 The Concept Sizing Tool: Choice and Evolution 94
6.6.3 Sizing Strategy and Optimisation Algorithm 95
6.7 Aircraft Sizing Tool Disciplinary Modules 97
6.7.1 Geometry 99
6.7.2 Aerodynamics 99
6.7.3 Stability and Control 102
6.7.4 Structures 103
6.7.5 Mass 105
6.7.6 Propulsion 106
6.7.7 Performance 110
6.7.8 Avionics and Payload 112
6.7.9 Cost 113
6.7.10 Reliability, Maintenance and Mishaps Models 117
6.7.10.1 Cost of Reliability Improvements 119
6.7.10.2 Weight of Reliability Improvements 120
6.8 Value Model 121
6.8.1 Cost-Benefit Model 122
6.8.1.1 Monetising the Mission Benefit 124
6.8.1.2 Discount Rate 126
6.8.2 Operational Simulation 126
6.8.2.1 UAV Model 128
6.8.2.2 Performance Model 130
6.8.2.3 Payload Model 131

6.8.3 Output of the Operational Simulation and Numerical Noise 134
6.9 Assumptions and Limitations 136
6.10 Summary and Final Remarks 138

7 Value Trade Space Exploration Using DUADE 140

7.1 Introduction 140
7.2 Summary of the Assumptions about the Design Problem and the Mission Scenario 140
7.3 Exploration of the Design Space Using the Aircraft Sizing Tool 141
7.3.1 The Choice of the Intermediate Objective Function 142
7.3.2 The Impact of Parameters and Constraints on the Optimal Aircraft Characteristics 146
7.3.2.1 Analysis of the Results 148
7.4 Exploration of the Design Space Using the Value Model 152
7.4.1 Baseline Search and Rescue Scenario 152
7.4.2 The Effect of Performance Requirements on Mission Effectiveness and Operational Cost 152
7.4.3 Effect of Simultaneously Varying the Performance Parameters 156
7.4.4 Trade Space Exploration Using the Cost-Benefit Model 160
7.4.5 The Impact of the Aircraft Configuration on the Value Metrics 168
7.5 Design Indications 170
7.6 Final Remarks 173
7.6.1 Benefits of DUADE System Design Loop 173
7.6.2 Mutual Value Dependency of the Performance Parameters 173
7.6.3 Challenges of Modelling the Operational Simulation 174
7.6.4 The Role of the Intermediate Objective Function, Design Variables and Performance Parameters 175
7.6.5 Supporting Value Driven Design After the Concept Phase 179
7.7 Summary 181

8 Conclusion 183

8.1 Introduction 183

8.2 Novel Contribution 183
8.3 Review of Research Hypotheses 184
8.3.1 Design for Additive Manufacturing of UAV Airframes 184
8.3.1.1 Answers to the Research Questions 184
8.3.2 Development of a Value Driven Design Framework for the Design of Search and Rescue Unmanned Aerial Vehicles 186
8.3.2.1 Answers to the Research Questions 187
8.4 Further Research 189
8.4.1 Additive Manufacturing of Airframes 189
8.4.2 Value Driven Design Framework for the Design of Unmanned Aerial Vehicles 190

Appendix A. Mechanical Properties of Direct Metal Laser Sintering Materials I

Appendix B. Examples of Rapid Manufactured UAVs II

A.1 Introduction II
A.2 DECODE-2 II
A.2.1 The Aerodynamic Optimisation of DECODE-2 Fuselage III
A.2.1.1 The Value-Driven Design Point of View VI
A.2.2 Manufacture and Flight Tests VII
A.2.2.1 Mishaps XI
A.2.3 Lessons Learned XII
A.3 SPOTTER XIII
A.3.1 Manufacture and Flight Tests XVII
A.3.2 Mishaps XIX
A.3.3 SPOTTER and the DUADE Workflow XX
A.3.4 Lessons Learned XXI
A.4 Summary XXII

Appendix C. Adjacency Matrices XXIV

Appendix D. Spreadsheet Interface of the Concept Design Tool XXVI

Appendix E. DECODE-2 Project Timeline XXIX

Appendix F. Geometrical Parameters of the Fuselage of DECODE-2 XXX

Appendix G. Performance Flight Tests XXXII

G.1 Measuring and Recording Data XXXII

G.2 Take-Off and Landing Distance XXXII

G.3 Maximum Speed XXXIII

G.4 Stall Speed XXXIV

G.5 Climb Rate XXXIV

G.6 Glide Ratio XXXV

G.7 Fuel Consumption XXXV

Appendix H. 2SEAS-3i Project Timeline XXXVI

List of References XXXVII

List of Tables

1 – Additive manufacturing techniques and their bonding process. 45

2 – Mechanical properties of SLS Nylon 12 (source 3T-RPD [185]) and Aluminium 7075. 47

3 – Specification and performance of SULSA. 61

4 – Table displaying the disciplinary modules, software and their level of integration with CDT. 98

5 – Components reliability model inputs (table excerpt). 118

6 – List of parameters defining the Aircraft Model in the Operational Simulation.....130

7 – Performance requirements used as fixed parameters in the design optimisation of a sub 20 kg UAV (table excerpt). 143

8 – Results of the design optimisation of a sub 20 kg UAV with three different objective functions.....144

9 – Initial parameters' vector used in the trade study. 147

10 – Mechanical properties of DMSL materials in the horizontal (XY) and vertical (Z) direction with respect to the building plane (source 3T-RPD [279]). I

11 – Design variables and objective functions for the DECODE-2 UAV. V

12 – DECODE-2 specifications and performance. X

13 – Comparison between the specification and performance at maximum take-off mass of 2SEAS-20 and SPOTTER. XVII

14 – Adjacency Matrix of the tail assembly of DECODE-2. XXIV

15 – Adjacency Matrix of the tail assembly of SPOTTER. XXIV

16 – Adjacency Matrix of the re-designed tail assembly of DECODE-2. XXV

17 – DECODE-2 project timeline. XXIX

18 – 2SEAS-3i project timeline. XXXVI

List of Figures

1-1 – Cost-Knowledge-Freedom shift for future design methods [28]. 4

2-1 – Decision-making process [33]. 9

2-2 – Aircraft design process. 11

2-3 – The design wheel [37]. 11

2-4 – Increasing the number of design parameters [25]. 12

2-5 – DoD Systems Engineering Process [69]. 17

2-6 – The V-model [33]. 19

2-7 – The spiral model of system life cycle [33]. 20

3-1 – Lottery example. 30

3-2 – Test of additive independence condition [147]. 34

4-1 – Additive manufacturing processes classified by the form of the starting material 45

4-2 – **a.** "Cake" of powder containing the final part. **b.** Technician removing powder from the final part [21]. Note the 3D printed hinge. 47

4-3 – **a.** CAD model of SPOTTER's fuel tank (Mk1). **b.** SLS fuel tank (Mk1) with trailing edge distortion (circled). **c.** CAD model of the fuel tank (Mk2). The extra stiffener introduced to prevent warping is highlighted. **d.** SLS fuel tank (Mk2) showing no trailing edge distortion. 49

4-4 – Hot-wire foam cutting. 51

5-1 – **a.** Supermarine Spitfire elliptic wing [191]. **b.** Geodesic structure visible on a Vickers 290 Wellington [192]. 55

5-2 – The rebuilt time of a CAD model is the time required for updating the geometry if a design parameter is changed. In very complex models, software

latency can become a major obstacle to productivity. Above: this model of an integral fuel tank requires a rebuild time of almost one hour. 58

5-3 – SULSA three-view drawings. 60

5-4 – Parametric model of SULSA. The wing sections were generated and updated using a purposely designed computer code and imported into the CAD software. 60

5-5 – Transparent view of SULSA showing the geodesic-inspired airframe. 62

5-6 – SULSA mark 2 taking off from HMS Mersey. 63

5-7 – SULSA mark 2 during the Project Triangle trials in the Antartic. 64

5-8 – SPOTTER's inner wing assembly. The integral fuel tank is shown in transparency. 66

5-9 – Two views of SPOTTER's integral fuel tank. 67

5-10 – Fuel tank section view. 67

5-11 – Calculation of the stress and deformation on the fuel tank due to a 7g inertial load. Note: deformation is magnified by a factor of 10. 68

5-12 – Example of design iteration: the hole in the baffle of the fuel tank was reinforced to avoid stress concentration. 69

5-13 – Example of design iteration: the redesign of the tank's cap increased the fuel volume by 30%. 70

5-14 – Design for confined complexity method. 74

5-15 – Exploded view of the tail assembly of DECODE-2. Only chunks to the left of the plane of symmetry are shown. 78

5-16 – Exploded view of the tail assembly of SPOTTER. Only chunks to the left of the plane of symmetry are shown. 78

5-17 – Network representation of the tail assemblies of: **a.** DECODE-2 and **b.** SPOTTER. The nodes in red correspond to the parts produced using AM. 79

5-18 – Degree of Centrality of the physical elements of the empennage assemblies of: **a.** DECODE-2 and **b.** SPOTTER. The bars in red corresponds to the parts produced using AM. 79

5-19 – Detail of the 3D printed spar clamping mechanisms. 80

5-20 – Part of the subassembly of the tailplane of DECODE-2. **a.** Collapsed view **b.** Exploded view. 81

5-21 – Part of the re-designed tail assembly. The servo mounts have been integrated into part 7, thus reducing the mass and cost of the subsystem. 81

5-22 – **a.** Network representation of the redesigned tail assemblies of DECODE-2. **b.** Degree of Centrality of the physical elements of the empennage assemblies of DECODE-2. 82

6-1 – DUADE workflow. 85

6-2 – Baseline scenario showing lifeboat stations (yellow squares) and incident positions (dots) [65]. 88

6-3 – DUADE System Design Loop. 89

6-4 – Aircraft configurations available in the baseline version of the AST. 90

6-5 – Examples of research vehicles designed using the AST. **a.** DECODE-1, a 10 kg MTOM glow fuel aircraft; **b.** SULSA, a 3 kg electric powered entirely 3D printed aircraft; **c.** DECODE-2, a 23 kg MTOM petrol engine aircraft; **d.** SPOTTER, a 35 kg MTOM twin engine aircraft. 91

6-6 – Aircraft Sizing Tool modules. All high-level variables are coordinated by the CDT. Low-level variables are managed in the high-LOD geometry tool and can be shared with disciplinary modules for detailed analysis. 92

6-7 – Different level of abstraction of the DECODE-2 aircraft geometry in the Aircraft Sizing Tool: **a.** Cartoon representation of the aircraft used in the Concept Design Tool; **b.** Geometric model used for the CFD analysis; **c.** High-LOD CAD geometry; **d.** Picture of the airframe during flight tests. 100

6-8 – Coefficient of pressure (cp) distribution over SPOTTER's UAV wing at the AoA=3° and 30 m/s calculated using a Vortex Lattice Method code. 101

6-9 – Dimensionless roll rate of DECODE-1 UAV measured during flight test versus design value. 102

6-10 – Flight Envelope generated by the Concept Design Tool. 103

6-11 – Example of bending moment distribution along the wing span obtained with a VLM code. The picture displays the bending moment on the SPOTTER's wing at AoA=3° and 30 m/s. 104

6-12 – SPOTTER's wing static load test (7 g). The ultimate load distribution was approximated using sandbags and lead weights. 104

6-13 – Example of mass estimation relationship in the CDT. The equation estimates the mass of the stabilisers' skin and secondary structure given their area. The linear regression was obtained using data from five previously built UAVs and includes vertical, horizontal and V-tail stabilisers. 105

6-14 – Regression analysis for capacity, power, and mass of RC aircraft engines. 106

6-15 – BSFC curves for a two-stroke petrol engine (3W 28i) with and without EFI, and a four-stroke petrol engine (OS GF40). The test was performed using a two-bladed 18x10 inch Biela propeller at 10°C in static flow condition. 107

6-16 – Measured and calculated static thrust for a two-bladed 18''x10'' inch Biela propeller at 10°C. 108

6-17 – Regression analysis for propeller diameter vs engine size. Data presented were obtained from the RCFAQ database [244] and from Top-Flite manufacturer chart [245]. 109

6-18 – Propeller efficiency $\eta prop$ as a function of the propeller Advance Ratio J and the pitch to diameter ratio (p/d). Experimental data for APC Sport propeller series (11 in diameter) [241]. 109

6-19 – UAV unit cost estimation model (excerpt). The colour of the nodes reflects how strongly a small change in each node's value impacts the value of the UAV unit cost; green indicates a strong positive influence and red a strong negative influence. 115

6-20 – Wing cost estimation model (excerpt). 116

6-21 – Landing crash probability as a function of the UAV kinetic energy at landing. 119

6-22 – Reliability Cost Estimating Relationship of military systems [262]. 120

6-23 – SAR Value Model. 123

6-24 – Model of the operational cost of the SAR vessels (excerpt). 123

6-25 – UAV total cost (excerpt). 124

6-26 – Incident survival probability based on water immersion time [65]. 127

6-27 – UAV search pattern and camera footprint [65] 127

6-28 – Interface between the Aircraft Model and Operational Simulation. 129

6-29 – Geometry of airborne imagery collection [219]. 133

6-30 – Graphical study of the cumulative mean and confidence interval of one of the outputs of the Operational Simulation. 134

7-1 – **a.** Number of incidents per lifeboat station. **b.** Cumulative distribution of the incidents as a function of the distance from the UAV base at Lyme Regis. 141

7-2 – DUADE Bi-Level System Design Loop. 142

7-3 – Geometry of the results of the design optimisation of a sub 20 kg UAV using three different objective functions: **a**. Fuel efficiency at cruise speed **b**. Minimum empty cost **c**. Minimum empty mass. The payload is displayed in red and the engine in yellow. 144

7-4 – Effect of the performance parameters on the UAV mass. 149

7-5 – Effect of the performance parameters on the UAV cost. 150

7-6 – Effect of the performance parameters on the mission performance. 154

7-7 – Effect of payload mass and UAV range on: **a**. Average finding time **b**. Number of saved lives. Note that input axes are rotated to enhance the picture readability. 157

7-8 – Effect of payload mass and UAV range on: **a**. Total lifeboats utilization time **b**. UAV total flight time **c**. UAV fuel used **d.** Number of take-offs **e.** UAV total

maintenance time **f.** UAV mishaps number. Note that input axes are rotated to enhance the picture readability 159

7-9 – Effect of payload mass and UAV range on: **a**. UAV total fuel cost **b**. UAV maintenance cost. Note that input axes are rotated to enhance the picture readability. 160

7-10 – Effect of payload mass and UAV range on the UAV life-cycle cost. 160

7-11 – UAV life-cycle cost per additional saved life; the labels on the x axis display the value of range (km) and payload mass (kg) separated by an underscore. 161

7-12 – Scatter plot of the number of additional saved lives and UAV life-cycle cost. The labels on the data points display the value of range (km) and payload mass (kg) separated by an underscore. The red line is the Pareto front. 162

7-13 – Effect of payload mass and UAV range on the total Surface craft cost..... 163

7-14 – SAR total cost per saved life; the labels on the x-axis display the value of range (km) and payload mass (kg) 163

7-15 – Effect of payload mass and UAV range on the UAV dry mass. 164

7-16 – Scatter plot of the total number of saved lives and SAR total cost. The labels on the data points display the value of range (km) and payload mass (kg) separated by an underscore. The red cross is the Pareto front. 165

7-17 – Modified scatter plot of the total number of saved lives and SAR total cost: the designs with a dry mass higher than 19 kg have been excluded. The labels on the data points display the value of range (km) and payload mass (kg) separated by an underscore. The red line is the Pareto front. 166

7-18 – Value added by the UAV to the SAR mission. The labels on the x-axis display the value of range (km) and payload mass (kg). The red bars correspond to UAVs with a dry mass higher than 19 kg. 167

7-19 – Effect of payload mass and UAV range on the Value added by the UAV to the SAR mission..... 168

7-20 – Comparison of five UAV configurations (displayed in **e.**) in terms of **a.** MTOM, **b.** UAV unit cost, **c.** total SAR cost, **d.** Number of saved lives. The red bars in **c.** and **d.** are the sample standard deviations. 169

7-21 – Breakdown of the UAV life-cycle cost of the design 600_3.25.....171

7-22 – Military UAV class A and B mishaps per 100,000 hours as a function of the cumulative flight hours [275].....172

7-23 – Side-by-side comparison of UAV optimised for empty unit cost (left column) and fuel burn rate (right column). Effect of UAV landing speed and range on: **a**. and **b**.Maximum take-off mass **c**. and **d.** Engine max power.**e**.and **f.** Value added by the UAV. Note that input axes are rotated to enhance the picture readability. 178

7-24 – Value model versus reality.....181

A 1 – DECODE-2 detail design activities.....III

A 2 – DECODE-2 aerodynamic optimisation loop. IV

A 3 – Size and shape comparison between: **a.** DECODE-2 baseline geometry **b.** Aerodynamically optimised blended wing-body geometry..... V

A 4 – Detail of the curves used to control the parametric geometry of the fuselage. VI

A 5 – Life-cycle cost and value comparison between the DECODE-2 baseline design and aerodynamically optimised blended wing-body geometry. The red bars are the sample standard deviations..... VII

A 6 – **a.** Port wing of DECODE-2 showing the Styrofoam skin, 3D printed Nylon ribs, and the carbon fibre main spar. **b.** Central fuselage of DECODE-2 showing the GISM structure. VIII

A 7 – **a.** DECODE-2 during the pre-flight checks. **b.** iFlyer in flight with the BBC colour scheme. VIII

A 8 – Side-by-side comparison of the fuselage of DECODE-2 (on the left) and iFlyer (on the right). IX

A 9 – **a.** Damage to the rear undercarriage mount. **b.** Damage to the camera mount dome.....XII

A 10 – a. Transparent view of SPOTTER showing the aircraft structural design. b. Subassembly of the 3D printed fuselage. c. Phase of the assembly of the composite wing. XIV

A 11 – Three-view drawings of SPOTTER.....XV

A 12 – **a.** Trails of 23 automatic flights at Ramsgate port. **b.** Automatic landing touch-down points [21].....XVIII

A 13 – **a.** Moment of the crash landing. **b.** The payload pod and the fuel tank survived the crash undamaged. XIX

A 14 – Damage resulting from the automatic landing mishap. XX

A 15 – Concept Design Tool Excel interface. XXVI

A 16 – Wing area (a_wing) variables network map. The colours indicate the parameter group; the size of the nodes indicates the number of relations with other nodes. XXVII

A 17 – Geometric parameters used for the aerodynamic optimisation of the fuselage of DECODE-2 XXX

A 18 – Telemetry data recorded during a take-off test of SPOTTER on 30/04/2014. XXXIII

A 19 – Telemetry data recorded during a maximum speed test of SPOTTER on 30/04/2014. XXXIII

A 20 – Telemetry data recorded during a stall speed test of SPOTTER on 30/04/2014. XXXIV

A 21 – Telemetry data recorded during a climb test of SPOTTER on 04/03/2015. XXXIV

A 22 – Telemetry data recorded during a glide test of SPOTTER on 30/04/2014. XXXV

Author's Publications

In the course of developing this thesis, the author has published the following scientific papers:

Journal Papers

- A Value Based Decision Environment: Vision and Application -- D. Gorissen, E. Quaranta, M. Ferraro, B. Schumann, J. van Schaik, M. Bolinches, A. Keane, J. Scanlan – Journal of Aircraft 51 (5), pp. 1360–1372 (2014).
- Better Design Decisions through Operational Modelling during the Early Design Phases -- B. Schumann, M. Ferraro, A. Surendra, J. Scanlan, H. Fangohr – Journal of Aerospace Information Systems 11 (4), pp. 195–210 (2014)
- The Challenges of using Value-Driven Design for practical design of UAVs -- A. Surendra, M. Ferraro, B. Schumann, J. van Schaik, J. Daniels, D. Gorissen, J. Scanlan, A. Keane - Journal of Aerospace Operations – Journal of Aerospace Operations 1 (4), pp. 377–386 (2012).

Conference Papers

- Design and Flight Tests of a Civil Unmanned Aerial Vehicle for Maritime Patrol: The Use of 3D-Printed Structural Components -- M. Ferraro, A. Lock, J. Scanlan, A. Keane – 4th Aircraft Structural Design Conference - Royal Aeronautical Society pp. 1–14 Belfast, UK (2014)
- Toward Value-Driven Design of a Small, Low-cost UAV -- M. Ferraro, D. Gorissen, J. Scanlan, A. Keane, K. Takeda, E. Quaranta, B. Schumann, J. van Schaik, M. Bolinches – 53rd AIAA/ASME/ASCE/AHS/ASC Structures, Structural Dynamics and Materials Conference pp. 1–9 Honolulu, Hawaii (2012)
- Architecting a Decision Environment for Complex Design Evaluation -- D. Gorissen, E. Quaranta, M. Ferraro, J. Scanlan, A. Keane, K. Takeda – 53rd AIAA/ASME/ASCE/AHS/ASC Structures, Structural Dynamics and Materials Conference pp. 1–7 Honolulu, Hawaii (2012)

DECLARATION OF AUTHORSHIP

I, Mario Ferraro

declare that this thesis and the work presented in it are my own and has been generated by me as the result of my own original research.

Value Driven Design of Additive Manufactured Unmanned Aircraft

I confirm that:

1. This work was done wholly or mainly while in candidature for a research degree at this University;
2. Where any part of this thesis has previously been submitted for a degree or any other qualification at this University or any other institution, this has been clearly stated;
3. Where I have consulted the published work of others, this is always clearly attributed;
4. Where I have quoted from the work of others, the source is always given. With the exception of such quotations, this thesis is entirely my own work;
5. I have acknowledged all main sources of help;
6. Where the thesis is based on work done by myself jointly with others, I have made clear exactly what was done by others and what I have contributed myself;
7. None of this work has been published before submission:

Signed: .....

Date: .....

Acknowledgements

This work would have been impossible without the help and support of many people. There are several persons I would like to express my sincere gratitude to.

Firstly, I would like to thank my supervisor Prof. Jim Scanlan for his support and guidance.

Then, I would like to thank the members of the DECoDE project for their cooperation and friendship. They are Dirk Gorissen, Erika Quaranta, Ben Schumann, Jeroen van Schaik, Marc Bolinches, and Prof. Andy Keane.

A big thank you to the colleagues and friends that worked with me at the 2Seas-3i and BERISUAS projects: Andrew Lock, Mantas Brazinskas, Mehmet Erbil and Bob Entwistle.

Finally, to all members of the Computational Engineering and Design Group for helping creating a stimulating atmosphere to work in.

Definitions and Abbreviations

3D – Three-Dimensional

ABS – Acrylonitrile Butadiene Styrene

AD – Axiomatic Design

AHP – Analytic Hierarchy Process

AM – Additive Manufacturing

AoA – Angle of Attack

AST – Aircraft Sizing Tool

BBC – British Broadcasting Corporation

BSFC – Brake Specific Fuel Consumption

CAD – Computer-Aided Design

CB – Cost-Benefit

CDT – Concept Design Tool

CE – Concurrent Engineering

CFD – Computational Fluid Dynamics

CKF – Cost commitment, Knowledge about design, and design Freedom

CNC – Computer Numerical Control

CoG – Center of Gravity

COTS – Commercial-Off-The-Shelf

ConOps – Concept of Operations

DECODE – Decision Environment for COmplex DEsigns

DoC – Degree of Centrality

DUADE – DECODE Unmanned Aircraft Design Environment

DFM – Design For Manufacturing

DMSL – Direct Metal Laser Sintering

DoF – Degrees of Freedom

EASF – Extensive Attribute Scaling Factor

EFI – Electronic Fuel Injection

EPP – Expanded PolyPropylene

FBRC – Fuel Burn Rate at Cruise

FDM – Fused Deposition Modelling

GISM – Geodesic-Inspired Semi-Monocoque

GRS – Grid Reinforced Structures

IMO – Individual Manufacturing Operation

IOF – Intermediate Objective Function

IPPD – Integrated Product and Process Development

LOD – Level Of Details

LUAS – Light Unmanned Aerial Systems

MBSE – Model-Based Systems Engineering

MDO – Multidisciplinary Design Optimisation

MTOM – Maximum Take-Off Mass

NL – Netherlands

NP – Neutral Point

NPV – Net Present Value

QFD – Quality Function Deployment

RIR – Reliability Improvement Ratio

RM – Rapid Manufacturing

RNLI – Royal National Lifeboat Institution

ROI – Return On Investment

RP – Rapid Prototyping

SAR – Search And Rescue

SE – Systems Engineering

SLS - Selective Laser Sintering

SM – Static Margin

SUA – Small Unmanned Aircraft

SV – Surplus Value

TOPSIS – Technique for Order of Preference by Similarity to Ideal Solution

UAV – Unmanned Aerial Vehicle

UAS – Unmanned Aerial Systems

UA – Unmanned Aircraft

UK – United Kingdom

UV – Ultraviolet

VDD – Value Driven Design

VLM – Vortex Lattice Method

VM – Value Model

VSL – Value of a Statistical Life

XPS – eXtruded PolyStyrene

1 Introduction

1.1 Unmanned Aerial Vehicles, Rapid Manufacturing and the Future of Aircraft Design

An Unmanned Aerial Vehicle (UAV) – also known as an Unmanned Aircraft (UA)[1] – is an aircraft that operates with no human pilot on board. UAVs can be remotely piloted and/or are capable of automated or autonomous operation. According to the UK Civil Aviation Authority (CAA) definition, UAVs do not include systems that are not reusable or that are classified as guided weapons [1].

UAVs are far from being a recent development: the very first heavier-than-air flying machines were unmanned aircraft. Remotely piloted aircraft have been used by the military as weapons or aerial targets for training since as early as World War II. Modern UAVs (systems capable of flying a complex pre-programmed mission) started to appear in the second half of the 20th century. However, until the last decade of the century, their use was limited to military applications due to the complexity and cost of the technology. The UAVs were flying dull, dangerous and dirty missions, where the cost and risk for manned aircraft were deemed too high.

In recent years, the reduction in cost and size of the enabling technology has generated an increasing interest in UAVs from commercial companies, public bodies, and research instructions. It is recognised that UAVs can perform some tasks more cost effectively than manned planes. Moreover, the affordability of UAVs has generated new business opportunities and demand for new services that were made possible by the access to this technology.

The current and future applications of UAVs include search and rescue, disaster relief, cargo and parcel delivery, wildlife protection, surveillance and reconnaissance, aerial imagery for the media

[1] Other terms used to refer to UAVs are Unmanned Aerial System (UAS), Drone, Remotely Piloted Aircraft (RPA), and Remotely Piloted Aircraft System (RPAS). All these terms are generally used to refer to the same concept, although their definition might vary slightly across different sources. For example, the UK CAA CAP 722 regulation [1] defines RPAs as a subset of UAs that are constantly under the control of the remote pilot. Similarly, it defines UAS and RPAS as the collection of system elements required for the operation of the UAV, thus including the UA, the remote piloting station, the communication link, and so on. However, these terms are used inconsistently in the CAP 722 regulation (For example, the mass-based classification of the unmanned aircraft uses the term UAS while UA should be used).
In this document, the term UAV is used to refer to the unmanned aircraft while the UAS refers to the aircraft plus the supporting system elements. The terms SUA and LUAS will be used to refer to the specific UAV categories defined in CAP 722.

industry, crop monitoring, pipe monitoring, archaeological and geological surveys, and remote sensing in general.

UAVs, like any other aircraft, have to comply with the air navigation rules set by the national CAAs. Not all the countries have dedicated rules for UAVs, and when they are in place there is little uniformity between different countries[2].

In general, large UAVs provide higher mission capabilities in terms of larger payload capacity, greater endurance and higher flying speed. Their design is less constrained by mass restrictions and can result in a more reliable aircraft by exploiting redundant and sophisticated flight systems. However, higher regulatory requirements translate into higher development cost, increased development time and operational restrictions. For this reason, SUA and LUAS are often a higher value solution in many civil applications.

Having a low development time and cost implies that SUA and LUAS benefit less from versatility and can be designed for a single specific mission. When the mission value is high compared to the system cost, bespoke disposable systems can be a valuable solution.

The benefit of a rapid design cycle can only be fully harvested if it is coupled with a manufacturing process that can translate the "blueprint" of the UAS into the final product in a very short time scale. Thanks to the evolution of Rapid Manufacturing[3] (RM) techniques, it is now possible to produce an airframe within days of conception [2]. The physical scale of SUA and LUAS makes materials like ABS (Acrylonitrile Butadiene Styrene) and Nylon plastic viable options for structural airframe components. These materials can be formed into very complex geometries without the need for tooling by utilising Additive Manufacturing (AM) techniques. Analogously, Computer Numerical Control (CNC) machining can be used to shape light and inexpensive parts made out of Polypropylene or Polystyrene foam.

In the past decades, AM, also known as three-dimensional (3D) printing, was mainly used to create prototypes or models for engineering, scientific or design purposes. Nowadays, AM is still

[2] In the UK, the CAA divides the unmanned flying vehicles into three main categories: systems lighter than 20 kg are defined as Small Unmanned Aircraft (SUA); systems whose mass is between 20 kg and 150 kg are defined as Light Unmanned Aerial Systems (LUAS); systems above 150 kg are defined as UAS. SUAs do not require an airworthiness approval or a registration of the vehicle. They can be operated within Line Of Sight (LOS) in not densely populated areas and below 400 feet (122 m) of altitude. A special permission is required for aerial work and to operate in more risky operating environments. LUAS generally require airworthiness approval and airframe registration but it is possible to obtain an exemption to these requirements on a case by case basis. In general, a lower mass, lower complexity, and highly safe LUAS is more likely to obtain the exemption certificate. An operating permission is always required for LUAS and is granted on the basis of a thorough risk analysis.

[3] Please see Chapter 4 for the definition of Rapid Manufacturing, Additive Manufacturing, Rapid Prototyping and 3D printing.

sometimes referred to as Rapid Prototyping but the use of 3D printing to produce end-products is well established [3]. Business analysts predict a large expansion of the AM market and an increasing demand for mass customisation and bespoke products [4–7]. It is expected that improvements in the current techniques and the appearance of new and more refined technologies will generate an overall decrease in the production cost and an increase in the product quality.

Recently, the aviation industry has started to consider 3D printing as a competitive manufacturing option for at least some parts of the final product [8–10]. Large aerospace companies have been investing in this technology and the first 3D printed components have been used on military and commercial flights [11–13]. In the world of small unmanned aircraft, 3D-printed parts have been used as major structural components and largely 3D printed airframes have been starting to appear [14–17]. The author has been pioneering this trend by realising and flying the world's first entirely 3D printed aircraft (named SULSA) [2] and with the DECODE and 2SEAS projects [18–22], where Light UAVs were largely produced by Selective Laser Sintering (SLS) Nylon printers.

In a more general context, Mavris *et al.* [23] identified three key areas of improvement of the future aircraft design process: Cost commitment, Knowledge about design, and design Freedom (CKF). Figure 1-1 presents schematically the variation of CKF during the various phases of the current system development and the aspiration of the future design process. It is commonly suggested in the literature that between 50% and 85% of the development cost of a product is committed by the end of the concept design phase [24–27], although the majority of the costs are incurred in later phases. Therefore, decisions that significantly reduce the design space, result in major cost commitments, and have the largest impact on the success of the final product generally happen in the very early design phases, when the knowledge of the problem and the proposed solution is poor and/or incomplete. To remedy this situation, the future design process should aim at increasing the knowledge in the early development phases and at delaying the commitment to early decisions for as long as possible.

The use of inflexible manufacturing processes is one of the main causes of the early cost commitment and reduced design freedom. Therefore, the use of RM promises to deliver a large improvement to these two aspects. However, the benefits of RM need to be evaluated concurrently with the ability to produce competitive products in terms of cost and performance; the production cost and the availability of high-performance materials of RM (and particularly of AM) are still significantly worse if compared to more traditional manufacturing techniques. These, together with other technological and legal limitations, are the reasons why it has not yet been

proposed that a large-scale commercial aircraft be designed for rapid manufacturing. However, for UAVs up to a certain scale, RM can be the most valuable solution.

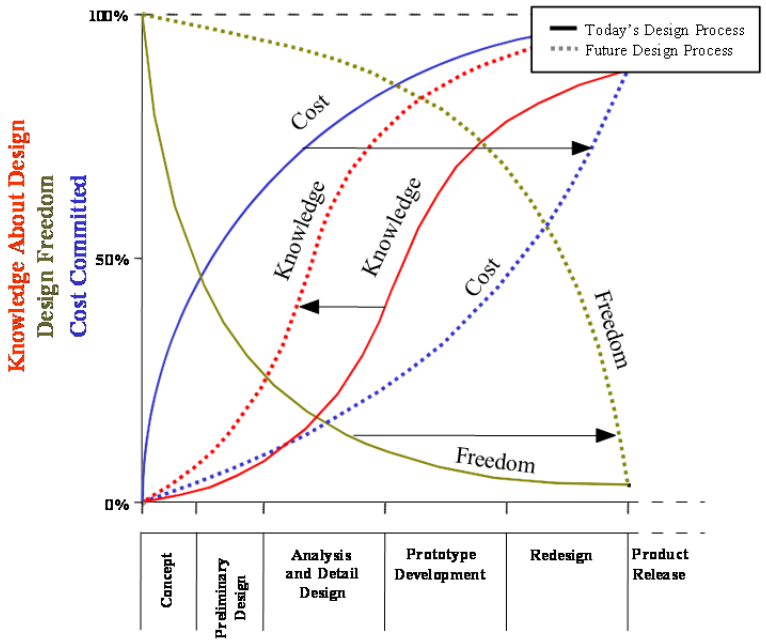

Figure 1-1 – Cost-Knowledge-Freedom shift for future design methods [28].

Design decisions can be better informed by accounting for multiple aspects of the system life-cycle from the early design stages. For example, manufacturability, maintainability, and reliability of a system are often overlooked in the initial design phases. Systems Engineering (SE) was developed to address the need for a more comprehensive approach to the aircraft design, trying to find an optimal balance between the product's performance, cost and development time. However, traditional SE was developed for large organisations and complex multi-year programs. This resulted in rigid design frameworks where the system's requirements are established at the beginning of the development cycle and then propagated down to the subsystems and components. These models have the advantage of reflecting the hierarchical structure of large design organisations and providing designers with clear goals but, in practice, often result in major cost and schedule overruns [29]. The problem lies in the fact that requirements allocation drives the engineers toward solutions that meet all the requirements rather than the ones that generate the best overall value. As a result, designers dedicate the majority of their resources to the satisfaction of difficult-to-meet requirements while overlooking easily achievable improvements.

In recent years, research has focused on the development of Value Drive Design (VDD) [30], a novel SE and design process based on requirements flexibility and the use of a value model to

guide design decisions. The main idea behind VDD is straightforward in principle, but its practical implementation presents many challenges. For example, it is not trivial to define what the system value function should be, particularly for applications that do not present a clear way to generate positive cash flows. Furthermore, in order to generate an accurate ranking of alternative solutions, VDD requires modelling of the entire system life-cycle, including system development, service life, and disposal. Unfortunately, many of the disciplinary models required for such analysis are neither available nor sufficiently mature to be trusted by the engineers. Additionally, there is the problem of presenting the decision makers with a clear and intelligible map of the VDD trade-offs. Finally, requirements flexibility entails frequent interaction between the subsystems' developers which is a problem for large projects involving many design entities. For all these reasons VDD is not currently used in the aerospace industry [31].

Nevertheless, the requirements flexibility introduced by VDD is a key requisite for the exploitation of the benefits of RM. The transition to the future design process (i.e. the CKF curves shift described in Figure 1-1) requires a high flexibility in both the design and the manufacturing process. The application of the VDD methodology to the design of small and light UAVs is less affected by the problems indicated above (for example, regarding the communication between design teams) and it can be seen as the first step toward the integration of VDD into the development processes of major aerospace programs.

1.2 Research Questions and Hypotheses

There are two main points of interest in this research. The first is the study of the design opportunities and constraints posed by the access to AM techniques in the context of UAV design. The second is the study of the practical implementation of VDD for mission-specific rapid-manufactured unmanned aircraft.

The development of small and low-cost rapid-manufactured UAVs represents a particularly interesting academic case study (as well as being commercially interesting, as discussed in Section 1.1). On one hand, these systems require the solution of a complex design problem that presents many of the challenges encountered in larger aerospace development programs (multidisciplinary problems, integration of several components, cost-performance balance, and so on). On the other hand, their scale and the use of AM allow a small design team to rapidly develop the product. Therefore, the result of the design process can be tested in real life, providing important feedback to the research project.

1.2.1 Design for Additive Manufacturing of UAV Airframes

At the beginning of this project, there were no examples in the literature of largely 3D printed airframes. The author's research group at the University of Southampton had been experimenting with Fused Deposition Modeling (FDM) of small components of the secondary structure of UAVs. However, these components were only used for non-flight-critical parts such as camera-holding brackets. Nevertheless, there was a strong interest in the creation of plastic 3D printed UAV structures for the reasons discussed earlier in this chapter.

Therefore, one of the research topics discussed in this work is the use of AM for the production of structural components of UAVs. In particular, this study is focused on the design possibilities and limitations associated with the use of Selective Laser Sintering of Nylon (which is one of the most common and high-quality 3D printing techniques).

The main research hypothesis can be stated as follows:

Hypothesis 1 – *The extensive use of additive manufacturing can improve the design process of small low-cost unmanned aircraft by increasing its flexibility and reducing the development time and cost.*

In order to verify or reject this hypothesis, this research answered the following questions.

1 - Is it possible to produce an entire UAV by using only 3D printed components and COTS avionics systems?
2 - Are the available materials suitable for the use in UAV structural components?
3 - What is the development time of a 3D printed airframe?
4 - What are the major advantages and disadvantages of 3D printed structures?
5 - Should 3D printed airframes be designed differently to conventional ones? If a partly 3D printed airframe is designed, what parts are best produced using AM?

1.2.2 Development of a Value Driven Design Framework for the Design of Search and Rescue Unmanned Aerial Vehicles

As already discussed in Section 1.1, the main obstacles to the adoption of the VDD process are related to its practical implementation. By focusing on a specific application, it is possible to unveil the problems and opportunities that VDD entails. Therefore, it was decided to focus this study on the following design problem: the design of a rapid-manufactured UAV to support maritime Search and Rescue (SAR) operations.

VDD relies on the presence of a design environment where a quantitative analysis of the design trade-offs can be performed. That is, it is possible to measure the benefits and detriments that result from a particular design decision. This implies the existence of several interconnected disciplinary models and a system value model used to rank design alternatives. In particular, the value of a system is derived from the ability to fulfil its mission. Therefore, the value model has to include a way to predict if, and how well, the system will be able to perform the mission. In the case of UAVs with no predetermined flight path (such as flying from point A to point B), this can be achieved through the use of an operational simulation. In the end, in order to progress with the design, engineers need to understand the relationship between the design variables (i.e. the wing span), the technical performance parameters of the system (such as the UAV flight speed), the mission-level performance (such as the number of successful rescue operations), and ultimately the overall value for the stakeholders.

The main research hypothesis can be stated as follows:

Hypothesis 2 – *A Value Driven Design framework based on a holistic system model and a life-cycle operational simulation can improve the understanding of the problem, support design decision making and guide the system design toward the highest value for the stakeholders.*

In order to verify or reject this hypothesis, this research answered the following questions.

1 - What process should be used to design mission-specific UAVs?
2 - How should the system value of mission-specific UAVs be measured?
3 - Is it possible to link technical system requirements to mission level performance and ultimately to the system value? Is it possible to link low-level (detail design) variables to the system value?
4 - What are the practical obstacles preventing the adoption of a VDD approach for the design of UAVs?

1.3 Original Contribution to Knowledge

The original contribution to knowledge of this work can be summarised in the following points:

- The demonstration that the use of AM technology and materials is a viable option for the production of structural components of airframes with a maximum take-off mass up to 35 kg.
- The analysis of the merits and limitation of AM for UAV design through a number of case studies.

- The introduction of a design principle that can guide engineers during the design of partly 3D printed airframes based on a simple manufacturing complexity measure, engineering judgment and a basic network analysis of the system physical architecture.

- The development of a design framework for mission-specific rapid-manufactured aircraft where an aircraft sizing tool, an agent-based operational simulation, and a value model are used concurrently to make design decisions about the system characteristics.
- The demonstration of the benefits of using a detailed life-cycle simulation from the concept design stage.
- The demonstration of the importance of providing the decision maker with a comprehensive set of simulation outputs in order to facilitate the understanding of the factors and dynamics that contribute to the value generation.

1.4 Thesis Structure

The first part of this thesis presents an introduction to the state of the art of engineering design and the available additive manufacturing processes. Chapter 2 contains an introduction to aircraft design, optimisation, and Systems Engineering. It also discusses the importance of the selection of system requirements, the definition of the concept of operation and the simulation of the mission scenario. Chapter 3 describes the role of system value models in engineering design and presents the concept and applications of VDD. Chapter 4 introduces rapid manufacturing, focusing on the peculiarities of additive manufacturing.

Chapter 5 discusses the impact of additive manufacturing on the aircraft design process. It also presents case studies showing the application of additive manufacturing for the production of unmanned aircraft airframes. Finally, it introduces the principle of confined complexity that can be used to guide the design of the physical architecture of partly 3D printed airframes.

Chapter 1 describes the implementation of a design framework that aims to support VDD of small low-cost UAVs for civil applications (DUADE). In particular, a SAR mission is used as the test case scenario. Chapter 7 describes the application of DUADE for the trade space exploration of system requirements, mission effectiveness, life-cycle cost, and overall system value.

Chapter 8 presents the conclusion of this thesis.

2 Aircraft Design and Systems Engineering

2.1 Introduction: Engineering Design as a Decision Making Process

Engineering design is a non-unique iterative process, the aim of which is to reach the best compromise of a number of conflicting requirements [32].

The design activity is in essence equivalent to the decision-making process. The decision-making process involves a series of steps that can be summarised as shown in Figure 2-1.

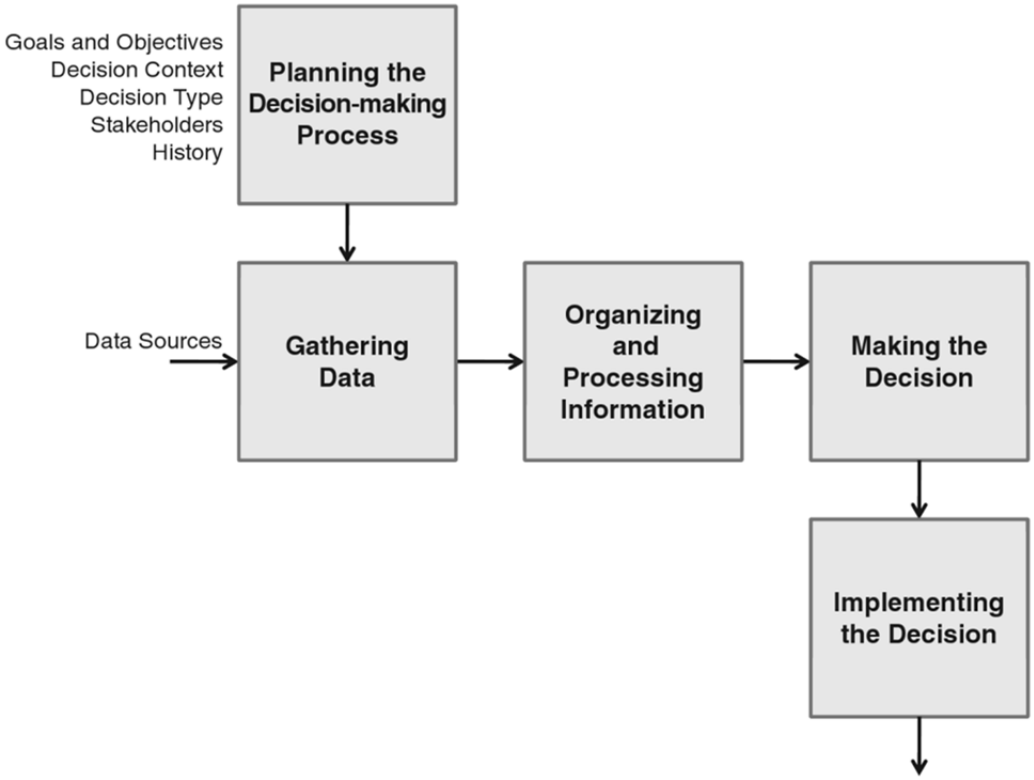

Figure 2-1 – Decision-making process [33].

One can distinguish two key inputs required to perform a rational decision:

First of all, the decision maker needs to have a clear understanding of the goals, context and stakeholders' needs and requirements. Moreover, they need to have a clear way to assess the goodness of an option and to rank alternatives. This implies the creation – conscious or unconscious – of a system value model that can rank design alternatives. This subject will be discussed in Chapter 3.

Second, the decision maker needs to gather information in order to be able to predict, or at least estimate, the outcome of the decisions. This requires the understanding of the control variables and trade-offs and is referred to as the analysis phase.

The design of complex artefacts involves decision making over a potentially infinite number of variables. Some of these decisions are more relevant than others. In order to make a problem treatable, the number of variables needs to be reduced by creating simplified models of the problem. The understanding of the problem leads to the establishment of constraints, requirements and variable bounds that guide the designer toward a suitable solution. This phase of problem understanding is often the most difficult, time and resource consuming. In the past decades, research in the aerospace field has focused its efforts on the creation and improvement of disciplinary analysis tools, producing significant advances in the instruments available to the engineers. The increasing computational power has also allowed the analysts to routinely use high-fidelity physics-based models for disciplines like the fluid dynamics or structural analysis. In comparison, little research efforts have been aimed at improving the design process as a whole.

The impact of decisions needs to be propagated to all the aspects of the system and its environment. In the past, and during each stage of design, a chief engineer would assimilate information from a number of disciplines and use experience, intuition, and judgment to make top-down decisions in seeking good trade-offs. A good example of this was Kelly Johnson, renowned for his work on many aircraft designs, including the U2 and SR-71 [34]. Observational studies in engineering design offices confirm that experience is still a fundamental requisite to correctly understand trade-offs and reasons behind design solutions [35,36]. However, the increasing scale and complexity of aerospace engineering programs and the increasing demand for systems that account for non-traditional engineering discipline and environmental constraints have gradually increased the need for design methodologies and tools that facilitate a holistic approach to the system design. The life span of today's major aerospace development programs is measured in decades, and often they involve multiple design entities, suppliers, sub-contractors and stakeholders based in many different geographical locations. At the same time, the development of small unmanned aircraft demanding a quick development time has introduced new challenges for the designers and engineers that are called to tackle similar integration problems but on a smaller scale and with fewer resources available.

This chapter presents a brief introduction to the aircraft design process, the Systems Engineering approach and the emerging methods and tools.

2.2 Aircraft Design

A simple diagram of the classical approach to aircraft design process is given in Figure 2-2. Design starts with a set of requirement to be met and ends with the production of the aircraft. The actual design effort is conventionally divided into three phases: the conceptual design, the preliminary design, and the detail design. Feedback loops may occur when the information obtained in the next design phase brings to light problems or major improvement opportunities that impact the previous design decisions.

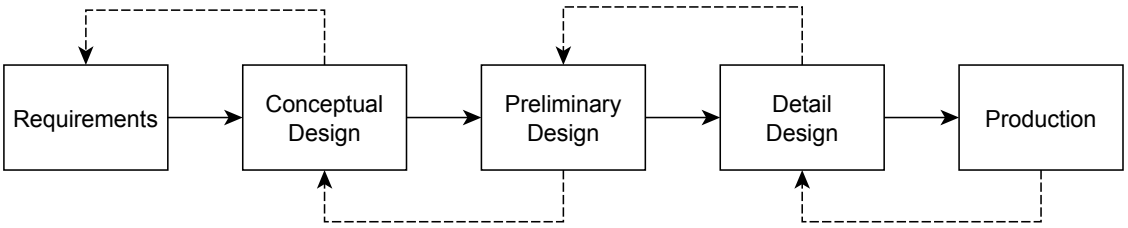

Figure 2-2 – Aircraft design process.

1 - The **conceptual design** is where the high-level questions about the aircraft configuration, size and technology are addressed. In this phase, different configurations are generally explored and the design team gains an understanding of the performance trade-offs of the various design alternatives. This is an iterative process in nature and Raymer [37] describes it as a "design wheel" (Figure 2-3): preliminary trade studies generate a set of requirements that lead to the choice of a concept. Design analysis assesses the feasibility of the aircraft and leads to an iteration in the preliminary sizing and trade studies.

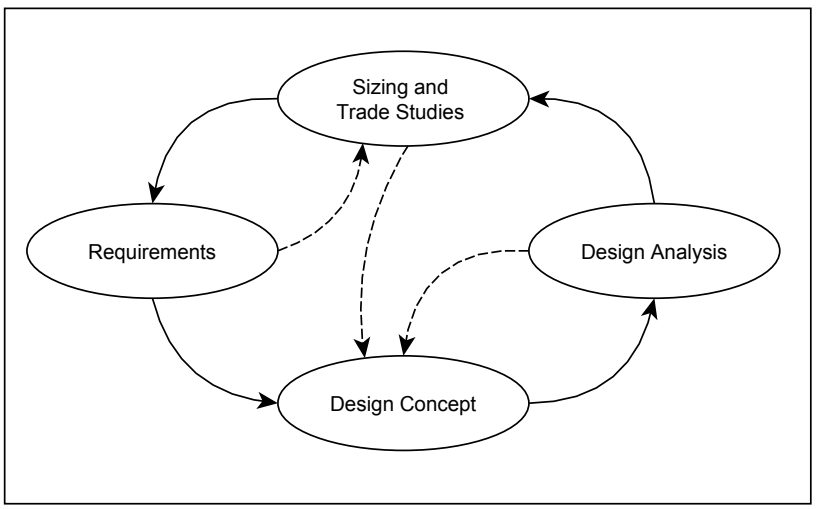

Figure 2-3 – The design wheel [37].

At the beginning of the conceptual design, many possible configurations are explored. Typically there is a qualitative screening of possible solutions which ends with the definition of a concept space which contains the most promising alternatives that are worth investigating in more detail. Then there is the primary sizing of the candidate aircraft which is performed initially taking into account only very high-level parameters such as the take-off weight, wing area and propulsive power and progressively introducing more parameters such as the position and dimension of the control surfaces, the size of the fuselage etc. It is worth noting that during this process of refinement the design space is gradually reduced while the number of variables that are explicitly considered increases as shown in Figure 2-4.

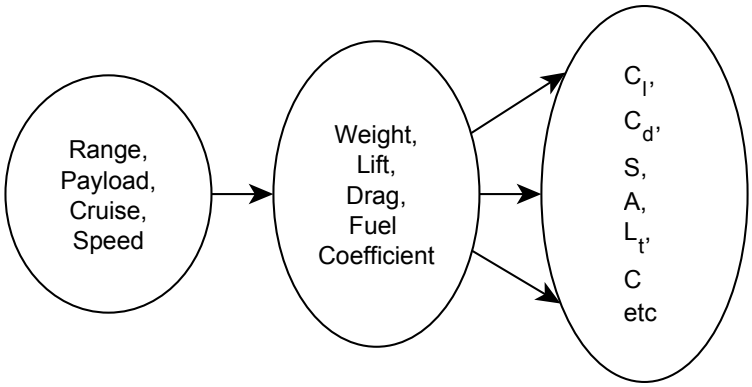

Figure 2-4 – Increasing the number of design parameters [25].

The conceptual design ends when all the major decisions about the aircraft systems have been taken and only small revisions of the configuration are expected.

2 - During the **preliminary design** phase, the aircraft systems are analysed in more depth and lower level variables, such as the fuselage skin thickness or the undercarriage wheel diameter, are considered. There is still some level of iteration with the conceptual design phase but given the computational cost of the more detailed analyses and the increasing number of variables to be considered, the engineering team tends to "freeze" the configuration as soon as possible. An accurate cost estimation of the aircraft is expected as one of the outputs of this phase.

3 - Finally, **detail design** is when the actual parts to be produced are designed with the manufacturing process in mind. This is a very time expensive activity as all the smallest design components are considered and the number of design variables increases rapidly. The design team commits to the decision taken during the conceptual and preliminary

design phases and revisions occur only if major problems are encountered. On the other end, the design of local features is a highly constrained problem and the decisions on the lowest level variables have a negligible impact on the overall system [25].

The process ends with the start of the production phase, even though the product development often continues in the years after the first version is released.

The end of each phase represents a milestone in the product development and the designers benefit from tackling these design stages sequentially because they can focus on less complex problems. On the other hand, commitment to early design decisions can cause the final product to deviate substantially from the optimal solution. This is caused by the fact that designers have to make choices relying on a poor understanding of the problem and scarcity of information. This is particularly true when unconventional configurations or novel technologies are exploited and little or no past experience can be exploited.

The design process has evolved during the last decades to meet the increasing complexity of aerospace systems. Although the basic steps of the design phases are the same, more emphasis is placed on the development of a holistic approach to product development that includes life-cycle metrics and non-traditional disciplines such as economics. The Systems Engineering (SE) approach has provided the ideal framework for multidisciplinary optimisation and has stressed the importance for a continual feedback between system requirements, function, and design synthesis.

2.2.1 Design Optimisation

Design optimisation is a systematic way to explore the design space in search for a solution that maximises an objective function. An optimisation problem can be stated as follows

$$\max_{\boldsymbol{x}\in\boldsymbol{X}} f(\boldsymbol{x},\boldsymbol{p}) \qquad \text{subject to } \boldsymbol{g}(\boldsymbol{x},\boldsymbol{p}) \leq 0, \boldsymbol{h}(\boldsymbol{x},\boldsymbol{p}) = 0 \qquad \text{2-1}$$

where f is the objective function to be maximised, $\boldsymbol{x}$ is the vector of the design variables controlled by the optimiser, $\boldsymbol{p}$ is the vector of parameters that influence the objective function but cannot be changed by the optimiser, $\boldsymbol{g}$ and $\boldsymbol{h}$ are the inequality and equality constraints, respectively.

Over the years, many algorithms have been proposed to solve this problem[4]. One of the possible classifications distinguishes between “local” and “global” algorithms. The first are based on the idea of sequential refinement of an initial guess value. The main difference among them has to do with the strategy they employ to establish the direction and size of the step they take in the successive refinements. Good examples of this class of algorithms are the Newton and Quasi-Newton methods which rely on the calculation or approximation (respectively) of the Hessian matrix, that is the matrix of the second-order partial derivatives of the objective function with respect to the design variables. This class of algorithms can be very effective in finding local optima but the solution will depend on the starting point.

Global optimisation algorithms search the design space by using a population of points. Having multiple starting points they can reject local optima and identify the global best solution. Evolutionary and stochastic algorithms are examples of global algorithms that are not gradient-based. These methods can explore the design space very efficiently at the price of a lower accuracy in finding the refined optima.

2.2.2 Multidisciplinary Design Optimisation and Aircraft Sizing Tools

Optimisers can be used to solve a vast range of problems. In the field of aircraft design, they are routinely used to size the aircraft at the conceptual stage as well as to enhance the performance of a particular subsystem at the detail design stage. Whenever several specialist analysis disciplines are considered at once, the optimisation problem is called a Multidisciplinary Design Optimisation (MDO)[5].

Particularly in the early phases of design, it is important to have models that cover multiple disciplines (such as aerodynamics, structures, cost, performance, and so on) in order to find a balanced solution. The integration between design and analysis disciplines remains the great challenge of MDO. Design frameworks can follow two approaches: either the design environment is designed to include all the aspects of the systems analysis/synthesis in a single tool or it is a composition of specialised tools that communicate with a central one. The first kind can be defined *integrated* sizing tools and the second kind *coordinated* sizing tools.

The first approach has been used in several aircraft conceptual design environments [38–51]. Integrated aircraft sizing tools provide the great advantages of being self-contained. This generally results in a better controlled interaction between the design modules and in an easier

[4] A good review about the optimization algorithms can be found in [280].
[5] Reviews on the state of the art of MDO can be found in the literature [152,281,282].

management of the design variables and parameters. On the other hand, there are two main limitations with this class of tools. The first is that they are generally limited to specific types of vehicles, due to the sizing algorithm being coded into the sizing tool. The second is that the analysis tools and disciplinary models are hard coded into the tool and are difficult to modify or change. This makes difficult or impossible to refer to the same tool at later stages of design, when information available is higher and there is the need for more detailed models.

Coordinated design environments have the potential to be more flexible and can handle different Levels of Details (LOD)[6] of the analyses. They also resemble more closely the structure of design companies, in which disciplinary experts provide analysis for their domain. Moreover, the central module can be used to coordinate design from the concept to the detail design phase, providing a common environment to perform trade-off analysis. The main problem with this class of tools is that the variables and parameters that are used in detail design and analysis models are generally different from the high-level parameters that are used in the conceptual design. An example is the wing area, which is one of the main concept sizing variables but is not explicit in the final Computer-Aided Design (CAD) drawings. Moreover, different disciplinary models are interested in different levels of abstraction of the geometry and hence different parameters (for example the aerodynamics model of the aircraft will not have the internal structure details while the structural model will focus on the main structural element only). The result is that engineers spend substantial periods of time linking various analysis tools. If the design parameters are not properly controlled and managed there is the risk of divergence between the data used by different disciplines. A number of frameworks have been proposed to automate the non-creative activates of design, like the work needed to generate the aircraft geometry models for the various analysis [52–56]. However, experience has shown that automated and sophisticated tool integration is very difficult to support and rarely generates a net value for an organisation in the long term [57]. Good examples of the coordinated design environments are Dimensional Addition and Detail Insertion (DADI) developed at the Queen's University of Belfast [25], Parametric Aircraft

[6] Engineers employ models to predict the impact of design decisions on the characteristics of the final system. A number of disciplinary models are routinely used by aircraft engineers; these include models to simulate the physics of the systems (such as the vehicle aerodynamics) and models of the processes (such as manufacturing or maintenance). Some models are based on first order approximations and can produce an output using only a few key input variables; others are designed to be able to capture higher order effects and require a more detailed input. They are generally referred as low- and high-fidelity models. However, this use of the term fidelity is incorrect. Fidelity can be defined as: "The degree to which a model or simulation reproduces the state and behaviour of a real world object or the perception of a real world object, feature, condition, or chosen standard in a measurable or perceivable manner […]" [283]. Instead, models should be classified by their Level Of Details (LOD) where the LOD can be defined as the degree to which a model is responsive to the details of the input. The model fidelity is a consequence of the LOD, the accuracy of the input and correctness of the equations governing the model.

Configuration Schema (PACS) developed by German Aerospace Centre (DLR) [58] and Parametric-based Comprehensive Aircraft Design (PCAD) developed by Konkuk University [59].

The problem of linking the subsystems and the high-LOD world to the overall system balancing has led to multilevel optimisation strategies. The optimisation problem can be decomposed in order to create a hierarchy of problems, each with his own objective function, while the central coordination is maintained. Examples of decomposition strategies are the Bi-Level Integrated System Synthesis (BLISS) [60,61], the Collaborative Optimisation (CO) [62], Analytical Target Cascading (ATC) [63] and Concurrent Subspace Optimisation (CSSO) [64]. Each of these methods proposes a different strategy to decompose the main objective function and control the target functions and constraints of the subspace problems and their interaction. BLISS uses weighting coefficients of the subsystem objective function to influence the outcome of the subsystem-level optimisation; CO and ATC use a similar approach based on target values to drive the subsystem optimisation, with CO oriented toward a discipline decomposition and ATC toward component decomposition; for each subspace problem, CSSO exploits low-LOD or surrogate models of the other subspaces to achieve a concurrent optimisation of all the subsystems and the overall system.

Another limitation of classical conceptual design tools is that many non-technical disciplines, such as maintenance and manufacturing, are often neglected [6].

Finally, despite the fact that some of these design environments provide a basic mission description, this is usually limited to the definition of flight segments [65].

2.3 Systems Engineering

A system is a set of elements that interact to achieve a stated purpose. The purpose is called a mission [66].

Systems Engineering is a methodical, disciplined approach for the design, realisation, technical management, operations, and retirement of a system [67].

The necessity to guide the engineering of complex systems led to the formalisation of Systems Engineering in the decades following World War II [33]. This Systems Engineering approach focuses on the system as a whole and is concerned with the identification and management of external factors as well as the mere engineering design. The customer needs, the operational environment and all the other external factors that can impact on the system life cycle are considered as part of the design problem. The ultimate target of a Systems Engineering process is to achieve the “balance” among conflicting goals – such as performance, cost and schedule

constraints – that leads to the best value for the system user. This involves the ability to make decisions involving incommensurable attributes of the system that are strongly interdependent of each other.

There are many possible approaches to the Systems Engineering process, good examples are the ones used by NASA [67], INCOSE [68] and the Department of Defence (DoD) of the United States [69]. In Figure 2-5 the framework proposed by the DoD is described. The inputs to the process are the end-users needs and requirements and the external constraints. During the requirement analysis phase, the inputs are analysed and translated into a set of technical requirements that define unambiguously and completely what the system must do. The functional analysis and allocation provide a decomposition of the system into lower-level functions (functional architecture) which are simpler to analyse. The requirements are flown down at the lower-level subsystems and a better understanding of the system capabilities, priorities, and functional conflicts is used to improve the definition of the system requirements. During the design synthesis, the system physical architecture is developed, which maps the physical subsystems to their functions. The knowledge about the system increases and a design loop ensures that the functional architecture is updated to reflect the implication of the new information. The role of the system analysis and control is, on one hand, to provide the technical management of the process activity and, on the other hand, to perform the design and trade-off studies that provide the rigorous and quantitative data to support design decisions and requirements and functions selection. Finally, the final solution is compared to the initial requirement in the verification loop.

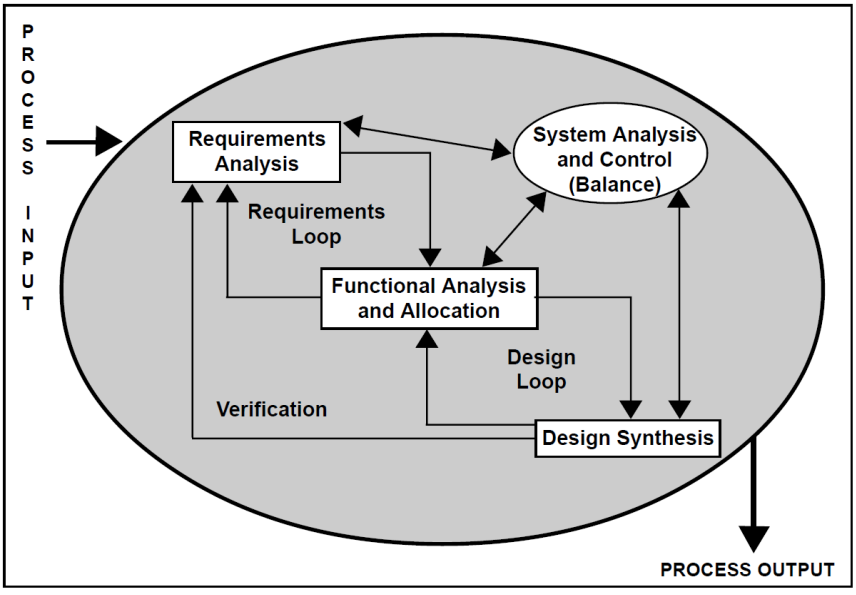

Figure 2-5 – DoD Systems Engineering Process [69].

2.3.1 Reductionist and Holistic System Models

A system can be described as following either a reductionists or a holistic approach. In the first case, the system is considered to be entirely defined by the sum of its parts. This implies that it can be divided into simpler subsystems each of which is analysed separately. The holistic approach studies the system as a whole and aims to capture complex interactions between subsystems that cannot be explained by the reductionist approach. These interactions are called emergent behaviours.

In theory, the reductionist approach presents a number of advantages. First of all, it enables a more straightforward task distribution among the design entities. This is particularly useful for large projects when several companies in different geographical locations participate to the system development. It also favours a modular approach to the system and the independent development of subsystems which can be tested and de-risked individually. As demonstrated by the Axiomatic Design (AD) theory [70–73], limiting the interactions between system elements results in a more controllable and robust design process. In particular, AD applies a *divide-and-impera* strategy to system design by proposing that the coupling between design parameters should be eliminated by design. This is a sound principle but it can be difficult or impossible to apply in practice.

Many design methodologies that help the decision makers to capture the interaction between system requirements, design variables and the subsystems dependencies have been proposed over the years. In particular, there are a number of matrix-based methods that help to map and understand these combinatory behaviours [74]. Examples are the “house of quality” of the Quality Function Deployment (QFD) [75,76] and the N^2 diagrams or Design Structure Matrixes [77,78]. These methods are very useful in identifying the qualitative dependencies but are based on very approximate quantitative description of the interactions. This makes them very useful in the very early stage of concept design but they cannot support advanced trade space analysis.

In designing aerospace systems, the coupling between disciplines and subsystems plays an important role in the success of the final product. The interaction between mass, performance, aerodynamics and structures of an aircraft is just one of the possible examples. When emergent behaviours cannot be neglected, the system description must be holistic and the interaction between the system elements must be modelled accordingly. In order to achieve this, the document-centric approach to SE needs to be replaced by the Model-Based Systems Engineering (MBSE) [79]. MBSE is the formalized application of modelling to support system requirements, design, analysis, verification and validation [80]. Although the use of model-centric approaches for

many engineering disciplines has become widespread with introduction of computers in the 1950s and 1960s, in the SE field the transitioning process is still immature [79].

2.3.2 Waterfall, Spiral and Agile Product Development Models

The life cycle of a system is the evolution from concept design to product production, operation and ultimately disposal. Systems Engineering provides life cycle models that support and guide the system development. Here three models are presented (the waterfall, spiral and agile product development models), from the more rigidly structured to the more flexible.

Reductionism favours a top-bottom approach to the system design, that is, the system life cycle is described as a series of sequential processes, each providing the input to the following one. This "waterfall" approach is based on the hypothesis that there is limited feedback between the subsequent processes and the interaction between project phases are limited to successive steps [81]. One of the classical incarnations of the waterfall model is the V-model (Figure 2-6). The V-model has the advantage of providing a specific deliverable for each of the subsequent phases and a clear way to keep track of the project progress. It also emphasises the test and acceptance phase by planning for them early on. On the other end, it is a rather rigid model and does not provide a clear strategy to deal with the problems encountered during the test phase, especially because the validation happens toward the end of the process when modifications are very costly if not impossible.

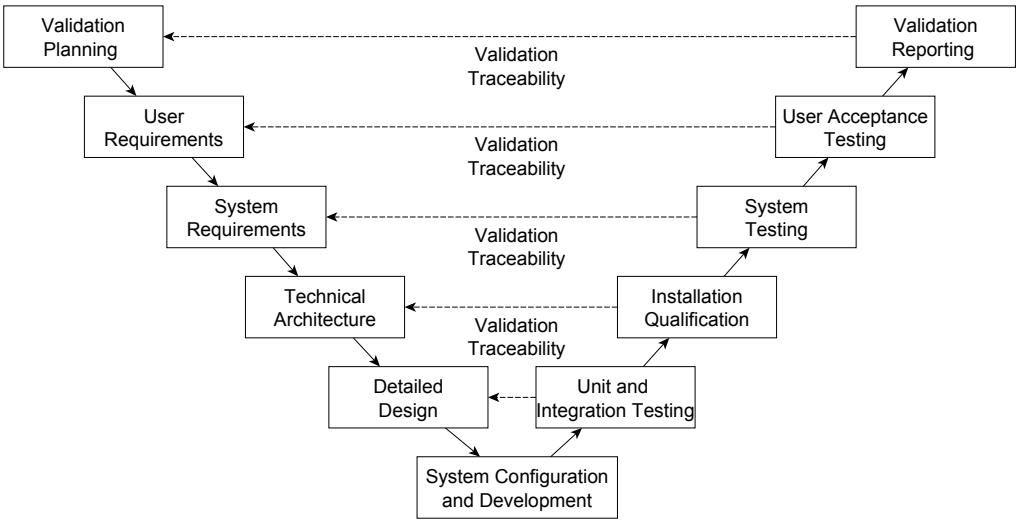

Figure 2-6 – The V-model [33].

The spiral life cycle model emphasises the iterative nature of the system development [82]. Unlike the waterfall approach, it relies on the continuous repetition of the Systems Engineering process throughout the system lifecycle. In particular, it aims at exploiting the information that is gained

during the system development to apply correction and steer the solution toward a better result. The spiral model is more flexible than the waterfall model and is well suited to the development of systems whose requirements and technical challenge are uncertain or difficult to predict from the beginning. It also encourages the creation of working prototypes and it has a deeper focus on risk management. In a spiral development cycle, the focus is shifted from the timeline of the project to the achievement of the product requirements. This is beneficial because it reduces the risk of delivering a product that does not meet the specification. However, it also increases the risk of greatly extending the duration of the development program.

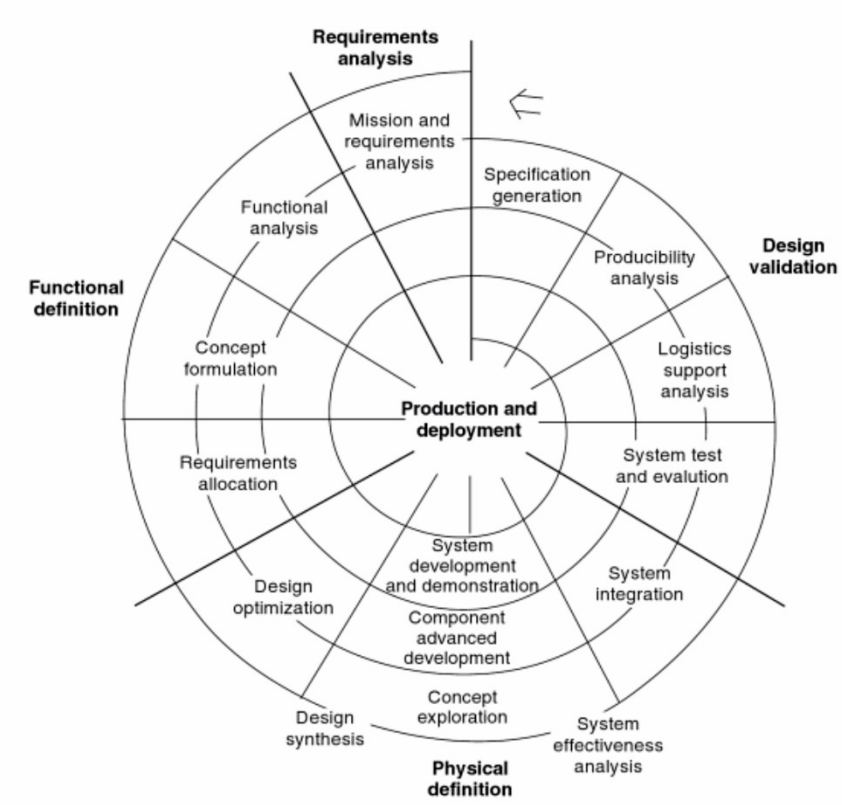

Figure 2-7 – The spiral model of system life cycle [33].

Agile Systems Engineering methods have been developed to deal with constantly changing environments and fast evolving technologies. They have their origin in the software development world but have found their application in many other engineering fields [83,84]. The main idea behind agile Systems Engineering is to prioritise quick and iterative product development over more structured approaches. Top-down approaches tend to generate a substantial amount of documentation and require a significant effort in the process control and management. This is beneficial for large and long-term projects, but it can represent an obstacle for small and time-critical projects. Agile development divides the work packages in time or workflow chunks (e.g. in the Scrum method [85] or in the methods inspired by the Kanban process [86]), and demands that these chunks must be kept small (typically 2-8 weeks). It also emphasises the need for a constant

communication flow between small groups of engineers working in parallel. By doing so it favours communication and bottom-up innovation. Moreover, the short time available to achieve each task pushes the engineers to prioritise the essential work ensuring that minimal resources are spent in low impact activities.

2.3.3 Concurrent Engineering and Integrated Product and Process Development

"Concurrent Engineering is a systematic approach to the integrated, concurrent design of products and their related processes, including, manufacturing and support. This approach is intended to cause the developers from the very outset to consider all elements of the product life cycle, from conception to disposal, including quality, cost, schedule, and user requirements" [87].

As explained in the definition above, the Concurrent Engineering (CE) method has been developed to include life cycle consideration as soon as possible in the system development. This is achieved by simultaneously developing models, performing analysis and making decisions for all the aspects that influence the product success and the stakeholders' satisfaction. One classical example is the concurrent design of the manufacturing process together with the product design. In this way, possible problems and opportunities are identified early on, when changes to the design are still possible without major cost and time penalties [88,89]. CE, and the analogous Integrated Product and Process Development (IPPD) [90], can be seen as structured and systematic applications of the spiral life cycle model.

The application of the principles of CE and IPPD has been investigated in a number of scientific publications [91–94] and promoted by institutions like the European Space Agency [95], DLR [96], NASA [67] and DoD [90] but their full potential has not been exploited yet. The problem lies in the difficult task of translating the core principles into practical models due to the lack of models for some of the key disciplines and the difficult management of product information across different models and different level of abstraction [25,97].

2.4 System Requirements, Concept of Operation and Mission Simulation

The system's requirements selection is a good example of an early design decision that has vital importance for the achievement of a successful product. It requires a good understanding of the project stakeholders' needs, the environment in which the system will operate and the trade-offs involved with the achievement of a certain level of performance in each of the key system functions. Techniques to elicit the system requirements from the stakeholders' expectation include structured matrix methods like in the QDF or the COncept Design Analysis (CODA [98]) or prescriptive approaches that rely on the analysis of customer statements [99]. Requirements are

typically established in the very early stages of the design phase and feedbacks are limited to the concept design stage. However, at that stage, the designers do not have yet a clear understanding of the simultaneous impact of the requirements, product design variables, and technologies available [100].

Systems like aircraft and spacecraft are designed to fulfil a very specific mission and benefit the most of the modelling of a Concept of Operations (ConOps). The ConOps is the description of how the system will be operated during its life cycle to meet the customer expectations [67]. By doing so the main technical challenges can be exposed and the system requirements can be clearly identified and quantified. The use of mission models and simulations enhances the problem understanding because it provides the quantitative base for trade-off analyses involving the system requirements and performance.

Many COTS aircraft design tools include a mission model that can be used to optimise the system performance, estimate the fuel consumption and the operational cost. Most of these models are limited to the definition of flight segments (such as “taxi”, “take-off”, “climb”, “cruise”, and so on). Examples include FLOPS [39], ACSYNT [101], RDS [102] and PIANO [103]. This approach is perfectly reasonable for the class of aircraft these tools have been designed for, that is, transport vehicles whose typical mission is to fly from point A to point B. At the other end of the spectrum there are tools that incorporate sophisticated flight simulators that include six Degrees of Freedom (DoF) models of the aircraft and control surfaces and actuators models, like the one proposed by Krus *et al.* [104,105]. However, this LOD is not required during the initial phase of design when the properties of the aircraft are still uncertain. Pacelab Suite [106] include an advanced mission simulation tool which is aimed at marketing and acquisition studies for transport aircraft rather than design studies. There are also COTS mission simulation software, like FLAMES [107] and STK [108], that provide high LOD 6 DoF flight models and can simulate the interaction of multiple vehicles in detailed terrain and atmospheric environments. However, these tools are intended for strategic studies, aiming at assessing the performance of the current assets rather than support the design of novel vehicles.

The mission simulation tools aimed at supporting the design of UAVs requires characteristics in between the simple flight segment models and the high LOD 6 DoF ones. They must be detailed enough to be able to distinguish between design alternatives and capture the meaningful interaction between the UAVs and the other agents in the environment. At the same time, they must avoid sophisticated models that require a too detailed description of the system whose characteristics are not entirely defined yet. Duquette [109] argued that a low LOD flight model based on few high-level aircraft parameters can provide a realistic enough representation of the

UAV behaviour, and proposed the use of its model for the control algorithms study and flight strategy optimisation. Wei [110] used an agent-based simulation environment for the study and coordination of swarm of UAVs.

A number of studies about the use of operational simulation as a design support tool for UAVs and combat aircraft have been published. Soban [111] demonstrated that design parameters can be linked to system effectiveness metrics by the use of mission scenarios. Similar studies were performed by Evans [112], Nilubol [113] and Cassidy *et al.* [114]. Thokala [115,116] created a design tool for life cycle cost and performance optimisation of turbojet combat UAV based on a number of mission scenarios. As noted by Schumann [65,117], the key limitations of these tools are the impossibility to simulate multiple vehicles, the lack of models for interaction and cooperation with other agents and the lack of geographical and environmental models. In 2015, Yifeng *et al.* [118] presented a study based on the optimisation of UAVs design in a system-of-systems context. This study included the presence of multiple UAVs cooperating to the fulfilment of a mission but crucially neglected any cost consideration in the assessment of the mission performance.

2.5 Summary

This chapter has presented the aircraft engineering design process and the Systems Engineering approach to product development. It has briefly described some multi-disciplinary optimisation strategies applied by aircraft synthesis tools and presented some system life-cycle models. A brief discussion about the importance of the concept of operation and mission models in the understanding of system requirements have been provided as well.

Each of the models and frameworks described in this chapter has its own strengths and weaknesses. The choice of a design or life cycle framework needs to account for the specificity of the product of interest. For example, transport jet aircraft or satellite systems will benefit from more structured approaches that are more effective at managing the interaction and cooperation of large organisations over long time spans. In comparison, light and low-cost UAVs will benefit from simpler and more agile SE processes.

One of the most critical activities of SE is the establishment of the performance requirements. It has a big impact on the final value of the aircraft but it is often performed using only the experience and judgment of the decision makers. In many cases, the analysis of the reference market and the examination of similar systems can provide the required performance benchmarks. Nonetheless, in the case of bespoke UAVs, those data are rarely available. Therefore, the performance requirements must be obtained from the analysis of the ConOps.

However, the ConOps does not provide information about the feasibility of a system that meets these requirements as well as the cost and performance trade-offs involved.

An end-to-end mission simulation can be used to provide the quantitative relationships between the aircraft performance and the mission cost and effectiveness but it has been rarely used as an integral part of the design cycle. Overall, the design environments proposed so far have failed to integrate aircraft sizing tools, life-cycle cost models and detailed operational simulations where the performance of the system is evaluated concurrently with its interaction with the environment and the other agents involved.

3 System Value Models and Value Driven Design Methodologies

3.1 Introduction

The need to compare and rank design alternatives in a systematic way led to the development of system value models. System value models have been the object of extensive studies in economics and decision theory. In this work, the interest lies in their application to the aerospace systems design. Good reviews of aerospace system value models are given by Collopy [119] and Ross *et al.* [120]. Value models are particularly useful in trade studies: with traditional Systems Engineering, trade-offs between performance, cost, risk and schedule are not straightforward because these are incommensurable metrics. Moreover, attributes like reliability, flexibility and robustness are often ignored (or not included in the optimisation loop but only taken into account as "best practices"). The aim of a value model is to integrate all these performance and characteristics into a single figure of merit.

Design approaches based on explicit value models have been referred in the literature as value-driven design [30], value-centric design [121] or value-based design [122] methodologies. Some authors assign slightly different meaning to them, but in this work they are used as synonyms.

This chapter will briefly introduce the concept of value models and value-driven design and will shortly present the current status of the research.

3.2 Value-Driven Design

3.2.1 What is Value-Driven Design?

Value-Driven Design (VDD) is a design methodology that uses economic theory to improve Systems Engineering and optimisation [30]. The design goal is not a set of particular performance parameters but the *value* of the final product. The main improvement of a value-based design process over the traditional approaches lies in the systematic and simultaneous evaluation of cost and benefits of design alternatives [120]. Although the basic idea of VDD is some decades old, research started to focus deeply on this subject after the instigation of the Value Driven Design Program Committee by the American Institute of Aeronautics and Astronautics [123]. They define VDD as *an improved design process that uses requirements flexibility, formal optimisation and a*

mathematical value model to balance performance, cost, schedule, and other measures important to the stakeholders to produce the best outcome possible [123]. VDD entails a flexibility of the requirements so that the final design is obtained from the exploration of an entire solution space.

3.2.2 How is VDD Different from Traditional Systems Engineering?

The VDD philosophy can be applied to assist the decision makers from the conceptual to the detail design stage, improving the system design.

In the conceptual design phase, VDD can lead the sizing and requirements definition for the system. At this stage, traditional cost-centric and requirement-based engineering would optimise the system to achieve a minimum life-cycle cost while meeting a desired performance level or, inversely, the best performance given a maximum program cost. By using a VDD approach, the design team can identify the most valuable options by recognising the best trade-off between cost and performance and other attributes.

In the preliminary design phase, VDD can help identifying the subsystems which are more important to the success of the product and hence require more attention form the designers. The traditional Systems Engineering is based on the assumption that in order to meet the overall system requirements, all the subsystems have to meet their own requirements. VDD instead intends to *optimise the system performance while giving a range of performance parameters to the subsystems* [124].

Finally, at the detail design stage, when components are designed in isolation, the VDD does not flow down requirements but objective functions [30]. By linearly decomposing the system value functions into component value functions a distributed optimal design can be achieved [29]. This reduces the risk of cost and schedule overrun [125].

3.2.3 How is VDD Implemented?

References [30,119,120,126] present good reviews of the several implementations of Value-Driven Design proposed over the years. All the approaches share the same simple philosophy: the optimal system is the one that maximises the value for the stakeholders. The way the value is defined, the way the stakeholder preferences are aggregated, and the way the VDD is operationalised may differ in the various approaches.

Nevertheless, the general framework for the practical implementation of VDD can be summarised as follows:

1 - Define the problem and identify the stakeholders.
2 - Define what value means for the stakeholders and establish the “point of view” of the value model.
3 - Define the system to be designed.
4 - Create a system value model to coherently measure value of alternative systems.
5 - Generate candidate systems.
6 - Measure the value of the candidates and select the best.

Although this appears to be a straightforward process, each of the steps listed above presents its own challenge [31].

3.3 Stakeholders Analysis

Typically the stakeholders of an aerospace project include the customers, i.e. the ones purchasing the product, the companies that are involved in the design and realisation of the product and all the other people or institutions that are going to interact in one way or another with the system.

However, not all these stakeholders will be interested in the same attributes of the system. The example of an airliner can clarify the problem. In this case, the customers are represented by the airlines that are interested in purchasing the aircraft. Their main goal is to maximise their profit and hence they will be interested in a system that would allow them to sell more tickets and/or at higher prices while reducing the operating cost. The companies that design and build the aircraft will be interested in maximising their own profit, and hence they want a system that can be sold to the airliners at the highest price while minimising the resources needed to realise it. The users will be the passengers that will be interested, apart of course from the cost of the ticket, in having a comfortable, quick and safe trip. Other stakeholders will include, for example, people that are part of the environment in which the system operates, like people leaving in the proximity of airports which are concerned about noise and pollution.

Aggregating and quantifying the needs of the stakeholders is a difficult problem which has a literature of its own. Arrow’s impossibility theorem [127] states that it is not possible to use the preference of individuals in a group to establish the preference of the group as a whole, unless some assumptions are introduced, like the existence of a main decision maker that can assign weights to the preference of the group individuals.

Focusing on the VDD methodologies, Collopy [119] points out that in order to build a coherent value model one should identify what is the “point of view” of the model, or in other words, identify the main decision maker. He suggests that the most appropriate final decision maker is

the organisation that is financing the project. How and if the voice of the other stakeholders is taken into account is not entirely clear. One way of accounting for the preferences of secondary stakeholders is to model the impact of their level of satisfaction on the value for the primary stakeholder (returning to the former example, one can assume that passengers would pay more for their ticket if the seats are more comfortable, hence increasing the value for the airliner as well). However, this method is not always straightforward to apply or implement [31].

Different approaches for aggregating and the preference of multiple stakeholders include the introduction of group voting strategies or averages of the individual preferences [128,129]. However, these methods lack a solid theoretical foundation. The use of Game Theory[7] to achieve multiobjective decisions with multiple stakeholders has been studied by Papageorgiou *et al.* [130].

3.4 How to Define and Measure Value

The term "value" can be a source of confusion, given the fact that it has many different and often vague definitions which depend on the context and disciplines. For example, the renowned economist Adam Smith distinguished between *value in use* and *value in exchange*, the first being the utility of possessing or consuming a good and the second the power of purchasing other goods given by the possession of that particular good [131].

In the engineering context, value can be defined as a numerical encoding of preference that has the property of order, that is, given three alternatives *a, b* and *c*, if $a < b$ and $b < c$, then $a < c$). This implies that value mast be expressed by a single ordinal number [119].

3.4.1 Decision Under Uncertainty: Value and Utility

Preferences can be modeled by noticing that given a set of alternatives *X*, for each pair of elements *a, b*, the decision maker can either prefer one of the two, be indifferent or judge the elements incompatible. This can be represented mathematically by introducing the binary relation $\succcurlyeq$ on $X \times X$, where $a \succcurlyeq b$ means that either the decision maker prefers a to b or they are indifferent [132]. The cases of indifference, strict preference and incompatibility can be derived from the $\succcurlyeq$ operator and the logical *AND* and *NOT* operators. However, in practical situations, it is useful to represent preferences numerically through functions that assign real numbers to each of

[7] Game Theory studies the optimal strategies of rational decision makers in cooperative and non-cooperative situations.

the elements of *X* such that the higher the number the more preferred is the element. Such functions $v: X \longmapsto \Re$ are called *value functions*[8] and can be defined as

$$for\ all\ a, b \in X, \qquad a \succcurlyeq b \Leftrightarrow v(a) \geq v(b) \tag{3-1}$$

In a deterministic world, each *act* of the decision maker leads to a unique consequence. This implies that the value of the act is equal to the value of the consequence, that is, the decision maker will prefer the action that leads to the preferred consequence. In a non-deterministic world, each act can have several consequences which occur with a certain probability. According to the *expected utility theory* [133], first formulated by Daniel Bernoulli in the 18th century, the decision maker will prefer the action that leads to the highest expected *utility*. The *utility* is a particular scale of value that takes into account the risk attitude of the decision maker. In more details, the outcome of a decision can be modeled by a set of consequences $(x_1, x_2, \dots, x_n)$ and their probabilities to occur $(p_1, p_2, \dots, p_n)$. The sets $(x_1, p_1, x_2, p_2, \dots, x_n, p_n)$ are called *lotteries* in decision theory terminology. The *utility theorem* by Von Neumann and Morgenstern [134] states that there is a *utility function u* such that

$$v(act) = \sum_{1}^{n} p_i u(x_i) \tag{3-2}$$

u is unique within an affine transformation. In other words, the value of an act can be computed as the *expectation* of the utility of the outcomes. The theorem is derived from the following four axioms that basically define the rationality of the decision maker:

1- Completeness: given two options *a, b* the user can either prefer one of the two or being indifferent between the two.
2- Transitivity: given three options *a, b, c*, if $a \succcurlyeq b$ and $b \succcurlyeq c$, then $a \succcurlyeq c$.
3- Continuity: there is a probability *p* such that the decision maker is indifferent to a lottery between two outcomes *a,c* with probability p and $(1-p)$, respectively, and a certain intermediate outcome b. Formally: if $a \preccurlyeq b \preccurlyeq c$, then there exist a probability $p \in [0,1]$ such that $pa + (1-p)c = b$.

[8] Often the functions v are called utility functions in the literature [36]. However this is source of confusion because the term utility function is also used with a different meaning when decisions under uncertainty are considered.

4- Independence: the preference between two lotteries does not change if they are mixed with a third lottery. Formally that is: given three lotteries *a, b, c* and $T \in (0,1)$, if $a \succcurlyeq b$ then $aT + c(1-T) \succcurlyeq bT + c(1-T)$.

Strictly speaking, the case of decision under risk and under uncertainty should be distinguished. In the first case, the probabilities of the outcomes are known (similar to throwing a dice), in the latter case the probabilities are subjectively assigned by the decision maker. However, Equation holds in both cases.

The utility function can be derived through interviews with the decision makers by utilising the following methodology [119]. Given the worst consequence x_0, the best consequence x_1 and an intermediate consequence x_i, a choice is presented to the decision maker in which the options are either a lottery in which there is a p probability of getting x_1 and a $(1-p)$ probability of getting x_0 or the certainty of getting x_i (Figure 3-1).

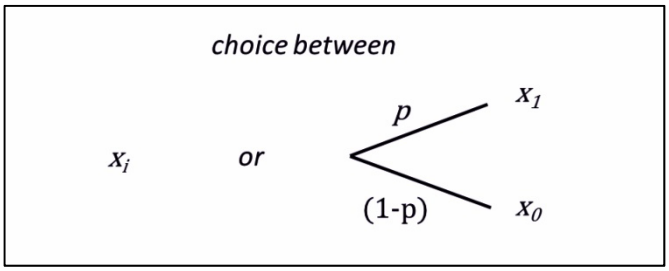

Figure 3-1 – Lottery example.

There is a particular probability p_i at which the decision maker is indifferent to the choice. In this case the following relation holds

$$p_i = \frac{u(x_i) - u(x_0)}{u(x_1) - u(x_0)} \qquad 3\text{-}3$$

If the utility function is normalised such that $u \in [0,1]$ than $u(x_i) = p_i$. The utility function can then be defined by iterating this process for as many outcomes x_i as needed.

The utility curve gives a measure of the decision maker attitude toward risk. In particular, assuming that a (deterministic) value function v exist for the possible outcomes of a decision, the risk aversion is defined as

$$\gamma = -\frac{u''(v)}{u'(v)} \qquad 3\text{-}4$$

where $u'(v)$ and $u''(v)$ are the first and second order derivatives of the utility function with repect to value.

If the utility-value curve is a concave function, the decision maker is risk adverse; if it is convex is risk seeking and if the second derivative is null is risk neutral.

In summary, in deterministic situations, a value function can be defined to map the decision maker's preference over a set of (certain) outcomes. The decision maker preference in a non-deterministic situation is expressed through a utility function that defines his risk attitude.

3.5 Decision with multiple objectives

Often the decision maker is presented with a set of alternatives for which he finds it difficult to identify a single utility function that would map his overall level of satisfaction with the outcomes of the decision. This is the case when multiple contradictory goals are pursued. In this circumstance, the set of possible outcomes is a multidimensional space and the various properties in which the decision maker is interested are called *attributes or criteria*.

The construction of an overall utility function of multiple attributes is impractical and very challenging due to the cognitive limits of the decision maker. However, the problem can be simplified if the overall utility function can be decomposed into multiple *single attribute* utility functions. There are several decomposition forms (additive, multiplicative, multilinear, and so on) that have been studied in the literature and which holds under particular conditions.

This paragraph describes some of the techniques to deal with decisions with multiple objectives.

3.5.1 Trade Space Exploration

Trade space exploration is a fundamental activity in the making of design decisions. Through trade-off analysis it is possible to compare and rank a series of alternatives with respect to a number of desired characteristics. In order to perform a trade space exploration, the following steps are involved:

1 - Define evaluation criteria
2 - Define control variables and constraints
3 - Generate candidate systems
4 - Compare system and analyse results

The evaluation criteria can be a collection of system attributes such as performance, cost and mission effectiveness. They can also be desired characteristics of the system that do not have an obvious numerical representation (one example might be the aesthetics of a product). In this case,

the judgment of the decision makers is used to assign a numerical score to the various alternatives.

The performance of each system in the different criteria needs to be presented to the decision maker in a systematic and intelligible way. Multidisciplinary design tools often offer the possibility to perform quantitative analysis to evaluate the impact of control variables on different attributes of a system. For example, the Georgia Institute of Technology developed a tool based on the response surface methodology, named Unified Trade-off Environment for the analysis of the simultaneous impact of requirements and aircraft characteristics [100,135,136]. The design method called TIES (Technology Identification, Evaluation, and Selection) was developed to address the challenges related to the uncertainty, multidimensionality and life-cycle considerations while assessing the impact of immature technologies infusion [28,137]. Hollingsworth developed a method for systematic exploration of the requirement space and identification of technologies' limits [138]. A multi-LOD concept design environment focused on Unmanned Aerial Vehicle has been developed by Dufresne *et al.* [139]. Stump *et al.* have developed a virtual design environment to allow simulation-based design as well as virtual exploration of design trade-offs for the complex design space of an engineering product [140]. Visual comparison of alternative systems can be performed through the use of Spider Charts or parallel coordinates plots. In a Spider Chart, the score of the candidate systems is plotted in a multi-axes graph where each axis represents one of the criteria. In this way, it is possible to identify the systems that perform particularly well in many of the criteria and simultaneously expose weaknesses and strengths of each candidate.

If on one hand multi-attribute trade space exploration is desirable because it presents the decision maker with a complete set of information; on the other hand, it does not provide a clear way to identify the optimal system: the decision maker has to rely on their judgement to evaluate the relative importance of each attribute and find the best compromise solution.

3.5.2 Pareto Front

Pareto fronts can be used to screen out suboptimal systems: a candidate system is part of the Pareto set if none of the attributes can be improved without worsening at least another. Pareto fronts can be represented by curves or surfaces in two- or three-dimensional attributes spaces. For more than three attributes the graphical representation of Pareto sets becomes less intuitive and it is more difficult to judge trade-offs. There are methods to visualise multiobjective Pareto fronts in bi-dimensional spaces such as the hyper-radial visualisation method proposed by Chiu *et al.* [141]. These methods rely on the grouping of attributes into two auxiliary functions that

become the orthogonal axes of a bi-dimensional space. If on one hand, they allow the decision maker to visualise the distribution of Pareto set, on the other end they hide meaningful information about the nature of the trade-off involved because the auxiliary functions do not have an obvious meaning.

Finally, it is worth nothing that Pareto fronts do not present the optimal solution but a set of non-dominated alternatives because there is no aggregation or relative weighting of competing goals.

3.5.3 Technique for Order of Preference by Similarity to Ideal Solution

The Technique for Order of Preference by Similarity to Ideal Solution (TOPSIS) [142] is based on the idea that the best candidate in a multi-attribute space is the one whose characteristics are the closest to the utopia solution, that is the point that has the best possible score in all the criteria, and farthest from the negative ideal solution. The distance between each alternative and the utopia point is measured as a Euclidean distance in the multidimensional normalised attribute space. Weighting is used to establish the relative importance of the attributes. However, it is difficult to keep the consistency of judgment when assigning the weights to various criteria [143].

3.5.4 Analytic Hierarchy Process

Analytic Hierarchy Process (AHP) [144] is a widely used multi-attribute decision support tool. The method's strength relies on the fact that the decision makers can obtain both the criteria weighting coefficient and the candidate ranking using simple pairwise comparisons. The selection problem is subdivided into smaller problems that create a hierarchy. The matrix of pairwise comparison between decision criteria is generated and the relative weightings are obtained by solving the eigenvector problem

$$M \times w = \lambda_{max} w \tag{3-5}$$

where M is the matrix of pairwise comparison, w is the vector of weighting factors and λ_{max} is the highest eigenvalue of M.

The AHP assumes preference independence among the various criteria. For large numbers of criteria, the pairwise comparison becomes a difficult task and inconsistency problems are likely to occur. One of the main criticism of AHP is that it subject to rank reversal, that is, the preference order of the alternatives can change if a new alternative is introduced [143].

3.5.5 Multi-Attribute Utility Theory

Keeney and Raiffa [145], demonstrated that under the following axioms, a multiplicative form can be used to combine the utility functions.

1- Preferential independence: the preference order between two consequences of an attribute is independent of the level of all the other attributes.
2- Mutual utility independence: the utility function of an attribute is independent of the level of all the other attributes (up to a positive linear transformation).

Given the vector of attributes $\bar{x}$, the i^{th} single attribute utility function $u_i(x_i)$ for the i^{th} attribute x_i, the overall utility function $u(\bar{x})$ is

$$1 + Ku(\bar{x}) = \prod_{i=1}^{N}[Kk_i u_i(x_i) + 1] \qquad 3\text{-}6$$

where k_i is a scalar constant which represent the multi-attribute utility value of x_i when it is at his best and all the other attributes are at the worst value and can be interpreted as a weighted ranking of the attributes relative importance [146].

The scaling factor K can be obtained solving the equation

$$K + 1 = \prod_{i=1}^{N}[Kk_i + 1] \ , \quad K\epsilon(-1,1), k_i \neq 0 \qquad 3\text{-}7$$

If the further condition of *mutual additive independence* is verified, the Equation 3-6 becomes a simple weighted sum of objectives,

$$u(\bar{x}) = \sum_{i=1}^{N} k_i \, u_i(x_i) \qquad 3\text{-}8$$

with $\sum_{i=1}^{N} k_i = 1$. The condition of mutual additive independence is well explained by Figure 3-2

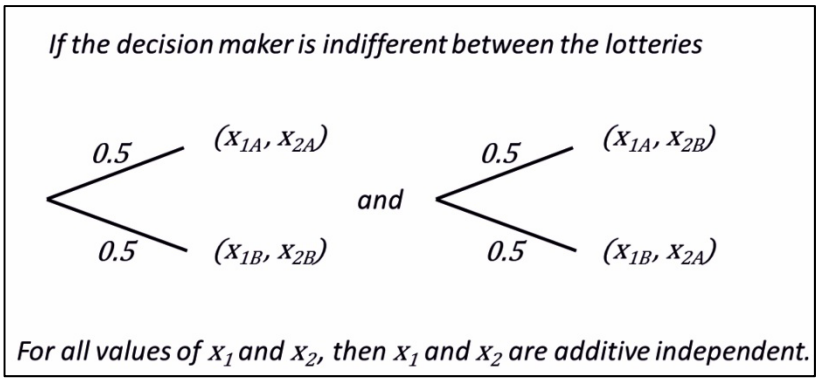

Figure 3-2 – Test of additive independence condition [147].

The multi-attribute utility approach can be very useful in engineering decisions because it allows the decision maker to establish trade-offs between attributes otherwise difficult to compare such as performance, cost, reliability, and so on. However, its operationalisation presents some difficulties:

- The hypotheses of utility and preferential independence are often not valid in real situations for at least some of the attributes. This can be overcome in certain situations by redefining the attributes, for example aggregating some of them. The condition of *mutual additive independence* is almost never verified in practice.
- Utilities are dimensionless metrics whose real meaning is difficult to be understood by the stakeholders and engineers. When they are combined together, the overall Multi-Attribute Utility (MAU) is obtained. The MAU provides a ranking of the alternatives but at the same time does not provide a quantitative insight of the difference between them.
- The method requires the elicitation of the single attribute utility functions through stakeholders' interviews, which can be a long and difficult process.

3.5.6 Decisions with Multiple Objectives: "Stanford School approach"

An alternative to the Keeney and Raiffa approach, known as the "Stanford School approach", has been proposed by Matheson and Howard [148]. In this case, the value functions for each attribute are combined under certainty and then the utility function is applied to the overall value to represent the risk attitude of the decision maker. The foundation for this approach is provided by the utility transversality [149] which states that once a value function has been defined, the risk attitude (i.e. the utility curve) in multi-attribute decisions can be defined independently for only one of the attributes; all the other risk attitudes must be derived from this.

3.6 Monetising Value: Worth Models

The Stanford School approach simplifies the problem because it removes the need for the hypothesis of utility independence. However the problems of defining a common (certain) value function for all the attributes such that they can be meaningfully aggregated remains. Collopy [119] proposes that this value scale should be worth (i.e. the value expressed in monetary units). The main point is that worth is a metric intelligible to everybody and that everybody uses in daily decisions. On the other hand, this definition of value implies that all the characteristics of a system that are important to the stakeholders are quantifiable into monetary units. Often this problem does not present a trivial solution. However, Keeney and von Winterfeldt suggest that in many practical situations it is possible to apply an Equivalent-Cost Procedure by asking the decision makers for value trade-offs [150].

The use of worth implies that the deterministic value functions can be aggregated through an additive model. Although this is not true in general, in many cases it is possible to obtain additive models by redefining the attributes or by defining extra attributes that account for the non-additive effects [150].

3.6.1 Implications of Monetising Value: Risk Attitude and Discount Rate

The Stanford School approach still requires converting the value obtained under certainty to utility in order to account for the risk attitude of the decision maker. If value is expressed as worth, this is equivalent to assess the risk tolerance with respect to money. Collopy [119] provides an interesting discussion on the topic whose conclusion can be summarised as follows:

- Defining the risk tolerance ρ as the reciprocal of the risk aversion γ defined in Equation 3-4, in the hypothesis of constant ρ, the worth-utility curve can be expressed as

$$u = \rho\left(1 - e^{-\frac{w}{\rho}}\right) \qquad 3\text{-}9$$

  Where *e* is the exponential function, w indicates worth and the utility scale is such that it is zero when the worth is zero.
- For companies, risk tolerance can be estimated approximately as 1/6 of the total company equity[9].
- The presence of risk adversity implies the presence of a risk premium. That is, if a value is placed on each possible prospect as if they were certain and then they are weighted by their probabilities and summed, the expected worth is obtained. If instead the values are first converted to utilities, the expected utility is computed and then they are converted back to worth through Equation 3-9, the "certain equivalent worth of the expected utility" is obtained. The difference between the two is due to the risk attitude of the decision maker. When there is risk neutrality the two values are equivalent.
- A quantitative measure of the risk premium θ can be obtained as

$$\theta \approx \frac{\sigma^2}{\rho} \qquad 3\text{-}10$$

  where σ^2 is the variance of the worth distribution for the possible consequences of the decision. When $\theta \approx 0$ the condition of risk neutrality holds. This condition holds when the

[9] Collopy based this estimate on a study by Howard [284] that observed that, for a small sample of oil and gas companies, the risk tolerance was proportional to the size of the company and could be estimated as one-sixth of the total equity or 6% of the annual revenue. A more recent study has confirmed the existence of a statistically significant positive relationship between firm size and risk tolerance, at least for the petroleum industry [285]. No such study has been published for aerospace companies.

decision maker is a public entity such as a government. In case of companies the following criterion for risk neutrality can be applied

$$\text{Risk neutrality when: } \frac{\sigma^2}{MC \times PV} < \frac{1}{6}\% \tag{3-11}$$

Where MC is the market capitalisation of the firm and PV is the estimate of the value of the program object of the value model. In practice risk neutrality can be assumed for all the real world engineering decisions [119]. This implies that the value models reduce to a worth model.

In a worth model, one should discount the cash flows to take into account of the time value of money (money today is worth more than money tomorrow). This is typically done by introducing a discount rate r such that the Net Present Value (NPV) of future cash flows $D(t)$ is

$$NPV = \sum_{t=0}^{N} \frac{D(t)}{(1+r)^t} \tag{3-12}$$

where N is the number of discrete periods considered (generally years) and r has been assumed constant with time. The discount rate should only be used to obtain the present value of money, thus indicating the time preference of the decision maker. It should not be increased to interpret the risk preference of the stakeholders [119].

3.7 Metrics for Worth Based Value Models

Engineers and value modellers are often tempted to define value as performance divided by cost. This definition has the great advantage to avoid the problem of assigning a monetary value to the system performance. However, excluding some special cases [151], this metrics generally leads to wrong results [119].

MDO research agenda indicates as one of the priorities the inclusion of manufacturing and cost models into the design loop in order to design for NPV or Return On Investment (ROI) [152].

Provided one has solved the problem of monetising the value of a system, there are a number of possible ways to establish a ranking of the alternative systems. In this paragraph, some of the most widely used metrics are discussed.

3.7.1 Return On Investment

ROI is a metric that indicates how efficiently an enterprise or a particular business generate profit given a certain investment. In its simplest form, ROI can be calculated as

$$ROI = \frac{G - C}{C} \quad \text{3-13}$$

Where G is the gain from the investment and C is the cost of the investment. It is often expressed in percentage (for example, an investment that generates £11 given a cost of £10 has a ROI of 10%).

ROI is a very flexible metric that can be used to compare very different systems. However, it presents some criticalities. First of all, ROI does not explicitly account for the duration of an investment: the same ROI can be realised with two different systems, one of which may take one order of magnitude more time to generate the profit. ROI also does not take into account of the cash flows and possible constraints on the invested capital. For example, one system may generate a better ROI in the long term but require a substantial initial investment and an initial series of negative cash flows; all this is "hidden" to ROI. Finally, ROI does not indicate the investment that provides the best profit but the one that provides *proportionally* the best return, that is, ROI would favour an investment that returns £12 with a cost of £10 over an alternative that provides £23 spending £20 despite the fact that the latter generates a higher profit.

3.7.2 Net Present Value

As already discussed in Section 3.6.1, Net Present Value (NPV) measures the current value of future cash flows. It is calculated by using Equation 3-12.

NPV currently accounts for the time value of money and correctly ranks the alternatives according to their value. However, it relies on the assumptions that future cash flows are known a priori. The discount rate chosen for a particular project has a large influence on the final NPV, but unfortunately there is no definite method to select it. One possible way is to choose r according to the interest rate that needs to be paid for borrowing the money required for the project. Alternatively, one can look at the expected return of projects of similar field and risk. In any case the selection of the appropriate discount rate requires some expert judgment and therefore value models based on NPV will be influenced by this.

3.7.3 Surplus Value

Surplus Value (SV) is similar to NPV in the fact that uses cash flows and discount rates to establish the current value of a project. It is used to simplify the NPV model in the case of multiple manufacturing companies contributing to the realisation of a system. According to this model, If one assumes that there were only a single company designing the overall system, the subsystems that maximise the value for that company are equivalent to the subsystems that maximise the value for each subcontractor [153,154]. SV relies on a number of simplifying hypotheses discussed in [153] and [155], including the existence of a single producer and a single customer.

3.7.4 Real Options

When evaluating a project using the NPV or the SV, one implicitly assumes that the decisions made at the beginning will be held throughout the development of the project. However, in the real world, decision makers will react to the outcome of future uncertain events such as market demand variation. This means that they will decide to drop a program that becomes clearly unprofitable or maybe to invest more if new information indicates that it could lead to a higher profit. The Real Options model tries to capture this behaviour to present decision makers with a more accurate picture of potential gains and losses. Real Options can be priced using the Black-Scholes model or the Binomial Option Pricing model. However, these methods have been developed primarily for the stock market and are based on hypotheses (like the “random walk” hypothesis for the price of the asset) that are not satisfied in the aerospace manufacturing world [119]. An alternative method, based on the principle of flexible strategy, phased investment and Monte Carlo simulation has been proposed by Miller and Clarke [156].

3.8 Cost and Operational Effectiveness Analysis

Worth models are very useful and straightforward for the cases in which there is a reference market for the service provided by the system, such as the commercial transport planes or satellite communication systems. They are in principle applicable also to situations in which there is no such reference market, but there are cases where it is preferable to avoid monetising value. Selva and Crawley [157] suggest to use a rule-based method to establish the most appropriate value model according to the system role. In particular, they distinguish the case in which the benefit can be measured as profit, performance or utility. In particular, monetising value implies the existence of a function that can map utility (or any other desirable output of a system) to money. In the absence of an objective criterion to establish this correspondence, the judgement of the value modeller and the stakeholders is used. This process can introduce inconsistencies or

be based on inexplicit or not well understood hypotheses. On the other hand, the resources needed to develop a system and deliver a service can often be readily measured in terms of money (materials, energy and labour have reference markets).

In the aerospace world, systems are often developed for a specific mission whose output cannot be readily translated into some form of monetary profit. Military and scientific systems are a good example of this. In these cases, the goodness of the system is measured in terms of performance (the probability of hitting a target for a missile system or the quantity of data acquired by a sensor, for example). In such cases, the use of an end-to-end simulation can provide an objective measure of the benefit of a system; the technical attributes of the system are not assessed individually but are considered as means to achieve the mission goal. For example, the impact of the range or endurance of a SAR vehicle can be assessed indirectly by the number of successful rescue operations that can be performed. Combining this with a cost model able to capture both acquisition and operational cost of the system, the application of Cost-Benefit (CB) analysis becomes possible. In particular, the decision maker can be presented with a bi-dimensional graph comparing different levels of service effectiveness with the associated costs. In a sense, the decision maker is allowed to postpone their judgement on the value of a particular performance until the final result of the analysis is available. In some cases, the mission benefit can be converted into monetary units to achieve a single cardinal number for the system value and compare the performance of systems designed to achieve more than one independent goal.

3.9 Some Applications of VDD to Aerospace Systems

In recent years, VDD has received an increasing attention from the aerospace community.

The Massachusetts Institute of Technology developed an approach to take into account market demand uncertainty in NPV-based design optimisation of commercial aircraft [122,158,159]. The approach is based on Real Options theory and addresses the uncertainty problem by recognising that strategic decisions occur at different times during the system development. Other studies have been proposed where the multi-attribute utility is used as system value metric [146] and the problem of changing scenarios over time is addressed [160–162]. In 2010, Ross *et al.* published a study in which different value models, including Multi-Attribute Utility Theory, NPV and Cost-Benefit analysis, where compared in the case study of a satellite system design [120]. The study demonstrated that different perceptions of value lead to different recommendations of “best system”.

Castagne *et al.*[163] used the SV theory to build a value model for the design and optimisation of an aircraft fuselage panel. The results showed how a value model can identify the best trade-off

between weight and manufacturing cost. In a similar study, Vučina *et al.* [164] used NPV-base value model as the objective function for an evolutionary algorithms optimisation of a sandwich panel. Cheung *et al.* [154] studied the application of VDD to an aero engine. Also, in this case, SV was used to model the system value. The authors also described a methodology to implement a VDD model and to decompose the system value model into component value models. Hollingsworth and Patel [165] used a value model based on SV for initial concept sizing of commercial transport airplanes, showing that the best design can deviate from the one obtained by minimising the gross weight. Keller and Collopy [166] proposed the application of VDD principles to the design of Space Launch Systems.

Maybe the most advanced project based on the VDD[10] philosophy is the System F6 program launched in 2008 by the U.S.A. Defense Advanced Research Project Agency (DARPA). The goal of the System F6 was to demonstrate the feasibility and benefits of a fractionated spacecraft system over a traditional monolithic satellite [121,167,168].

Four industrial teams – Lockheed Martin Company (LM), Northrop Grumman Corporation (NG), Orbital Sciences Corporation (OSC) and Boeing Company (BC) – participated to the DARPA F6 program, Part I. The system value model architectures developed under system F6 were explicitly mission agnostic, in the sense that they were designed to support different missions and payload scenarios. DARPA did not provide a guideline for the development of a system value model. The result was a significant disparity among the work performed by the industrial teams. Different approaches were proposed for the input and output structures, the LOD, the mission considerations, and so on. Interestingly, even the definition of the spacecraft value was different among the four VDD tools, with LM and OSC opting for NPV while NG chose utility versus life-cycle cost. BC chose to measure value as benefit versus cost but at the same time included a tool to convert a given benefit into monetary units. All the tools were using Monte Carlo simulation to account for the life-cycle uncertainties. The different tools were assessed through a comparative study involving the value analysis of different mission and spacecraft architecture scenarios. The tools did not show agreement in the identification of the best spacecraft system [169].

After initially awarding the contract to OSC, the project was eventually cancelled in 2013, due to its high cost, poor management choices and lack of interest from agency financing the project [170].

[10] In the publication related to the DARPA System F6 Program, the term “Value-Centric Design” is used instead of Value-Driven Design.

3.10 Summary

Value Driven Design is a Systems Engineering and design philosophy that revolves around the concept of value maximisation. VDD methods offer the possibility to perform trade-offs between incommensurable characteristics of a system, such as performance, cost, risk, schedule, and so on.

One of the main characteristics that differentiate VDD from traditional SE is the flexibility of requirements. In VDD, requirements are not simply allocated at the beginning of the system design phase but are treated as design variables for the exploration of the solution space.

Central to VDD is the creation of a system value model. This involves the identification of the stakeholders' needs and the definition of a value function that can be used to compare and rank design alternatives.

Virtually all design decisions occur under uncertainty. The expected utility theory provides a model to guide decision under uncertainty. When more than one attribute is important to the decision maker the creation of an overall utility function can be intractable. Some approaches exist to decompose the problem and analyse the single attributes individually. The multi-attribute utility analysis tackles the problem by defining individual utility functions for each of the attributes and then combining the utilities together. The drawback of this approach is that engineers and decision makers have to deal with a dimensionless measure which has little meaning to them and that prevents a meaningful quantitative analysis of the alternatives.

The Stanford school approach solves the problem by aggregating deterministic value functions over the attributes and then defining a utility function for the final deterministic value. If the attributes are carefully defined, worth can be used as value function. The worth model can be converted to the final value model by accounting for the risk tolerance of the decision maker. In engineering design, the decision maker can be assumed risk neutral in most cases. The main problem with worth models is the difficulty in assigning a monetary value to attributes or performance for which there is no reference market. However, the problem of mapping attributes to worth is in essence no different than mapping attributes to an arbitrary value scale.

For systems designed to accomplish a single specific mission, the analysis of Operational Effectiveness versus Cost provides a powerful tool to present decision-makers with the necessary information. The results of this Cost-Benefit analysis can be presented both in a graphical way or alternatively benefits can be converted into monetary unit to obtain a single number representing value. However, in this case, the model reduces to a worth model and it is subject to the same limitations.

There is no consensus on the best system value model for a particular application with different models leading to different system recommendations. Therefore, the choice of a system value model must be treated as a design decision, with the hypotheses, implications and limitations understood.

4 Rapid Manufacturing and Additive Manufacturing

4.1 Introduction

The terms Rapid Manufacturing, Rapid Prototyping, Additive Manufacturing and 3D printing are often used to refer to the same process: the computer controlled creation of 3D objects through layer deposition of material. The use of these terms as synonymous has historical reasons but it is sometimes confusing and it is here proposed to differentiate their meaning. The author will refer to Additive Manufacturing (AM) to indicate the class of manufacturing processes that generate the final object through the deposition, sintering, photocuring or gluing of the raw material. 3D printing will be used as a synonym of AM. Rapid Prototyping (RP) will be used to refer to the use of AM processes to create models of the final product. Rapid Manufacturing (RM) will be used to indicate any production process that is computer controlled and does not require a significant set-up time, thus including Computer Numerical Control (CNC) machining and AM.

4.2 What is Additive Manufacturing?

Additive Manufacturing is a class of manufacturing techniques that entail the creation of 3D objects through the computer-controlled deposition of material. All the AM techniques share the same workflow that can be summarized in the following steps:

1 - A model of the object is created using computer-aided design (CAD) software.
2 - The model is converted into a file format compatible with the 3D printer's software.
3 - The printer user decides the orientation in which the model will be built.
4 - The model is divided into thin "slices" (layers) parallel to the printer's building plane.
5 - The first layer of the object is built by merging together the particles of raw material.
6 - The next layer is built on top of the previous one until the object is complete.
7 - The object is removed from the printer and the support material (when present) is eliminated.

The production of parts through AM does not require any tooling and, once its CAD model is completed, very little pre-processing is necessary in order to obtain the final product. By building the object layer-by-layer, AM enables the production of objects of almost any shape. This allows the designer to focus on primary goals such as functionality, strength-to-weight ratio, and aesthetics of the object rather than on manufacturability.

Several AM techniques have been developed over the years. The main difference between the various AM processes involves the initial state and the method of bonding the raw material. Also, each technique can make use of a specific set of raw materials. The advantages and limitations of each technique have been described in a number of previous publications [171–176]. Figure 4-1 and Table 1 presents a classification of some of the main AM techniques.

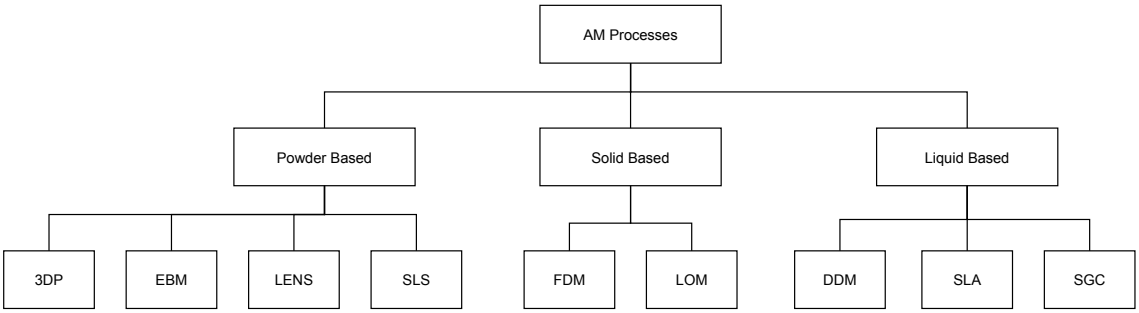

Figure 4-1 – Additive manufacturing processes classified by the form of the starting material.

AM Process	Technology	Bonding
3DP	Three-Dimensional printing	Gluing
DDM	Droplet Deposition Manufacturing	Deposition
EBM	Electron Beam Melting	Sintering
FDM	Fused-Deposition Modeling	Deposition
LENS	Laser Engineered Net Shaping	Deposition
LOM	Laminated-Object manufacturing	Gluing
SGC	Solid Ground Curing	Photocuring
SLA	Stereolithography	Photocuring
SLS	Selective Laser Sintering	Sintering

Table 1 – Additive manufacturing techniques and their bonding process.

4.3 Additive Manufacturing Compared to Injection Moulding and High Pressure Die Casting

If AM is compared to more traditional mass manufacturing techniques such as injection moulding (IM) for plastic objects and high pressure die casting (HPDC) for metals, a number of differences can be highlighted:

- **Tooling and manufacturing constraints**. Parts produced through injection moulding or die casting require tooling and hence have to be designed to account for the geometrical constraints that those imply. For example, the designer has to account for draft angles and anticipate the split line position. Re-entrant shapes and parts with not nearly constant wall thickness are very difficult to obtain. AM removes most manufacturing

constraints and allows the designer to focus on the production of parts optimised for functionality and assembly [8,177,178].

- **Time to beginning of manufacturing**. The design and manufacture of tooling required in IM and HPDC generally involve a lead time of several weeks. With AM it is possible to avoid this delay, hence the production of the parts can start immediately after the design is complete.
- **Production time per part**. Once the mould is ready, IM and HPDC can produce parts at a much higher rate: for a similar sized object, the production though AM can require a time four or five orders of magnitude higher. Rapid manufacturing of tooling [179–181] has the potential to deliver the advantages of both worlds, but the final part is subject to the same geometrical constraints as for conventional IM.
- **Cost drivers**. The main production cost associated with IM and HPDC is tooling cost. This implies that the cost-per-part is highly influenced by the number of parts produced (the larger the production run, the less expensive is the single part). Conversely, in AM the main cost is due to the 3D printing machine depreciation. Therefore, the cost-per-part depends on the time required to print each object rather than the number of objects produced. The most immediate consequence is that AM is cheaper than IM and HPDC when small quantities of the final parts are required. The size of the production batch at which the cost of AM and IM or HPDC is equal depends on the specific 3D printing techniques and the geometry and characteristics of the part. Previous studies have been focused on establishing the economic convenience of AM: some authors have looked at the cost of production of a part originally designed for IM [173,182] while other studies have focused on the opportunity of cost saving that arises from redesigning the part to fully exploit the advantages of AM [8,183]. The general trend indicates that the cost competitiveness of AM is increasing over time and the size of the production batch at which the production cost is equivalent for AM and IM or HPDC can be estimated in the range of tens of thousands units for plastic parts and tens or hundreds of units for metal parts.

4.4 Selective Laser Sintering of Polyamide

Of all the AM techniques, Selective Laser Sintering (SLS) is the one that provides the best compromise between cost and process accuracy. It is available in a variety of materials that include plastic, metal, and combinations of them. This work is focused on the applications of SLS of polyamide (commonly known as Nylon) 12, which is the most common material used in plastic AM. Nylon has good long term stability, chemical resistance, and decent mechanical properties.

These properties make it ideal for end-usable products as well as for prototypes. However, the mechanical properties of the sintered material can be worse than the equivalent injected moulded version and are a function of the sintering process [184]. Table 2 compares the mechanical properties of a typical SLS Nylon 12 version to Aluminium 7075, vastly used in the aerospace industry.

Mechanical Properties	**SLS Nylon 12**	**Al 7075**
Density	900 to 950 kg/m³	2810 kg/m³
Tensile Modulus	1.7 ± 0.15 GPa	71.7 GPa
Tensile Strength	45 ± 3 MPa	503 MPa
Elongation at Break	20 ± 5%	11%
Specific Tensile Modulus	1.77 x10^6 m^2/s^2	25.5 x10^6 m^2/s^2
Specific Tensile Strength	4.88 x10^4 m^2/s^2	17.9 x10^4 m^2/s^2

Table 2 – Mechanical properties of SLS Nylon 12 (source 3T-RPD [185]) and Aluminium 7075.

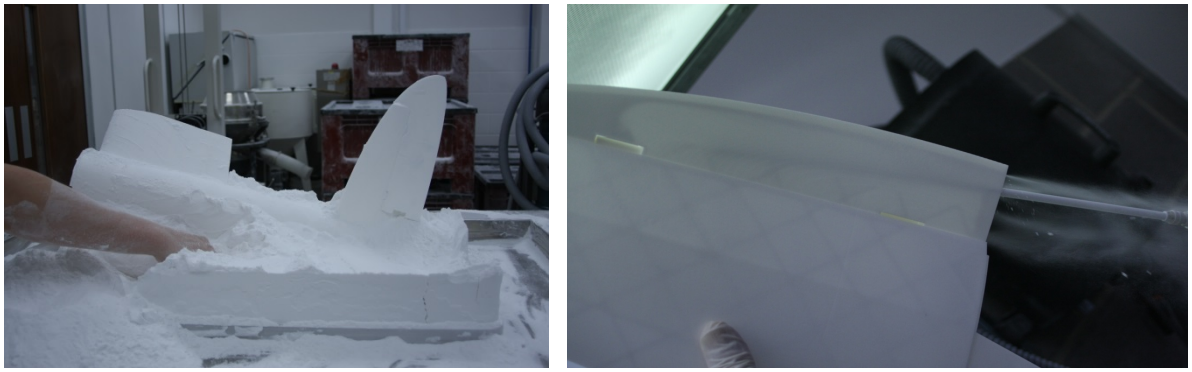

a. b.

Figure 4-2 – **a.** "Cake" of powder containing the final part. **b.** Technician removing powder from the final part [21]. Note the 3D printed hinge.

In SLS, the objects are obtained by sintering together the powder of raw material. In order to minimise heat-caused distortion and facilitate bonding, the printing chamber, and the powder are heated to a temperature a few degrees below the melting temperature of the polymer. Thin layers of powder (of the order of a tenth of a millimetre) are sequentially applied while a laser beam fuses together the Nylon particles at each layer. The powder that is not sintered offers support to the 3-dimensional object and can be recycled for the next build. In the end, the object is contained into a "cake" of loose powder (Figure 4-2a). A cooling period is generally required before extracting the object in order to avoid distortion due to high temperature gradients. Air blasts are used to remove the residual powder from the final part, as shown in Figure 4-2b.

SLS can produce objects of virtually any shape including integrated assemblies of multiple parts, like hinges (Figure 4-2b). However, there are some limitations that designers have to account for:

- **Maximum size for a single part**. The size of the printing chamber limits the maximum size of the object obtainable as a single part. Currently, the largest machines on the market have a building volume of the order of one-tenth of a cubic metre.
- **Cooling distortion**. As previously described, the SLS printing process is performed at a relatively high temperature and a cooling period is required before the object can be removed from the powder bed. During this phase, structures presenting a great inhomogeneity in terms of wall thicknesses can develop distortion due to different cooling rate. This can be mitigated by allowing a longer cooling time while in the power bed but it is best practice to account for these at the design stage and to avoid geometries prone to this problem whenever possible. Figure 4-3 shows an example of cooling distortion on an SLS fuel tank. The distortion was partly caused by the difference in stiffness between the rear spar supports and the trailing edge of the top surface. To mitigate this problem, an extra lateral stiffener has been introduced on the bottom side of the fuel tank top surface, as close as practical to the trailing edge (Figure 4-3c). The final 3D printed part is shown in Figure 4-3d.
- **Detail resolution**. The typical layer thickness for an industrial SLS printer is 0.1 mm and the resolution obtainable in the layer plane is generally comparable. However, the accuracy with which details like holes and slots can be reproduced depends on the orientation in which the part is built, and the ratio between the wall thickness and the details to be printed. Resources discussing detail resolution, tolerances, and design guidelines can be found in the literature or on companies website offering SLS services [186,187].
- **Surface finish**. The surface finish of SLS Nylon parts is rough and partly porous. This can be a disadvantage for outdoor application resulting in the absorption of water and dirt. A better finish can be obtained by applying surface treatments at the cost of additional time, cost and weight.
- **Enclosed cavities and powder removal**. One of the few geometrical limitations of Nylon SLS is the impossibility to print enclosed cavities: unless one is not concerned about trapping unused material, it is necessary to provide an escape path for the unsintered powder. Even when there are not enclosed cavities, the part geometry can be such that it is very difficult to remove the unused powder. It is best practice to account for the powder removal process during the design phase.

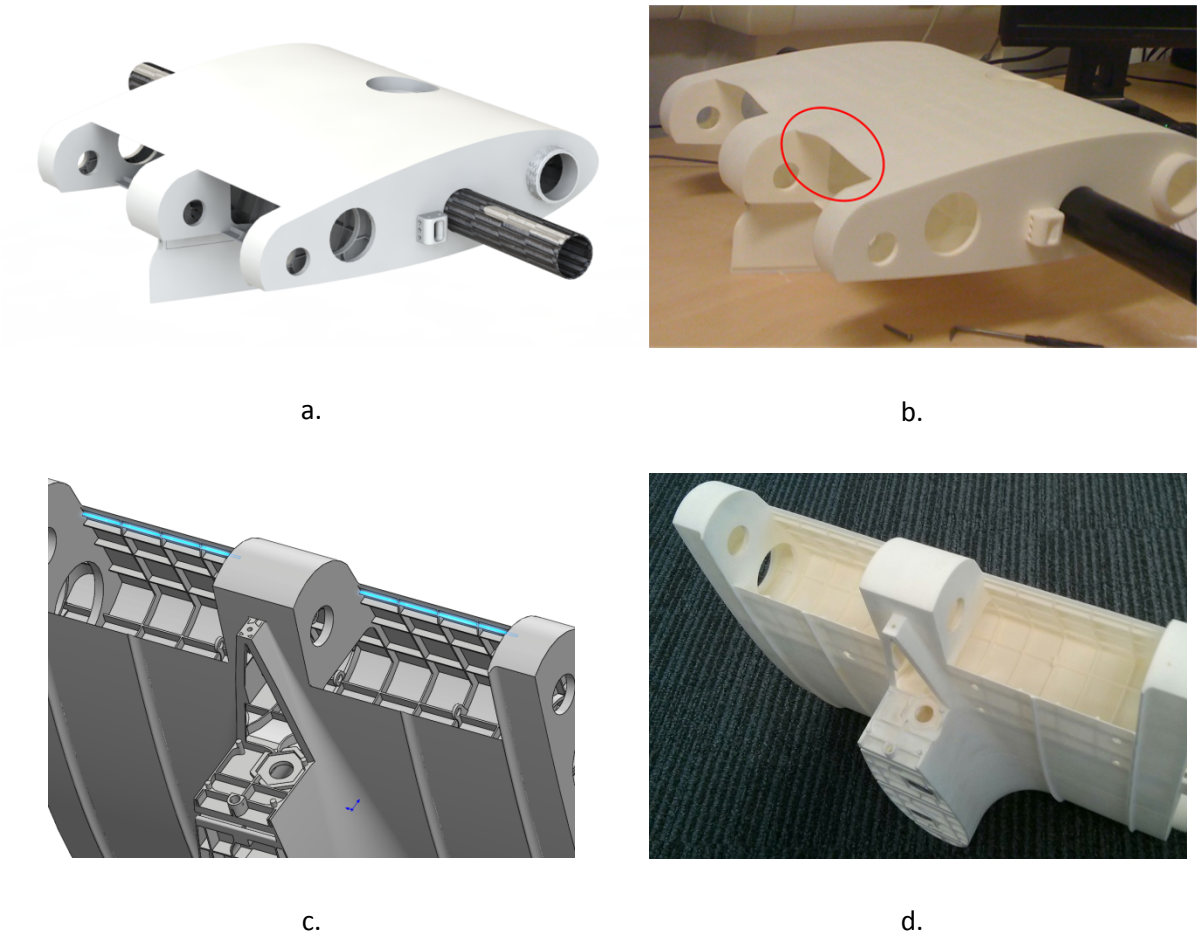

a. b.

c. d.

Figure 4-3 – **a.** CAD model of SPOTTER's fuel tank (Mk1). **b.** SLS fuel tank (Mk1) with trailing edge distortion (circled). **c.** CAD model of the fuel tank (Mk2). The extra stiffener introduced to prevent warping is highlighted. **d.** SLS fuel tank (Mk2) showing no trailing edge distortion.

4.5 Direct Metal Laser Sintering

SLS of alloys, also called Direct Metal Laser Sintering (DMSL), is analogues to SLS of plastic but with some key differences that limit its applicability for the production of low-cost UAV.

First of all, the commercial cost per unit volume of 3D printed metal parts is currently an order of magnitude higher than the one of Nylon[11].

Materials available include Aluminium, Stainless Steel, and Titanium alloys. Despite these materials have superior mechanical properties[12] if compared to Nylon 12, their density is also several times higher and the minimum wall thickness achievable with DMLS is in the same range

[11] For example, the price per volume of Aluminium AlSi10Mg is 25 times higher than the one of Nylon 12 (7.0 $/ cm^3 against 0.28 $/$cm^3$ – source Shapeways [286]) .
[12] The mechanical properties of DMLS materials are listed in Appendix A.

of the one achievable with plastic SLS[13]. Therefore, the use of AM of metal for parts that are not designed to absorb a significant mechanical stress can result in a mass penalty.

Moreover, metallic AM parts experience a complex thermal history during fabrication, typically involving high cooling rates, that introduces complexities to the analysis of their properties not typically found in conventional processes. Fabrication defects can vary within and between builds in one machine and across different machines and are influenced by the orientation and location of the parts within the building chamber [188]. This is particularly important for the fatigue properties of the material which are dominated by processing defects such as residual stress, micro-porosity, and surface finish [189]. No published work exists for low cycle fatigue, fatigue crack growth, fracture toughness, impact, creep, creep-fatigue, multiaxial testing, or environmental effects [188]. This limit the use of metal AM for structurally critical applications.

Finally, the parts fabricated with DMLS have to be anchored onto a platform in order to hold them in place and dissipate heat. Moreover, they require temporary support structures for the walls angled at more than 45° from the normal to the build platform. The removal of the support material (typically achieved through CNC machining) requires additional post-processing work and impacts the cost of and speed of production. Moreover, the designers have to ensure that the support material can be accessed by the cutting tools. Therefore, some of the geometries obtainable with plastic SLS (such as a hollow sphere with small holes for powder removal) cannot be obtained using DMLS. This limits the design advantage of metal AM over CNC subtractive manufacturing.

4.6 Fused Deposition Modelling

Fused Deposition Modelling (FDM) is also a very popular technology. In FDM, the layers are created by extruding melted plastic material through a nozzle. The plastic quickly solidifies once it has reached the printing area. Two different materials are used in this process: the building material (typically ABS plastic), and the support material, the sole function of which is to support the part's layers. At the end of the process, which typically lasts a few hours depending on the size and complexity of the part, the support material is removed and the part is ready to use. FDM can be cheaper than SLS but there are three main disadvantages:

- The range of shapes that is possible to create is limited by the vertical development of the part and by the possibility to access and remove the support material, particularly if light-weight structures are required.

[13] The recommended minimum wall thickness is 1.0-1.6 mm for metal and 0.8 – 1.2 mm for plastic [187].

- The mechanical properties of the parts are very anisotropic. The bond between subsequent layers is not as strong as the bond on the same layer plane. As a result, the maximum tensile stress achievable perpendicularly to the layers is sensibly lower than the one in the layers' plane.
- The layers thickness and detail resolution are generally worse than SLS.

For these reasons, the use of FDM is often limited to rapid prototyping or to manufacture of non-structural components.

4.7 Other Rapid Manufacturing Technologies for Low-Cost UAVs

There are other RM techniques that must be considered for the production of low-cost UAVs. Here the focus is on numerically controlled and tool-less manufacturing techniques because they share some of the advantages of additive manufacturing. They also have a very short set-up time and can lead to the final object with minimal post-processing.

4.7.1 CNC Foam Cutting

Solid plastic foam materials like Expanded PolyPropylene (EPP) and eXtruded PolyStyrene (XPS) are widely used on small UAV and aircraft models. They have a very low density and low cost and can be cut into shape using relatively low temperature hot-wire. EPP also exhibits excellent impact resistance but is less rigid than XPS. CNC foam plotters can cut foam blocks into the desired geometry. Although foam plotters with more axes are commercially available, the majority of the foam cutters have either 2 or 4 degrees of freedom. With a 4-axis foam cutter (Figure 4-4), it is possible to cut a high-performance wing featuring taper, sweep, dihedral and a linearly varying wing section. However, wing shapes featuring compound curves are not possible.

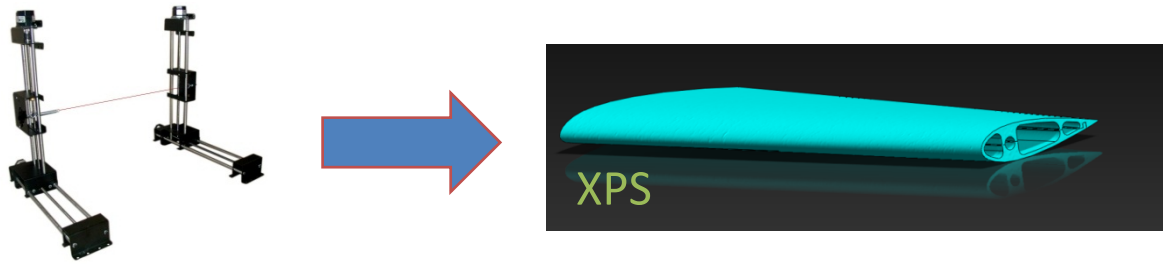

Figure 4-4 – Hot-wire foam cutting.

The process accuracy depends on the size of the block, the shape to be cut, the temperature and speed of the wire. These parameters influence the amount of foam that evaporates as a result of the passage of the hot wire (cut thickness). If the wire proceeds at different speed at the two ends of the block (which is what happens when a tapered wing chunk is cut) the thickness of the cut

will vary across the span, unless an appropriate correction is applied. For long foam blocks in the direction of the wire, there is typically a difference between the cut thickness at the borders of the block and at the inner part. This is due to different cooling of the wire. According to the author's experience, the best way to control this inaccuracy source is to limit the span of the blocks: it has been found that for blocks length up to about 50 cm the cut thickness can be controlled within a tolerance of $\pm$0.5 mm.

4.7.2 CNC Subtractive Manufacturing

Similarly to AM, subtractive CNC manufacturing, such as milling and turning, does not require tooling and the final object is obtained through the operation of a computer-controlled machine that follows a set of instructions generated from the CAD model. The main difference between AM and subtracting CNC machining is the lower level of complexity that can be achieved by the latter: subtractive CNC machining must remove material from a larger block and hence is limited in the amount of detail that can be obtained, particularly in parts that present cavities or geometries that are difficult to access by the cutting tools. Complex geometry can still be achieved by dividing the part into smaller ones and then merging them in a second stage. This, however, adds to the time and cost of producing the object. Moreover, subtracting machining is inherently a high-waste process while some of the AM techniques are virtually waste-free. On the other hand, subtractive CNC machining offers a superior range of materials and can produce parts with an extremely high tolerance control. It can also be less expensive than AM, depending on the part geometry.

4.8 Summary

This section has briefly presented some rapid manufacturing technologies employed in UAVs manufacturing and rapid prototyping. The focus has been on additive manufacturing and in particular on SLS of plastic materials. Some of the main differences with tool-based manufacturing have been highlighted and advantages and disadvantages of AM have been discussed.

5 The Impact of Additive Manufacturing on Aircraft Design

5.1 Introduction

This Chapter presents some of the advantages introduced by AM from the design and product development points of view. The practical implementation of the principles described is demonstrated through two case studies, describing the design and test of an entirely 3D printed aircraft and the iterative development of a multifunctional integral fuel tank.

The design of partly 3D printed aircraft is also discussed, focusing on the analysis of the system architecture as a mechanical network and introducing the principle of confined complexity as a method to exploit the strengths of AM and integral design while minimising their drawbacks.

5.2 Concept Generation

Design For Manufacturing (DFM) is the name used to indicate the engineering process that emphasises the importance of manufacturability from the early product design stage. Its aim is to reduce the manufacturing cost while not compromising quality and development cost. Typically, the development of a new part starts with the generation of high-level concepts. These concepts constitute a rough description of the product function and its physical shape. Soon after, the most promising ideas have to be evaluated in terms of manufacturability. An experienced designer will be able to assess the manufacturability and the production cost from the early design stages. This implies that manufacturing considerations influence the concepts generation, as well. Although this might be beneficial in filtering out ideas difficult to realise, at the same time, it can inhibit the exploration of the whole design space preventing the designer to “think out of the box” and generate novel and better solutions. Therefore, the first great advantage of AM manufacturing comes at the concept design stage, that is, the designer can freely generate ideas without worrying too much about the manufacturing process itself, knowing that almost any shape that can be modelled using CAD software can be built.

5.3 Process Flexibility and Product Delivery Time

The reduced development time and the process flexibility are probably the most valuable benefits that AM brings to the system development.

Parts produced with this technique are typically available within hours of the completion of the design. Therefore, the overall product delivery time can be greatly reduced if AM is coupled to rapid design techniques. Alternatively, a quick manufacturing process can benefit the design by providing more time to perform analysis and improve the system, ultimately improving the quality of the final product. Despite the fact that the production unit cost of AM parts can be higher than other processes for medium size batches, the rapidity with which new parts can be manufactured can generate savings in opportunity cost, for example helping companies to meet tough deadlines [190].

AM flexibility implies that the designers do not have to commit to a particular geometry. This has three benefits:

- **Adaptability**. The designers can make use of information that becomes available at a late stage and can easily adapt the system to unforeseen problems or opportunities.
- **Continuous development**. The products can undergo a continuous evolution with each subsequent release, incorporating improvements or modification as a result of the evaluation of the previous version. Although this is something that happens with every engineering system to a certain degree, AM makes it possible without major cost or time penalties. This is particularly useful for small UAVs that benefit from reduced certification requirements and are not subject to the same level of hardware version control of manned systems.
- **Customisability**. AM offers the possibility of easily creating different versions of the hardware to meet customer demand. The same UAV configuration can be scaled or morphed to adapt to different missions or to accommodate different payloads. Moreover, in the case of novel and bespoke systems, often customers do not fully understand their own requirements until after starting using the product. 3D printing makes possible to integrate customer feedback loop in the system design, and to do it independently for each individual customer.

Examples of rapid development, adaptability, customisability and continuous development are presented in the case studies of Section 5.7.

5.4 Manufacture of Geometrically Complex Structures

The geometrical complexity of a structure is a property that is difficult to define in absolute terms. It is linked to the ease with which a structure can be designed, manufactured or assembled. In the context of UAV design and referring to traditional manufacturing techniques, structures can be considered complex when they exhibit a large number of features, non-straight edges, non-

constant wall thicknesses, non-right angles, and are constituted of assemblies of many different parts[14]. Traditional DFM principles discourage the design of geometrically complex parts because they are expensive and difficult to manufacture. AM effectively removes these disadvantages.

a. b.

Figure 5-1 – **a.** Supermarine Spitfire elliptic wing [191]. **b.** Geodesic structure visible on a Vickers 290 Wellington [192].

Aviation history is full of examples of potentially effective design ideas that have been abandoned because of manufacturing complexity. One classical example is the elliptical wing used on the Second World War fighter the Supermarine Spitfire (Figure 1-1a). The elliptical planform guarantees the lowest induced drag for untwisted wings. This (small) aerodynamic advantage comes at the expense of manufacturing complexity[15]. The fact that the elliptic wing has practically disappeared from the aircraft world is indicative of relative importance between the aerodynamic gain and the manufacturing difficulties. However, the fate of the elliptical wing would have been different if its production time and cost were the same compared to straight or tapered wings. The best 3D printed wing is probably an elliptic wing because it can deliver the advantage of the reduced drag without manufacturing penalties.

[14] Manufacturing complexity of an object can be linked to the number of operations required to obtain the object and the difficulty of each individual operation [209].

[15] When the first batch of Spitfire entered production, the manufacture of the wing was still an unsolved problem for a long time, so that, in 1938, 346 bodies were produced but only 10 wings were available [287]. In general, the production of the Spitfires took twice as long compared to the German fighters.

Other examples of geometrically complex but efficient designs are lattice structures and grid reinforced structures (GRS)[16]. Both these kinds of structures present a lattice of stringers interconnected to create a grid. The difference between the two is that in lattice structures almost the entire load is carried by the lattice while the skin has mainly aerodynamic functions. In the case of GRS, the skin absorbs a significant load and the stringers are used mainly to stabilise the structure against buckling. Of course, intermediate structures are possible, as well. Most modern aircraft are built using a semi-monocoque approach in which the airframe skin absorbs the tensional load, while the stringers absorb the compression load. This also can be viewed as a GRS. However, even this approach requires the assembly of hundreds of frames and stringers. With 3D printing, the excellent structural properties of the GRS airframe can be achieved without the assembly complexity or the high waste of material of subtractive manufacturing.

Section 5.7 provides an example of a 3D printed airframe featuring both an elliptical wing design and a semi-monocoque fuselage with geodesic inspired reinforcement lattice.

5.5 Structural and Aerodynamic Optimisation

Because of the ease with which it can produce complex geometries, AM is particularly suitable for design optimisation. Optimisation requires fine tuning of a number of design parameters; if these parameters are carefully chosen, the higher their number the higher is the control on the final result. On the other hand, many design parameters correspond to a highly complex shape.

One example is the aerodynamic optimisation of an airframe. A straight, un-tapered and untwisted wing can be described using only three parameters (i.e. wing span, area, and airfoil). By adding more parameters (such as taper ratio, twist, sweep, crank, different airfoils, and so on), a better aerodynamic shape can be obtained at the expense of increased manufacturing complexity. Potentially, the entire airframe surface could be discretised into thousands or more points and

[16] An example of lattice structure is the geodesic airframe that was successfully used on the Vickers Wellington Second World War bomber (Figure 5-1b) and abandoned because of its high cost and building time. The isogrid is a GRS obtained by machining a solid block of material to obtain a panel reinforced by a triangular lattice of stringers. The structure obtained is isotropic within the plane of the structure and result in an excellent stiffness-to-weight ratio. Despite the relatively high cost and high waste of material associated with its manufacturing process, the isogrid is still in use for some space applications [288].
The anisogrid structure is constituted by a lattice of helical, circular and axial stringers that are generally used to stiffen aircraft's or rockets' fuselages [289,290].The main attraction of anisogrid structures is the fact that they can be optimised such that the main load on the stiffeners is axial, in which case composite materials with unidirectional fibres can be exploited to their full potential. The anisogrid structure can be designed with or without a load bearing skin. Many studies have focused on the unstressed skin configuration [291–293] because it is easier to manufacture, but comparative studies indicate that a load bearing skin can lead to a more efficient design [294].

each could be controlled independently in order to achieve the best overall efficiency. Ignoring for the moment the computational problem related to the exploration of such a large design space, it is clear that the optimisation result benefits from a manufacturing process that imposes no constraints on the geometrical shape of the final product. An example of aerodynamic optimisation of a 3D printed airframe is given in Section B.2.1.

The same is true in the case of structural optimisation. In aerospace applications, the need for strong and lightweight parts is paramount and structural optimisation can reduce the total mass of an aircraft by optimising the airframe for the particular load scenario. As in the previous case, the control over a large number of parameters can lead to better performance at the cost of structural complexity. For example, the thickness of each individual stringer can be controlled independently, or the thickness of the airframe skin can be continuously changed to match the more or less stressed areas. Topology optimisation [193–195] makes it possible to determine an optimal structural layout independently of the designer. The optimal structure is the result of the exploration of a vast design space and often is a rather complex geometry. It is common practice to post-process the result of the optimisation and generate a CAD model of the structure that resembles the optimisation result but is not an exact copy. This is done to overcome the shortcomings of the topology optimisation: firstly, the result is generally obtained using a coarse model of the structure due to the constraint on computational resources; secondly, the approximations introduced in the definition of the load cases can result in structurally weak points. It is left to the experience of the engineers to translate the result of the topology optimisation into a well-engineered structure. This, however, can be a very long and demanding task. Perhaps in the future, with access to increased computational power, it will be possible to obtain the ready-to-manufacture model of the structure directly from the output of the topology optimisation. However, it is likely that the definition of a fully comprehensive model of the load cases and design constraints will remain the main obstacle to the full automation of the structural design and the experience of the engineers will still be required to judge and complement the result of the optimisation.

Periodic structures – like the ones described in Section 5.4 – can represent a good compromise between conventional discreet structures and fully free-form structures. Periodic structures can be controlled and optimised using a relatively small number of parameters but have a great potential in terms of weight saving and customisation.

5.6 Non-Monetary Cost of Geometrical Complexity

There is a final consideration to be made regarding geometrical complexity: the more complex a structure is, the more difficult and time-consuming it becomes to design it. This is due to a number of factors: first of all, it is more difficult for the designer to predict the behaviour of a complex structure under a certain load. Even using computer simulation, complex structures can require a significantly higher pre-processing time.

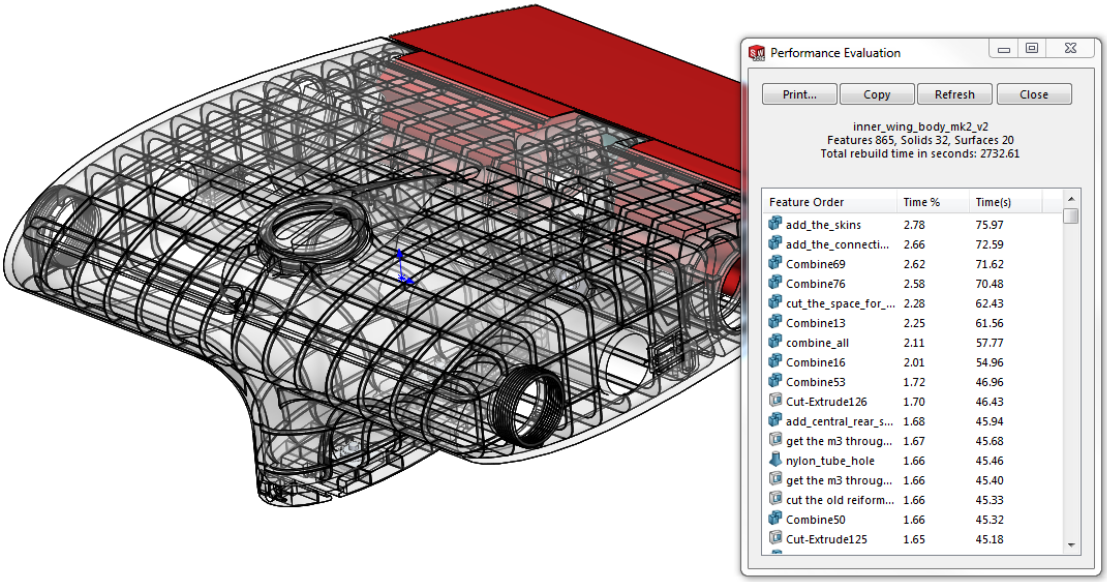

Figure 5-2 – The rebuilt time of a CAD model is the time required for updating the geometry if a design parameter is changed. In very complex models, software latency can become a major obstacle to productivity. Above: this model of an integral fuel tank requires a rebuild time of almost one hour.

Furthermore, as the number of details of a particular part increases, the chance of making design mistakes rises. On one hand, this problem is mitigated by the fact that AM does not have fixed costs, and hence the mistakes can be corrected relatively cheaply. On the other hand, mistakes on large 3D printed parts can still be quite costly.

Finally, the performance of CAD software becomes worse as the number of features added to the part increases, to the point that the software latency can become a major obstacle to the productivity of the designer. In his 6 years of experience as a UAV designer, the author had the opportunity to design a number of very complex SLS parts, mostly using SolidWorks [196], one of the most popular CAD software for mechanical design. In order to harvest the benefit of rapid manufacturing, a great effort was put into creating parametric models that were robust with respect to design changes. In this way, concept sizing and detail design could proceed in parallel.

On some occasions, the CAD design of these parts was computationally demanding so that the performance of the CAD workstation decreased to the point that the modification of the geometry would take an impractically long time (Figure 5-2). There are some workarounds that can be exploited to continue the development the part. One possible approach is to save the part and import the body in a new file. This has the effect of losing the feature history, effectively freezing the design up to that point. Of course, the disadvantage is that the model is no longer parametric. There are CAD software tools that use a history-free geometry modelling approach [197] and can handle complexity slightly better from the computational point of view. However, the author's opinion is that the lack of a feature history tree is a large disadvantage precisely in the case of complex parts: history-based CAD software force the designer to think rationally about the relationship between the various parts of the structure and enable the creation of parametric models where a large number of features can be controlled by a relatively low number of variables.

5.7 Case Studies

5.7.1 Southampton University Laser Sintered Aircraft – The World's First Entirely 3D Printed Airframe

The author designed the world's first entirely 3D printed aircraft. The aircraft, named SULSA (Southampton University Laser Sintered Aircraft), was developed in 2011 and was conceived as a technology demonstrator. The task was to demonstrate that it is possible to conceive, design, build and test fly a small 3D printed unmanned aircraft in the span of just two weeks. The main operational advantage of all-printed airframes is linked to the portability of SLS production systems. Provided one has access to a printer and the material powder, an airframe can be built anywhere and at any time. Possible applications include the use of UAV for scientific research in very remote areas like the Antarctic [198], or even for space exploration missions [199].

Another benefit of the experiment was to assess the suitability of SLS Nylon as a main structural material for small scale UAVs. The design requirements included a tool-less and fastener-free assembly and the use of a minimum number of individual parts. The avionics and servo actuators were COTS components simply clipped into purposely designed slots on the airframe. The aircraft had to be catapult launched, limiting the total mass of the aircraft to a maximum of 4 kg. The aircraft layout is shown in Figure 5-3. It features elliptic wing and tail planform and a pusher V-tail arrangement.

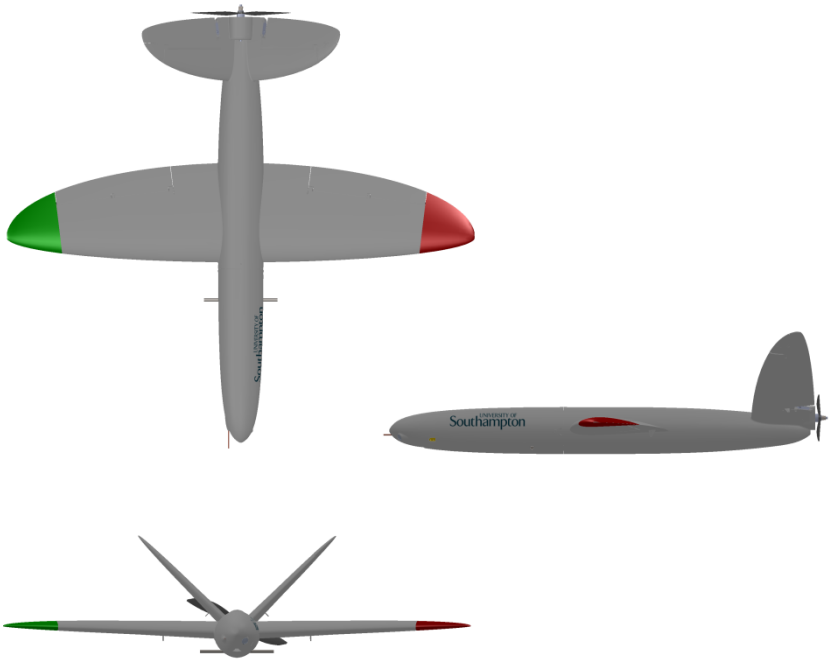

Figure 5-3 – SULSA three-view drawings.

The wing planform was selected to minimise the induced drag. A linear washout of 2 degrees was introduced to prevent tip stall at high angles of attack. The wing and tail geometry were designed by controlling the sections through a numerical program linked to the CAD software (Figure 5-4). In this way, it was also possible to control the wing skin thickness along the wing span. This parametric model enabled the designers to initiate the detail design phase while the airframe sizing was still not completed. This resulted in a very fast development time: it took only 10 days and two engineers to complete the manufacture-ready model.

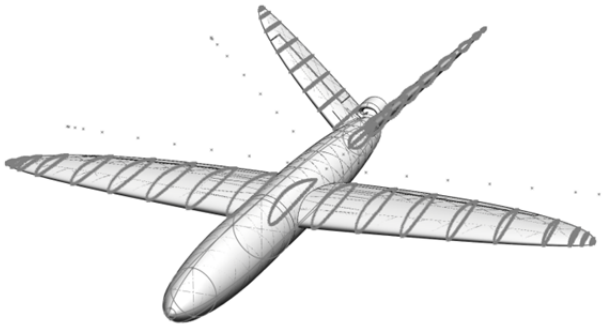

Figure 5-4 – Parametric model of SULSA. The wing sections were generated and updated using a purposely designed computer code and imported into the CAD software.

The choice of the configuration was driven by the requirements of catapult launched take-off and belly landing. The airframe was sized using the design environment discussed in Chapter 1. Due to the short time constraints, only a low-LOD aerodynamic analysis was performed using vortex

lattice code and empirical methods. The dimensions and flight performance of SULSA are summarised in Table 3.

Specifications	Length	1.1	m
	Wing span	1.2	m
	Wing area	0.24	m^2
	Aspect ratio	6	-
	Take-off mass	3.2	kg
	Motor	Axi 2820/12, 990 rpm/V	-
	Battery	4S LiPo	-
	Propeller	11x5.5	inch
Performance	Maximum Speed	40	m/s
	Cruise Speed	25	m/s
	Stall Speed	12	m/s
	Endurance	30	min

Table 3 – Specification and performance of SULSA.

The fuselage was designed using a Geodesic-Inspired Semi-Monocoque (GISM) structure (Figure 5-5). It was obtained by adding the fuselage skin to a reinforcement grid constituted by stringers laid in crossing helix patterns. The control of the local properties of such a structure can be obtained by acting on one of the following degrees of freedom: the skin thickness, the number of stringers, the pitch angle of the stringers, their thickness and height. In this case, the latter option was selected because it was the easiest to implement in the CAD model: the height of the stringers was adjusted locally to account for high loading areas (e.g. the wing attachment points) while the stringers and wall thicknesses were kept at the constant minimum thickness of 1 mm. In the regions of stress concentration, such as the launch bar attachment point, further structural reinforcements were added and superimposed to the GISM. The result was a very rigid and lightweight structure that demonstrated excellent performance during normal operation.

Given the scale of this UAV system, one of the most demanding load cases was the transport and handling of the airframe. The helix reinforcement provided very good strength and rigidity against handling pressure load. Finally, the reinforcement lattice provided a way to transfer local loads to the main structure: local features such as the servo holding structures could be easily connected to the lattice avoiding excessive stress concentration on the skin.

There are two main drawbacks with this structure. The first is related to the SLS production process: the structure created by the reinforcement lattice, the external skin, and all the added features, create an intricate “trap” for the Nylon powder. Despite all the designers’ effort resulting in a structure with no enclosed cavities and with clear paths for the air blasts used to

remove the powder, it was often not possible to completely de-powder the airframe. Small pockets of compacted powder accumulated at the joints of the lattice and, depending on the angle at which they could be accessed by the air blasts, they proved to be very difficult to dislodge. It was not infrequent, after an SLS GISM fuselage had received a small impact, to discover a thin layer of powder particles on the internal components, even after a few years of operations. Typically, the mass of powder that remains trapped in the structure after the factory de-powdering process is negligible; however it can constitute a problem if the airframe carries sensors or other equipment that can be damaged by the presence of powder.

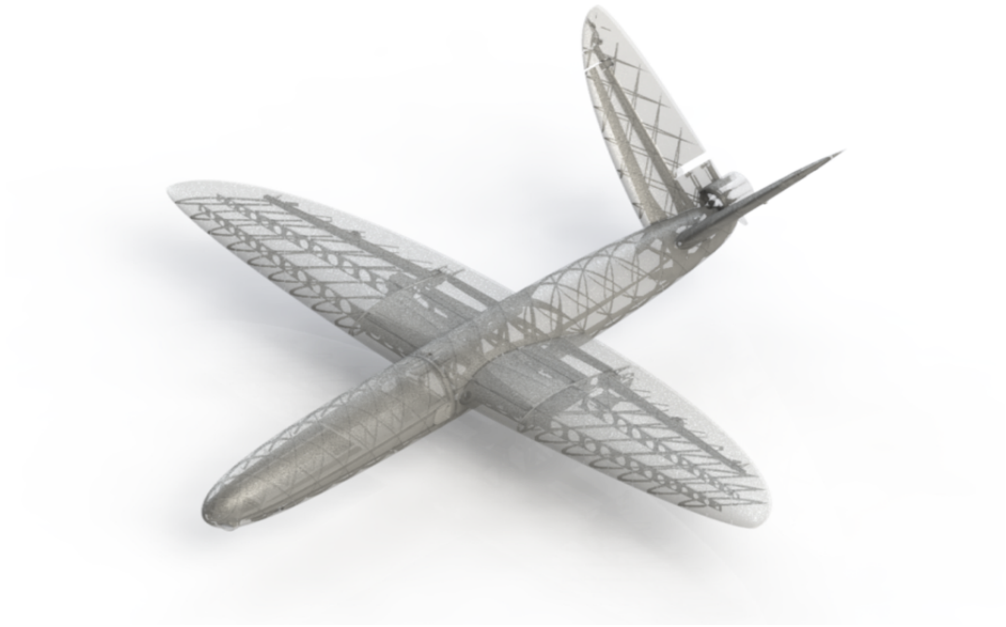

Figure 5-5 – Transparent view of SULSA showing the geodesic-inspired airframe.

The second drawback of the GISM is the lack of simple models that can predict the behaviour of the structure and its failure modes. Although this can be overcome by dedicated finite element analysis (FEA), it is still a limitation in the context of rapid design and manufacturing. Moreover, the FEA of such multi-features structures can be difficult and time-consuming. One of the main challenges is the separation of structural components from functional ones: when dealing with integral structures, simplified models of the structure cannot be easily created without losing information on regions of possible stress concentration.

Another interesting design feature that was tested on SULSA was the possibility to simultaneously print the aerodynamic surfaces and their control flaps as unique hinged parts: this concept was applied to both wings and tailplanes, hence removing the need for assembly (Figure 4-2). However, the correct dimensioning of the hinges' interfaces was a non-trivial task, requiring a few test parts to be built. The main problem with this kind of coupling is that, on one hand, there is

the risk of bonding the hinge pin and sleeve together if there is not enough clearance between the two. On the other hand, there is the risk of ending up with a coupling that is too loose, losing accuracy in the control of the ailerons or ruddevators. In the end, the compromise solution was sufficient to achieve a safe control of the airframe, but still not entirely satisfactory. Another difficulty was introduced by the difference in the outcome of the SLS process with respect to the orientation of the parts in the printer. This meant that the test parts printed to establish the best hinge interference for the wing (that had to be printed horizontally) could not be used for the tailplanes (that had to be printed diagonally and at an angle of 88 degrees of each other).

Figure 5-6 – SULSA mark 2 taking off from HMS Mersey.

The original SULSA airframe was first flown in July 2011. Four years after the initial tests, the airframe was used to test the feasibility of the operation of 3D printed low-cost reconnaissance aircraft for the Royal Navy (Project Triangle). The Project Triangle aspiration was the development of a system that could potentially be manufactured on board or alternatively, could be collected from harbours anywhere in the world.

In order to continue the Project Triangle tests, the mark 2 version of the airframe was developed in 2015. The main difference with the mark 1 version was the redesign of the nose cone and avionics tray to allow for the integration of a High Definition (HD) camera system. The wing and tail hinges were not printed in place this time: a 6 mm carbon fibre composite rod was used to provide the pivot, while the hinge sleeves were integrated into the wings and ailerons that were printed as separate parts. This small diversion from the fully 3D printed airframe concept enabled a significantly superior control over the performance of the hinged parts. Other differences

included a modification in the servos clamping system and the introduction of a bolt retaining the nose and real fuselage together.

The Project Triangle demonstration flight was successfully performed in July 2015, when SULSA mark 2 took off from HMS Mersey and landed on a nearby beach after a short autonomous mission (Figure 5-6). In March 2016, SULSA was used in a series of trials in the Antarctic where the vehicle was used to assist the navigation through icy waters of the Royal Navy's ice patrol ship HMS Protector (Project Albatross [198]). A further research program aiming at optimising SULSA for maritime application is currently under evaluation.

Figure 5-7 – SULSA mark 2 during the Project Triangle trials in the Antartic.

The lessons learned from the SULSA project can be summarised as follows:

- SLS Nylon is a suitable material for structural components for small UAV. It combines decent mechanical properties with a relatively low density. Despite having a specific tensile modulus one order of magnitude lower than high-grade aluminium (Table 2) and a poor impact resistance if compared to EPP foam, it offers good performance for this application. It could be argued that, given the superior material performance, an equivalent airframe made out of aluminium would be much lighter than the Nylon version. However, given the relatively low-stress levels on the airframe skin, almost all the SLS parts produced by the University of Southampton for use on UAVs have used the minimum practical wall thickness of 1mm. Ignoring the effect of stringers, an aluminium structure with equivalent tensile strength would have a wall thickness of only 0.09 mm (which is about the same thickness of a soda can). The weight equivalent part made out of

aluminium would have to have a wall thickness of circa 0.3 mm (but with superior strength and stiffness). However, part of the weight advantage of the aluminium would be reduced by the necessity to bond stringers to the skin (as opposed to the case of the SLS fuselage, where the stringers are an integral part of the structure). Further weight savings are achieved by exploiting the geometrical flexibility of the SLS process and integrating functional elements into structural components (for example, the servo actuators holders are fully integrated into the GISM structure). Moreover, the production of the SLS airframe requires significantly fewer man-hours and enables the exploitation of more advanced geometries. Finally, SLS enables the engineers to have an excellent control of local structural properties.

- Despite its attractive properties, an entirely printed airframe is probably not the best option from the design and production point of view. The introduction of some small "compromise" solutions, such as the presence of a limited number of fasteners or the use of carbon fibre rods for the hinge axis, can bring great benefit to the robustness of the design and final product while retaining most of the advantages of a fully 3D printed airframe. Although there might be applications in which even small items like fasteners are hard to obtain, at present, the technology to print electronics components, batteries and servos is not mature. Therefore, the user that would want to print the airframe in very remote locations will still need to carry a stock of components, of which fastener could just be a small portion.
- The time span that occurs between the initial concept development and the first flight of a small, entirely 3D printed aircraft can be extremely short. The initial phase of the design process can be automated through the use of parametric models and integrated analysis software. However, the most time-consuming activity remains the creation of the detailed CAD model. Extra care is required to ensure that the parts can be de-powdered effectively.
- There are very few data on the long-term stability of SLS Polyamide 12 parts. Schmid *et al.* [200] published a study on the effect of automotive fluids on SLS materials. Other works have looked at the effect of Nylon powder degradation on the mechanical properties of the final SLS part [201]. Exposure to UV radiation causes a change in the properties of all plastics. Despite having a better weathering resistance compared to other kinds of Nylon [202–204], Polyamide 12 mechanical properties are still affected by exposure to sun radiation, oxygen and air moisture. Generally, parts' surfaces are affected first and hence it can be inferred that the performance degradation is more severe for thin and porous parts like the one used on 3D printed airframes. The first SULSA airframe was exposed to a moderate level of sun radiation for 4 years (mostly indirect sunlight). The material

colour shifted toward a yellower hue, but no test was performed to assess the change in its mechanical properties. No structural problems were detected during normal operation, and the airframe performed well under high-stress conditions such as the catapult launch and the belly landing. However, a dedicated study is recommended for long term use of structural SLS Nylon components.

5.7.2 Integral Fuel Tank

The inner wing of SPOTTER is a very good example of how SLS manufacturing can be used to obtain high-performance multifunctional structures at a competitive price. SPOTTER is a research UAV designed by the author and currently undergoing iterative development at the University of Southampton[17].

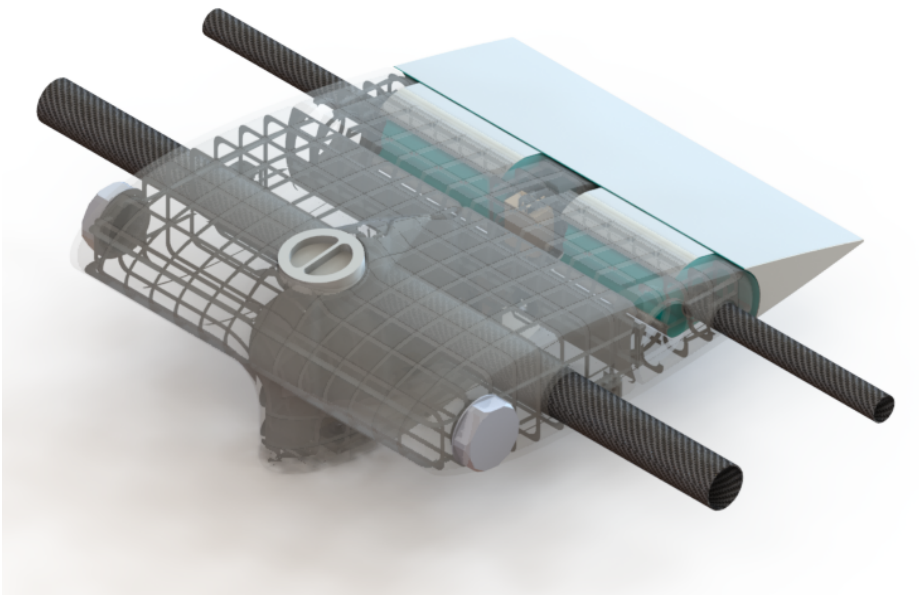

Figure 5-8 – SPOTTER's inner wing assembly. The integral fuel tank is shown in transparency.

Figure 5-8 shows the inner wing assembly: a large 3D printed fuel tank is connected to the inner flap and the wing spars. The fuel tank is shown in Figure 5-9. It exploits an integral design approach in order to decrease the total cost of the airframe by reducing the number of parts and hence reduce the assembly cost. The part serves many functions: it contains the fuel and contributes to the lift generation of the aircraft. It provides the hinge line for the central flap and the mounting point for its servo actuator. Moreover, the fuel tank provides the structural

[17] More details on SPOTTER are given in Appendix A.

connection between the aircraft main spars and the payload[18]. The interface used for the installation of the payload and its retaining mechanism are features of the same integral structure. Furthermore, the part is used to connect the two fuselages (on each side of the fuel tank) and provide the cable routing between them and to the payload pod. Finally, the mounting points for the fuel level sensors are part of the structure, as well. The part has many other built-in connection interfaces, these allowing technicians to quickly couple the tank with other mechanical parts and avionics sub-systems.

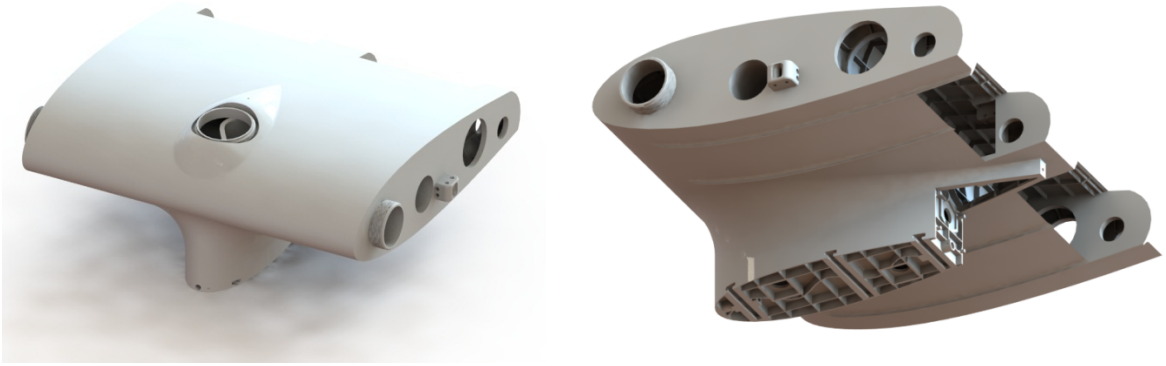

a. b.

Figure 5-9 – Two views of SPOTTER's integral fuel tank.

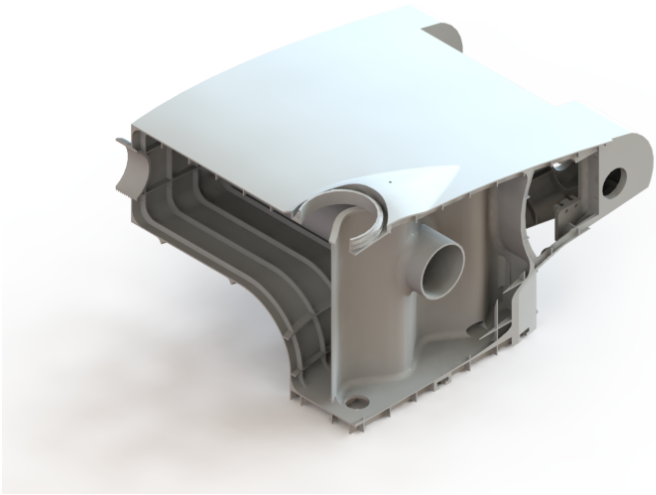

Figure 5-10 – Fuel tank section view.

The fuel tank is a GRS with a wall thickness of 1.2 mm. Local structural reinforcements are used to avoid stress concentration in highly loaded areas or where opening or irregularities are present.

[18] SPOTTER is designed to have a modular payload stored in a custom designed pod. The pod is connected to the aircraft by sliding the payload interface into the T-slots visible at the bottom of the fuel tank in Figure 5-9b.

The total mass of the structure is 980 g and it can contain up to 8 litres of fuel. The structure was designed to carry a 5 kg payload and absorb loads of more than 7g with no damage.

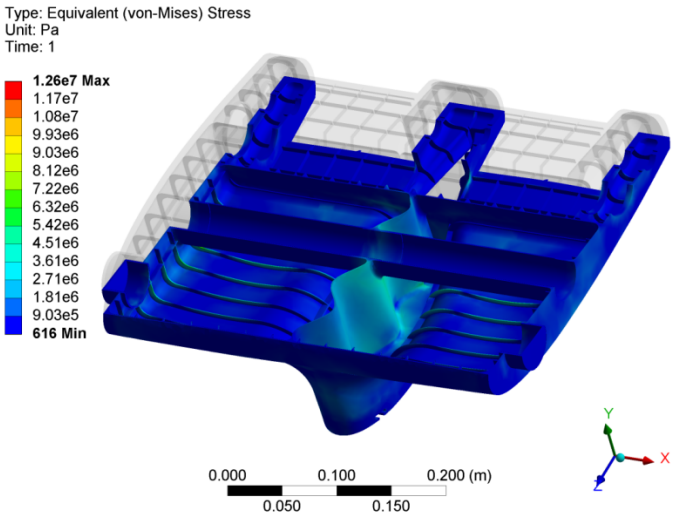

a.

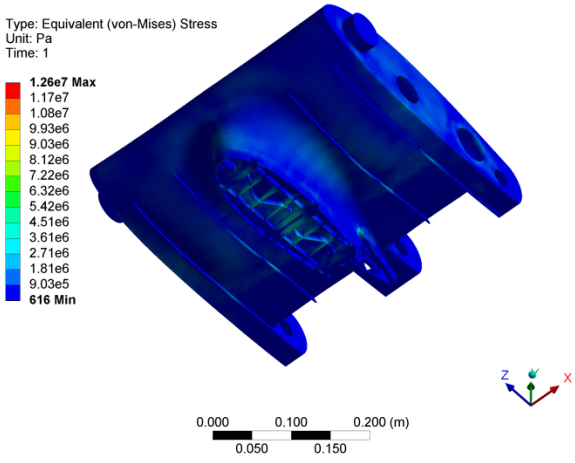

b.

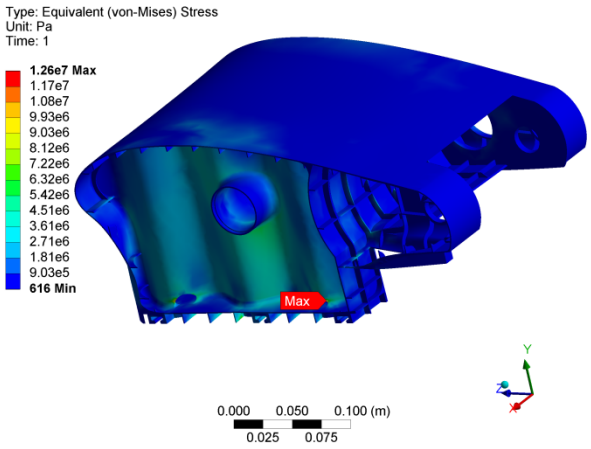

c.

Figure 5-11 – Calculation of the stress and deformation on the fuel tank due to a 7g inertial load. Note: deformation is magnified by a factor of 10.

The tank presents a T-shaped cross section that ensures that the fuel pick-ups are submerged until the tank is completely empty. This geometrical feature is also exploited to provide a payload mounting pylon that has an airfoil shaped section in order to reduce the aerodynamic drag. The lower surface of the tank presents external stringers in order to avoid trapping fuel in the reinforcement framework, as visible in Figure 5-9 and Figure 5-10. A longitudinal baffle prevents the fuel from sloshing from one half of the tank to the other. The corrugated wall of the baffle provides the necessary stiffness while avoiding the complication of the framework. Small holes at

the bottom of the baffle connect the two sides of the tank so that the aircraft can exploit the whole fuel load even when one engine is inoperative. A tank liner is used to seal the tank and avoid absorption of fuel by the porous 3D printed Nylon.

One of the greatest advantages of 3D printing is the fact that the designers don't have to commit to early decisions and can continue to improve and adapt the design at no extra cost. The integral fuel tank has undergone a series of design iterations as a result of knowledge gathered through further analysis, more demanding requirements and changes in the other airplane's systems. Two examples are described below.

Figure 5-11 shows the result of stress computation performed on one of the design iterations of the part using a finite element model[19]. In this test, the model was constrained with frictionless supports at the spar locations (approximated as infinitely rigid) and the inertial load of fuel and payload during an asymmetric 7g landing was applied. The pictures show how both the framework and the baffle contribute to transfer the load to the carbon fibre spars, leaving the skin with a relatively low stress level. The safety factor is higher than 5 in all the points apart from a small region of stress concentration around the baffle's holes where it is 3.5 (Figure 5-11c). Thanks to the flexibility of AM, it was possible to reinforce this region in the next iteration of the part (Figure 5-12).

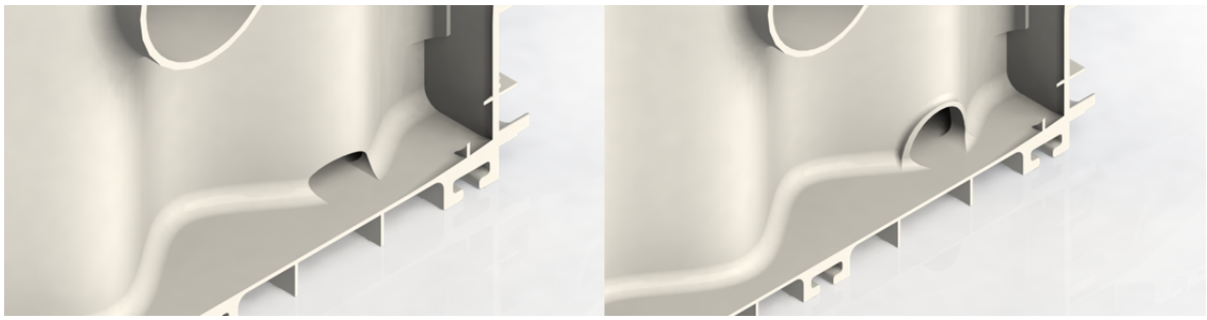

a. b.

Figure 5-12 – Example of design iteration: the hole in the baffle of the fuel tank was reinforced to avoid stress concentration.

Another example of a design iteration is shown in Figure 5-13. In the first version of the integral fuel tank, the tank's cap was designed such that, when screwed in, it was completely flush with

[19] The tank is supported at the interface with the carbon fibre spars though frictionless supports. The load is applied at the wall of the fuel tank and at the payload interface. The load applied simulates the inertial load of the fuel and payload mass during an acceleration of 7g whose direction is (x,y,z)=(-0.17,0.97,0.17).

the upper surface of the wing. To achieve this, the cap thread was penetrating into the tank volume (Figure 5-13a). This was causing two problems: firstly, it was not possible to exploit the volume of the tank above the level of the cap's interface; secondly, the female thread was on the inside of the tank and hence it was difficult to protect it from the tank liner during the sealing operation, which in turn caused a poor coupling between the two threaded parts. The second iteration, shown in Figure 5-13b, solved both issues. The fuel cap interface was slightly raised over the wing's top surface and protected with an aerodynamic fairing, and the thread coupling was reversed (male thread on the tank and female on the cap). In this new version, the fuel capacity was increased by 30%.

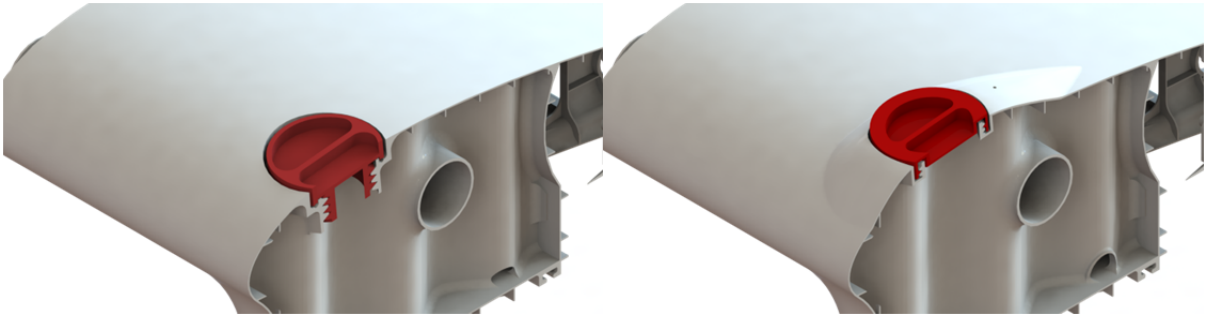

a. b.

Figure 5-13 – Example of design iteration: the redesign of the tank's cap increased the fuel volume by 30%.

This example has shown how designers can exploit the geometrical flexibility of SLS manufacturing in order to produce complex parts where structural and functional features are merged into a single part produced in a single operation. This has the potential of reducing the mass (thanks to the efficient integration of structural and non-structural elements) and the assembly cost of the airframe. Moreover, the absence of fixed costs encourages the continuous development of the part.

5.8 Design for 3D Printing: the Implication on the System Architecture

Despite all the advantages of SLS manufacturing described in the previous paragraphs, 3D printed parts are still a suboptimal solution in many applications. For example, highly stressed parts with a simple geometry – such as the wing spars of medium sized UAVs – can exploit the vastly superior mechanical properties of composite materials while relying on COTS standardised units (such as

carbon fibre reinforced plastic tubes). Other parts with no major structural requirements but with a relatively simple shape can make use of the inexpensive and low-density CNC cut foam[20].

The use of 3D printed components becomes advantageous when the designer is able to generate mass and/or cost savings by integrating many features and functions into the same structure. However, integral designs can be disadvantageous with respects to other aspects system life-cycle, as explained in the following paragraph.

Partly 3D printed airframes can be designed to fully exploit the strengths of AM while avoiding its weaknesses. In order to do that, the designers need to think in terms of system architecture and recognise where the use of 3D printed components can result in a superior solution.

5.8.1 System Architecture and Product Modularity

A product can be defined as the collection of its parts and subassemblies of parts. These are the *physical elements* of the system and are sometimes referred as *chunks*. Alternatively, the product can be modelled as the collection of operations and transformations by which the overall performance is obtained. These are defined *functional elements*. The *system architecture* is the scheme by which the functional element of a product are arranged into physical elements and by which these elements interact [205].

The system architecture has a strong impact on the product performance, development time, flexibility, manufacturability and cost [206]. Its main characteristic is the degree of modularity: in strictly modular systems, each physical element implements completely one functional element and the boundaries and interactions between the chunks are clearly defined. At the other end of the spectrum, in strictly integral systems, the chunks contribute to the implementation of many functional elements and the interactions between the physical elements are diffuse and difficult to isolate and define; boundaries between physical elements are sometimes non-existent. In reality, most products have a hybrid architecture, in which some functional elements are implemented modularly and some require an integral approach.

The other important characteristic of the system architecture is the coupling between the physical elements. There is high coupling between two chunks when the modification of the first requires the modification of the second to ensure the functionality of the product. Integral system architectures are generally associated with high coupling between chunks. Modular architectures

[20] Given the same volume, the cost of a 3D printed Nylon component is two orders of magnitude higher than the cost of a CNC cut Styrofoam equivalent. The density of nylon is 25 times higher than the Styrofoam one.

can present decoupled or coupled physical elements, depending on the type of interface between the chunks and the way their interaction is defined.

Highly modular and decoupled designs (also known as *segregated architectures* [207]) present a number of advantages:

- **Problem decomposition**. The modular system architecture enables the designers to perform efficient problem decomposition: by mapping each functional element to a single physical element it is possible to design, test and build each subsystem independently. By specifying clear interfaces and interactions between physical components it is possible to clearly define subsystems' requirements and therefore facilitate the interaction with design teams, subcontractors, and the supply chain. Once the interfaces have been defined, there is relatively little need for a central coordination of the product development. Physical elements can be developed at different times and the design of each chunk is less complex and hence the probability of satisfying its functional requirements is higher.
- **Product variety and design adaptability**. In a segregated architecture, chunks can be modified and upgraded independently. This makes product changes less costly and enables the firm to produce a high variety of products based on the same design[21]. Segregated product architectures also increase the design adaptability [207]. Adaptable design allows the design firm to save money, time and design cost by reusing the plan (design) or even parts in an assembly or adapting with minimal change the existing ones to meet needs of different customers. This is a great advantage in the context of rapid development of UAVs.
- **Efficiency**. In a modular design, it is possible to use standard components which usually provide a higher performance for a given cost. Each functional element can be assigned to a team of specialists resulting in better performance.
- **Maintenance, wear and reuse**. Maintenance can be performed independently on different chunks. The product life is not limited by the subsystem with the shortest life, if

[21] Variety can be defined as the property of a product that can be produced in several different versions to adapt to customer demand within a particular time period [205]. The flexibility of a manufacturing process is the ability to produce a high variety of products without major cost and time increases. Injection moulding is a relatively inflexible process: a change in the product geometry requires the manufacture of new tooling and substantial investments. AM and CNC subtractive manufacturing are very flexible processes. Products designed with a modular architecture can have a high variety even if the manufacturing process used is inflexible: the variety can be achieved through the use of multiple versions of the same modules or through a platform system to which optional modules can be added. Products designed with an integral architecture can only achieve a high variety by exploiting a flexible manufacturing process.

this can be replaced easily. Physical elements can be reused for different projects that require similar functional elements.

On the other end, integral architectures, while requiring a higher effort in coordination and management of the design tasks, can generate superior results when the performance of the product is highly dependent on global attributes[22]. Moreover, integral architectures are in general cheaper to manufacture and less time consuming to assemble because of the reduced number of parts obtained by integrating components. The reduced number of interfaces often results in lower weight and space savings [208].

5.8.2 The Principle of Confined Complexity

A careful design of the system architecture can allow partly 3D printed aircraft to exploit the benefits of integral components while achieving a high degree of physical modularity. This can be achieved by exploiting the principle of *confined complexity*. Confined complexity can be described as the concentration of the majority of the features that introduce elements of complexity into a few physical elements of the structure. This applies to both geometrical complexity (such as in the case of structures difficult to manufacture) and functional complexity (such as in the case of parts requiring multiple interfaces with subsystems). Confining complexity to 3D printed parts enables the designer to simplify the geometry and function of the other chunks. As a consequence, the simplified chunks can be produced at a lower cost and can exploit high-performance materials not available for AM.

[22] The product performance can be defined as the collection of measurable attributes that constitute the ability of the system to perform a set of tasks measured against a set of benchmarks. In the case of an aircraft, examples of product attributes are the maximum range, the payload capacity, the aerodynamic efficiency, the maximum structural load factor, etc. More in depth, one can distinguish between *local attributes* and *global attributes*. Local attributes are the characteristics of the system that depend on the properties of a single or a few chunks. The maximum coefficient of lift of a wing and the maximum thrust produced by an engine are examples of local attributes. Global attributes are those that arise from the interaction of many chunks, like the total mass of an airplane or its aerodynamic efficiency. In some cases, global attributes of a system are simply the sum of the attributes of its parts. For example the mass of a product is the sum of the mass of the subsystems. However, in many practical situations the global attributes of the overall product is dependent on the complex interaction of its components. For example, the aerodynamic drag of the overall aircraft is often higher than the sum of the drag of its parts in isolation due to the interference drag. In some cases, synergies between the product parts and can lead to the improvement of the product performance. In general, local attributes can be optimized using modular system architecture while the optimization of global attributes requires a holistic approach and hence it is best suited to the integral approach. For example, function sharing between two or more physical elements can lead to a reduction of mass and production cost. In a similar way physical nesting of product parts can result in a more efficient use of space at the cost of interface coupling. These approaches require integral system architectures.

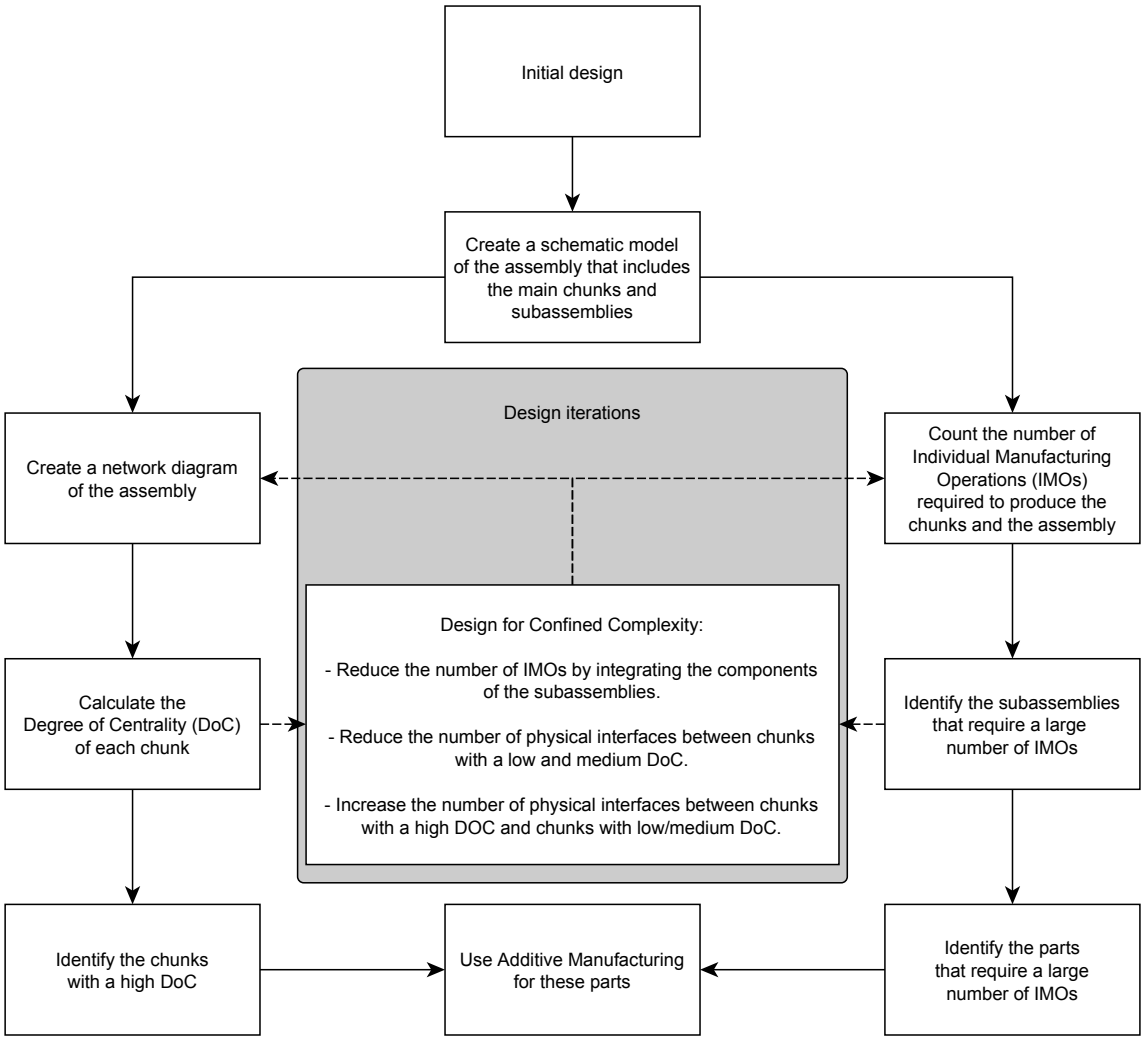

Figure 5-14 – Design for confined complexity method.

Product complexity in the context of manufacturing and assembly has been the object of several studies in the past years [209]. For example, methods inspired by the Axiomatic Design theory [71] identify complexity with the Information Content defined in the second axiom (and therefore with the opposite of the probability of meeting the functional requirement). ElMaraghy and Urbanic [210] proposed a measure of complexity inspired by Shannon entropy[23] [211] where quantity, diversity, and difficulty of production of the features of a part are combined to achieve an overall product complexity index. These methods are useful to quantify complexity in a systematic way but require substantial work from the designer in the encoding and interpretation of the relative difficulty of manufacturing operations (for example, the same manufacturing operation, such as creating a hole in a component, can be more or less problematic depending on

[23] Shannon entropy H is a measure of the average content of information of a given event (in this context it is interpreted as the information content required for the description of a particular part). It is given by the formula $H = -\sum_i p_i \log_q p_i$; where p_i is the probability that the given event is in the status i and q is an arbitrary number larger than 1.

the particular manufacturing technology used, the geometry of the part, the tolerance and surface finish required, and so on). According to the author's experience, in the context of rapid development and one-of-a-kind products, methods that require a considerable upfront time investment are often neglected by designers who rather rely on their instinct and judgment. A simpler way to quantify the manufacturing complexity of a product is the count of the Individual Manufacturing Operations (IMOs), i.e. the individual operations required to produce it. This method is far from being perfect and neglects many important aspects (for example how difficult, expensive or time consuming is any individual operation) but it is very simple to implement and, if complemented by the designer's judgment, can be very effective. In this interpretation, confining complexity to 3D printed parts is equivalent to reducing the overall complexity of the product because these components can be produced in a single operation.

Another method to identify the parts that are good candidates for the use of AM is to refer to the network theory and the concept of Degree of Centrality (DoC) [212]. In particular, the physical system architecture can be thought as a network, where the nodes are the chunks and the edges are the physical interfaces between them[24]. The DoC is a measure of the number of connections of each node[25]. In order to calculate it, a network of n elements can be represented in a matrix form by assigning a numerical index $i \in [1, n]$ to each node. The Adjacency Matrix A contains information about the presence of an edge between each pair of nodes. For example, A_{ij} – i.e. the element of A corresponding to the nodes i and j – is defined as follows

$$A_{ij} = \begin{cases} 1 & \text{If there is an edge between nodes } i \text{ and } j. \\ 0 & \text{Otherwise.} \end{cases} \quad \text{5-1}$$

C_i, the DoC of the node i, can be calculated using Equation 5-2.

$$C_i = \sum_{j=1}^{n} A_{ij} \quad \text{5-2}$$

Most assemblies present a small number of chunks with a high DoC (sometimes called hubs) and a small number of low DoC nodes [213]. Hubs provide the alignment foundation for multiple parts and are likely to be geometrically complex and therefore there is the opportunity to generate cost

[24] The representation of assemblies as networks has been studied in the context of assembly sequences by De Fazio and Whitney [295], Mathew and Rao [296], Demoly *et al.* [297].

[25] A slightly different approach accounting for the strength of the connection has been proposed by Li and Xie [298]. The authors developed an algorithm to automatically partition large assemblies and identify subassemblies with the aim of favouring the reuse of modules in the context of one-of-a-kind products.

and mass savings by adopting integral design and AM[26]. Moreover, the physical elements with a high DoC are the ones that are most likely affected by the changes of the other parts of the assembly. Thus, they would greatly benefit from the flexibility of AM.

The network analysis of the assemblies and the analysis of the IMOs can also be used as tools to improve the design of the subsystems by identifying opportunities for confining complexity. Figure 5-14 shows a graphic representation of the process: the model of the assembly and its main components is used to calculate the DoC of each chunk and the number of IMOs required for each part and subassembly. Using an iterative approach, the designer modifies the physical architecture of the product in order to reduce the overall number of IMOs, for example integrating adjacent parts. Concurrently, physical interfaces are re-designed in order to reduce the coupling between parts with a low and medium DoC while increasing the connection between parts with a high and low DoC[27]. This process results in the creation of a small number of complex chunks that provide the common platform for the interfaces with a large number of simpler components. According to the principle of confined complexity, these complex chunks – identified by both a high DoC and a large number of IMOs – are the parts to be produced by AM. Note that using AM for these parts reduces their number of IMOs to one.

An example of the application of the principle of confined complexity is presented in the following paragraph.

5.8.3 Case study: The Network Analysis of the Empennage Assembly of two UAVs

Figure 5-15 and Figure 5-16 show the exploded view of the tail assemblies of DECODE-2[28] and SPOTTER, respectively. For simplicity, the pictures only show the components to the left of the longitudinal plane of symmetry. The corresponding network diagrams are shown in Figure 5-17 where the nodes corresponding to 3D printed components have been highlighted in red.

DECODE-2 features an inverted V-tail configuration where pitch and lateral control are achieved using four ruddervators (two of which are displayed in Figure 5-15 with the number 2 and 9).

[26] Parts with simple geometries can have a high DoC because of their physical size. For example, long structural chunks interface with many components (such as the wing spars interfacing with the wing skin and ribs). However, if the geometry of the part and of the relative interfaces is simple, the use of 3D printing is not recommended.

[27] Note that the absolute value of the DoC is influenced by the size of the assembly: in large assemblies constituted of many parts, the average DoC of each chunk is higher than in in small assemblies with fewer parts. In this discussion, “low”, “medium”, and “high” DoC are used in a relative sense, i.e. a chunk with a high DoC is a chunk that has a high DoC relatively to the average DoC of the other parts in the same assembly.

[28] DECODE-2 is a rapid-manufactured UAV presented in Section B.2.

SPOTTER uses a more conventional empennage with individual rudders and elevators (chunks 13, 4 and 15 displayed in Figure 5-16). The V-tail configuration requires fewer parts but introduces a coupling between the requirements of pitch and lateral control. This results in a less robust design as the two functional requirements cannot be controlled independently and therefore the correction of any design error is problematic[29].

In both cases, the designer used AM for relatively complex-shaped parts acting as interfaces between simpler chunks and between COTS components. For example, chunk 1 in both assemblies is used to create the interface between the CNC cut foam wing skins and the carbon fibre spar, and to provide the hinge point for the control surfaces. The carbon fibre spars are constrained to the 3D printed parts by using a printed clamping mechanism (Figure 5-19). By doing so, the designer transferred all the complexity of the interface to the 3D printed body and minimised the manufacturing operations.

However, the analysis of the networks in Figure 5-17 and the graph of the DoC in Figure 5-18 highlight that confined complexity was achieved more effectively in the case of the empennage of SPOTTER. In particular, the node corresponding to the part 12 of Figure 5-16 has a very high number of connections: the part is used to provide the interface between the horizontal tail plane and the vertical one; it contains the clamping mechanism for the connection to the tail boom and hosts the mounting points for the servo actuators of both the vertical and horizontal control surfaces. More importantly, by concentrating the interfaces into part 12, the designer created a decoupled architecture: any modifications to the servo actuators (corresponding to the nodes 9, 10 and 14) or the tail boom (node 6) can be absorbed by modifying part 12 only. Similarly, the modification of the vertical tailplane subassembly (corresponding to the cluster of nodes in the bottom left part of Figure 5-17b) or the horizontal tailplane subassembly (corresponding to the cluster of nodes in the top right part of Figure 5-17b) only affects node 12. Note that the horizontal tail plane could be further divided into two subassemblies, one on to the left and the other to the right of part 12, that would also be decoupled if it wasn't for the spars (node 2 and 3) penetrating the whole length of the horizontal plane.

[29] The V-tail violates the Independence Axiom of the Axiomatic Design Theory [72].

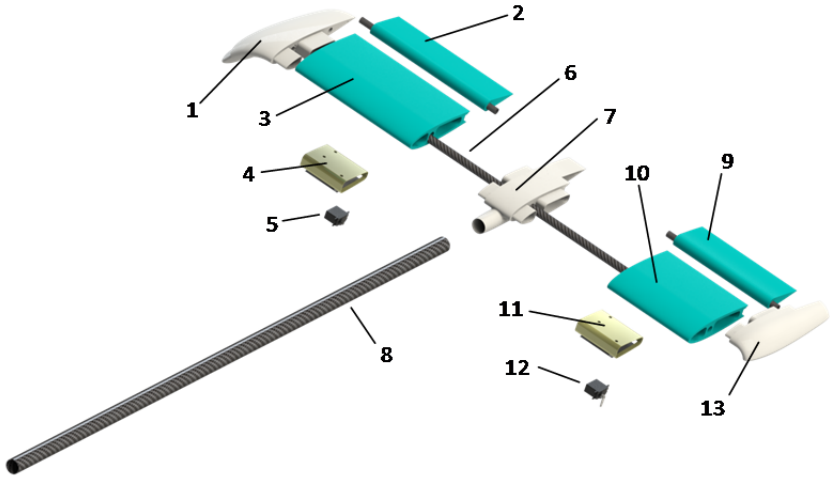

Figure 5-15 – Exploded view of the tail assembly of DECODE-2. Only chunks to the left of the plane of symmetry are shown.

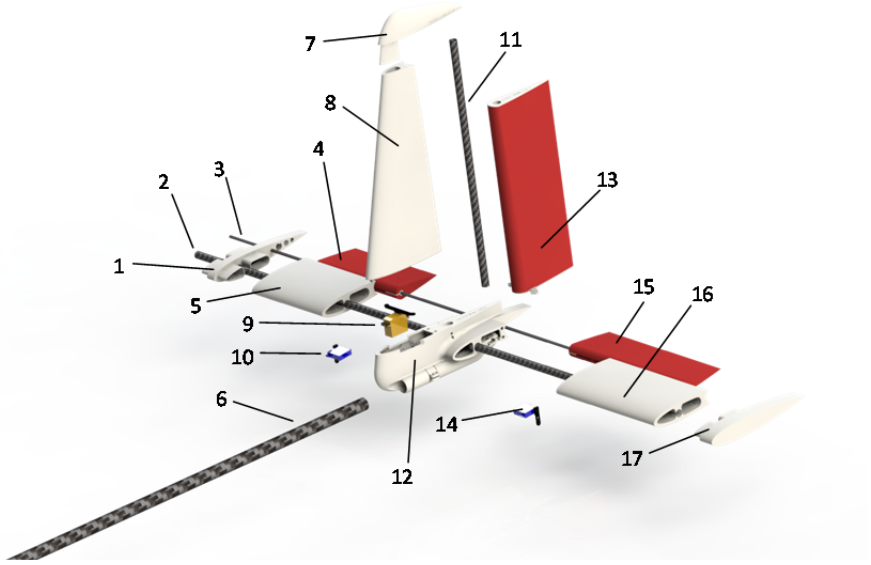

Figure 5-16 – Exploded view of the tail assembly of SPOTTER. Only chunks to the left of the plane of symmetry are shown.

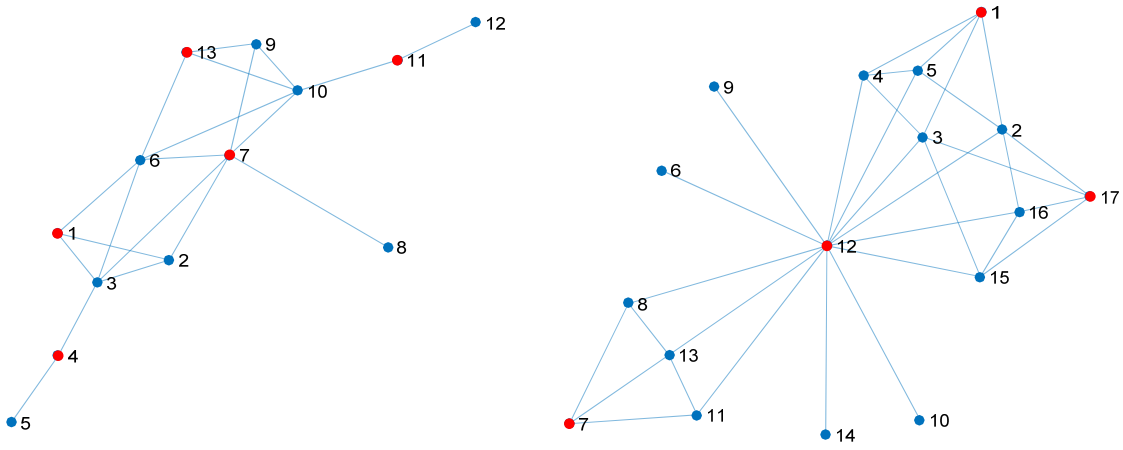

a. b.

Figure 5-17 – Network representation of the tail assemblies of: **a.** DECODE-2 and **b.** SPOTTER. The nodes in red correspond to the parts produced using AM.

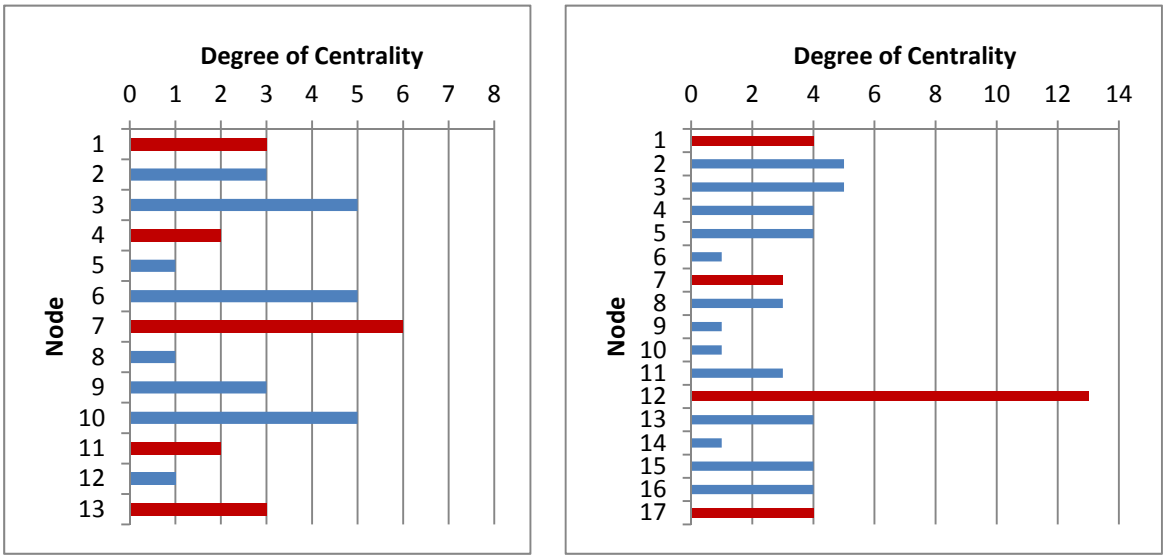

a. b.

Figure 5-18 – Degree of Centrality of the physical elements of the empennage assemblies of: **a.** DECODE-2 and **b.** SPOTTER. The bars in red corresponds to the parts produced using AM.

Part 7 of the tail assembly of DECODE-2 (shown in Figure 5-15) is used with a similar function to part 12 for the SPOTTER's tail assembly. However, in this case, the designer missed the opportunity to integrate the servo mounts into the same 3D printed object. As a consequence, the design of parts 3 and 10 includes an extra interface (with part 4 and 11, respectively) that increases the manufacturing complexity. Figure 5-20 shows a detail of a part of the DECODE-2's tail assembly: the servo actuator is connected to the CNC cut XPS wing skin though a 3D printed interface bonded to the skin. The interface between parts 3 and 4 required the cut of a slot into

the lower surface of part 3. This operation cannot be performed by the CNC plotter but requires the manual intervention of a technician. Overall the production of this part requires four IMOs:

1- Cut of part 3 from the Styrofoam block.
2- AM of part 4.
3- Cut of the slot in part 3.
4- Bonding of part 3 and 4.

Further four manufacturing operations are required for the production of the symmetric assembly constituted by parts 10 and 11.

Figure 5-19 – Detail of the 3D printed spar clamping mechanisms.

The servo mounts could have been integrated into part 7 (as shown in the preliminary sketch in Figure 5-21) at the cost of a small mass increment but with no increase in the parts cost[30]. On the other hand, parts 4 and 11 would have been eliminated, corresponding to a net saving of 54 g and £14[31] plus the cost of the additional manufacture and assembly operations. The number of IMOs would have been reduced to three (the cut of parts 3 and 10 and the 3D printing of part 7) from the original nine.

The network representation of the re-designed tail assembly is shown in Figure 5-22. The network structure and the graph of the DoC show that the modification resulted in a less coupled design where part 7 became the main hub of the assembly.

[30] The overall mass increase of the re-designed part 7 is 4.0 g, which correspond to 2.5% of the total mass of the part. This was achieved by integrating the servo mounting feature to the pre-existent structural features. The cost of the 3D printed components is estimated using the bounding box volume of the parts. The overall volume of the part is kept constant and therefore the cost of the part is unchanged.
[31] The cost of the SLS Nylon parts per unit of the bounding box volume used in this calculation is 0.025 £/cm^3.

a. b.

Figure 5-20 – Part of the subassembly of the tailplane of DECODE-2. **a.** Collapsed view **b.** Exploded view.

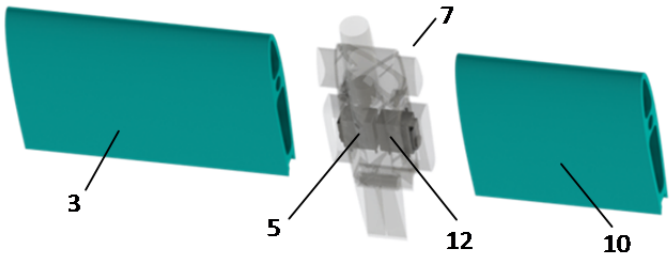

Figure 5-21 – Part of the re-designed tail assembly. The servo mounts have been integrated into part 7, thus reducing the mass and cost of the subsystem.

5.9 Summary

This Chapter has discussed the impact of AM on the aircraft design with a focus on small UAVs. The main advantages connected to the flexibility and rapidity of AM have been discussed, starting from the impact on the concept design and examining the implication on the product adaptability and the continuous system development. The opportunities for the exploitation of complex geometries for the creation of optimal structural and aerodynamic designs have been briefly presented together with the implication of geometrical complexity on the detail design phase.

These considerations have been drawn from the author's experience gained during the development of aircraft made largely through SLS manufacturing. A number of case studies have been presented, including the design and test of the first entirely 3D printed aircraft. These examples have proven that AM can be considered as a viable technology for the production of small unmanned aircraft. The short development time and the possibility of iteratively improving the design proved to be two of the most valuable advantages introduced by AM.

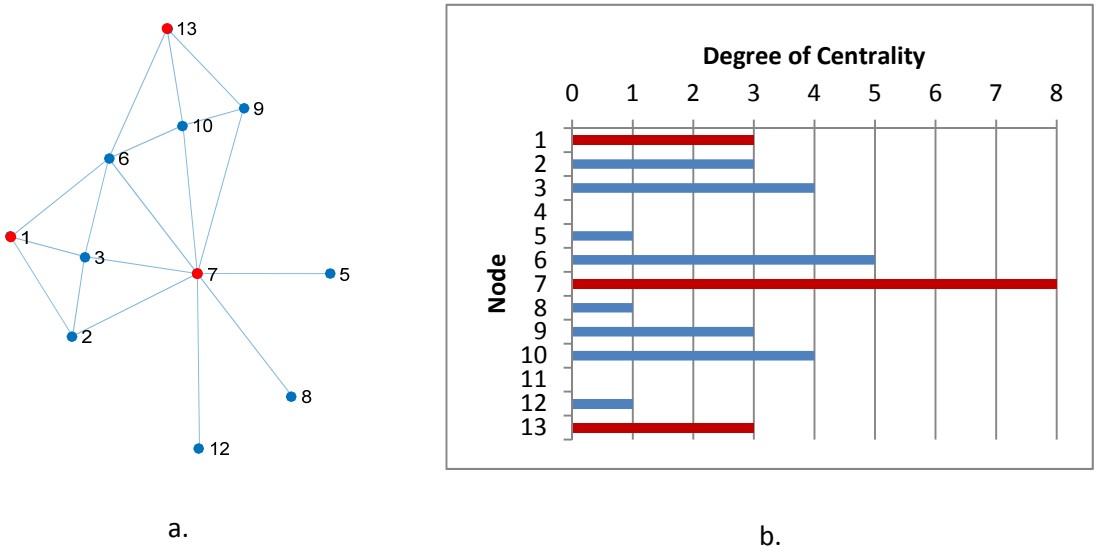

a. b.

Figure 5-22 – **a.** Network representation of the redesigned tail assemblies of DECODE-2. **b.** Degree of Centrality of the physical elements of the empennage assemblies of DECODE-2.

Finally, the principle of confined complexity was introduced to guide designers during architectural designs decisions that involve the use of 3D printed components. If the physical system architecture is though as a network, confined complexity is achieved by creating a few nodes with a high DoC and multiple nodes with a low DoC. In this way, the complex features can be condensed into a few 3D printed hubs while the geometry of the non-printed parts can be simplified, hence reducing the overall manufacturing and assembly cost, reducing the overall mass, and allowing the exploitation of mechanically superior materials.

6 Development of a Value-Driven Design Environment for Unnamed Aerial Vehicles

6.1 Introduction

Aircraft design software can provide an efficient way to manage the design variables and coordinate the various disciplinary problems. However, the analysis capability of most commercially available tools is limited to the assessment of the system technical performance (in terms of aerodynamics, structural efficiency, range and sometimes unit cost). The analysis of the system's operative capability and life-cycle cost is more rarely accounted for in the preliminary design decision. As a result, designers have a clear understanding of the relationship between design parameters and technical performance (such as the impact of the wing span on the aircraft mass or its range); but they do not have the tools to assess the impact of design variables on life-cycle performance (like the relationship between wing span and the cost of maintenance operations during the lifespan of the aircraft).

The DECODE (Decision Environment for COmplex DEsigns) research project at the University of Southampton investigated the decision-making process in the context of system design. As a member of DECODE, the author developed a UAV design environment able to improve decision making and support the VDD, named DUADE (DECODE Unmanned Aircraft Design Environment). In order to achieve this, DUADE was based on the integration of multidisciplinary analysis tools that included a system operational simulation as well as more traditional design disciplines such as aerodynamics and structures. DUADE was designed to support an agile spiral development approach where RM and system testing was treated as part of the design loop.

This chapter describes the DUADE workflow and its modules. In addition, it introduces the main case study investigated in this work: the design of a UAV to support maritime SAR operations. Although the DUADE workflow can be applied to a variety of design problems, the use of a specific case study provides the opportunity to explore and understand the challenges of the practical implementation of the VDD philosophy.

6.2 Design Principles

The design of DUADE was based on the following considerations.

- Requirement identification and allocation is one of the most critical activities of the system design. In most cases it is performed in the early stage of a project and therefore its outcome is negatively affected by the scarcity of information and poor understanding of the problem. The new design environment should allow the decision makers to explore the requirement space and assess quantitatively their impact on life-cycle cost and mission level performance.
- The identification of the optimal design solution relies on the establishment of a system value model that can be used to compare and rank systems on the basis of their performance on different attributes. The value model should be as simple and transparent as possible. Ideally the value model should capture the impact of the system usage on the overall mission environment.
- The use of AM and other RM techniques reduces the system development time and cost. As a consequence, the design of UAVs can be optimised for the fulfilment of a specific mission. Moreover, the use of AM and COTS components simplifies the concurrent engineering task because the cost and time of the manufacturing process can be estimated very accurately. Therefore, the new design environment should include both an analytical unit cost model and a detailed model of the mission (ConOps).
- RM favours the iterative approach to system design because the design-built-test-correct loop can happen within the timespan of a few weeks. The new design environment should be able to support design at different levels of detail and to integrate information obtained during tests.
- The decision makers require a tool to establish quantitative relationships between design variables and the overall system value. For mission specific system this can be achieved by integrating a life-cycle operational simulation based on the ConOps into the design environment.

6.3 DUADE Workflow

The DUADE workflow is shown in Figure 6-1. The process is divided into two phases: the problem definition phase[32] and the system design phase.

It is here assumed that the design workflow is intended for a UAV design/manufacturing organisation. In this case, the problem definition starts with the stakeholders' analysis which has two different goals:

1 - The identification of the value drivers.

2 - The definition of the system mission scenario (ConOps).

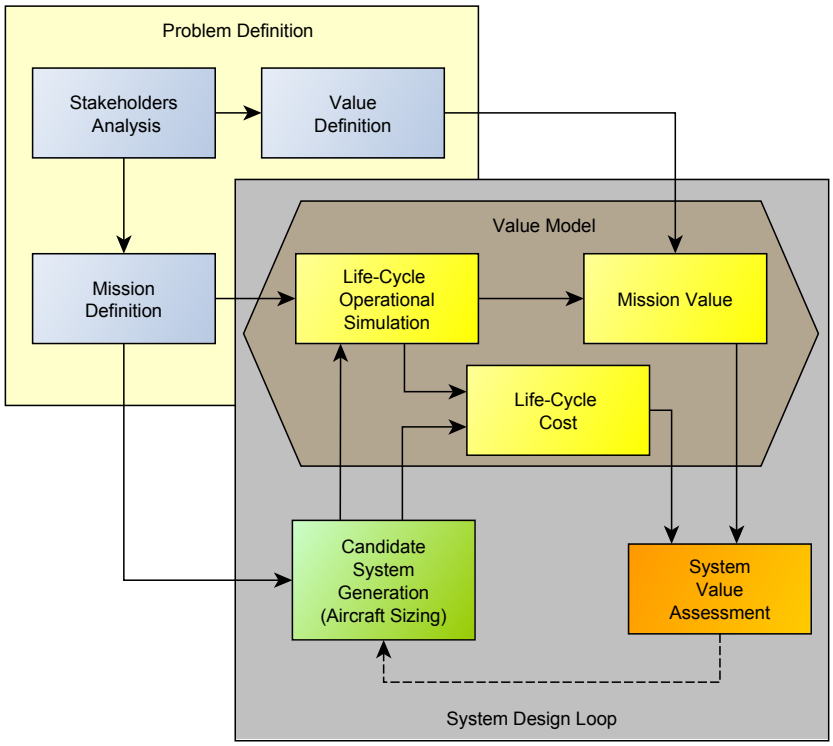

Figure 6-1 – DUADE workflow.

[32] The problem definition can be treated at different levels of abstraction. The first step is the identification of the stakeholders and the mission the system must accomplish to satisfy their needs. It is helpful to start with a mission statement that describes what the problem is, but does not implicitly suggest any solution. For example, a mission statement could be: "transport n passengers from city A to city B". This encourages the decision makers to consider different means of transportation (aircraft, train, coach, and so on). However, this level of abstraction is not operatively useful for an aircraft manufacturer company. Although considering solutions alternative to aerial transportation can provide a very valuable performance benchmark, the design company will be more interested in what kind of aircraft (as opposed to what kind of generic transportation means) can best satisfy the customer needs.
The other important aspect to consider is the definition of the system and its boundaries. In the example of the transport aircraft, one can identify the system to be designed as the airframe only, or one can include all the resources that are needed to achieve the mission, including hardware, software, personnel involved, infrastructures, airspace management service, and so on. Also, in this case, the correct level of abstraction depends on the subject using the design workflow.

The first is necessary to capture the inputs of the system value model. In particular, the design team should try to understand the fundamental needs of the stakeholders and their main goals for using the system. However, unlike traditional Systems Engineering, this phase should not result in the allocation of technical requirements to the system but in the definition of the metrics that will be used to assess the system value.

One of the fundamental hallmarks of DUADE is the integration of an agent-based operational simulation at the earliest phases of the design loop. The operational simulation provides the means to assess the UAV mission effectiveness and provides the quantitative measure of the inputs of the value model. The mission scenario needs to describe the tasks that the system is expected to perform during its service life and must include the description of the operative environment and the agents that interact with the system.

Once the design problem has been clearly defined, the System Design Loop can start. Using the information about the mission scenario, the first candidate UAV system can be generated. This UAV is then evaluated using the Life-Cycle Operational Simulation and the System Value Model. The output is a number that represents the UAV value according to the stakeholders' perception. The process is then iterated by changing the characteristics of the candidate system until an optimal system is identified. The design exploration can also proceed in parallel with multiple design solutions evaluated at the same time since every design solution is independent of each other.

This chapter will describe in more details the implementation of this framework with the focus on a particular test case: the design of a civil UAV for maritime patrol. Here the main focus is on the implementation of the system design loop, rather than the problem definition phase. Therefore, the problem definition will be described only briefly.

6.4 Problem Definition

The goal of the Problem Definition phase is to answer the following questions:

1 - Who are the stakeholders?
2 - What are the fundamental needs they are trying to satisfy?
3 - What are the tasks and operations that they are currently performing in order to satisfy these needs?
4 - How would they use the product?
5 - What is the operational scenario? What are the other agents involved?
6 - How would they assess the value of the product?

The thorough study of the problem definition phase and the techniques available to answer the questions above are beyond the scope of this work. However, the system design loop cannot proceed without a clear statement of the problem. Moreover, problems and difficulties in the practical implementation of the system design loop can only be unveiled by the application of the framework to a specific problem. For this reason, an exemplar case study has been selected and it is presented in the following sections.

6.4.1 Case Study: Design of a UAV for Search and Rescue Missions

DUADE has been primarily developed to assist the design of a UAV for SAR and other maritime patrol missions.

This case study has been chosen for two main reasons: firstly, it is a realistic application; the recent improvements in the unmanned aircraft technology and the consequent reduction of the cost of UAVs have piqued the interest of many governmental agencies in the topic. Organisations such as police units, coast guards, and port authorities are considering the option of integrating their operations with UAVs in order to cut the costs, improve their service and reduce the risk for the organisation members. Recent examples are the European Community funded project 2Seas-3i[33] and 2Seas-BERISUAS[34] which aimed to promote the use of UAVs in the maritime environment.

The second reason is that the problem presents many challenges; although the UAVs have found extensive use in warfare and intelligence applications, there are not many examples of civil UAVs performing this kind of missions. The system requirements are not easy to elicit and the impact that UAVs would have on the current operational scenarios is hard to assess. Moreover, the potential end-users have little or no understanding of the UAV technology and the system capabilities required.

In the proposed scenario, the UAVs are meant to join the Royal National Lifeboat Institution (RNLI) lifeboats in SAR missions in a region of the South English Coast. The RNLI is a charity organisation that employs volunteers to rescue victims of incidents at sea. The RNLI is funded by donations and legacies; their income in 2011 was £162.9M against an expenditure of £140.6M [214].

[33] Integrated coastal zone management via Increased situational awareness through Innovations on unmanned aircraft systems. Website: http://www.2seas-uav.com/

[34] BEtter Response and Improved Safety through Unmanned Aircraft Systems. Website: http://www.berisuas.eu/

6.4.2 Problem Definition and Assumptions

The following assumptions are used: the main stakeholder is represented by the RNLI who is the organisation that is financing the project. The RNLI fundamental needs can be summarised as improving their SAR mission performance by saving more lives and decreasing the cost of their operations. The rescue operations are currently performed using lifeboats deployed from stations located around the UK coastline. In real life, the SAR operations are performed in cooperation with coastguard helicopters, but their presence has been neglected in this initial study. The geographic area of interest is a part of the south coast of England as presented in Figure 6-2. In this area, there are 10 RNLI lifeboats stations (yellow squares in the picture) that are equipped with a lifeboat each. The dots represent the historic distribution of incidents involving people immersed in water, which has been obtained from the data available from the RNLI website [214].

Figure 6-2 – Baseline scenario showing lifeboat stations (yellow squares) and incident positions (dots) [65].

A UAV will be based in the Lyme Regis station and will assist the rescue operations by helping to locate the victims in less time and hence increasing their survival probability. It is also assumed that the UAV will be the only flying vehicle operating in the area at the given altitude and that its position is signalled by transponder, so that other vehicles do not interfere with its flight path[35]. The impact of the UAV on the operation will be measured with a Cost-Benefit analysis, whose inputs are the number of saved lives and the cost of the rescue operations.

[35] This condition is unrealistic in the current regulatory framework. However, according to the author, the institution of flight levels dedicated to UAVs and the use of cooperative sense-and-avoid strategy are likely to be introduced in near future.

6.5 System Design Loop

The system design loop is described in Figure 6-3. It is composed of two main modules: the Aircraft Sizing Tool (AST) and the Value Model (VM).

The AST is a piece of software used to generate the model of a feasible UAV and to provide its properties to the Value Model. In order to achieve this, a multidisciplinary design optimisation ensures that the aircraft satisfy all the design constraints and maximise a user-defined Intermediate Objective Function (IOF). The system disciplinary models are coordinated by a central module that contains the aircraft sizing algorithm and low-LOD disciplinary models, and ensures that the coherence of the system description is maintained. In this way, it is possible to perform the system optimisation by considering multiple disciplines at once while avoiding the complication of the coordination of multiple optimisation loops. The data coming from high-LOD models and prototype testing can be fed back to the central module and the low-LOD optimisation reiterated in a spiral refinement process.

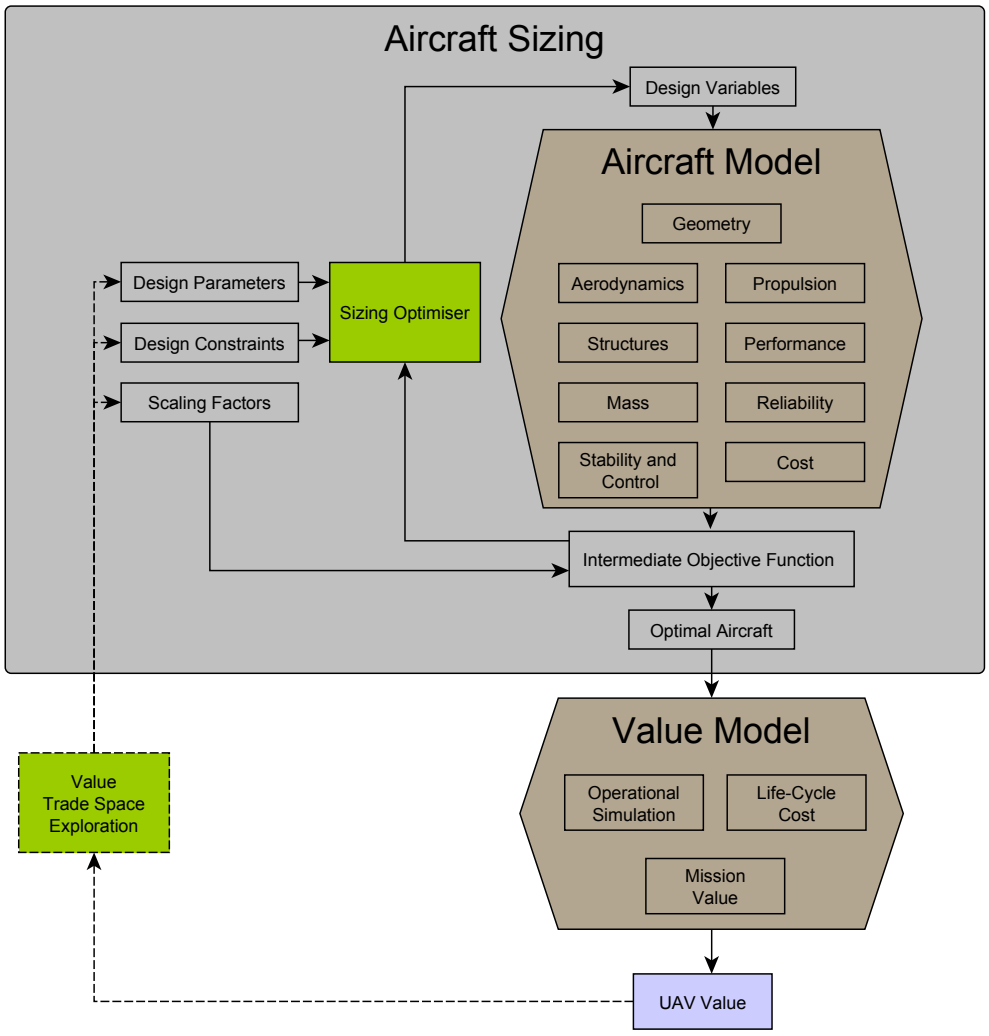

Figure 6-3 – DUADE System Design Loop.

The VM provides a tool to assess the quality of the design alternatives given the mission requirements. The system's ConOps is translated into the Life-Cycle Operational Simulation that provides the data for evaluating the life-cycle cost and the mission effectiveness of the system. This information is then used to rank the design alternatives. The system design loop is closed by studying the impact that design parameters, constraints, and AST objective functions have on the final value of the system.

In other words, the system design loop can be seen as a bi-level design activity, where the low-level one is responsible for providing the best aircraft that satisfies a certain number of requirements according to a local objective function. The high-level design loop is responsible for establishing the design requirements that lead to the best overall value according to the VM.

The advantage of this approach is that the AST and the VM can also be used independently of each other. For example, the user might compare existing systems by inputting their parameters to the VM. Similarly, the AST can be used independent of the VM to design aircraft using a more conventional approach.

6.6 Aircraft Sizing Tool

The AST was developed with two main goals in mind. The first was to allow the designers to perform trade space exploration and VDD studies by studying the impact of the different characteristics of the UAV system on the mission performance.

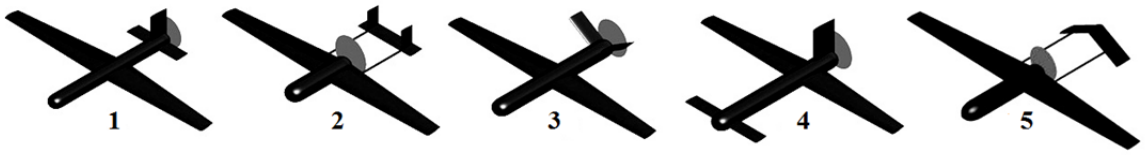

Figure 6-4 – Aircraft configurations available in the baseline version of the AST.

The second was to perform the sizing calculation for the research aerial vehicles developed and built by the University of Southampton. Since the AST was not aimed exclusively at theoretical studies, the model required a higher level of details and more specific assumptions than equivalent academic codes. For this reason, the code was not intended as a generic design tool. Instead, it was tailored for the particular class of vehicle of interest, that is fixed-wing UAVs with a

maximum dry mass between 3 and 40 kg. In particular, the analysis was initially restricted to UAVs with a single internal combustion engine in a pusher propeller configuration[36].

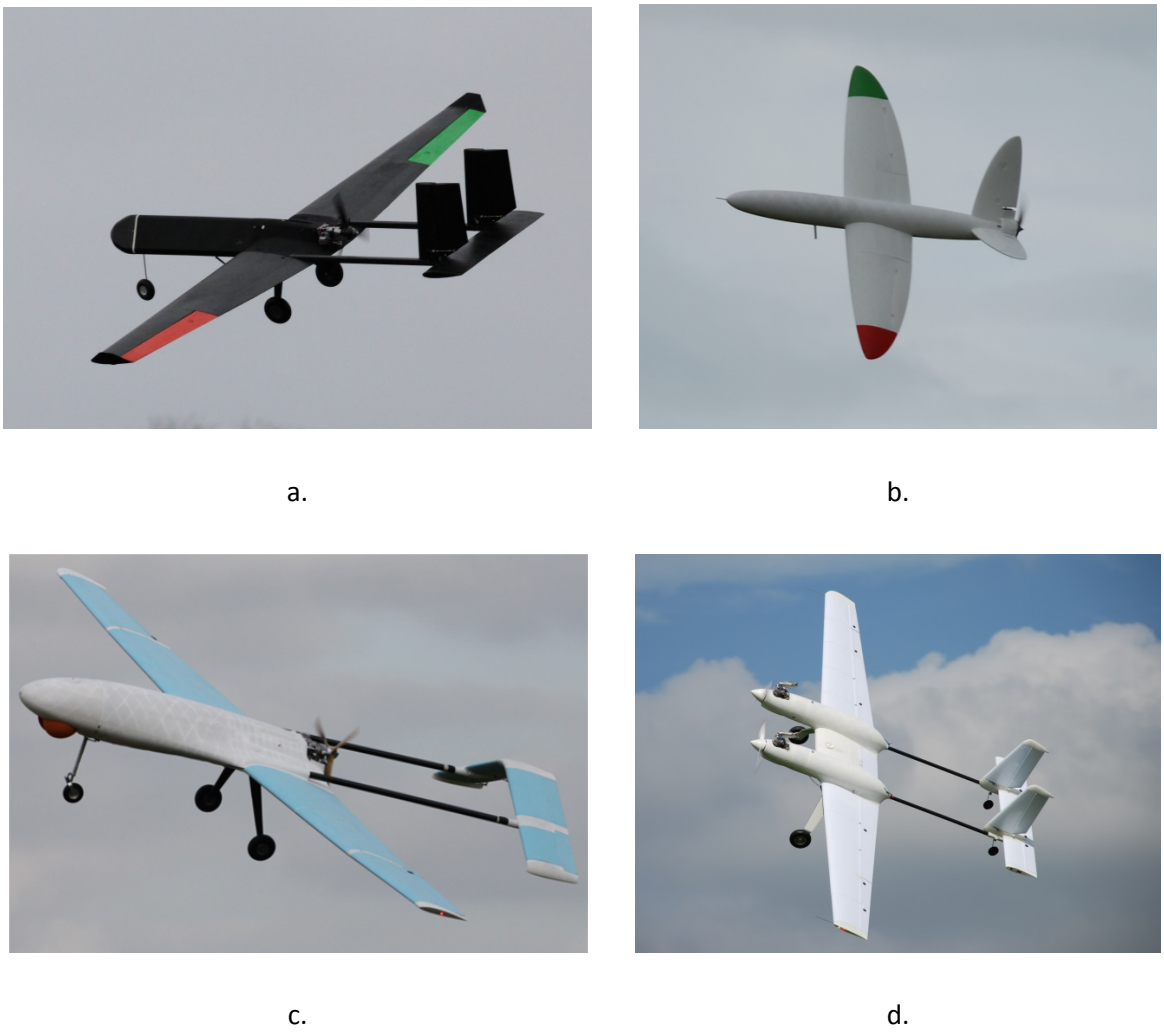

a. b.

c. d.

Figure 6-5 – Examples of research vehicles designed using the AST. **a.** DECODE-1, a 10 kg MTOM glow fuel aircraft; **b.** SULSA, a 3 kg electric powered entirely 3D printed aircraft; **c.** DECODE-2, a 23 kg MTOM petrol engine aircraft; **d.** SPOTTER, a 35 kg MTOM twin engine aircraft.

The base code is capable of analysing five different variants of this aircraft configuration, presented in Figure 6-4. The materials and building techniques used for the production of these vehicles are briefly discussed in Section 6.6.1. By knowing the technologies employed it was possible to develop cost and mass estimation relationships more accurate than the ones

[36] It was assumed that the payload is an optical sensor mounted in the nose of the aircraft. The pusher-engine configuration provides the sensor with an unobstructed view of the ground and prevents residuals of the fuel combustion from dirtying the sensor lens.

presented in the design handbooks[37]. Derivations of the AST were used for the design of aircraft with different configurations and propulsion technologies, including twin-fuselage/twin-engine UAVs and electric propulsion UAVs.

The AST was used to guide the design and production of several research vehicles which were successfully tested in flight (some examples are presented in Figure 6-5).

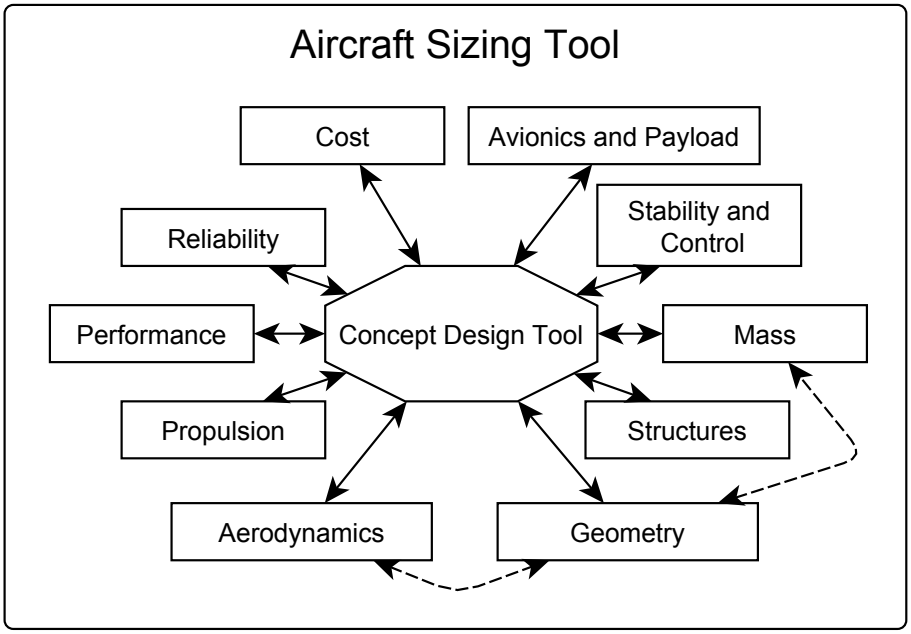

Figure 6-6 – Aircraft Sizing Tool modules. All high-level variables are coordinated by the CDT. Low-level variables are managed in the high-LOD geometry tool and can be shared with disciplinary modules for detailed analysis.

The AST is composed of multiple disciplinary modules that are coordinated in a central piece of software named Concept Design Tool (CDT). The aircraft design variables and parameters are organised in a two-level hierarchy: the top level parameters (such as the wing span, the tail length or the engine size, for example) are controlled through the CDT. These are the variables and parameters that are used in the aircraft sizing, optimisation or disciplinary analyses and can have an influence on the overall architecture or performance of the aircraft. The low-level parameters exist only in the CAD tool and are considered detail design variables that have little impact on the overall system. The bi-level variables' hierarchy implies that the concept and preliminary design phases are performed simultaneously; this enables the designer to understand the implication of architectural choices, typical of the concept phase, via a quantitative analysis rather than a

[37] For example, Raymer [37] and Gundlach [219] provide cost and mass estimation relationships based on statistical methods.

qualitative one. For example, one can see whether a particular empennage configuration requires a higher undercarriage and larger wheels and then evaluate if there is an overall benefit or penalty in terms of mass, drag and control capability.

The disciplinary modules of AST are described in Section 6.7. They include traditional aeronautical engineering disciplines such us aerodynamics and structures as well as a cost model and a component reliability model. The avionics and payload of the UAV are not explicitly modelled in the AST, but their mass and cost are estimated using empirical relationships derived from the experience of the UAV design team at the University of Southampton.

Some of the disciplinary models present different levels of analysis LOD. For example, the aerodynamics coefficients can be obtained using low-LOD methods derived from empirical and design handbook equations, or high-LOD methods that rely upon physics-based codes (Vortex Lattice method or Reynolds Averaged Navier-Stokes equations). In this way, AST can support the design of the UAVs in the spiral refinement cycle.

The user can access the AST using different interfaces. The most direct one is based on a structured spreadsheet, in which the design variables and constraints can be switched on and off according to the designer's needs. Customised design constraints and relations can be easily defined as well. A second interface is provided by a MATLAB® [215] client that can be used by the designer to perform extensive trade studies.

6.6.1 Design Philosophy and Manufacturing Processes

The design philosophy adopted here focused on the simplicity and rapidity of the manufacturing process. In particular, the designers were committed to avoid any labour intensive process and tried to exploit the benefits of RM techniques discussed in Chapter 4. COTS components were used when available at a competitive price. The following building techniques were adopted for the main components of the aircraft:

- The main structural elements of the wings and control surfaces were carbon fibre composite tubes. The reasons for this choice are the excellent strength-to-weight ratio, the low price and the large availability on the market of these components. In particular, the wing main spar was a single carbon fibre tube through the quarter point line of the wing. This was judged a better solution compared to others involving two or more tubes because of its assembly simplicity.
- The aerodynamic shape of the wings and control surfaces was realised using extruded polystyrene (XPS). This material has a low density (38 kg/m^3) and relatively high rigidity. Furthermore, it is inexpensive and easy to form into the desired shape. The foam blocks

were cut using a foam plotter. One of the main drawbacks of the extruded polystyrene is that it is easy to dent or damage by handling. For this reason, a protective external layer (glass fibre cloth or Mylar) was applied to the wing. This also increased the overall rigidity of the structure.

- The fuselage and all the parts that act as interfaces between different components and/or have complex geometrical features were produced using AM processes. In particular, SLS Nylon 12 components were extensively used.
- The engines and propellers were bought off-the-shelf relying on components available from the radio controlled aircraft hobbyists' market. The same is assumed for the undercarriages, wheels and servo actuators.
- Avionics was a composition of COTS parts and components that were designed and manufactured in-house.

6.6.2 The Concept Sizing Tool: Choice and Evolution

A number of commercial and open source tools are available to support the aircraft design at the concept and preliminary design stage; well-known examples include ACSYNT [101], FLOPS [39], AAA [44], RDS [102] and the more recent ADS [42] and CEASIOM [216]. Those tools were originally developed for aircraft whose size and construction methods are far from the sub-40 kg class of aircraft that are the object of the current study. Moreover, they generally involve the use of empirical relations whose assumptions and range of validity are difficult to assess.

These considerations led to the decision of developing a concept design tool which was initially based on basic principles present in classical aircraft design books [37,217–219] and that was gradually calibrated with empirical data obtained from previous UAVs designed and built in our group. The CDT was initially implemented in a formally structured spreadsheet, as well as in the commercial PaceLab Suite® [106] programming environment in order to evaluate the merit of a more free form approach versus a more structured and formal one. The other attraction of PaceLab Suite® was the possibility of automatically generating the geometry used in the high-LOD analyses. However, PaceLab Suite® was abandoned after the first few months of the research project due to the unsatisfactory performance of the geometry engine, the general preference of the designers for the more flexible spreadsheets and the high cost of its licence.

The choice of a spreadsheet as the main design environment has some advantages that can be summarised as follows [220]:

- The designer has absolute control of the variables, constraints, and methods.
- The design tool can be easily calibrated to the problem.

- Spreadsheets are widely used and well understood amongst the engineering community.
- The designer "learns" about the problem, is aware of the assumptions and approximations introduced and has instant feedback of the result of the computation.
- Spreadsheets can be very accurate and powerful if enough details are included.

Raymer [221] demonstrated that a relatively simple spreadsheet can be used as an aircraft sizing tool with satisfying results if one is ready to sacrifice flexibility in terms of the number of configurations explored. In his example, he also compared the development time of the spreadsheet versus the time needed to code the RDS tool, pointing out that the ratio is 1:100. Moreover, he estimated that the time needed for the average user to become familiar with the spreadsheet and start designing is about 10 times faster.

On the other hand, the use of spreadsheets presents also many drawbacks, as pointed out by Scanlan *et al.* [222]. These include:

- The flexibility of the spreadsheets which allows (and somehow encourages) the developer to create unstructured and complex webs of references which make the spreadsheet very difficult to use and understand for a third party.
- Errors are often very difficult to detect, particularly when large formulae with many terms are used, due to the use of cell references instead of variable names[38].
- Spreadsheets are not easily scalable and they are not very well suited to support computations that involve multiple configurations.

In order to mitigate these problems, the spreadsheet used for the concept design was provided with a clear structure: variables and parameters are organised using a column-based scheme and a two-level naming system; disciplinary calculations are performed in dedicated worksheets with a clear input/output structure; conditional formatting and filtering functions are used to manage the variables and constraints of the sizing optimisation. A more detailed description of the spreadsheet interface of the CDT is provided in Appendix D.

6.6.3 Sizing Strategy and Optimisation Algorithm

The CDT includes different disciplinary modules: Geometry, Aerodynamics, Stability and Control, Structures, Mass, Reliability, Propulsion, Performance, and Cost.

[38] Assigning names to cells can mitigate this problem, but most users don't use this function [299].

The sizing of the aircraft is obtained by solving the multidisciplinary problem generated by the mutual relations between design variables and analysis disciplines. For example, structures that are able to absorb larger loads will have a larger mass and, at the same time, heavier aircraft will require their structure to be stronger. This generates information loops that are resolved by the introduction of surrogate variables. The use of surrogate variables is better explained with an example: for a given flying speed and lift coefficient, the wing area S_w needed to sustain the aircraft depends on the weight of the aircraft W. Similarly, the weight of the aircraft is obtained by knowing the wing area. If a surrogate variable for the aircraft weight is introduced W_{sur}, this can be used to calculate the wing area. By knowing the wing area, the mass module can calculate the actual weight W. The loop is then closed by imposing that $W_{sur} = W$ to ensure the physical consistency of the model.

A solution to the problem involving surrogate variables can be found iteratively. However, in the case of the CDT, surrogate variables are used in the solution of aircraft optimisation problem. The optimisation process produces an aircraft that satisfies all the design constraints, ensure the physical consistency and maximises a user-defined objective function. The objective function is typically a combination of aircraft characteristics that are desirable for the designer. For example, the user can assign a weighted sum of performance and cost, in which case the scaling factors (or weights) can be adjusted to reflect the user preference.

At the prototype stage, the optimisation process was performed by using the Microsoft Excel Solver® [223] based on the Generalised Reduced Gradient Method [224]. This provided acceptable performance as long as the scale and complexity of the spreadsheet and optimisation problem was relatively small (less than 6 variables and 20 constraints). However, as the complexity of the CDT increased and more relations, variables and constraints were included, the Solver® was not able to achieve a solution and a more powerful and robust algorithm was required. This, together with the need for a tool more flexible than Excel for the communication with the other DUADE modules, led to the decision to compile the spreadsheet to the Python programming language. This was achieved thanks to the development of an automatic compiler and the relative Excel® plugin by one of the other members of the DECODE research team[39]. In this way, the extra flexibility needed was achieved while retaining the user-friendly spreadsheet interface. The generation of the Python code is entirely automatic, unless the spreadsheet user introduces macros or other functions using the Excel® API, in which case human intervention is required to keep the two codes synchronised.

[39] Dr Dirk Gorissen - Pycel: Compiling Excel spreadsheets to Python http://dirkgorissen.com/2011/10/19/pycel-compiling-excel-spreadsheets-to-python-and-making-pretty-pictures/ - accessed on 20-10-2011.

The compiled Python code allows the designer to exploit the optimisation algorithms available in the open source library OpenOpt [225]. After an initial screening of the available algorithms suited for constrained nonlinear optimisation problems, the sequential least square programming algorithm scipy_slsqp [226] was selected. This algorithm is based on a quasi-Newton method and hence it is best suited to find local optima. The starting points for the search were provided using data from similar vehicles or using the best judgment of the designer when these were not available. Evolutionary algorithms were discarded in the initial screening because they provided poor performance in satisfying equality constraints. Moreover, given the highly constrained design space, it was found that in most cases the same solution was achieved by the scipy_slsqp algorithm irrespective of the starting point.

The typical sizing problem involves 14 variables and more than 60 constraints; the optimisation generally converges to a solution within 5-10 minutes on a typical desktop machine[40].

The constraints and objective function of the optimisation are discussed in Chapter 7.

6.7 Aircraft Sizing Tool Disciplinary Modules

This paragraph provides a brief description of the disciplinary modules of the AST.

Table 4 provides a summary of the methods and software (indicated in brackets) used in the AST[41]. Per each disciplinary module, the table distinguishes between Low, Medium and High LOD models. There is also an "Experimental" row that displays the methods used to validate the results of the AST and/or provide feedback used in subsequent iterations of the design. The table also provides an indication of the level of integration of the various models with the CDT.

In particular, the Table 4 distinguishes between fully-integrated, semi-integrated and partly-integrated modules[42].

[40] Processors: 2.13 GHz eight-core. Memory (RAM): 12.0 GB.

[41] Table 4 is intended to give only a qualitative description of the AST modules to the reader. The table only shows the main method and software used by each disciplinary module; however, in some cases, the disciplinary calculations are obtained using a combination of different methods and software. For example, the medium-LOD Aerodynamics module uses the Vortex Lattice Method to calculate the lift and induced drag of the wings and empennage; however, the aircraft parasitic drag is still estimated using handbook equations. Similarly, the equations used to calculate the aircraft performance in the Operational Simulation are the same used in the low-LOD model; however, the Operational Simulation allows a more detailed calculation of the aircraft performance by providing a more detailed description of the mission phases.

[42] The classification of models by their level of integration is a qualitative one, as well. For example, the Operational Simulation is considered semi-integrated but, on one hand, it requires the user to carefully set the mission scenario; on the other hand, the result of the Operational Simulation can be automatically fed back to the CDT through the Value Trade Space Exploration loop displayed in Figure 6-3.

Discipline		Geometry	Aerodynamics	Stability and Control	Structures	Mass	Propulsion	Performance	Avionics and Payload	Cost	Reliability	Value
Level of Details	Low	three-view schematic drawing (Excel)	Handbook equations/ Empirical methods (CDT)	Handbook equations/ Empirical methods (CDT)	Handbook equations/ Empirical methods (CDT)	Lumped mass model/ Empirical methods (CDT)	Handbook equations/ Empirical methods (CDT)	Handbook equations/ Empirical methods (CDT)	Mass and Cost Estimate (CDT)	Cost Model (Vanguard Studio)	Component Reliability Table (CDT)	Custom value function (CDT)
	Medium	3D geometry model (VSP)	Vortex Lattice Method (Tornado)	Vortex Lattice Method (Tornado)	-	3D geometry model (VSP)	-	Operational Simulation (AnyLogic)	Operational Simulation (AnyLogic)	Value Model (Vanguard Studio)	Operational Simulation (AnyLogic)	Value Model (Vanguard Studio)
	High	CAD (SolidWorks)	RANS (Fluent)	-	FEA (ANSYS)	CAD (SolidWorks)	-	-	-	-	-	-
Experimental		Measures	Flight tests	Flight tests	Static tests	Mass Measures	Flight tests/ Wind tunnel	Flight tests	-	Cost Measures	In-service failure rate/ Bench tests	-

Level of integration with the CDT
Fully-integrated (automatic bi-directional interaction)
Semi-integrated (automatic input generation with manual intervention required for analysis feedback)
Partly-integrated (requires manual intervention for input and output)

Table 4 – Table displaying the disciplinary modules, software and their level of integration with CDT.

The fully-integrated modules are either hardcoded into the CDT or have a full automatic input/output exchange with the CDT and can therefore be used during the CDT sizing optimisation. The semi-integrated modules can receive the input parameters automatically from the CDT, but require some manual intervention to feedback the analysis results to the CDT.

Finally, the partly-integrated tools can obtained some of the inputs required from the CDT but still require manual pre-processing to perform the disciplinary analysis.

In the rest of this paragraph, the methods and tools used to model the AST disciplines are briefly described. In particular, the focus is on the Low-LOD methods that are used in the initial trade space exploration.

6.7.1 Geometry

The aircraft geometry is managed in the CDT by using a relatively small number of parameters (on the order of one hundred). Some of these parameters are independent and some are dependent on the other parameters. The number of independent parameters is determined by the number of geometrical relations and constraints that the user decides to consider.

The CDT provides the user with a cartoon representation of the aircraft that displays the size and position of the main structural elements (shown in Figure 6-7a.). The picture also indicates the position of the aircraft's neutral point (red line) and the Centre of Gravity (CoG) maximum aft and forward position (two light green lines). The CDT also automatically generates a 3D model of the aircraft using VSP geometry engine developed by NASA [45]. Similarly, a CFD-ready geometry is created using ANSYS® [227] geometric engine (example shown in Figure 6-7b.).

This low-LOD geometric model is linked to the high-LOD CAD module (Figure 6-7c.). Here the geometric variables controlled by the CDT are imported and treated as input in a parametric model. All the high-level geometric variables defined in the CAD module are not shared with the CDT. Some high-level design parameters can be used to control the aerodynamic or structural optimisation of the airframe during the detail design phase, in which case a link between the CAD module and the disciplinary module is created (Figure 6-6).

6.7.2 Aerodynamics

The Aerodynamics module computes the aerodynamic coefficients (drag polar and aerodynamic derivatives) that are used in the stability and control computation and in the performance estimation.

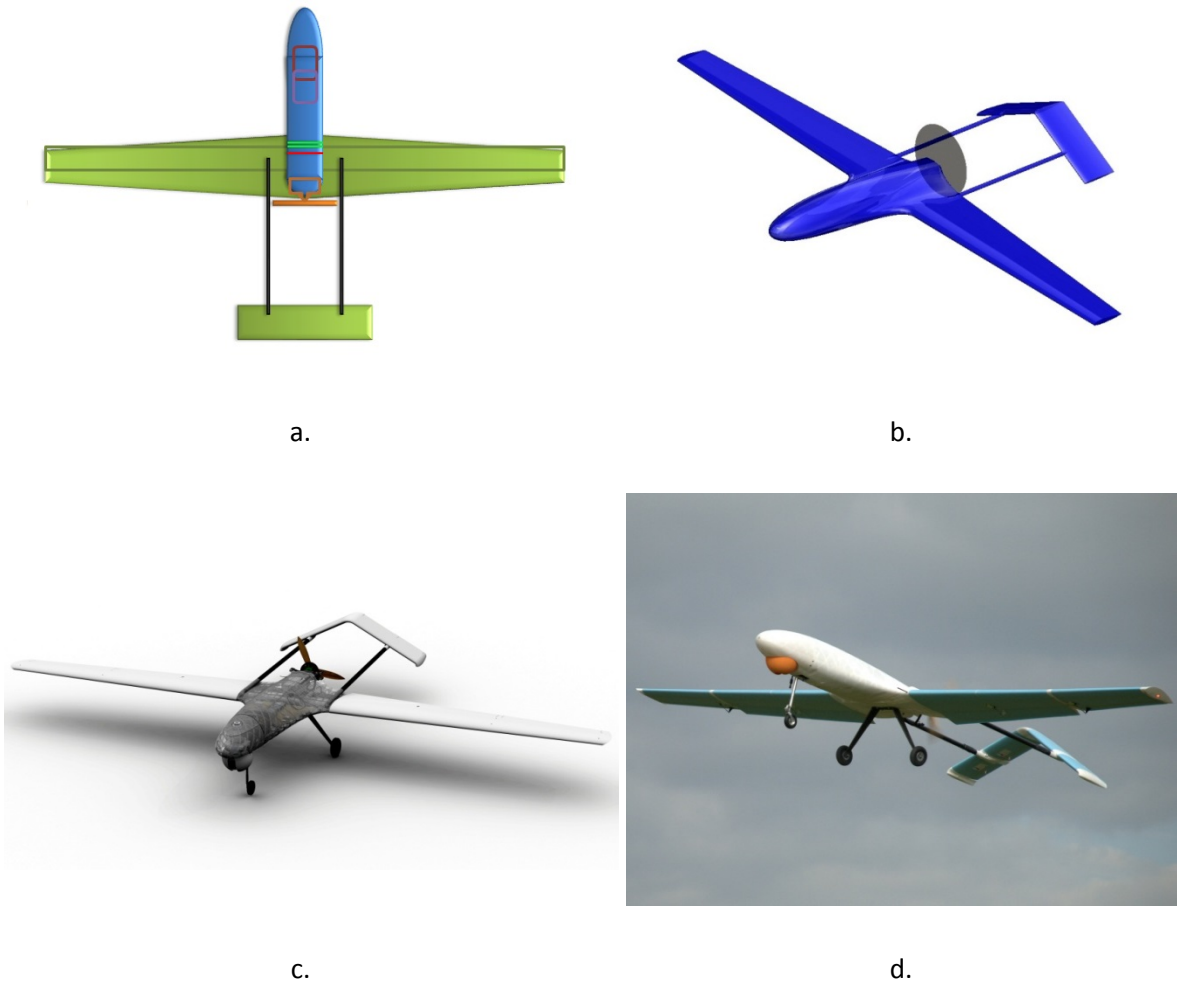

a. b.

c. d.

Figure 6-7 – Different level of abstraction of the DECODE-2 aircraft geometry in the Aircraft Sizing Tool: **a.** Cartoon representation of the aircraft used in the Concept Design Tool; **b.** Geometric model used for the CFD analysis; **c.** High-LOD CAD geometry; **d.** Picture of the airframe during flight tests.

The aerodynamic coefficients can be obtained through a low-LOD computation based on handbook methods and empirical equations ([37,217,228–230]) or through a physics-based simulation. The first is generally used during initial trade space studies while the second is reserved for later design phases when more accurate analysis is required.

The parabolic drag polar approximation is used. The coefficient of drag C_D is obtained using the following equation

$$C_D = k_1 + k_2 C_L + k_3 {C_L}^2 \qquad 6\text{-}1$$

where C_L is the coefficient of lift of the entire aircraft and the coefficients k_1, k_2, and k_3 depend on the aircraft configuration (cruise, take-off or landing). In the low LOD setting, the coefficients of the drag polar are estimated adding up contributions of individual aircraft components (wing,

fuselage, undercarriage, and so on) and then applying a correction for the interference drag. The drag values of the individual components are estimated using the equations and digitalised version of the tables available in the literature [231,232]. Aerodynamic derivatives (coefficient of lift, drag and moment *versus* angle of attack of the all aerodynamic surfaces and bodies, and effectiveness of the control surfaces per angle of deflection) are estimated using analogous methods [218,233].

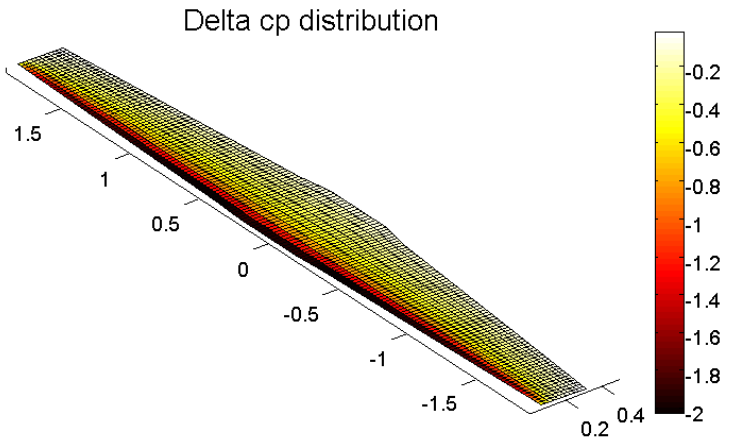

Figure 6-8 – Coefficient of pressure (cp) distribution over SPOTTER's UAV wing at the AoA=3° and 30 m/s calculated using a Vortex Lattice Method code.

The CDT is linked to a Vortex Lattice Method code (Tornado [234]) analysis software that can provide a physics-based first order approximation of the aerodynamic coefficients for the wing and empennage and their aerodynamic load distribution (Figure 6-8). Higher LOD analysis can be performed using a Reynolds Averaged Navier-Stokes (for instance using ANSYS Fluent® software [235]) for which a model of the basic aircraft configurations of CDT is automatically generated.

The output of the aerodynamic model is used to update the aerodynamic coefficients employed by the CDT for the sizing of the aircraft. This update is performed at each step of the sizing process in case of low-LOD calculations. If the high-LOD aerodynamic analysis is used, the aerodynamic coefficients are updated at the beginning of each CDT sizing cycle, during which they are kept constant. The entire process is reiterated until the convergence on the final aircraft geometry is achieved[43].

[43] More details on the use of high-LOD aerodynamic analysis in the sizing loop are given in Quaranta *et al.* [300].

6.7.3 Stability and Control

The Stability and Control module ensures that the aircraft retains a positive stability margin and there is sufficient control power in all the operating conditions. The stability computation is based on handbook methods and takes as input the aerodynamic coefficients and the CoG envelope of the aircraft. The low-LOD calculation of the Neutral Point (NP) position of the aircraft equipped with a foreplane control surface (canard) is based on Phillips [236].

The aircraft aerodynamic NP is calculated for both longitudinal and directional stability, by adding up the contributions of wing, empennage and fuselage and accounting for the effects of the induced angle of attack and propwash. The minimum Static Margin (SM) is obtained as the distance between the most aft position of the CoG of the aircraft and the NP; divided by the length of the main aerodynamic chord of the wing. The CoG is calculated for the aircraft with and without fuel and with and without payload. The minimum SM for the longitudinal stability is set to SM=0.1. Flight tests have confirmed that this value is acceptable for the vehicles of interest. An analogous process is used to ensure the directional stability of the aircraft. The importance of lateral stability of the aircraft was proven to be secondary and a neutral or slightly negative lateral stability value was deemed desirable as a safety feature to prevent a flyaway situation in the event of the electronic flight control failure.

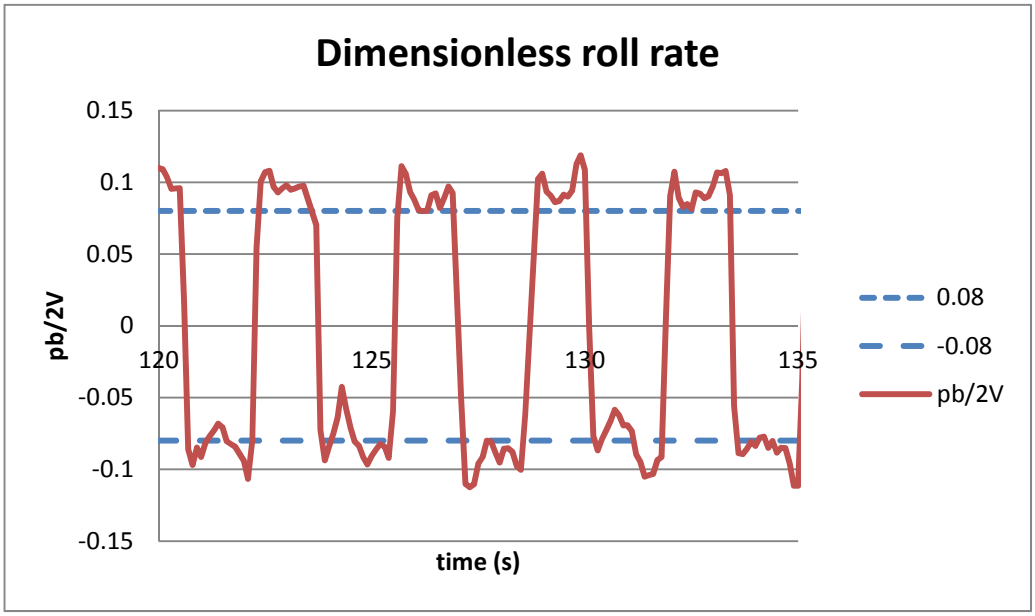

Figure 6-9 – Dimensionless roll rate of DECODE-1 UAV measured during flight test versus design value.

The control authority is calculated for each of the control surfaces of the aircraft using either handbook equations and tables or the Vortex Lattice Code. Different flight scenarios and CoG positions are considered, including landing with high-lift devices fully deployed and the ground effect. Acceptable levels of control authority were established using Roskam's [218] and Raymer's

[37] design books as main references. For example, a minimum dimensionless roll rate value of 0.08 is used to size the ailerons. Figure 6-9 shows the dimensionless roll rate measured during the flight tests of DECODE-1 airframe versus the design value. The data are in good agreement with the calculations. The test was performed by alternatively commanding a bank angle of ±50°. After a short transient, a constant roll rate was achieved. The difference in clockwise and anticlockwise roll rate was caused by the torque of the propulsion system.

6.7.4 Structures

The Structures module ensures that the main structural elements of the aircraft are able to resist the static and dynamic loads throughout the whole flight envelope[44].

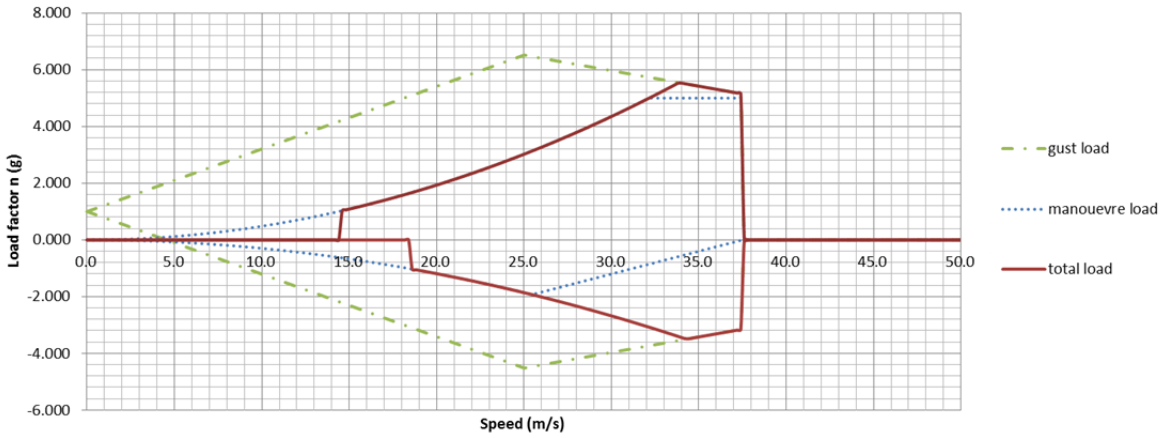

Figure 6-10 – Flight Envelope generated by the Concept Design Tool.

Since no airworthiness regulation applies to the structural design of this class of aircraft, an estimate of the manoeuvre and gust load factors is performed with reference to the Joint Aviation Requirements Part-23 [237]. Flight envelopes like the one shown in Figure 6-10 are automatically generated by the sizing software and the maximum loads are computed.

Only the structural model of wings, tail booms, tail planes and main undercarriage are included in the CST. The sizing of the structural elements is performed using the elastic beam theory and approximating the composite structures as a homogeneous material with the same elastic modulus and maximum tensile strength. The aerodynamic load distribution over the wingspan is

[44] The term "flight envelope" is used to refer to the boundaries of aircraft loading and flight conditions within which operation of the aircraft is satisfactory, and beyond which some aspect becomes unacceptable [301]. The whole flight envelope is a combination of several flight envelopes corresponding to different configurations of the same airplane: the configurations of landing gear, flaps, and other devices as well as the mass, and the CoG position, influence the performance and do matter for the structural integrity (for example, if the flaps are activated while the aircraft is flying at its maximum speed the result can be catastrophic).

approximated using the Schrenk method [238] or the Vortex Lattice Method code (Figure 6-11). A baseline safety factor of 1.5 is used.

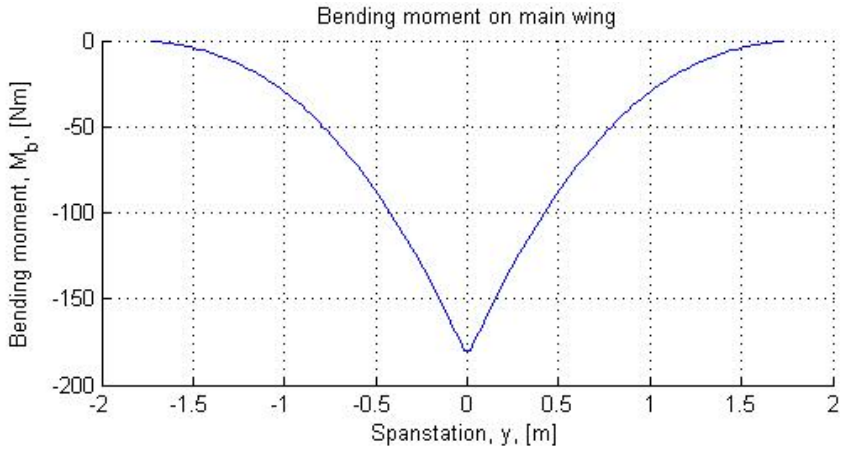

Figure 6-11 – Example of bending moment distribution along the wing span obtained with a VLM code. The picture displays the bending moment on the SPOTTER's wing at AoA=3° and 30 m/s.

The structural analysis of the other components is considered a detail design activity and only the impact of the components' mass is fed back to CDT.

Whenever possible, the structural performance of the primary structure was validated experimentally. For example, Figure 6-12 shows the wings of SPOTTER being tested at the calculated ultimate load[45].

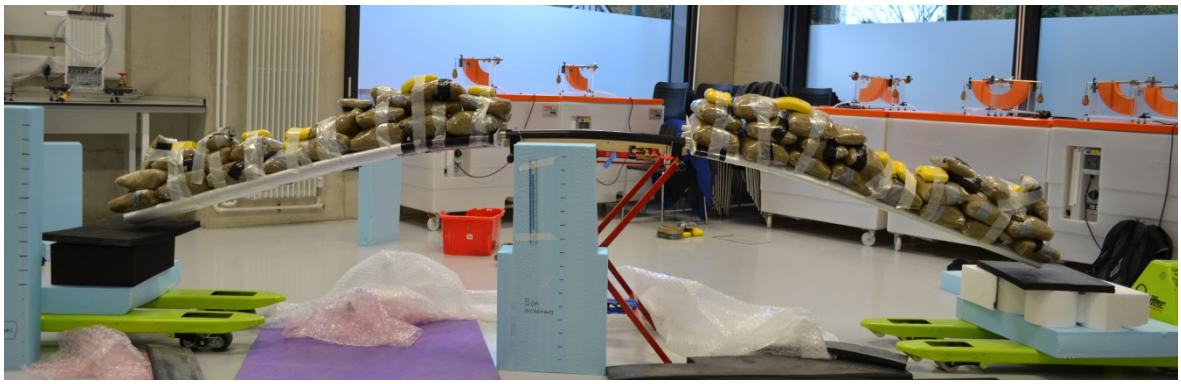

Figure 6-12 – SPOTTER's wing static load test (7 g). The ultimate load distribution was approximated using sandbags and lead weights.

[45] The static load was intended to replicate the load distribution in the direction of the wingspan. The torsion load was neglected. The load was applied for 15 second. The wing torsion box failed at 7.3 g due to the instability of the unintentional torsion load introduced by the sandbags. However, this load was not representative of the calculated aerodynamic load.

6.7.5 Mass

The Mass module calculates the mass of the aircraft and the overall envelope of the CoG.

Several aircraft mass estimation techniques are available in the literature. Some of these can only estimate the total mass of the aircraft; others provide mass estimation relationships for each of the main components of the airframe. In particular, references [239,240] provide statistical mass estimation relationships for different classes of manned aircraft. These techniques have two problems for this application: firstly, they are based on databases of vehicles whose size and building techniques are not comparable with the ones in this study. The second problem is that mass prediction in statistical methods does not respond to all the changes in the design variables.

In the CDT, the mass of each of the major aircraft subsystems is estimated using a combination of analytical methods and regression analysis. In particular, the mass of the main structural components is calculated using the information provided by the Structures module. The mass of the other components is obtained either estimating the material's volume or, when a sufficient database of similar structures exists, using regression analysis similar to the one displayed in Figure 6-13.

The mass and the position of the components are used to calculate the CoG and are fed back to the main sizing module. For each component, the mass estimation and CoG position calculated in the CDT can be overwritten with data coming either from the high-LOD CAD module or measures of the actual components.

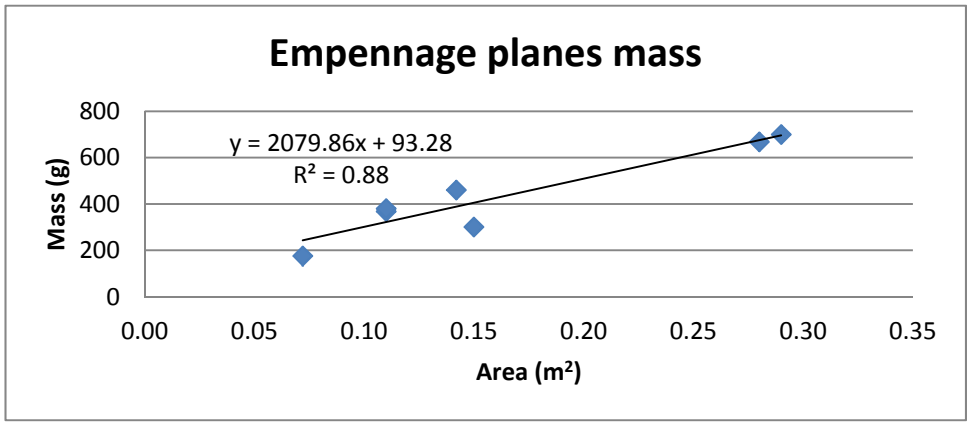

Figure 6-13 – Example of mass estimation relationship in the CDT. The equation estimates the mass of the stabilisers' skin and secondary structure given their area. The linear regression was obtained using data from five previously built UAVs and includes vertical, horizontal and V-tail stabilisers.

6.7.6 Propulsion

The Propulsion module provides an estimate of the performance of the engine/motor and propeller. A rubber engine model was built around a database of engines and motors available on the market for RC aircraft. Only limited information is available about the performance of these engines: displacement and mass are almost always available; power and fuel consumption are more difficult to obtain and often inaccurate. In particular, only maximum power and average fuel consumption are sometimes stated by the manufacturer; a torque-power-rpm map or detailed information about the fuel consumption is generally unavailable. However, a model that captures the basic performance of a typical engine was created for the initial sizing of the aircraft. Refined information can be introduced in the CDT once a particular engine has been identified and tests can be performed. A rubber engine model was created to link output power to mass (Figure 6-14).

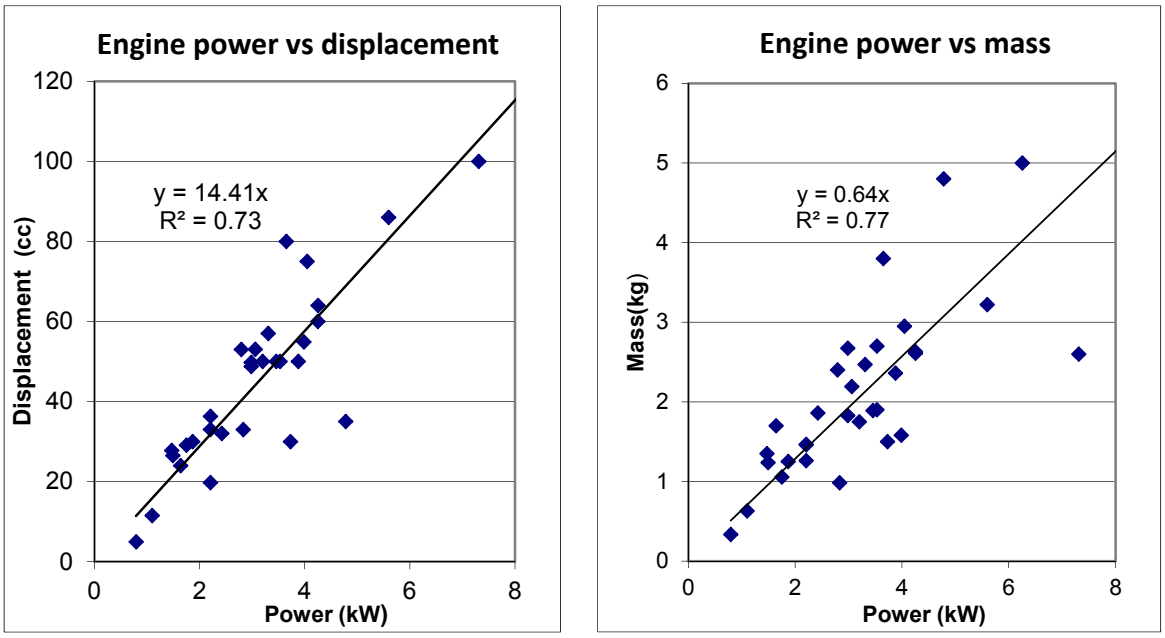

a. b.

Figure 6-14 – Regression analysis for capacity, power, and mass of RC aircraft engines.

The fuel efficiency of reciprocating engines is estimated using the Brake Specific Fuel Consumption (BSFC). The BSFC is measured in grams of fuel per kWh of power. Curves representative of typical two- and four-stroke model aircraft engines were estimated using the experimental measurements performed on a 3W 28i (with and without electronic fuel injection[46]) and OS GF40 engines (Figure 6-15). The experiments were performed in the engine test cell in static flow condition.

[46] The data for the 3W 28i with EFI were provided by the EFI manufacturer: Currawong Engineering, Kingston T, Australia.

The static thrust, engine rpm and fuel flow in g/h were measured[47]. The propeller used for the tests was a two-bladed 18 inch diameter and 10 inch pitch Biela propeller[48]. In Figure 6-15, the BSFC is plotted against the dimensionless power that was obtained as the ratio between the instantaneous power and the maximum engine power recorded in the test.

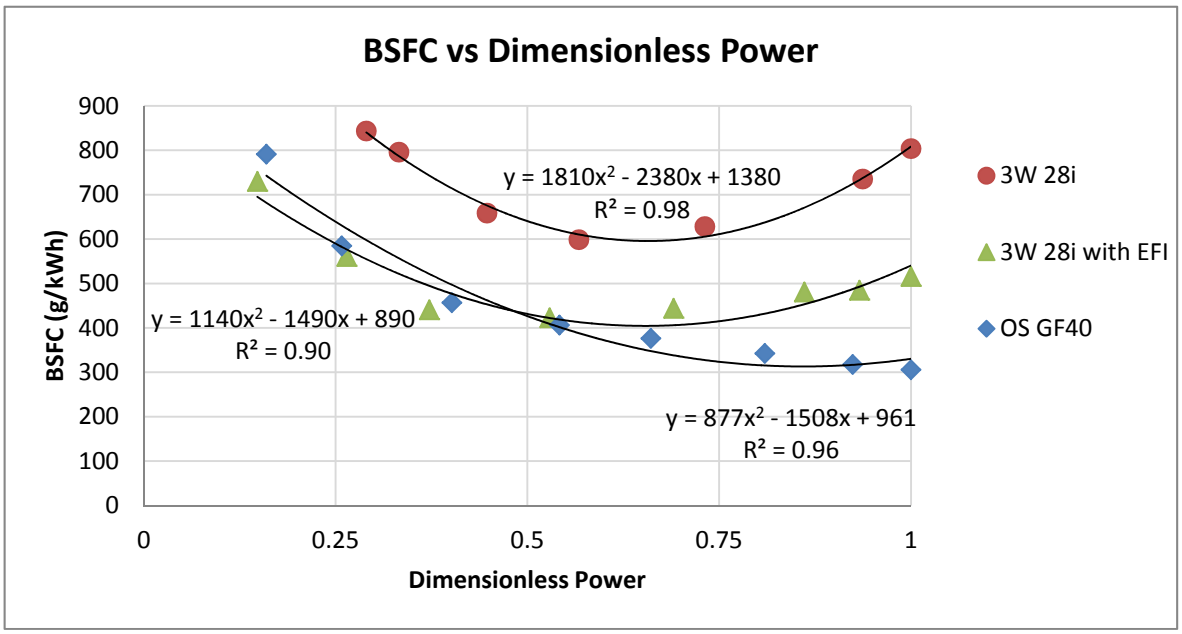

Figure 6-15 – BSFC curves for a two-stroke petrol engine (3W 28i) with and without EFI, and a four-stroke petrol engine (OS GF40). The test was performed using a two-bladed 18x10 inch Biela propeller at 10°C in static flow condition.

Figure 6-16 shows a comparison between the static thrust values measured in the engine test cell and the static thrust calculated using the following formula

$$T = C_T \rho f^2 d^4 \qquad 6\text{-}2$$

where T is the thrust produced (N), ρ is the air density (kg/m^3), f is the frequency of rotation (Hz) and d is the propeller diameter (m). C_T is the coefficient of thrust that depends on the propeller geometry and the airflow characteristics, such as the propeller advance ratio, the Reynolds number, and the Mach number at the propeller tip. The power P required to spin the propeller at the frequency of rotation f is

$$P = C_P \rho f^3 d^5 \qquad 6\text{-}3$$

[47] By assuming that C_P is constant in static flow condition, the engine power output can be directly linked to the frequency of rotation using equation 6-3.
[48] Propellers' dimensions (diameter and pitch) are in the vast majority of cases quoted in inch.

where C_P is the coefficient of power that depends on the propeller geometry and the airflow parameters.

In a static test with a given propeller geometry, the airflow is influenced only by f. Experimental studies on model aircraft propellers [241–243] have shown that, in static tests, C_T increases slightly with f, while is C_P is constant or slightly decreases. However, this effect is difficult to predict without an exact model of the propeller geometry. In this work, it was assumed that the variation of C_T and C_P with f is sufficiently small to be neglected during the calculation of the static thrust[49]. The calculated static thrust displayed in Figure 6-16 was obtained by using $C_T = 0.087$.

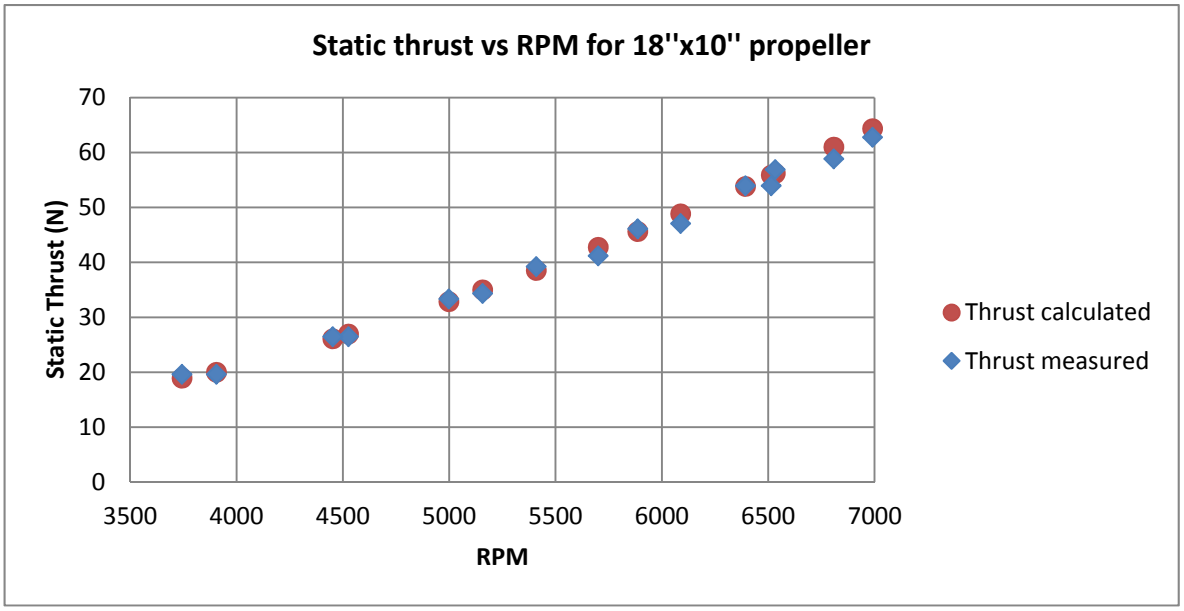

Figure 6-16 – Measured and calculated static thrust for a two-bladed 18''x10'' inch Biela propeller at 10°C.

In the initial sizing phase, the propeller diameter is matched to the engine using the regression analysis displayed in Figure 6-17. Propeller pitch in the RCFAQ database [244] presents a poor correlation with engine and propeller size. Hence, only the data from the Top-Flite manufacturer [245] were used to estimate the propeller pitch from its diameter. However, propeller's pitch can be treated as an independent variable during the aircraft sizing.

[49] The variation of the C_T and C_P are due to the local variation on the coefficient of lift and drag due to variation of the local Reynolds number. The tests performed by the University of Illinois at Urbana-Champaign were focused on small-scale propellers (most propellers tested had diameters between 7 and 11 inches) and were performed at Reynolds numbers typically between 10^3 and 10^5. The test with the largest propeller (19 inch) was performed to a Reynolds number of approximately 2.5×10^5. During the test displayed in Figure 6-15 and Figure 6-16 the maximum Reynolds number achieved was 5×10^5. The effect of the Reynolds number on the coefficient of lift and drag (and therefore on C_T and C_P) becomes less pronounces as the Reynolds number increases [230].

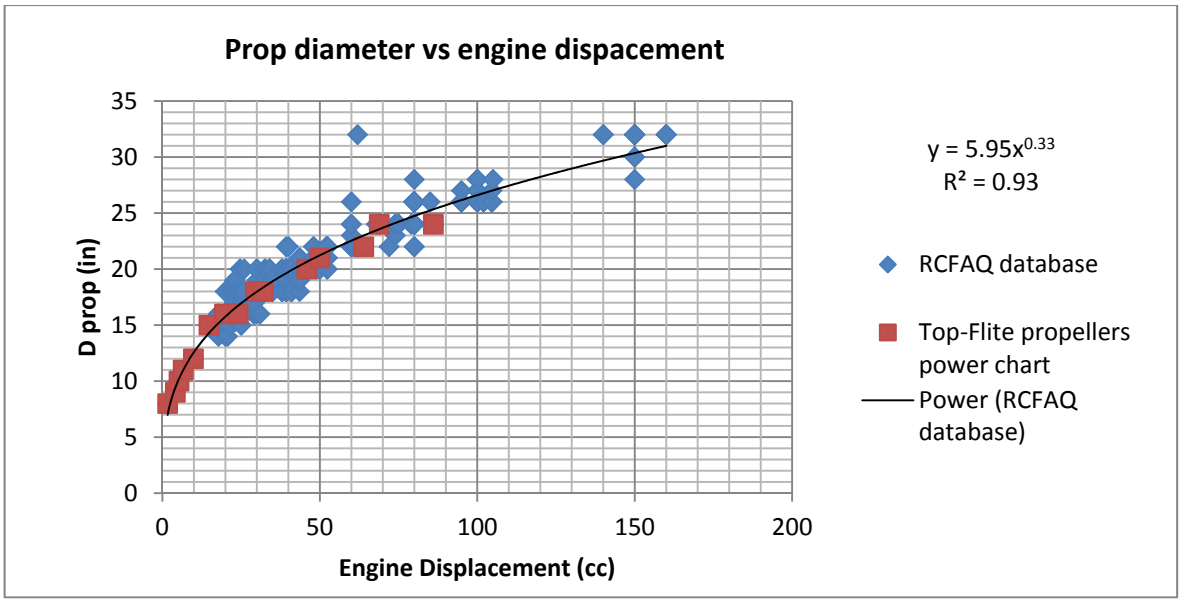

Figure 6-17 – Regression analysis for propeller diameter vs engine size. Data presented were obtained from the RCFAQ database [244] and from Top-Flite manufacturer chart [245].

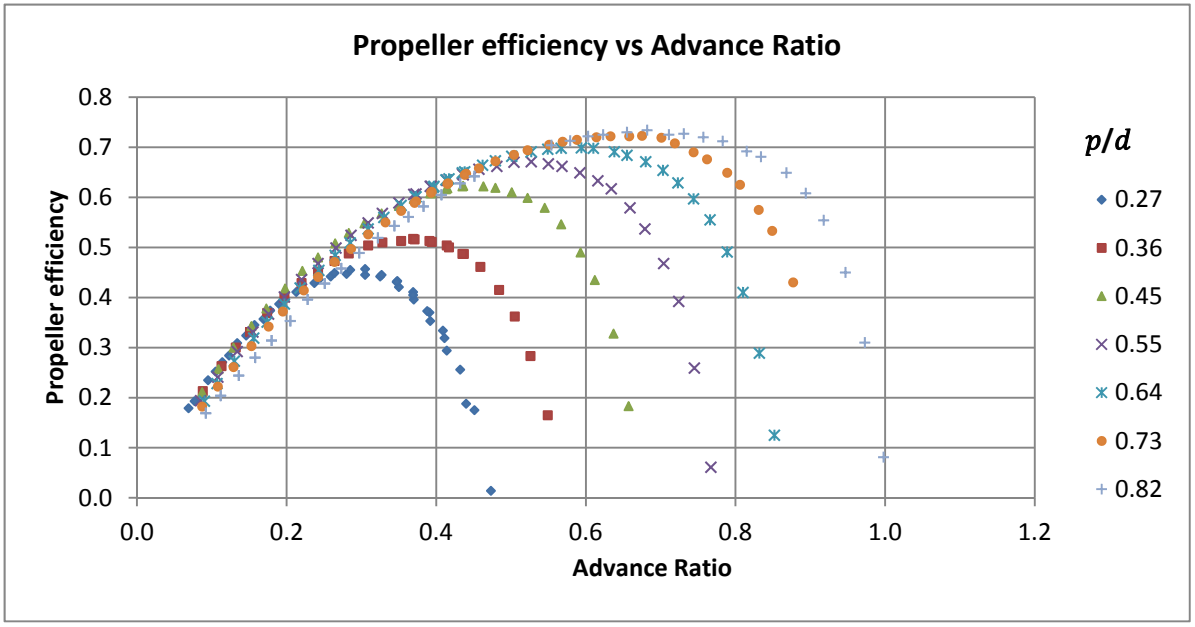

Figure 6-18 – Propeller efficiency η_{prop} as a function of the propeller Advance Ratio J and the pitch to diameter ratio (p/d). Experimental data for APC Sport propeller series (11 in diameter) [241].

Given the propeller geometry, it is possible to estimate the propeller efficiency as a function of the Advance Ratio. The propeller Advance Ratio J is defined as

$$J = \frac{v}{fd} \qquad 6\text{-}4$$

where v is the propeller forward velocity. The propeller efficiency η_{prop} is

$$\eta_{prop} = J\frac{C_T}{C_P} \quad 6\text{-}5$$

In the CDT, the value of η_{prop} as a function of J and the ratio between the propeller pitch and diameter p/d is initially estimated using an interpolation of the carpet plots shown in Figure 6-18. This plot is derived from the database published by Brandt *et al.* [241] where experimental tests of several model aircraft propellers performance are provided.

6.7.7 Performance

The Performance module calculates the most important aircraft performance including range, endurance and fuel consumption at any given speed, the maximum speed, the optimal cruise speed, the take-off and landing distances, the maximum rate of climb, and so on. The calculation relies on the coefficients obtained from the Aerodynamics, Mass and Propulsion modules.

The aircraft range and endurance are generally estimated using the Breguet equations. They are based on the assumption that the aerodynamic efficiency C_L/C_D, the propulsive efficiency η, the specific fuel consumption SFC and the true airspeed V are constant during the flight. In particular, for fuel powered aircraft, since the mass decreases over time, the assumption of constant aerodynamic efficiency is valid only if the aircraft gradually increases its altitude (cruise climb). However, the UAV will be most likely constrained to fly at a constant altitude and at a constant speed specified in the mission description. The range performance in cruise flight for a constant altitude and speed and for a drag polar in the form[50]

$$C_D = k_1 + k_3(C_L)^2 \quad 6\text{-}6$$

is given by Peckham in [246].

The range R equation 6-7 was derived for the more general case in which the drag polar is in the form of Equation 6-1 and the assumptions of constant specific fuel consumption SFC and propulsive efficiency η in the flight segment are kept

$$R = u\frac{2}{c}\left[\tan^{-1}\left(\frac{b}{c} + \frac{2}{c}W_1\right) - \tan^{-1}\left(\frac{b}{c} + \frac{2}{c}W_2\right)\right] \quad 6\text{-}7$$

where

[50] The coefficients k_1 and k_3 are defined in Equation 6-1.

$$u = q\frac{\eta}{SFC}\frac{S}{k_3} \tag{6-8}$$

$$a = \frac{k_1}{k_3}(qS)^2 \tag{6-9}$$

$$b = \frac{k_2}{k_3}qS \tag{6-10}$$

$$c = (4a - b^2)^{1/2} \tag{6-11}$$

$$q = \frac{1}{2}\rho V^2 \tag{6-12}$$

and ρ is the air density, V is the flight speed (true air speed), S is the wing area, W_1 and W_2 are the aircraft weight at the beginning and at the end of the flight segment respectively.

The fuel weight W_{fuel_b} burned after flying for the distance R at the speed V and at the altitude corresponding to the air density ρ, given the initial weight W_1, is

$$W_{fuel_b} = W_1 - \frac{c}{2}\left\{\tan\left[\tan^{-1}\left(\frac{b}{c} + \frac{2}{c}W_1\right) - \frac{R}{u}\frac{c}{2}\right] - \frac{b}{c}\right\} \tag{6-13}$$

While the weight of fuel W_{fuel_n} necessary to flight a distance R given the above flight conditions and for a given dry weight of the aircraft W_{dry} is

$$W_{fuel_n} = \frac{c}{2}\left\{\tan\left[\tan^{-1}\left(\frac{b}{c} + \frac{2}{c}W_{dry}\right) + \frac{R}{u}\frac{c}{2}\right] - \frac{b}{c}\right\} - W_{dry} \tag{6-14}$$

The assumption of constant SFC and propulsive efficiency η are not exact either: as the aircraft burns fuel, it gets lighter and a different engine output is required to keep the same speed and altitude. However, this inaccuracy can be limited by considering sufficiently small flight segments.

The other performance parameters are obtained by using the drag polar to compute the power required to flight at any given speed, altitude and mass and comparing it with the available propulsive power. Climb rate is obtained using the power excess approximation.

The take-off distance is calculated by integrating the instantaneous acceleration of the aircraft during the take-off run and until a 10 m obstacle is cleared. The acceleration is estimated using the aircraft mass and the estimated values of thrust, lift, aerodynamic drag and rolling resistance as a function of the aircraft speed. In order to obtain a conservative calculation, it is assumed a wind speed of 0 m/s in the direction of take-off. The landing distance is obtained in a similar way.

6.7.8 Avionics and Payload

Avionics systems include the flight control systems, the command and control communication link, the power management system and wiring of the airframe. These functions were not explicitly modelled in the CDT[51]. However, the cost and mass of the avionics systems were accounted for during the sizing operation. The avionics cost and mass estimate was based on the components available in the model aircraft market and the systems used on UAVs built at the University of Southampton. A list of the main avionics components was also created as an input to the Reliability model of the Operational Simulation.

The payload mass is considered an input to the system sizing. It is assumed that the payload consists of a camera and an automatic target detection system. A functional model of the payload is present in the operational simulation and briefly discussed in Section 6.8.2.3.

There are no data in the literature providing indication of the relationship between the mass of such payload systems and their performance. However, intuition suggests that the payload mass is positively correlated with the quality of the camera and automatic target detection system[52]. Therefore, a very simplistic model, based on the best judgment of the author, has been developed to link the payload performance to its mass[53].

The model assumes that the total mass of the payload (including camera, target detection system, batteries and supporting systems) is between 1 and 5 kg. The performance of the payload is linked to its mass using the following relations.

$$FOV_{H,V} = 20° + 5° \frac{W_{Payload}}{W_{Payload\_Max}} \qquad 6\text{-}15$$

[51] The range of the command and control communication link, as well as of the payload data link can be the limiting factors to the operational range of the UAV. The omission of a functional model for the communication links is justified by the following assumptions. In this study, it is assumed that most of the tasks performed by the UAV are completely autonomous or pre-programmed. It is also assumed that the requirements of the communication link can be satisfied through the use of low data rate satellite communication (for example, it is assumed that the payload data link is used to communicate the position of the target rather than pictures or videos).

[52] The payload mass can be linked to the performance of the camera target detection system in a number of ways. For example, larger camera lenses and sensors, anti-vibration systems, anti-fog systems, more powerful computers and larger batteries are examples of possible improvements over a baseline system that would be positively correlated with an increase in the system mass.

[53] By using a very simplistic model based on engineering judgment, the user can have an initial estimate of the importance of the aircraft payload capacity on the mission performance. The model can be easily replaced by a more accurate one once enough information about the mass-performance trade-off of the payload system has been acquired.

$$CDF = \frac{1}{2}\left(1 + \frac{W_{Payload}}{W_{Payload\_Max}}\right) \quad 6\text{-}16$$

where $FOV_{H,V}$ is the angular field of view of the camera system in the horizontal and vertical direction[54], $W_{Payload}$ is the payload system mass and $W_{Payload\_Max}$ is the mass of the heaviest payload considered in the study. CDF is the camera detection factor that is a scaling factor that reduces the probability of detecting the target calculated by the payload module in the ideal case. These equations imply that the UAV payload will have a field of view between $21°$ and $25°$ that correspond to a moderate zoom level (a focal length of 50-70 mm on a typical crop frame digital single-lens reflex camera). It is assumed that a heavier payload is able to process data from a wider FOV. It is also assumed that the payload mass is positively correlated with the quality of the camera and automatic target detection system (a 1 kg payload having a 40% lower probability of detecting the target than a 5 kg one).

6.7.9 Cost

The estimation of the cost involved in the development, procurement and operations of the product is a fundamental requirement for any value-based design methodology. Many examples can be found in the literature of aircraft design optimisation studies that used the minimisation of the Life-Cycle Cost (LCC) as objective functions [247–249]. Examples of cost estimation as a design decision and optimisation support tool were provided by Scanlan *et al.* [222] and Curran *et al.* [250].

The cost analysis relies on the use of Cost Estimation Relationships (CER) that link the system parameters to its cost. Many different models exist; extensive reviews can be found in the literature [24,27,251,252].

The classic cost estimating techniques can be divided into four categories [253]:

- The intuitive techniques rely on the judgement of experts that use their knowledge and experience to estimate the cost of a product, component or process. They can also provide simple relationships to scale the cost according to some key parameters.
- The analogical methods estimate the cost of the current project by comparison with similar past projects. This method is very useful at the early stages of system development when limited information about the system is available. However, it requires a database of sufficiently similar projects.

[54] Most digital cameras have individual sensors (i.e. pixels) arranged in rectangular arrays defined focal plane array. Here the horizontal and vertical direction are referred the orientation of the focal plane array.

- The parametric methods relay on the establishment of causal relations between a number of parameters (referred as cost drivers) and the cost of the project. These relations are typically obtained from regression of historical data. These methods are also referred as top-down approach.
- Finally, the analytical methods obtain the final cost by modelling the cost associated with the various phases and components of the project. For example, the production cost is obtained by calculation the raw material quantity and cost, the labour time and cost, and so on. The analytical methods provide the most accurate estimate of the real cost and provide a clear understanding of the cause-effect relationships. On the other hand, they are difficult to implement and require a detailed description of the product, technology and processes. These methods are also known as bottom-up approach.

A well-known CER tool for manned military aircraft conceptual design is the DAPCA (Development and Procurement Costs of Aircraft) model developed by the RAND Corporation [254]. This model estimates the cost of engineering, material and manufacturing costs based on some basic performance such as the maximum aircraft speed and the empty mass. Unfortunately, a similar tool for unmanned aircraft has not been developed yet. Part of the problem lies in the limited historical data available, but the greatest obstacle is probably represented by the great heterogeneity of the UAV systems which span several orders of magnitude in size, mass and complexity [219]. The situation is even worse for civil UAV systems, for which virtually no reliable cost data are available.

Attempts to develop CERs for military unmanned aircraft have been presented by Cherwonick [255] and Valerdi [256]. They are both based on the regression of cost data of military UAV correlated to general performance or mass.

In the presented work, the LCC of the UAV system has been estimated as

$$LCC = C_{SA} + C_{Ops} \tag{6-17}$$

where C_{SA} is the acquisition cost of the UAV system (the cost that the end-user has to pay to obtain the system) and C_{Ops} is the operational cost. The cost of disposal has been neglected for simplicity. The operational cost will be discussed in Section 6.8.1.

The acquisition cost is obtained as

$$C_{SA} = C_{Unit}\, N_u + C_{GS} \tag{6-18}$$

C_{Unit} is the unit cost of the UAVs, N_u is the number of UAV purchased and C_{GS} is the cost of the ground systems. Little information is available on procurement cost of the UAV ground control stations and communications equipment and no CER is available in the literature. Here, it is initially assumed that the cost of the ground systems is equal to the unit cost of the UAV as suggested by Chaput [257].

The unit cost is estimated using an activity based hierarchical model developed in Vanguard Studio® [258] and displayed in Figure 6-19.

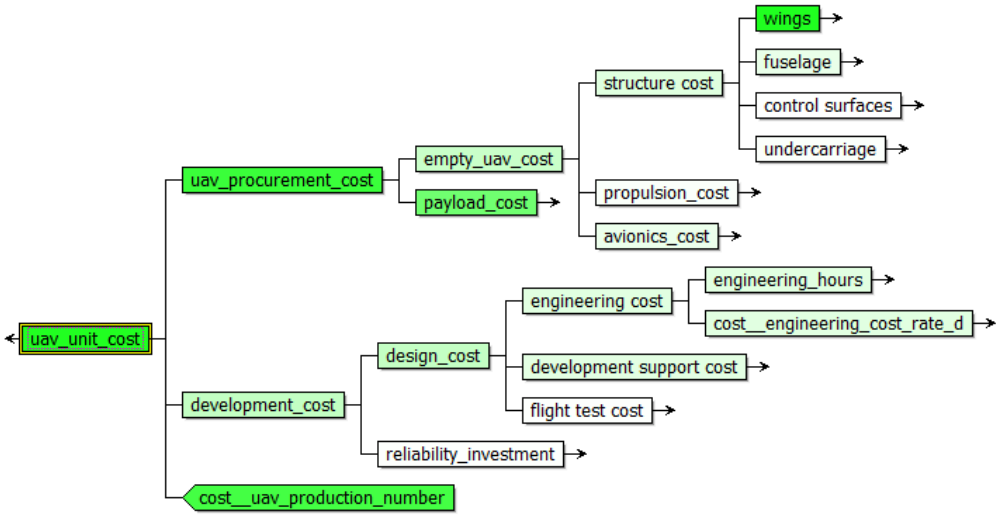

Figure 6-19 – UAV unit cost estimation model (excerpt). The colour of the nodes reflects how strongly a small change in each node's value impacts the value of the UAV unit cost; green indicates a strong positive influence and red a strong negative influence.

The unit cost is obtained as a sum of procurement cost and development cost. The procurement cost is obtained as a sum of the empty UAV cost and the payload cost.

The empty UAV cost is split into structure, propulsion and avionics cost. For each of these, there are further subcomponents. For example, the structure cost is divided into wing, empennage, fuselage and undercarriage cost. For each component, the cost is estimated as a sum of the raw material and the tooling and labour cost needed. These are computed using the aircraft dimension and parameters as input. Figure 6-20 shows an example of cost breakdown for the baseline structure of the wing. Such a detailed model is only possible if the main characteristics of the structural design and the manufacture processes used for the production of the airframe are known. In this work, it was assumed that the airframe components were designed and built according to the principles and manufacturing techniques described in Section 6.6.1 and Chapter 4. This model requires the introduction of parameters that are solely related to the

manufacturing process (for example the labour cost, the material cost, and so on) but are still controlled through the CDT.

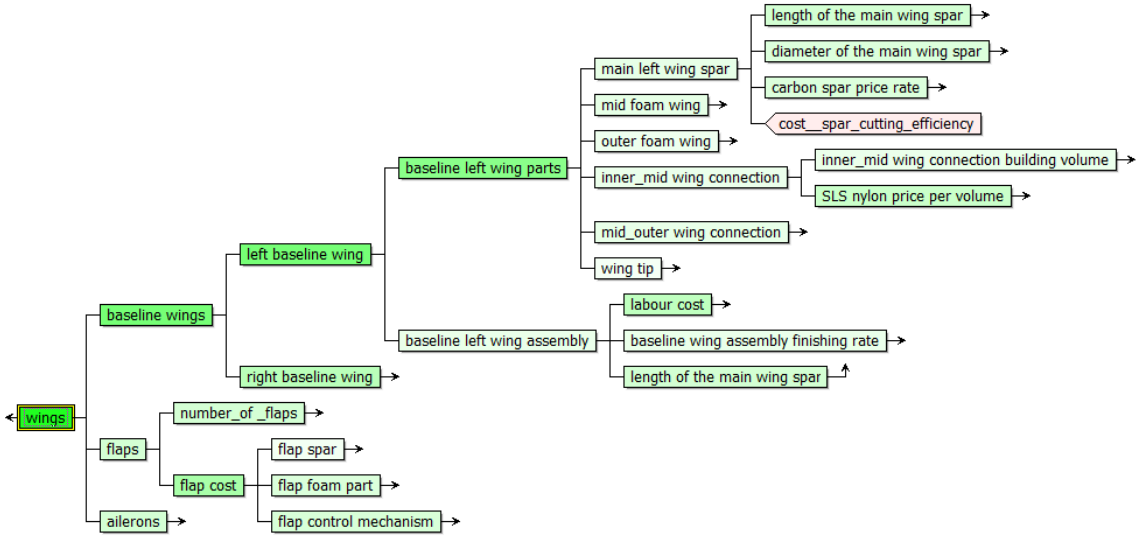

Figure 6-20 – Wing cost estimation model (excerpt).

The payload cost can vary considerably depending on the nature of sensors, on-board intelligence, link range and bandwidth. For this study, a simple equation linking the payload mass $m_{Payload}$ to its cost $C_{Payload}$ was used

$$C_{Payload} = k_{payload} m_{Payload} \qquad 6\text{-}19$$

The initial estimate of the value of $k_{payload}$ was selected as 5500 £/kg[55].

No reliable model exists to estimate the development cost of the small low-cost system described in this work. However, here a simple model has been used in which the development cost is obtained as a sum of engineering cost, development support cost and flight tests cost. These costs have been estimated using the DAPCA IV model as modified by Raymer [37]. However, Gundlach [219] suggests that the engineering hours and development cost of a small UAV can be estimated as one tenth of the ones necessary for manned aircraft. The author's experience confirms that the DAPCA model overestimates the development time and cost by approximately an order of magnitude. Therefore, a correction factor of 0.1 has been applied to the estimate of the engineering hours, development support cost, and flight tests cost.

[55] This value is based on the author's judgement and experience and it is inspired by an analogous relationship proposed by Chaput [257] for military surveillance UAV.

The model also includes a reliability investment component, which simulates the extra cost in terms of equipment quality and extra engineering effort required to achieve a reliability improvement with respect to a baseline level. This topic is presented in more details in Section 6.7.10.

6.7.10 Reliability, Maintenance and Mishaps Models

Reliability can be defined as the ability of a system or component to perform its required functions under stated conditions for a specified period of time [259]. It is typically measured in mean time between failure (MTBF) or main cycles between failure.

Component failures affect the system mission in a number of ways. First of all, if a critical component fails, the UAV will not be able to perform its mission. Second, if repairs are possible, it will imply a cost associated with labour and material required. Third, the failure of a critical component in flight can result in the loss of the system and possible damage to nearby objects.

The benefits of an increased reliability level are difficult to estimate using conventional aircraft design tools, but in the DUADE System Design Loop it can be estimated with the support of the Operational Simulation. Therefore, the AST was provided with a reliability model linked to the Operational Simulation.

The reliability of the UAV is simulated using a model based on component failures. A table listing the most critical components is created by the designer and imported into the Operational Simulation (Table 5). The probability of component failure is approximated through Weibull probability distribution curves [260]. In this model, the failure probability density function as a function of time (or cycles) $f(t)$ is controlled by two parameters λ and β, where the latter controls the shape of the distribution (basically, the failure rate increases with time if β>0, it is constant for β=0 and decreases with time for β<0). The parameter λ can be linked to mean time before failure[56]. The following equation was used to calculate $f(t)$

$$f(t) = \begin{cases} \frac{\beta}{\lambda}\left(\frac{t}{\lambda}\right)^{\beta-1} e^{-(t/\lambda)^{\beta}}, & t \geq 0 \\ 0, & t < 0 \end{cases} \qquad \text{6-20}$$

Table 5 indicates the deterioration mechanism (flight time or cycles) and the probability of the UAV crashing if the component fails. Redundant components are indicated in the last column of the table (quantity on-board). If a component fails, redundant components will prevent the UAV

[56] The MTBF can be calculated as $\text{MTBF} = \lambda \cdot \Gamma(n)$, where $n = \frac{1}{\beta} + 1$ and $\Gamma(n) = \int_0^{\infty} e^{-x} x^{n-1} dx$. The MTBF is equal to λ when $\beta = 1$ and it is 89% of λ when $\beta = 2$.

from crashing (unless all the redundant components fail during the same flight). However, the failure of a component will reduce the MTBF of the respective redundant components by a factor

$$R_{f\_i} = 0.1\frac{\lambda_i}{n_{rc\_i}} \qquad 6\text{-}21$$

where λ_i is the λ parameter of the Weibull distribution of the component i, and n_{rc_i} is the number of redundant components. The R_{f_i} factor was introduced to account for the fact that, after a component fails, each redundant component is stressed proportionally more (for example, in the case of a twin-engine aircraft, if one engine becomes inoperative, the second engine will need to output roughly twice as much power). Equation 6-21 assumes that, when multiple redundant components are present, the extra load is equally shared between them. Moreover, it assumes that the maximum reduction to the components MTBF is 10%, based on the author's judgment.

If a component fails and the UAV does not crash, the component is repaired once the UAV returns to base. The replacement time is included in the table as well. No planned maintenance operations are included in the Operational Simulation for the UAVs, while there is a planned maintenance model for the lifeboats.

Component	Deterioration mechanism	Weibull β	Weibull λ	Crash probability if fails	Replacement time (h)	Quantity on-board
Elevator control mechanism	hours	2	600	1	1	4
Rudder control mechanism	hours	2	600	0.1	1	2
Main undercarriage	cycles	2	800	0.8	1	1
Engine	hours	2	300	1	3	1
Ignition battery	hours	2	600	1	1	1
6 V flight systems battery	cycles	10	1000	1	0.5	2
GPS aerial	hours	1	1000	1	0.5	1
Autopilot	hours	1	1000	1	1	1
...	...	...	...	...	...	...

Table 5 – Components reliability model inputs (table excerpt).

Since landing accidents are one of the most frequent causes of mishaps for UAVs [261], a crash landing model was included. The model is based on the assumption that the probability of a landing mishap depends on the kinetic energy of the aircraft at landing. In the absence of reliable data that could support a more detailed model, an initial estimate of the kinetic energy-crash probability relationship was performed by the design team based on the experience of the University of Southampton with sub 20 kg UAVs landing on semi-prepared grass runways (Figure 6-21).

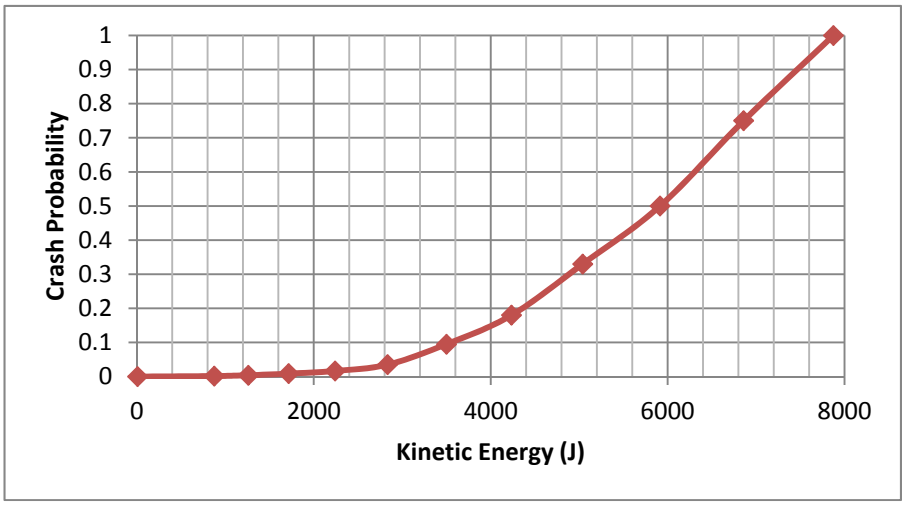

Figure 6-21 – Landing crash probability as a function of the UAV kinetic energy at landing.

6.7.10.1 Cost of Reliability Improvements

The achievement of a certain level of reliability is generally considered a design requirement rather than a design choice. However, several studies demonstrated that reliability is the prime driver in determining the operational and support cost of a product, which often represents a great part of the product life cycle cost [262]. This implies that investments in reliability improvements can generate substantial returns. However, excluding reliability targets that are established in operational and airworthiness requirements, reliability goals do not appear to be driving either management or engineering effort [263]. Part of the problem lies in the difficulty of estimating the investment required to achieve a specified gain in reliability.

Attempts to provide CERs that relate investments to reliability improvements can be found in the literature [262–265]. In particular, Forbes *et al.* [265] developed a basic model based on the regression analysis of 17 military systems (Figure 6-22). Equation 6-22 shows that the reliability investment increases with a power of the reliability improvement.

$$\frac{\text{Investment}}{\text{APUC}} = \left(\frac{\text{RIR}}{0.3659}\right)^{2.119} \qquad 6\text{-}22$$

The RIR (Reliability Improvement Ratio) is defined as

$$\mathrm{RIR} = \frac{\text{new MTBF} - \text{old MTBF}}{\text{old MTBF}} \qquad 6\text{-}23$$

where the MTBF can be replaced by the reliability measure which is more appropriate to the specific system. The reliability investment is also directly proportional to the average production unit cost (APUC), that is, it increases linearly with the complexity and size of the system. It has to be noted that the system considered in the study were very heterogeneous with respect to their technologies, size and complexity, spanning from small components to complete platforms. However, relation 6-22 seems to be valid across different technologies and systems [265].

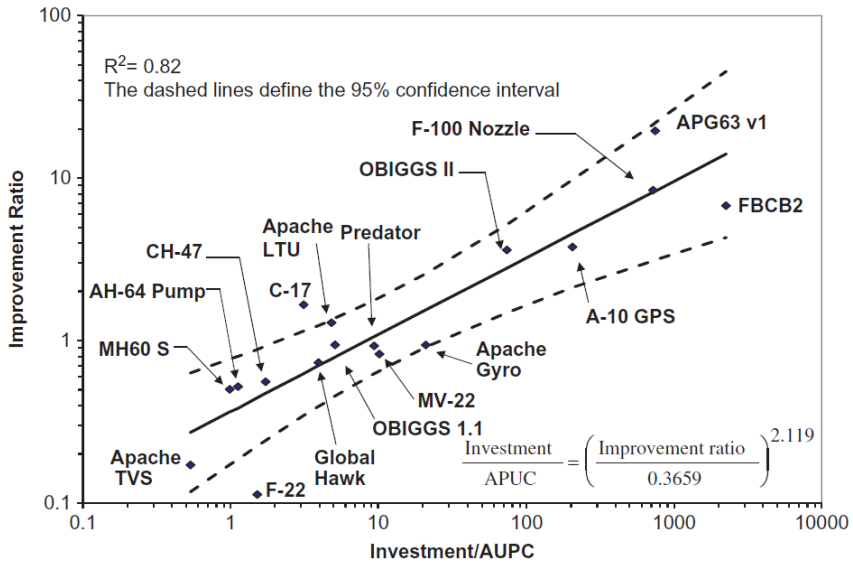

Figure 6-22 – Reliability Cost Estimating Relationship of military systems [262].

Although this study was limited to military systems and the sample size used in the regression analysis was small, equation 6-22 constitutes a very useful tool, particularly at the concept design stage, that allows the decision maker to estimate the cost of reliability improvements. In the broader context of VDD, this relation can be used to assess the benefit of increased system reliability on the mission performance versus the costs it incurs.

6.7.10.2 Weight of Reliability Improvements

The author's experience is that for small UAVs, the achievement of a reliability improvement is also linked to an increase in mass. This mass growth can be linked to the need for an increased robustness of the secondary structure which prevents damages from handling and transportation. It can also be linked to the introduction of larger and heavier servo actuators which operate at a

lower load factor. Finally, ruggedised avionics components, wiring and electrical connectors can result in a substantial mass increase.

There is no study available that can provide guidance on how to estimate the relationship between the UAV reliability improvements and the corresponding mass increments. Nevertheless, the author's opinion is that it is important to recognise that a relation between the two exists. In order to try to capture this effect, the equation 6-24 was used as initial estimate

$$\Delta W = W_0 \left(\frac{\mathrm{RIR}}{3}\right) \qquad 6\text{-}24$$

that is, it is assumed that the system mass increases linearly with the RIR and that a system that has a MTBF twice as long will be 33% heavier than the baseline.

6.8 Value Model

The implementation of the Value Model requires as input the definition of value for the project stakeholders. In Section 6.4.2 some assumptions about the problem definition phase have been made. The system mission can be summarised using the following value statement:

- "Improve the RNLI SAR mission performance by saving more lives and decreasing the cost of the operations"

This statement clearly indicates two main value drivers that are unambiguous and measurable which are the number of saved lives and the cost of the SAR operation. Intuition suggests that these goals are opposing each other, with an increase in saved lives positively correlated with a growth in operational cost. The statement is also solution neutral: the goals can be achieved using different lifeboats, changing the number of personnel involved, and so on. However, in this context, the interest is on the UAV design support framework. Therefore, the statement can be rephrased as follows:

- "Improve the RNLI SAR mission performance by saving more lives and decreasing the cost of the operations *by supporting the operations with an Unmanned Aerial Vehicle*"

This new statement introduces an additional hypothesis: only one UAV at a time will be used to support the SAR operations. This simplifying hypothesis is introduced to avoid the further complication of having to optimise the number of UAVs as well as their technical characteristics. Furthermore, it is assumed that the UAV will be designed and developed for this specific application as opposed to being acquired from the existing systems.

It is worth noting that the mission statement does not indicate any desired technical requirement for the system. In a conventional Systems Engineering process the system technical requirements would be obtained through a detailed stakeholder analysis combined with a functional analysis and allocation. The end result would be a set of targets regarding the UAV performance and characteristics (such as range, endurance, MTOM, cost, and so on). In the proposed approach, the stakeholders' analysis is performed with the primary goal of understanding the mission scenario. Part of the information acquired is indeed used to understand technical and environmental constraints that can be directly translated into system requirements (one example could be the maximum length of the runway available for the UAV). However, the main purpose of this phase is the collection of the information necessary to set an accurate operational simulation. This information includes the geographical area of interest, the number and type of vessels that participate to the SAR mission, the spatial and temporal distribution of the incidents, and details of how the rescue operation is currently performed. At the same time, a concept of operation of the UAV is created. This describes where the UAV is operated from, how the launch and recovery operations are performed, what the typical mission profile is. Information like the average distance between the UAV base station and the incidents location or the average search time of the SAR vessels can be used to design a baseline UAV. However, in this phase, there is little quantitative evidence to support decisions on system technical requirements. For example, the UAV could be designed to have enough range and endurance to support the SAR of all the incidents happening in the area or to be smaller and cheaper while being capable of supporting 80% of incident operations.

The goal of the value model is to provide the method and the quantitative analysis to help the decision maker to identify the best system for the required task. As discussed in Chapter 3, multi-objective design problems can be solved using a number of different techniques. However, in this case, the presence of only two fundamental needs of the main stakeholder – one of which is the reduction of the operational cost – makes the adoption of a Cost-Benefit model particularly attractive.

6.8.1 Cost-Benefit Model

The Cost-Benefit model was selected for this application because it allows the direct comparison of different systems on the basis of their cost and operational effectiveness.

It is worth noting that the value model assumes the "point of view" of the RNLI. Therefore, the "cost" in the CB analysis does not refer to the UAV system cost, but it is intended as the total operational cost of the SAR operation in the given area and timespan. Similarly, the "benefit" (i.e.

the number of saved lives) must be measured as the result of the collective effort of the RNLI, including both the UAV and the other vessels.

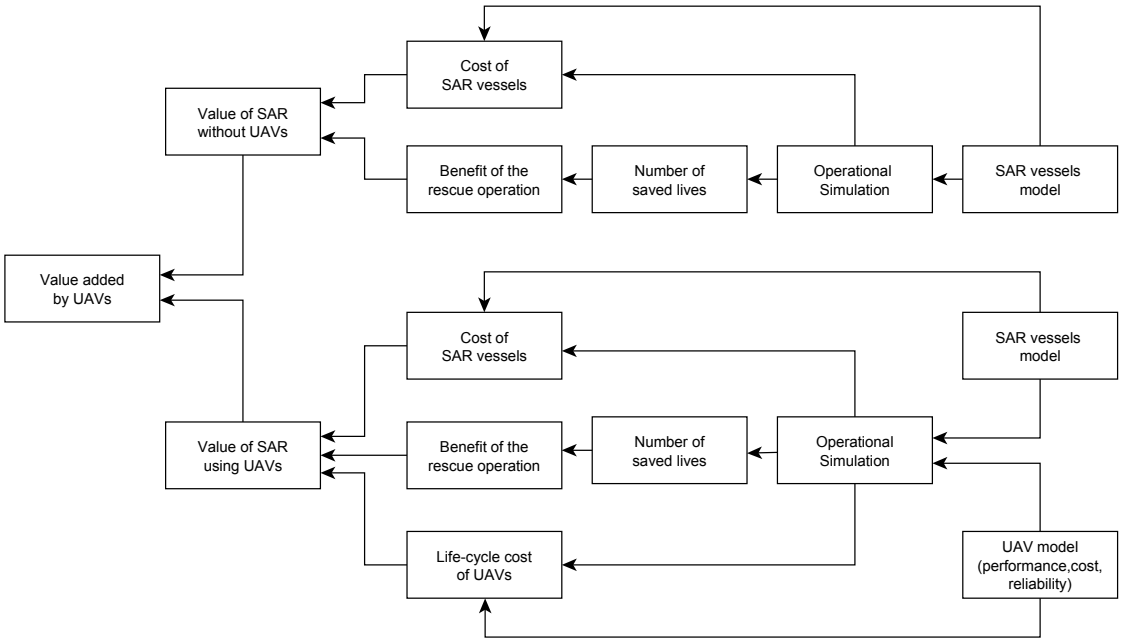

Figure 6-23 – SAR Value Model.

Figure 6-23 provides a schematic of the SAR value model. The impact of the UAVs on the SAR mission is assessed by comparing the mission performance in the case the RNLI is equipped with UAVs to the baseline case in which only the lifeboats are used for the SAR operations.

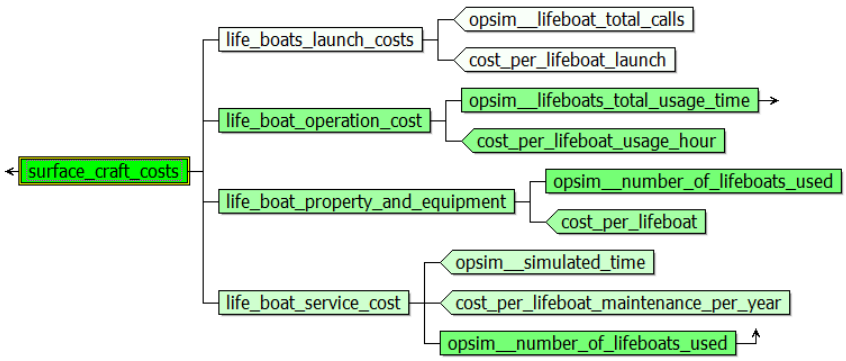

Figure 6-24 – Model of the operational cost of the SAR vessels (excerpt).

The cost of the baseline operation is obtained by calculating the total cost of the operation of the SAR vessels, as displayed in Figure 6-24. The model takes as input the output of the Operational Simulation (discussed in Section 6.8.2) such as the total number of lifeboat calls and the total time they spend in operation, the number of maintenance operations, and so on. These data are then

combined with costing parameters such as the cost of refuelling, launching and maintaining the equipment, accounting also for the cost and depreciation of the vessels in the simulated time.

The total cost of the UAV includes the unit cost of the UAVs, the ground system cost and the operational cost (Figure 6-25). The UAV unit cost was discussed in Section 6.7.9. The operational cost is obtained by using the inputs provided by the Operational Simulation and the relative cost parameters.

The impact of the UAV reliability is taken into account directly by the maintenance cost associated with components failure and by the cost of replacing the UAV when an incident results in the loss of the system. There is also an indirect cost associated with reliability, which is the degradation of the mission performance. This is also taken into account in the simulation: a less reliable UAV spends more time on the ground for repairs and has more probability of aborting a mission; hence, it results in a lower number of saved lives. UAV mishaps also have other types of indirect cost, which is bad publicity for the end user and the risk of causing damage to people or objects. These effects have been neglected in the model.

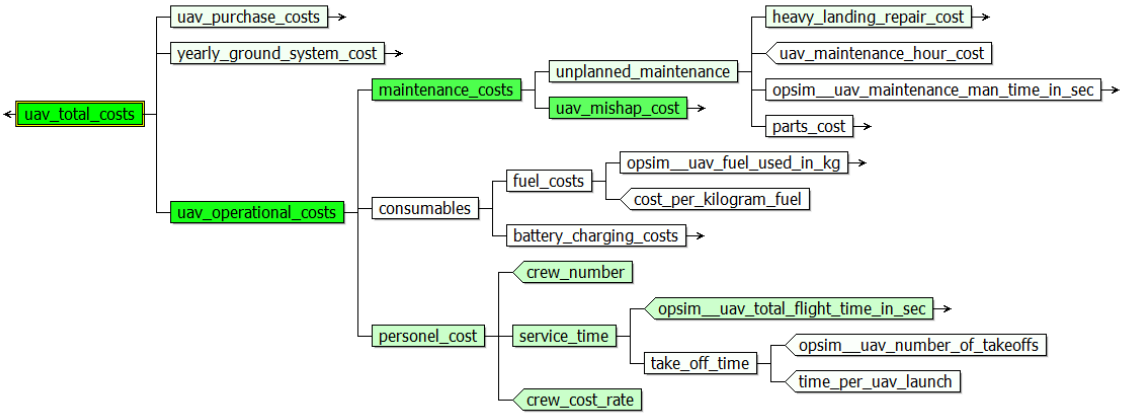

Figure 6-25 – UAV total cost (excerpt).

The Operational Simulation also provides a measure of the effectiveness of the SAR operation in terms of the number of lives saved.

6.8.1.1 Monetising the Mission Benefit

As already discussed in Section 3.6, converting the mission performance output into monetary units provides the most straightforward way to aggregate cost and benefits into a single value metric. However, in the absence of a reference market, this operation is particularly difficult. In this case study, the mission output is the number of rescued people which requires assigning a monetary value to the human life. This poses a moral problem as well as a technical one.

Nevertheless, decisions that impact people's safety and wellbeing (e.g. in the case of road works, hospitals, and life insurance) require implicitly or explicitly a judgement of this kind.

There are different possible approaches to estimate the monetary value of a human life. Here three of them are presented.

One approach is to refer to the value of a statistical life (VSL), which is the value that government agencies use to perform the cost-benefit analysis of investments in health and safety. Hence, the expected benefit of the SAR mission can be obtained as the expected number of saved lives times the VSL. For example, in 2015 the UK Department for Transport estimated the value of preventing a fatal road accident to be approximately £2M [266]. However, the estimate of the VSL varies massively depending on the methodology used and the agency performing the calculation [267]. In 2003, the median VSL was approximately £4M according to the estimate of by Viscusi and Aldy based on several worldwide market studies [268]. However, according to Doucouliagos *et al.* [269], the methods used in the literature to calculate the VLS do not account for publication selectivity bias and consequently overestimate the VSL that should be reduced by 70-80%.

An alternative approach is to extrapolate the benefit of rescuing a life from the data available about the current costs sustained by the decision makers in the SAR. By assuming that their net value is zero, one can obtain the cost per life rescued and use it as a proxy for the benefit of saving a life. By looking at the data published for the year 2011 [270], the total expenditure of the RNLI was £150.6M and the total number of people rescued 7976 (of which 354 were claimed as lives saved, i.e. where a life would have been lost if not for the intervention of the lifeguard). This means a cost of £18,900 per person rescued and £425,000 per life saved. There is a difference with the VSL approach of one order of magnitude.

A third approach would involve interviewing the decision makers and elicit their perceived benefit of a life saved. This would allow the modeller to enter non-linear value functions (i.e. the value of saving two lives might be different than twice the value of saving one).

The authors' opinion is that in this case study it is best to avoid monetising the benefit, at least in the initial trade space exploration phase. Expressing the SAR value in a single number enables an automatic candidate system ranking but at the same time hides important information. Instead, the candidate systems can be effectively compared using a bi-dimensional value plot, where the two orthogonal axes represent the two main value drivers. In this second case, the cost-benefit trade-offs can be readily understood by the decision makers. The final ranking of candidate systems can be performed a posteriori by using the most appropriate measures of the VSL.

6.8.1.2 Discount Rate

In this case study, the Operational Simulation replicates the SAR scenario for a single year only. This choice is justified by the fact that it is assumed that the UAV system development time is very short (months) and the system lifespan is limited to approximately one year at the rate of use of the simulated scenario. Therefore, the discount rate (expressing the time value of money only) has been neglected in the cost computation. The model can be easily updated to account for a multiple-years simulation by discounting the future cash flows according to the appropriate discount rate.

Risk neutrality is assumed for simplicity. This choice is justified by the discussion presented in Section 3.6.

6.8.2 Operational Simulation

The mission effectiveness of the UAV is measured through a stochastic Operational Simulation which has been developed as part of the DECODE project[57]. A more detailed description of the software is provided by Schumann [65] and Schumann *et al.* [22]. Here the basics are presented.

The Operational Simulation is an agent-based model in which the interaction of autonomous entities (agents) is simulated. The code was developed using the software AnyLogic 6.9.1 [271], which is a simulation modelling tool based on the Java programming language. In this case, the agents are represented by vessels that cooperate to accomplish the SAR mission. The vessels can be of different type: UAVs, lifeboats, helicopters, and so on. Each vessel has its own properties (such as moving speed, field of view and range) and interacts with the other agents following a series of pre-established rules (for example, two lifeboats will not get too close to each other in order to maximise the search area).

The SAR simulation focuses on incidents that occur at sea and that involve people immersed in the ocean. The goal of the mission is to locate the exact position of the victims in time to rescue them. The probability of surviving is related to the time spent in water according to the curve presented in Figure 6-26. The curve is based on the assumptions of constant water temperature of 14° C and people in good health condition, fully dressed and with a lifejacket ([272]).

[57] The Operational Simulation software code was developed by Dr. Benjamin Schumann. The author of this thesis contributed by designing the UAV mission profile and defining the mission logic, developing the UAV model used in the operational simulation, and by developing the software used to calculate the aircraft performance.

The geographical position (Figure 6-2), the temporal distribution and type of the incidents has been obtained from the historical data available from the RNLI website [214].

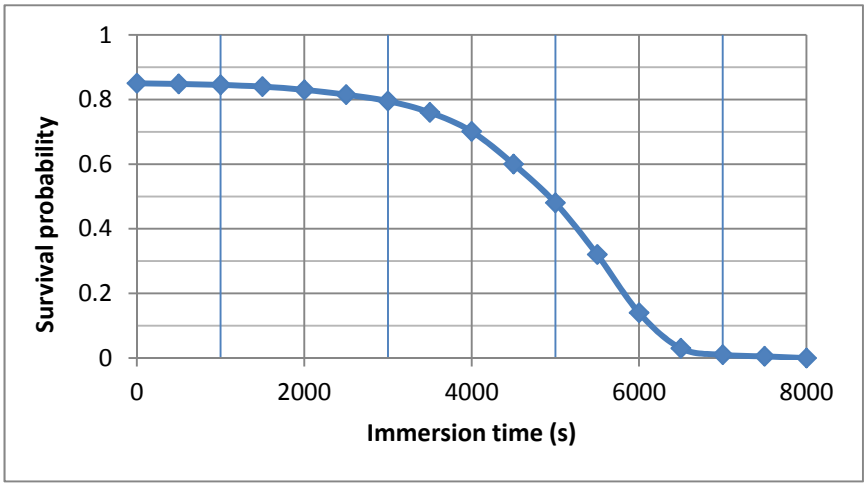

Figure 6-26 – Incident survival probability based on water immersion time [65].

When an incident occurs, the vessels are notified and they start searching for the victim. The vessels only know the position of the incident with an uncertainty that varies between 50 m and 3000 m depending on the type of incident: in some cases the victims are still in the proximity of the boats they fell off from, in which case their position is known with lower uncertainty. The UAVs operations have been modelled as follows: when an incident occurs within its operative range, the UAV takes off and dashes at maximum speed until it reaches a location near the real position of the incident, based on the position uncertainty of the incident. Then it starts the search phase: the UAV flies an expanding square pattern at a constant speed that allows the sensors to operate optimally Figure 6-27.

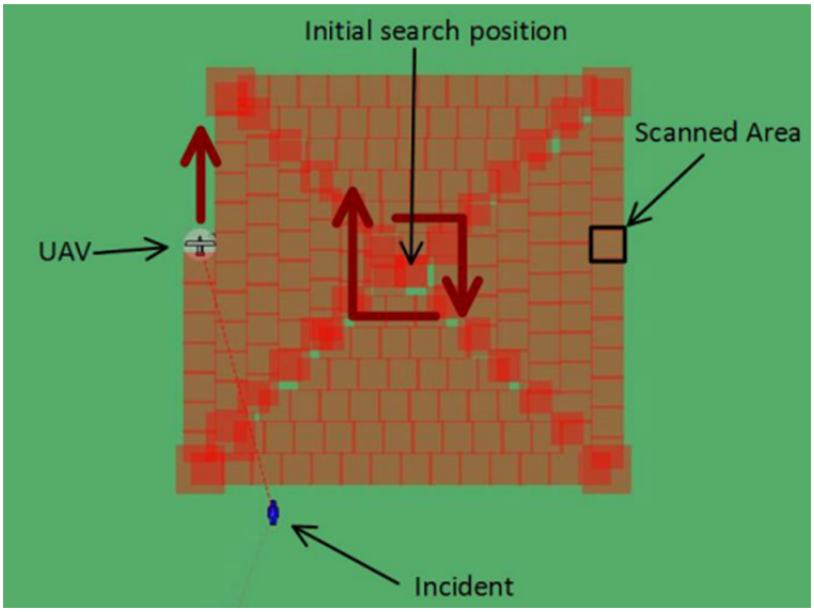

Figure 6-27 – UAV search pattern and camera footprint [65]

The pattern depends on the field of view of the on-board camera and the flight altitude. If the UAV flies over the incident, the victim position is identified with a probability that depends on the size of the target (heads of people immersed in the sea or the small boats in their proximity) and on the performance of the payload (sensors and processing system). If the victim is successfully detected, the position is notified to the operators and the closest lifeboat proceeds with the rescue operation while the UAV continues loitering over the incident position to acquire more information. False positives are possible, too: in this case, the error is detected after the UAV has spent some time loitering over the position and hence acquired more images. If another vessel spots the casualty before the UAV, the UAV is notified and flies over the location of the incident for the time required supporting the rescue operations. After the mission is completed, or earlier if the maximum flight time is reached, the UAV returns to the base to refuel and prepare for another mission.

6.8.2.1 UAV Model

During the simulation of the SAR operations, the UAV agent continuously needs to know its residual range and endurance in order to decide whether to carry on with the mission or to return to base and refuel. Plus, the simulation needs to record the amount of fuel used during the missions since this is an input to the operational cost of the UAV system. The kinetic energy at landing depends on the fuel used, too. The probability of successful target detection depends on the payload model. Finally, the UAV mishaps calculation requires inputs from the components' reliability model. All these data are obtained through the use of an aircraft model in the Operational Simulation.

Three alternatives were explored for the interface between the aircraft model and the Operational Simulation:

1 - The first option was to create lookup tables with the aircraft range and fuel consumption depending on the current mass, speed, altitude and other flight conditions. In this case, the lookup tables are uploaded into the Operational Simulation before the simulation starts and the performance parameters are obtained by interpolating the data in the tables. This approach is simple but requires a relatively large file to be shared between the aircraft model and the Operational Simulation.

2 - The second option was to create an external piece of software that the Operational Simulation can call by giving as input the current status of the aircraft (mass, fuel level, altitude, airspeed, and so on) and receiving the required performance as output. The main advantage of this approach is the flexibility: since the performance model is completely decoupled from the Operational Simulation, it can be managed externally and can be

modified for different kind of vehicles (for example one can model battery-powered UAV without having to change the Operational Simulation code). On the other hand, this approach can be computationally expensive if the communication between the two models is very frequent.

3 - Finally, the third option was to hardcode a performance model into the Operational Simulation software. In this way, the aircraft model and the Operational Simulation have to share only a minimal amount of data, required to describe the characteristics of the aircraft and its propulsive system. The computational time is reduced in comparison to option 2, but the flexibility of the model is reduced as well. Any modification to the performance model requires a modification of the Operational Simulation code.

Since the primary goal of Operational Simulation was to support the UAV design, both flexibility and speed of the simulation were important. In the end, it was decided to adopt a flexible interface that could be more easily developed and maintained. Hence, an external piece of software was developed to calculate the UAV performance[58].

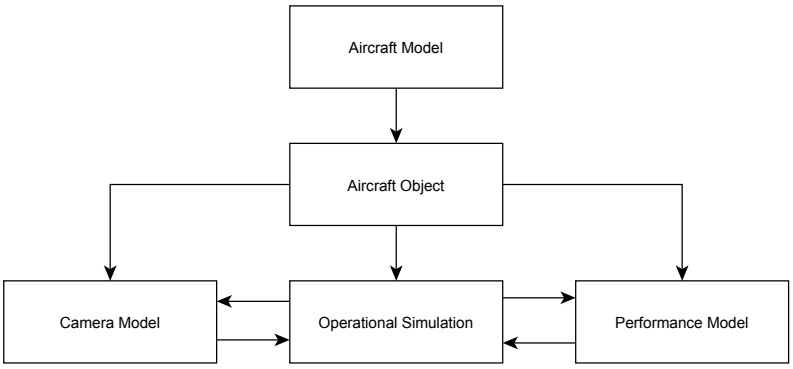

Figure 6-28 – Interface between the Aircraft Model and Operational Simulation.

The interface between the aircraft sizing tool and the Operational Simulation relies on the creation of an aircraft object (Figure 6-28). This has some properties that are relevant to the Operational Simulation only (e.g. the flying speed for each flying segment); some that are relevant to the camera model (which will be briefly presented later) and some are relevant to the performance model. The parameters are shared between the sizing tool and aircraft object using a structured text file containing the parameters shown in Table 6.

[58] The performance code was initially developed using the MATLAB® software because of the familiarity of the programmer with this language. An initial test demonstrated that this solution provides poor computational speed due to the suboptimal communication between the Java and MATLAB® based codes (every function evaluation required approximately 1 second). A second version of the performance function was coded using Java and compiled into a JAR file (Java ARchive file format). In this case, the function evaluation time dropped to 0.01 seconds which was more acceptable.

Parameter group	Parameter name	Parameter description
Aircraft size	a_wing	Wing area
	w_dry	UAV dry mass
	w_fuel	Max fuel load
	d_prop	Propeller diameter
Design performance	v_max	Maximum design speed
	v_typical	Design cruise speed
	v_stall	Lowest design speed (full flap and dry mass)
	altitude_max	Maximum design altitude
	altitude_typical	Cruise altitude
	reliability_improvement_ratio	Scaling factor for MTBF of components
Aerodynamics	k_x	Coefficients of the drag polar (cruise, take-off and landing configuration) 3x3
	cl_max	Maximum C_L of the aircraft
Propulsion	p_inst	Maximum continuous power of engine
	Rpm	Estimated engine cruise rpm
	sfc_x	Coefficients of a fourth degree polynomial for specific fuel consumption as a function of engine power output (5)
	zeta_a	Coefficients of a sixth-degree polynomial for propulsive efficiency as a function the propeller Advance Ratio (7)
Payload	camera_fov_hor	Camera field of view in the horizontal direction
	camera_fov_ver	Camera field of view in the vertical direction
	camera_pixels_hor	Number of pixels in the horizontal direction
	camera_pixels_ver	Number of pixels in the horizontal direction in the vertical direction
	camera_tilt_angle	Camera tilt angle
	camera_detection_factor	Scaling factor for the probability of target detection

Table 6 – List of parameters defining the Aircraft Model in the Operational Simulation.

6.8.2.2 Performance Model

The Performance model is used to compute the aircraft fuel consumption, endurance and range at any point in the simulation. If not specified in the UAV flight envelope or in the mission specification, the performance module can be also used to compute the maximum dash speed, the optimal flight speed that maximises range or endurance, the minimum landing speed, the climb performance and the engine power required to fly at any given speed.

The Operational Simulation performance model inputs are a set of parameters that describe the aircraft size, aerodynamics and propulsion system. The aircraft size parameters include the aircraft dry mass (i.e. with no fuel on board), the wing area and the maximum fuel mass. For the drag polar of the aircraft a parabolic approximation is used (described in Equation 6-1).

The maximum coefficient of lift is an input, as well. It is used to compute the optimal landing speed depending on the aircraft mass (which depends on the fuel on board at the moment of touch down). The propulsion parameters include the maximum continuous available power, the engine rpm, the diameter of the propeller and the coefficients of a fourth-degree polynomial describing the specific fuel consumption as a function of the engine output power and a sixth-degree polynomial describing the propeller efficiency curve as a function of the flight speed and rpm.

The Operational Simulation performs its computations at discrete time samples. During the time intervals, the UAV is assumed to fly at constant speed and altitude. The Operational Simulation calls the performance model using as input the distance flown during the last interval, the mass at the start of the interval, the altitude, and speed. It receives in output the mass of burned fuel and the maximum range at the specified return speed. The maximum range is compared to the distance from the UAV base and is used to check whether or not the UAV should abort the mission and return to base.

Similarly, a list of critical aircraft components (e.g. the one shown in Table 5) is passed to the Operational Simulation that at each time interval calculates subsystem failures using the internal reliability model.

6.8.2.3 Payload Model

The main purpose of the UAV in the simulated scenario is to provide a platform for optical sensors. In particular, it is assumed that the UAV is provided with a camera and an on-board processing system that is able to detect and recognise a target with a certain probability.

The camera model[59] is based on the model provided by Gundlach [219]. It takes as input the details of the camera system (such as field of view, number of pixels, and so on) and the flight altitude of the UAV and computes the camera footprint on the sea surface. If a target enters within the scanned area, the model computes the probability of detecting that target as a function of the size of the target and the properties of the camera system.

[59] The computer code of the Camera Model of the Operational Simulation was developed by Dr. Amrith Surendra.

In particular, the probability of detecting a target P_{TD} is calculated using the Johnson criteria [273] using the following equation:

$$P_{TD}(N) = \frac{\left(N/N_{50}\right)^{2.7+0.7\left(N/N_{50}\right)}}{1+\left(N/N_{50}\right)^{2.7+0.7\left(N/N_{50}\right)}} \quad 6\text{-}25$$

where N is the number of cycles of the target[60]. N_{50} is the number of cycles that correspond to a 50% detection probability. According to the Johnson criteria, N_{50} is equal to 0.75 for target detection[61].

N can be calculated by knowing the characteristic dimension of the target d_c, and the average ground sample distance GSD_{av}. By assuming that the targets appear as bi-dimensional objects when seen from the UAV flight altitude, the target characteristics dimension can be calculated as

$$d_c = \sqrt{w_t\, l_t} \quad 6\text{-}26$$

where w_t and l_t are the width and the length of the target. The GSD_{av} is the average of the horizontal ground sample distance GSD_H and vertical ground sample distance GSD_V[62]. These can be calculated using the following equations

$$GSD_H = 2\tan\left(\frac{FOV_H}{2\,Pix_H}\right) R \quad 6\text{-}27$$

$$GSD_H = \frac{2\tan(0.5\,FOV_V\,Pix_V)}{\cos(\theta_{Look})}\,R \quad 6\text{-}28$$

where FOV_H and FOV_V are the field of view in the horizontal and vertical direction; Pix_H and Pix_V are the number of pixels in the horizontal and vertical direction, respectively. R is the distance between the camera lens and the target, and θ_{Look} is the look angle; both this parameters are defined in Figure 6-29, where *h* is the flight altitude and *GR* is the ground range from the target.

[60] The number of cycles of a target is obtained by substituting the target image with pairs of black and white lines orthogonal to the direction of the characteristic dimension. Each pair of lines is a cycle and requires two pixels to be detected.

[61] Detection is defined as the probability of an imagery feature to be recognized to be part of a general group (i.e. ship, people, aircraft, and so on). Johnson criteria also provides N_{50} values for recognition and identification which require a higher level of details to be recognized.

[62] Here it is assumed that the horizontal row of the focal plane array of the camera is aligned with the horizon.

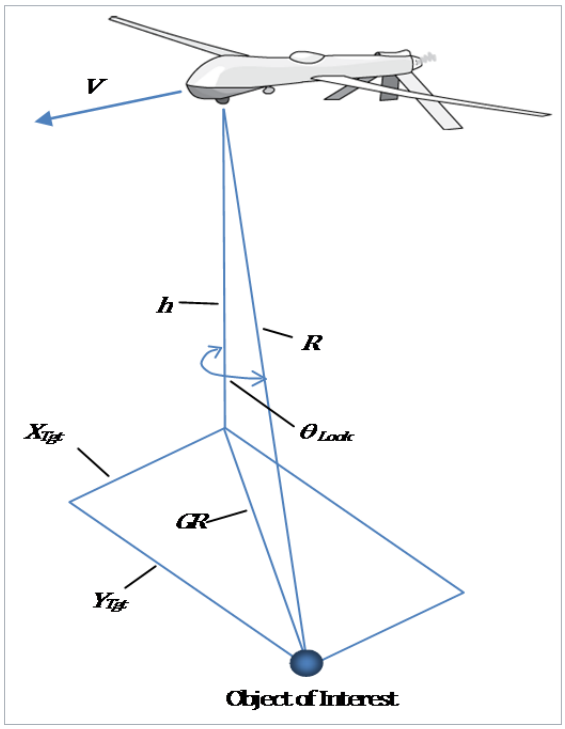

Figure 6-29 – Geometry of airborne imagery collection [219].

The number of cycles for a given target is

$$N = \frac{d_c}{2\ GSD_{av}} \tag{6-29}$$

Equation 6-25 provides the upper limit for the probability of detecting the target given its size and the properties of the camera system. However there are a number of additional factors influencing the probability of target detection. Some of these factors are related to the performance of the payload system (i.e. the quality of the lens, the amount of vibration, the quality of automatic target detection algorithm, and so on); some other factors are environmental (the quantity of light on the scene, the presence of fog or rain, and so on). For simplicity, the latter effects have been neglected in this initial study. To account for the effect of the performance of the payload, the probability of the payload automatically detecting the target P_{PTD} is obtained using the following equation

$$P_{PTD} = P_{TD}\ CDF \tag{6-30}$$

where CDF is the camera detection factor, defined in Equation 6-15.

The properties of the camera and the image processing system are linked to the payload mass as discussed in Section 6.7.8.

6.8.3 Output of the Operational Simulation and Numerical Noise

The Operational Simulation provides the user with a vast set of information regarding the mission performance. The number of saved lives, the UAV total flight time, the fuel used, the number of maintenance operations are few examples. These outputs are combined in the Cost-Benefit analysis tool but remain accessible to the designer for deeper analysis of the mission simulation.

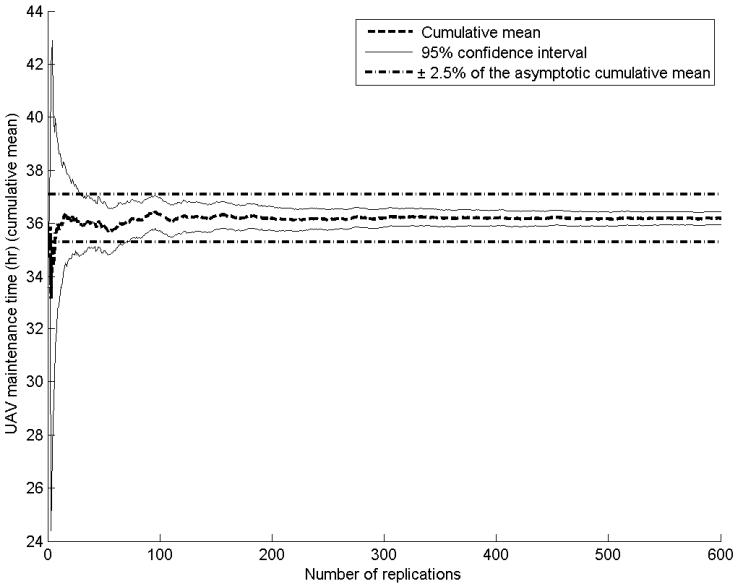

Figure 6-30 – Graphical study of the cumulative mean and confidence interval of one of the outputs of the Operational Simulation.

There are five random variables that influence the output of the Operational Simulation: the probability of a component's failure, the probability of the UAV crashing as a consequence of a component's failure, the probability of a landing mishap, the probability of target detection of the payload system, and the parameter governing the uncertainty of the incident position. Because of the stochastic nature of the Operational Simulation, the output can vary at each replication of the simulation. Therefore, the Monte Carlo method is used to obtain the results of the simulation and the sample mean and standard deviation of all the outputs are saved in the output file. The number of individual replications[63] used in a particular study depends on the trade-off between the width of the desired confidence interval of the outputs and the computational time available. By increasing the number of replications, the sample means approximate the real means of the

[63] Here, the term "replications" is used to indicate several independent repetition of the stochastic simulation with independent inputs. Instead, the term "iterations" is used when the output of the n^{th} simulation influences the output of the n^{th}+1 simulation.

outputs with increasing accuracy. However, a practical stop criterion is needed to establish a compromise between accuracy and computational cost.

In this study, the number of replications has been selected according to the graphical, and confidence interval methods proposed by Robinson [274]. In particular, the confidence interval method is based on the monitoring of the ratio between the width of a specified confidence interval (for example the 95% confidence interval) and the sample mean, as a function of the number of replications n. The number of replications is considered sufficient if

$$\frac{CI_{width}}{\mu} \leq \varepsilon \tag{6-31}$$

where CI_{width} is the width of the confidence interval, μ is the sample mean, and ε is a user specified error value. For the results presented in this work, ε was set to 0.05 and the 95% confidence interval was studied.

Given a sample of n replications, the 95% confidence interval $CI_{95\%}$ for the mean value can be calculated as

$$CI_{95\%} = \mu \pm t\frac{s}{\sqrt{n}} \tag{6-32}$$

where s is the sample standard deviation, and t is a value of the Student t-distribution that depends on the distribution degrees of freedom $(n-1)$ and the significance level (in this case it is 5% that corresponds to a 95% confidence interval). The confidence interval width is

$$CI_{width} = 2t\frac{s}{\sqrt{n}} \tag{6-33}$$

Figure 6-29 shows an example of graphical study of the cumulative mean and confidence interval for one of the most critical outputs: the total maintenance time of UAV during the simulated time. The study was performed by running the computer simulation six hundred times and calculating the cumulative mean of the UAV maintenance time. The curves display the cumulative mean, the 95% confidence interval and the ±2.5% error with respect to the asymptotic value of the cumulative mean.

The picture shows that one hundred repetitions are sufficient to obtain an estimate of the output mean value within a ±2.5% error. However, the cumulative mean curve is not sufficiently flat (minimal variability and no upward or downward trend) until about two hundred replications. An analogous study was performed for each of the outputs of the Operational Simulation. Two hundred replications were found to be sufficient to satisfy the stop criterion.

6.9 Assumptions and Limitations

The application of the DUADE workflow to a specific design problem has allowed the study of the practical implementation of a VDD framework. Several assumptions have been introduced regarding the operational environment and the stakeholders' value perception (Section 6.4), as well as the UAV configuration and building techniques (Sections 6.6 and 6.6.1), and the agents behaviour and mission profiles (Section 6.8.2). Nevertheless, the methodology can be applied to different missions and aircraft configurations.

The outcome of DUADE is affected by uncertainty, which can be classified as either aleatory or epistemic. Aleatory uncertainty is related to the inherent randomness of some phenomena and cannot be reduced by increasing the knowledge about the problem or by taking measures and conducting experiments. The random numbers used in the Operational Simulation are used to model aleatory uncertainty.

Epistemic uncertainty, instead, is due to the incomplete knowledge about the problem. Therefore, epistemic uncertainty is more difficult to control and quantify. In particular, there are three main factors of epistemic uncertainty in DUADE:

- The scenario uncertainty is due to the lack of knowledge about the decisions of the agents in future situations as well as about changes in the operational environment and other factors that may influence the development of the system of its operative life.
- The model uncertainty refers to the algorithms and mathematical relationships that are used to replicate and predict reality. DUADE modules are based on disciplinary models that use approximations, assumptions and judgement to obtain estimate of the future characteristics of UAV (such as its unit cost, performance or mission effectiveness).
- The parametric uncertainty is due to the lack of knowledge of the inputs of the various models used in DUADE. Examples of parametric uncertainty include the unit cost of a particular material or process, the MTBF of a particular component, and so on.

The study of the impact of uncertainty on the outcome of design decision is beyond the scope of this research[64]. Instead, this work is focused on the design insights that can be gained by the trade space exploration allowed by a design environment based on VDD and life-cycle simulation. Nevertheless, the reader should be aware of the following factors that can impact the quality of the results:

[64] Reviews of uncertainty based design methodologies and life-cycle cost estimation techniques are given by Yao et al. [302] and Goh et al. [27].

- The uncertainties concerning the aircraft properties were not modelled in this study: particularly at the beginning of the development cycle, there are many unknowns and decisions yet-to-be-made about the system properties. These can result in a poor estimate of the system cost and performance and therefore drive the design decision toward a suboptimal system.
- The disciplinary analyses are based on approximate models and therefore produce approximate results. Physics-based high-LOD models are available only for a few of the disciplinary modules. Nevertheless, a VDD approach cannot exist without the models of the other disciplines. Some coarse assumptions had to be made relying on engineering judgment (for example regarding the probability of a mishap occurring during landing, or the relationship between payload quality, cost and its mass, and so on). The quality of these approximations directly affects the quality of the value analysis.
- The Reliability Module is based on a number of assumptions whose accuracy is difficult to assess in the absence of extensive reliability data. For example, the deterioration mechanism of each component is linked to a single Weibull distribution and to a single deterioration mode. The parameters of the Weibull distribution have been estimated using the judgment and experience. The decrease of the life span of the redundant components is based on an unverified assumption. Similarly, the mass penalty of increased reliability components is based on the author's judgment.
- The stakeholders' value drivers are simplistic and do not account for secondary effects. For example, a UAV mishap can have a negative impact in terms of negative publicity, hence increasing the "cost" of mishaps. Similarly, the system benefit could include a model of the life hazard for SAR volunteers and link it to the UAV effectiveness. Other secondary attributes might be important for the stakeholders, such as noise, pollution, and so on.
- The effect of weather is not modelled in the operational simulation. Strong wind, precipitation and the sea state can affect the operational performance of the SAR agents favouring the use of UAVs or surface vehicles depending on the particular condition. This effect has been neglected in this study.
- The assumption of risk neutrality might not hold for the RNLI that is a charity with limited resources.
- The implication of the current legal requirements for operation of UAVs beyond visual line of sight has been neglected in this study. To date, UAVs with a dry mass between 20 and 150 kg (LUAS) can obtain an exemption from the airworthiness certification requirement on the basis of a Safety Case. This document describes the UAV system, the operational procedure, and includes a thorough risk assessment and mitigation strategy. The

preparation of this document and the subsequent assessment by the CAA can require several months and therefore exceed the development time of rapid-manufactured UAVs. The study presented in Chapter 7 was limited to UAVs with a dry mass not exceeding 20 kg in order to benefit from the reduced regulatory requirements. However, any UAV that is used for commercial operation[65] and/or at a distance exceeding 500 m from the remote pilot requires the authorization of the CAA and therefore is subject to an assessment process similar to the one required for LUAS. This legal obstacle can disadvantage the development of mission-specific systems in favour of larger and more versatile systems.

6.10 Summary and Final Remarks

This chapter has described the design and implementation of DUADE, a VDD environment applied to the design of small unmanned aircraft for civil application.

The DUADE workflow is divided into two phases: the Problem Definition and the System Design Loop. The Problem Definition phase is dedicated to the study of the stakeholders, their value drivers and the gathering of the information necessary to the creation of a concept of operation and mission simulation.

The System Design Loop revolves around the AST that generates the candidate systems and the VM that evaluates their merit according to the value drivers. The AST is a multidisciplinary design environment capable of producing an optimal UAV design with respect to a number of design parameters (including performance requirements, constraints and a used-defined objective function). The UAV mission efficacy and life-cycle cost is evaluated though an agent-based Operational Simulation and a life-cycle cost model. These provide the inputs to the Cost-Benefit model at the base of the VM. Following a VDD approach, the design requirements are considered the variables of the value trade space exploration rather than rigid design constraints.

The main challenge to the development of a VDD environment is posed by the need of providing a life-cycle model cable of capturing the quantitative effects of the system characteristics on the overall product value. This requires the introduction of several disciplinary modules, each based on a mathematical model, as well as a value model able to integrate the results of analyses.

In some cases, in the absence of well-established techniques or data evidence, the engineers are forced to develop basic disciplinary models that reflect their best judgment and intuition.

[65] Commercial operation is defined by the CAA as: “any operation of an aircraft other than for public transport […] in return for remuneration or other valuable consideration” [303].

Combining the results of evidence-based models and intuition-based models might appear to undermine the accuracy of the overall model's predictions. However, the alternatives to this approach are either to neglect some disciplines completely (risking to incur in unforeseen problems later on) or to leave the assessment of the matter to the instinct of the designers, leaving no record of the assumptions and reasoning behind certain design decisions. Instead, mathematical models based on engineering judgement are explicit; they can be validated or rejected through later experiments or data acquisition, and possibly replaced by improved versions.

Despite the difficulty of modelling several aspects of the system life-cycle, the VDD approach has the merit to force the designers to think systematically about all the aspects of the product development, identify the areas of poor or incomplete knowledge and express their assumptions in an explicit quantitative form.

7 Value Trade Space Exploration Using DUADE

7.1 Introduction

DUADE provides the designer with a powerful tool to explore the design space and identify the system characteristics that lead to the best overall value. This chapter describes the value trade space exploration applied to the case study presented in Chapter 1.

The study presents three steps. Initially, the impact of performance requirements on the aircraft characteristics is analysed. This allows the designers to understand the design space from the technical point of view and establish the relationship between aircraft performance and its mass and cost. Then, the study is extended to the mission level metrics that enable the study of the impact of technical characteristics on the overall mission effectiveness. Finally, the results of the analyses are combined into the Value Model to generate a ranking of design options and to provide further insights and guidance for the design decisions.

7.2 Summary of the Assumptions about the Design Problem and the Mission Scenario

The UAV design mission is the support of the SAR operation of the RNLI in a region of the South coast of England. It is assumed that all the information required in the Problem Definition phase has been acquired through interviews with the main stakeholder (the RNLI) and independent research. Two value drivers have been identified: the number of saved lives and the total cost of the SAR operations. It is assumed that the system life-cycle is limited to one year. Therefore, the discount rate of the future cash flows is neglected. Risk neutrality is assumed for the main stakeholder.

The area of interest and the distribution of the incidents can be seen in Figure 6-2. The UAV base is in Lyme Regis. Figure 7-1 shows the distribution of the incidents with respect to the closest lifeboat station and their cumulative distribution as a function of the distance from the UAV base. It is assumed that the position of the incident is known to the agents with an uncertainty between 50 m and 3000 m corresponding to a target size of 10 m and 0.2 m, respectively.

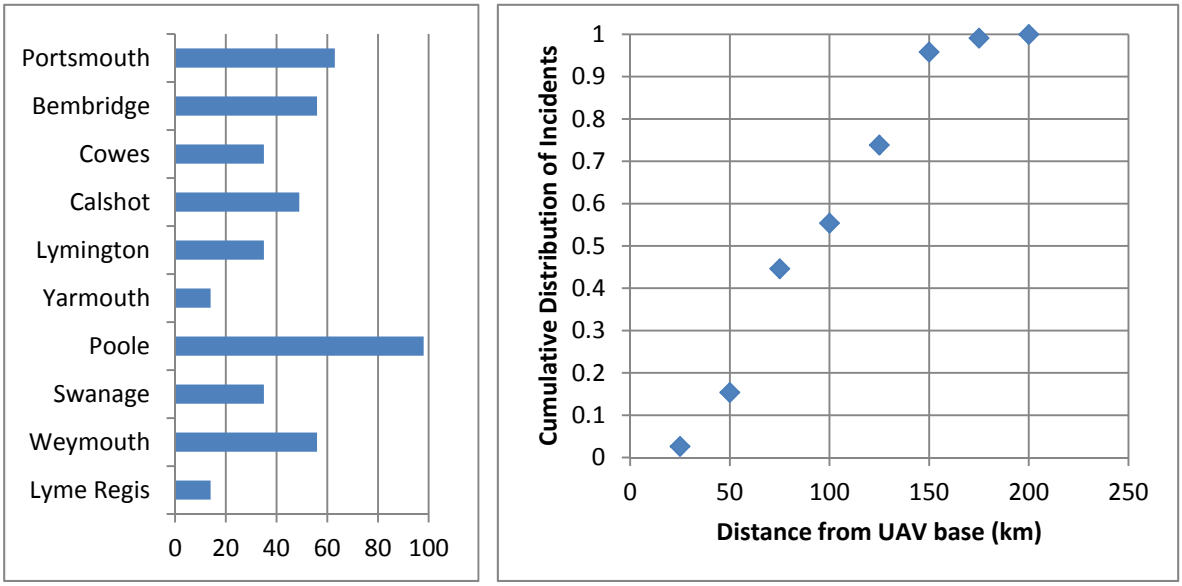

a. b.

Figure 7-1 – **a.** Number of incidents per lifeboat station. **b.** Cumulative distribution of the incidents as a function of the distance from the UAV base at Lyme Regis.

Each of the ten RNLI lifeboat stations in the area is equipped with a lifeboat with a cruise speed of 7 m/s and capable of a dash speed of 9 m/s and an hourly running cost of £850, including fuel cost[66]. The maximum operational time of the lifeboat is set to 10 h, after which the crew members need to be replaced. The effect of weather on the operations of the vessels is neglected for simplicity.

This study is limited to fixed-wing aircraft in the SUA category[67]. It is assumed that the payload is an optical target recognition system carried in the nose of the aircraft. The propulsion system is a combustion engine that drives a propeller in a pusher configuration. The UAV must be able to operate from a 100 m long grass runway. The UAV mission is performed autonomously, but one crew member is required to assist the take-off and landing operations and supervise the mission.

7.3 Exploration of the Design Space Using the Aircraft Sizing Tool

The bi-level System Design Loop used in DUADE is displayed in Figure 7-2. The aircraft sizing strategy was briefly introduced in Section 6.6.3: surrogate variables and equality constraints are used to decouple disciplinary problems while an optimisation process ensures the physical consistency of the model. The Sizing Optimiser controls the aircraft design variables (such as the

[66] These values are inspired by the Mersey class lifeboat [304,305].
[67] Small Unmanned Aircraft with a dry mass lower than 20 kg.

wing area, the fuselage length, and so on) with the aim of maximising the IOF. The IOF is a combination of important characteristics of the aircraft (such as the fuel efficiency and the unit cost); their relative importance is controlled by the designer through a vector of scaling factors. Design parameters and constraints are an input to the sizing optimiser, as well. The result of the sizing optimisation is an "optimal aircraft" that depends on the constraints, parameters and scaling factors.

The design space exploration can be performed at two levels:

- By using the AST, the user can explore the quantitative relationship between the performance requirements and the cost and physical characteristics of the aircraft.
- By using the VM, the user can estimate the mission efficacy and life-cycle cost of each design option hence creating a link between design parameters and product value.

This Section describes the design space exploration using the AST.

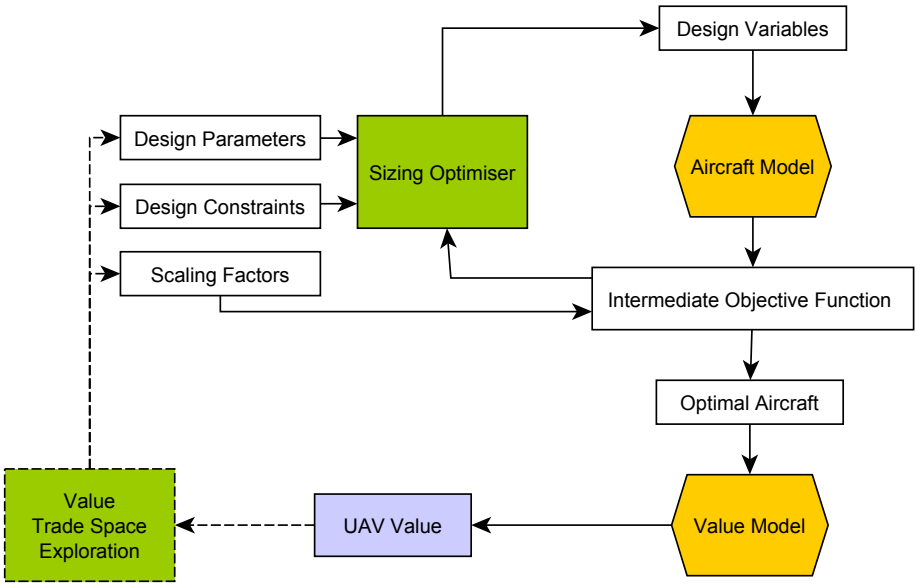

Figure 7-2 – DUADE Bi-Level System Design Loop.

7.3.1 The Choice of the Intermediate Objective Function

The sizing algorithm employed by the AST requires the definition of an Intermediate Objective Function (IOF). In the approach adopted here, the IOF is a function of the extensive attributes of

the UAV[68], while the aircraft performance parameters are treated as design requirements (constraints or parameters).

Design parameter	Value	Unit
Range at cruise speed	400	km
Maximum speed	37.5	m/s
Landing speed	13.0	m/s
Cruise speed	25.0	m/s
Payload mass	2.00	kg
Payload depth	0.200	m
Payload width	0.200	m
Payload length	0.250	m
…	…	…

Table 7 – Performance requirements used as fixed parameters in the design optimisation of a sub 20 kg UAV (table excerpt).

The following example demonstrates that the choice of different IOFs lead to different designs even if the performance requirements are identical. Table 7 shows a list of performance requirements to be satisfied by a sub 20 kg fixed wing UAV. There is more than one possible solution to this design problem. For example, the range requirement can be achieved by having a low aerodynamic efficiency but a large enough fuel fraction or by using a small amount of fuel due to a very efficient design. The designer will try to satisfy these requirements while maximising the aerodynamic and structural efficiency and minimising the UAV unit cost. However, in most cases these desired characteristics cannot be satisfied simultaneously and one or more aspects need to be prioritised.

Table 8 and Figure 7-3 show the results obtained using the CDT and three different objective functions[69]:

a - **Fuel efficiency** (i.e. the rate at which the fuel is burned during cruise. It was used as a proxy for the aerodynamic and propulsive system efficiency).

b - **Empty cost** (i.e. the cost of the UAV without payload).

c - **Empty mass** (it was used as a measure of structural efficiency).

[68] The extensive attributes are the attributes of a systems that result from the collective contribution of its parts and can be allocated as a "budget" to its subsystems (for example mass, aerodynamic drag, cost, and so on) [30,154].

[69] In all cases, it was assumed that the payload is positioned in the nose of the aircraft, forward of the front undercarriage leg, in order to provide an unobstructed view to the sensors. A pusher propeller and twin boom configuration was selected for this study.

	Optimisation Objective Function			
Design variable	**Fuel efficiency (a)**	**Empty cost (b)**	**Empty mass (c)**	**Unit**
Wing area	1.08	1.28	1.08	m^2
Wing aspect ratio	10.8	10.3	10.3	-
Wing taper ratio	0.321	1.00	1.00	-
Fuselage front bulkhead position	0.731	0.462	0.669	m
Horizontal tail longitudinal position	-1.40	-1.12	-1.19	m
Equivalent horizontal tailplane area	0.185	0.320	0.233	m^2
Equivalent horizontal tailplane aspect ratio	4.50	4.49	4.50	-
Equivalent vertical tailplane volume coefficient	0.0452	0.0391	0.0429	-
Maximum engine power	2.93	3.27	2.97	kW
Percentage of engine power at cruise	35.7	36.5	36.0	%
Nose ballast mass	0	1.89	0	kg
Fuel mass	1.86	2.12	1.92	kg
Maximum take-off mass	18.3	21.4	18.0	kg
Maximum load factor	5.52	5.51	5.57	g
Objective value				
Empty UAV cost	18600	15600	17800	£
Fuel burn rate at cruise	420	479	429	g/h
Empty mass	14.2	17.0	13.9	kg

Table 8 – Results of the design optimisation of a sub 20 kg UAV with three different objective functions.

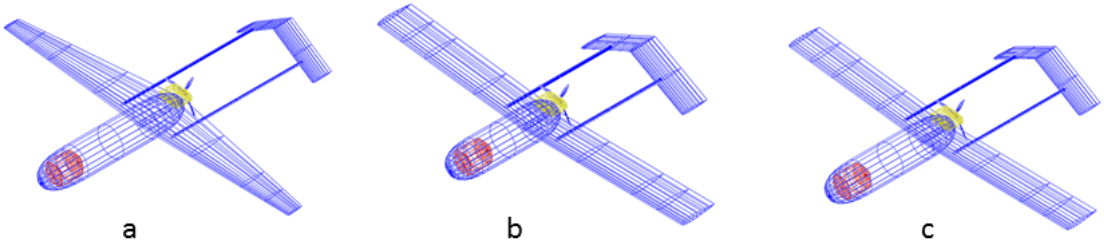

Figure 7-3 – Geometry of the results of the design optimisation of a sub 20 kg UAV using three different objective functions: **a**. Fuel efficiency at cruise speed **b**. Minimum empty cost **c**. Minimum empty mass. The payload is displayed in red and the engine in yellow.

The aircraft optimised for fuel efficiency (Figure 7-3a) is the one with the longest fuselage and the smallest wing and tailplane. Its wing also has the highest aspect ratio and the lowest taper ratio. These features increase the aerodynamic efficiency of the aircraft but increase its manufacturing cost (aircraft **a** is the most expensive of the three). Design **b** is optimised for unit cost. It uses ballast in the nose to ensure the correct position of the CoG while having the shortest fuselage. The fuselage is a large 3D printed structure and its size is one of the main cost drivers for the airframe cost. As a result, aircraft **b** is the heaviest design and it has the highest fuel burn rate.

Finally, the aircraft optimised for mass (Figure 7-3c) has intermediate fuel efficiency and empty UAV cost.

All of these three aircraft satisfy the design requirements and hence are capable of successfully fulfilling the mission. However, they are very different designs. The decision between the three candidate systems requires the existence of a value model that can be used to assess the relative importance of structural efficiency, fuel efficiency and unit cost. It is possible that the best system from the VDD point of view is neither of the ones above, but a fourth aircraft which is part of the Pareto optimal set with respect to the three objectives considered.

In the rest of this study, the objective function used for the aircraft optimisation will be a linear combination of the objective functions used in the example above. The optimisation problem is defined as follows

$$\max_{\boldsymbol{x}\in\boldsymbol{X}} \sum_{m=1}^{M} w_m \left(f_m(\boldsymbol{x},\boldsymbol{p}) - z_m\right) \qquad 7\text{-}1$$

$$\text{subject to } \boldsymbol{g}(\boldsymbol{x},\boldsymbol{p}) \leq 0, \boldsymbol{h}(\boldsymbol{x},\boldsymbol{p}) = 0$$

Where $\boldsymbol{x}$ is the vector of design variables, $\boldsymbol{p}$ is the vector of design parameters, M is the number of objectives, w_m is the scaling factor (normalised weight) of the m^{th} normalised objective f_m and z_m is the m^{th} objective reference point. $\boldsymbol{g}$ and $\boldsymbol{h}$ are the inequality and equality constraints, respectively.

The weighted sum was chosen because it is the simplest way to combine multiple objectives. There are some disadvantages in case of non-convex problems, namely not all the points of the Pareto solutions can be found and the same vector of scaling factors can represent different solutions in the Pareto optimal set. On the other hand, the method does not require a modification of the search algorithm and the objective weights can be treated as parameters in the optimisation process.

In particular, it was decided to use a combination of fuel burn rate at cruise and the UAV empty unit cost only. These two attributes have been chosen because they can be directly linked to one of the value drivers described in Section 6.4 (the UAV operative cost will depend on the cost of the fuel used during the mission and on the airframe cost itself). Moreover, the structural efficiency is already partially accounted in the fuel burn rate metric (the aircraft mass has a strong impact on the fuel consumption). The combined objective function $F(\boldsymbol{x},\boldsymbol{p})$ is

$$F(\boldsymbol{x},\boldsymbol{p}) = -\left[w_{FBC}\,\frac{\left(FBC - FBC_{ref}\right)}{FBC_{ref}} + w_{EUC}\,\frac{\left(EUC - EUC_{ref}\right)}{EUC_{ref}}\right] \qquad 7\text{-}2$$

$$w_{FBC}, w_{EUC} \in [0,1]$$

$$w_{FBC} + w_{EUC} = 1$$

where FBC and FBC_{ref} are the fuel burn rate at cruise and the relative reference value, EUC and EUC_{ref} are the empty unit cost and the relative reference value. w_{FBC} and w_{EUC} are the scaling factors for the two objectives.

7.3.2 The Impact of Parameters and Constraints on the Optimal Aircraft Characteristics

Understanding the relationship between the requirements and the aircraft characteristics provides an extremely powerful tool that the designer can use to perform trade space analysis. The following study demonstrates that the AST is able to provide a quantitative estimate of the effect of a change of the requirements or constraints on the optimal aircraft design[70].

The plots presented in Figure 7-4 and Figure 7-5 were obtained by optimising the UAV as a function of variables listed in Table 8 and the following parameters

- The **RIR** (Reliability Improvement Ratio, discussed in Section 6.7.10. It can be regarded as a system robustness factor).
- The aircraft **Range**[71].
- The **Maximum speed**.
- The **Landing speed**[72].
- The **Search speed** (i.e. the cruise speed used during search operation).
- The **Payload mass**.

[70] The optimisation parameters and constraints control the design space available for the CDT optimiser. Constraints are generally dictated by physical principles (for example, the aircraft structure must be able to absorb the aerodynamic loads) or imposed by practical limitations (for example, the maximum wing span might be limited due to storage or transportation requirements). Parameters and constraints can also be used to control performance or operational requirements (for example, the minimum requirement for the aircraft endurance or maximum speed), in which case they have to be considered design variables (although not an optimisation variable).

[71] In order to simplify the input structure, the Range requirement is associated to a simplified calculation that assumes that the aircraft flies at the Search speed, at the design cruise altitude and has an initial mass equal to the MTOM. This calculation overestimate the real range because it neglects the take-off and landing phases, as well as any flight segment that is flown at less efficient speeds. However, the performance model used in the Operational Simulation accounts for these effects and provides a more realistic operative range.

[72] The Maximum speed and Landing speed values are calculated assuming that the aircraft mass is the MTOM.

- $\boldsymbol{w_{EUC}}$, that is the scaling factor of the empty unit cost used in the combined objective function and defined in Equation 7-2. $w_{EUC} = 0$ implies that the aircraft is optimised for fuel efficiency; $w_{EUC} = 1$ implies that the aircraft is optimised for unit cost.

141 different designs were obtained by varying the parameters one at a time with respect to the initial parameters' vector, which is shown in Table 9. Five data points were used for each plot. The initial values are the middle values of the parameter interval, but for w_{EUC}[73].

Design parameter	Value	Unit
RIR	0.125	-
Range	500	km
Max speed	35.0	m/s
Landing speed	14.5	m/s
Search speed	25.0	m/s
Payload mass	3.25	kg
w_{EUC}	0	-

Table 9 – Initial parameters' vector used in the trade study.

The plots presented in Figure 7-4 and Figure 7-5 are organised following a matrix scheme where the columns correspond to the input parameters and the rows to outputs, that are defined below. The crosses indicate the data points; the red lines are splines used to help visualise trends.

The outputs displayed in Figure 7-4 are, from top to bottom:

- The aircraft **Fuel mass**[74].
- The maximum take-off mass **MTOM**.
- The **Empty mass** that is the mass of the aircraft without payload and fuel.
- The **Dry mass** that is the mass of the aircraft with payload but no fuel.
- The **IOF** (Intermediate Objective Function) that is the objective function of the sizing optimisation $F(\boldsymbol{x}, \boldsymbol{p})$ defined in Equation 7-2.

The outputs displayed in Figure 7-5 are defined as follows:

- The **Empty UAV cost** is the sum of the cost of structure, propulsion and avionics systems.
- The **UAV procurement cost** is the sum of the empty UAV cost plus the cost of the payload.
- The **UAV unit cost** is the UAV procurement cost plus the development cost.

[73] By optimising the aircraft for either fuel efficiency or cost, problems connected with additive objective functions are avoided and the plots can be easily interpreted. Fuel efficiency was selected for this study because it is influenced by physical principles of easier interpretation.
[74] It is assumed the mission always starts with the maximum fuel load.

- The **UAV system cost** is the UAV unit cost times the number of UAVs produced[75] plus the ground system cost.
- The **FBRC** is the Fuel Burn Rate at Cruise calculated at the MTOM.

7.3.2.1 Analysis of the Results

By studying the plots in Figure 7-4 the following insights can be obtained.

The impact on mass of the RIR is not particularly interesting given the very simple and coarse approximation introduced in Section 6.7.10. However, it is interesting to note that the plots show that the increase in structural mass (dry mass) requires an increase of the fuel load to achieve the same given performance.

An increased range requirement is positively correlated with an increase of the aircraft mass. The plot shows that there is a large impact on both the fuel mass and the structural mass (roughly 60% of the MTOM increase is due to fuel and 40% to structure). This result is in agreement with the designer's intuition: longer range requires more fuel, therefore, heavier structure and larger propulsion system and lifting surfaces to support the additional weight.

The increase in maximum speed has an impact mainly on the structural mass (it requires a larger propulsive system and a more robust structure). The increase in fuel load is a secondary effect due to the fact that a heavier aircraft requires more power (and hence fuel) to deliver the same cruise performance.

The curves corresponding to the landing speed variation present an interesting trend: the aircraft mass initially decreases with the increase of landing speed, reaches a minimum point around 16 m/s and increases again for higher landing speeds. This trend can be explained as follows: low landing speed requires low wing loading. Large wings are heavy because of their size and because the gust loads are comparatively more severe. These effects dominate the left-hand side of the mass plots. On the other hand, higher landing speeds require a more robust undercarriage to dissipate the additional kinetic energy. The mass increase of the landing gear system dominates the right-hand side of the curves.

[75] The number of UAVs produced is kept constant in this study.

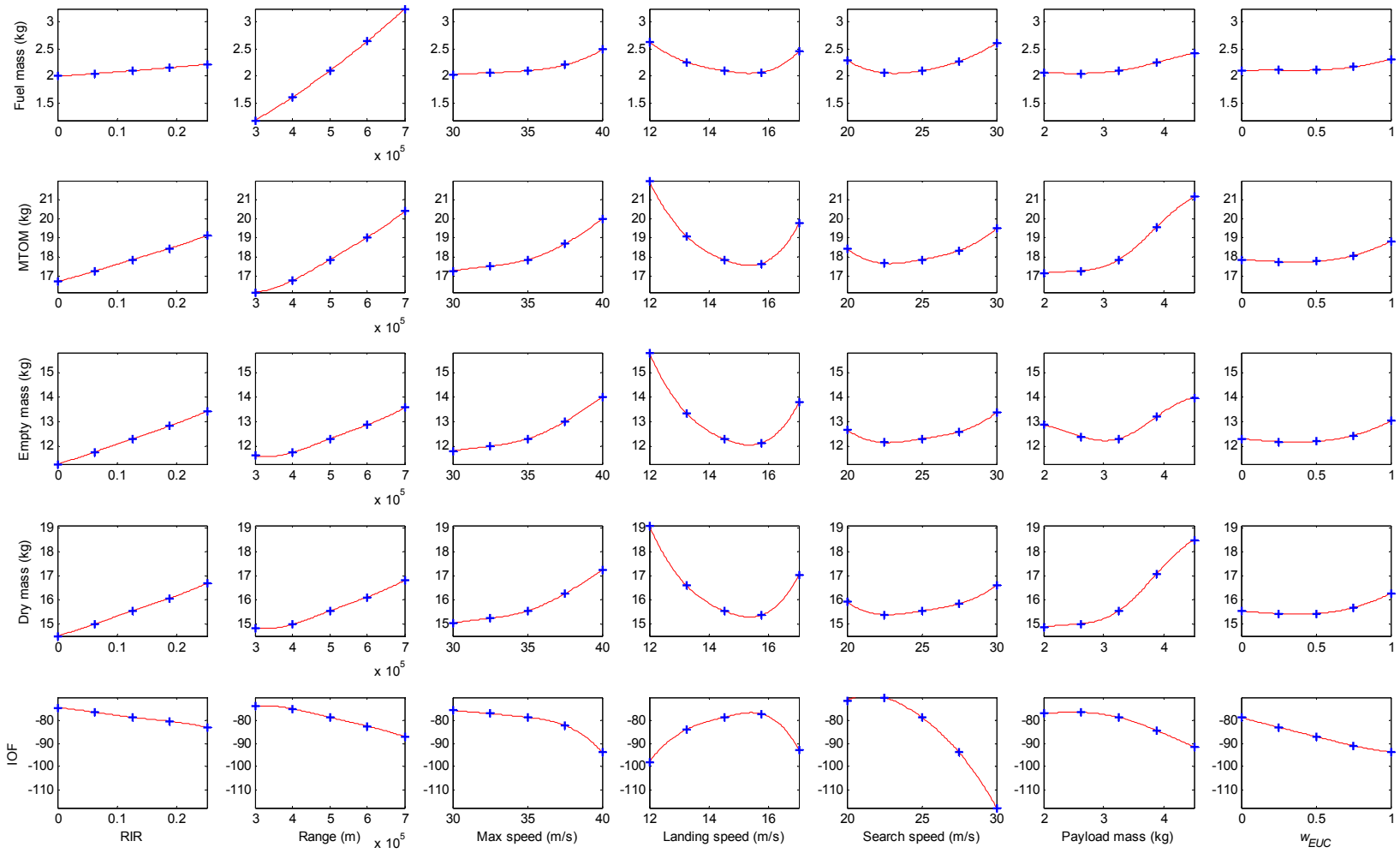

Figure 7-4 – Effect of the performance parameters on the UAV mass.

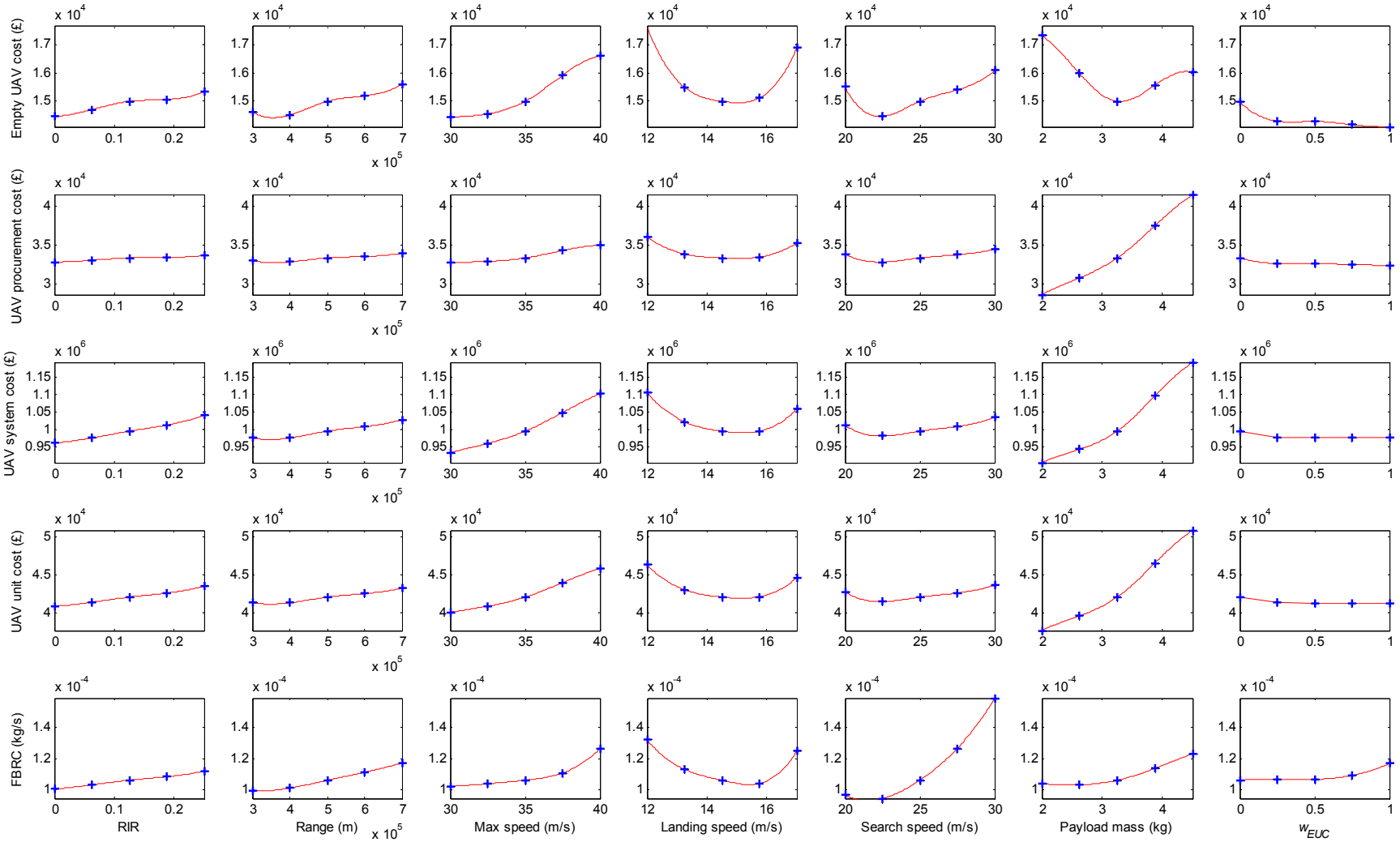

Figure 7-5 – Effect of the performance parameters on the UAV cost.

The search speed plots indicate that there is an optimum design speed for the given performance and payload point: an aircraft designed to cruise at 22.5 m/s will require less fuel and a lower structural mass to perform the mission. Note that this is different than the optimal cruise speed of a particular aircraft (which depends on the drag polar and propulsion system of that particular system). The search speed is a mission parameter and it is in general different than the optimal speed for range optimisation.

Unsurprisingly, the aircraft MTOM increases with the increase of the payload mass. However, it is interesting to note that the empty mass does not monotonically increase. This is due to the fact that, being positioned in the nose, the payload has a large impact on the CoG (and hence the stability and control) of the aircraft. With a light-weight payload, in order to have the CoG within the safe envelope, the aircraft needs to have either a longer fuselage or ballast in the nose. Since the curves in Figure 7-4 are obtained optimising the aircraft for fuel efficiency, the long fuselage option is preferred (similarly to the case presented in Figure 7-3).

The effect of w_{EUC} on the UAV mass is in agreement with the example in Section 7.3.1: by increasing the importance of the UAV empty cost over the fuel efficiency, an aircraft with a shorter fuselage and additional nose ballast is obtained.

The study of the plots in Figure 7-5 provides the following indications.

The general trend shown by the UAV cost diagrams highlights a positive correlation between the increase in aircraft performance and the cost of the UAV, particularly for the cases of the maximum speed, reliability, and range.

The effect of the landing speed on cost is similar to the one on the aircraft mass, with a minimum system cost corresponding to the minimum mass point.

Similarly, the search speed corresponding to the lowest UAV mass is also the one that corresponds to the lowest system cost.

The payload mass is the parameter with the highest impact on the aircraft cost; however, the cause is to be attributed to the relatively high cost per unit mass of the payload itself. The plot of the empty UAV cost shows that the impact on the airframe cost is not monotonic, although still significant.

Finally, the effect of increasing w_{EUC} is a corresponding decrease of the system cost, although this effect is small if compared to the impact of the other parameters.

The dominant parameter for the fuel consumption at cruise is the search speed. All the other parameters have a monotonic positive correlation with the fuel burn rate but for the landing speed, for which there is a minimum in the speed range considered.

7.4 Exploration of the Design Space Using the Value Model

DUADE can provide a quantitative analysis of the impact of the system performance on the mission effectiveness and operational cost. This is achieved by linking the Operational Simulation and the life-cycle cost model to the AST. The results presented in this paragraph were obtained by modelling the SAR mission described in Section 6.4.1 and Section 7.2.

7.4.1 Baseline Search and Rescue Scenario

A baseline SAR scenario was simulated in order to provide a reference point for assessing the mission effectiveness of the UAV. In the baseline SAR scenario only the RNLI surface vessels were included in the simulation. The results show that the RNLI vessels were cable of successfully rescuing an average of 280 persons with an average total cost of £9.03M[76].

The baseline simulation was also used to estimate the VSL. The Cost-Benefit model described in Section 6.8.1 was used and it was assumed that the value of the baseline SAR mission is equal to zero. The corresponding VSL is £32.2k[77].

7.4.2 The Effect of Performance Requirements on Mission Effectiveness and Operational Cost

The SAR scenario was updated to include the operation of the UAV. The same designs explored in Section 7.3.2 were tested. The Figure 7-6 shows the effect of the design performance parameters on some of the mission-level performance metrics. The outputs displayed in Figure 7-6 are defined as follows:

- The **Average finding time** is the time that occurs between an incident involving a person at sea is reported and the time the casualty is identified by either the UAV or any of the other vessel participating in the SAR operation.

[76] The results were obtained by averaging 200 replications of the simulation. The total number of accidents in the simulated scenario is 455. This implies that an average of 175 rescue operations were unsuccessful. This number is high if compared to the overall number of fatalities as a result of accidental drowning in the entire UK (the total in 2015 was 321 according to the data published by the National Water Safety Forum [306]). This difference can be explained by some of the model assumptions, such as the absence of SAR helicopters or the fact that the same survival probability function is applied to all the accidents (therefore assuming that all the accident are at life risk if not rescued by the lifeboats).

[77] This value has the same order of magnitude of the cost per rescued person calculate in Section 6.8.1.1.

- The **UAV mishaps number** is the number of UAV system failures resulting in a loss of the aircraft. It includes both landing mishaps and in-flight failures.
- The **Number of saved lives** is the number of people successfully rescued in the time period of interest.
- The **UAV total flight time** is the total time spent in flight during all the SAR operations in the given period.
- The **UAV fuel used** is the total fuel used during all the SAR operations in the given period.

The blue bars in the plots represent the sample standard deviation s. The 95% confidence interval can be calculated using equation 6-32. In this case (200 replications and a 95% confidence interval[78]), $t \cong 1.97$. Therefore

$$CI_{95\%} \cong \mu \pm \frac{s}{7.1} \qquad 7\text{-}3$$

i.e. the size of the 95% confidence interval is about seven times smaller than the sample standard deviation.

The UAV mishaps number and the number of saved lives appear to have relatively large confidence intervals if compared to the other metrics. This is partly due to the fact that they represent rare discrete events (particularly in the case of mishaps); and partly due to the fact that their relative range of variation is smaller than the ones of the other parameters; therefore their output noise is amplified by the scale of the plots.

The RIR does not have a major impact on the number of saved lives, the average finding time and the total UAV flight time. Thus, the data imply that a 30% increase on the baseline reliability levels does not significantly impact the mission performance[79]. Not surprisingly, the UAV mishaps number decreases by increasing the reliability factor, and the fuel used increases. The latter effect is due to the increased mass of a more reliable aircraft.

[78] The computational cost of the Operational Simulation for this test case is high because of the calculations associated with the payload module. For this reason, the number of replications of the simulation was limited to 200, which satisfy the simulation stop criterion described in 6.8.3.

[79] In the Operational Simulation, it is assumed that a spare UAV is always available at the base to immediately replace the crashed one.

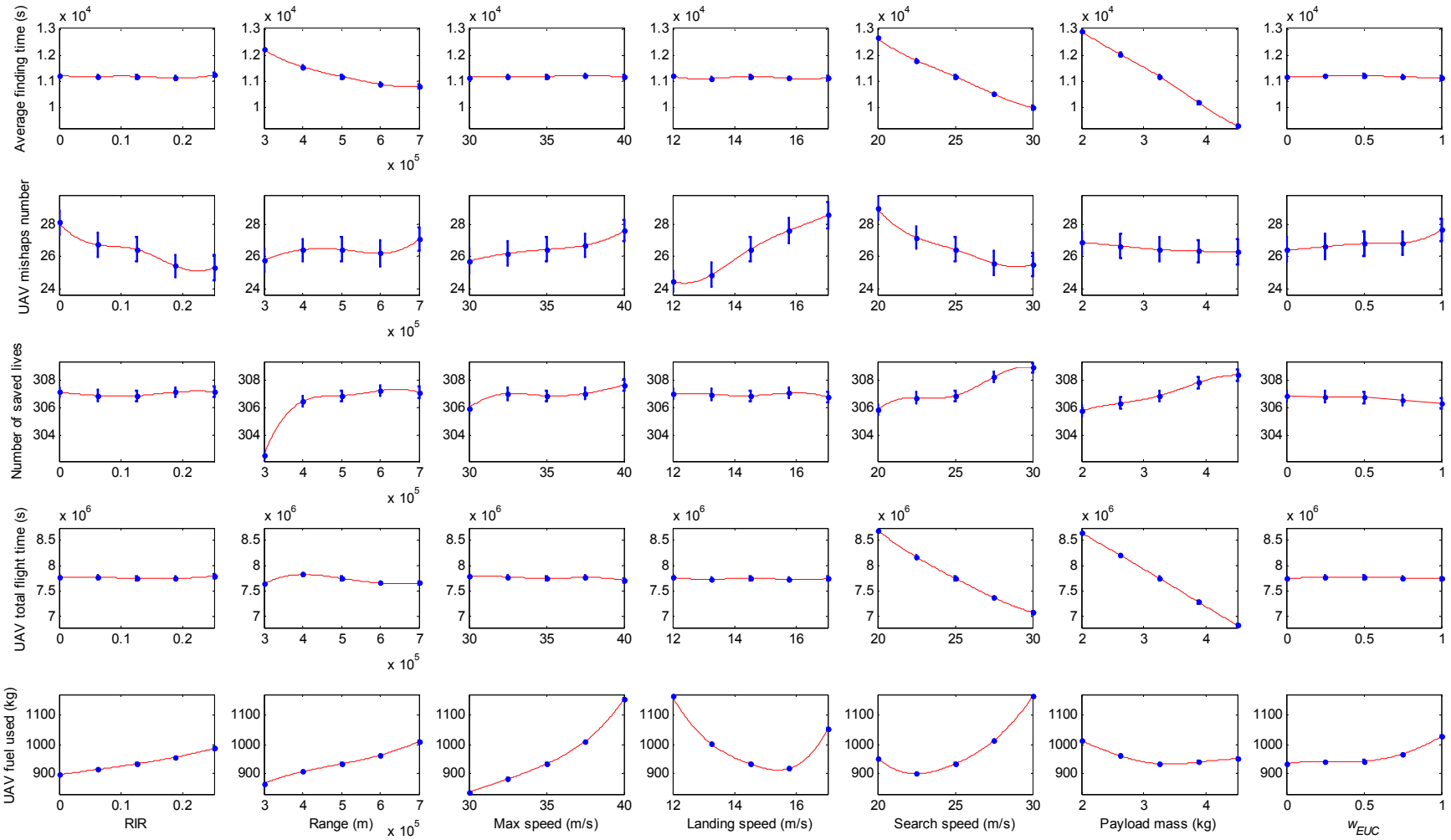

Figure 7-6 – Effect of the performance parameters on the mission performance.

Increasing range has a positive effect on the average finding time and the number of saved lives. This effect is to be attributed to the fact that the aircraft does not have to interrupt the mission to fly home and refuel and it can fly consecutive missions if more casualties occur in a short time span. Interestingly, the number of saved lives is not proportional to the average finding time. This can be explained by the non-linear function adopted for the survival probability versus immersion time. In particular, increasing the UAV range from 300 km to 400 km has a greater impact than increasing it from 400 km to 700 km. This is due to the fact that, in the first case, it has increased the probability of finding casualties early, i.e. when their probability of survival is the highest.

The UAV total flight time initially increases and then decreases by increasing the aircraft range. This can be explained by the fact that a UAV with a short range has to fly home more often to refuel. Sometimes the mission will be completed by other vessels before the UAV has the chance to fly back to the incident location. On the other hand, a long range UAV can spend more time on the incident location and hence decreases the time needed to spot the casualty by supporting the other SAR vessels. The total fuel used increases by increasing the range because the size and mass of the aircraft increase. The impact of range on the UAV mishaps number is small; probably due to two effects balancing each other in determining the number of landing mishaps: aircraft with longer range perform fewer take-offs and landings but at the same time are heavier and hence have a higher probability of crashing during each landing (according to the model used here) due to their increased kinetic energy.

The maximum speed does not have a large impact on the average finding time or the total UAV flight time, thus suggesting that the dash phase is a relatively short phase of the mission. However, faster aircraft save (marginally) more lives because they can locate sooner the recent incidents (high survival probability). The mishaps number and the fuel consumption increase with the aircraft max speed because of the increased mass it implies.

Landing speed has a negligible impact on the mission performance (average finding time, number of saved lives and UAV total flight time). On the other hand, it has a large impact on the UAV mishaps number (due to the variation of kinetic energy at landing) and the fuel consumption (due to the impact on the mass and drag of the aircraft). The plot suggests that the ideal landing speed is somewhere between 12 m/s and 13 m/s if the priority is to minimise the landing mishaps and between 15 m/s and 17 m/s if the priority is to minimise the fuel consumption.

Search speed is one of the most important parameters in determining the UAV mission performance. Increasing the search speed decreases the average finding time and total UAV flight time. The number of saved lives increases too. The UAV mishaps number decreases because of

the lower flight time. Despite the decrease in the flight time, the total fuel used increases because of the additional power required to fly at higher cruise speed (though there is a minimum around 22.5 m/s).

The payload mass is linked to the quality of the on-board sensor and has a great impact on the mission performance. Therefore, a higher payload mass decreases the average finding time and the total flight time and increases the number of saved lives. The increased UAV mass and the decreased flight time play opposite roles in determining the total fuel used and the mishaps number.

Increasing the importance of the UAV cost in the optimisation objective function has the effect of increasing the total fuel used. The number of mishaps slightly increases and the number of saved lives slightly decreases, probably due to the increased mass (and hence kinetic energy at landing).

The analysis of Figure 7-6 has provided some counterintuitive insights. For example, it has shown that a similar decrease in the number of UAV mishaps can be achieved by increasing the system reliability by 30% or by increasing the search speed from 20 m/s to 30 m/s. On the other hand, increasing the maximum speed of the aircraft has an opposite effect on the number of mishaps.

Figure 7-6 has also provided indications about ideal performance points. For example, there are optimal search and landing speeds that minimise the total fuel used and a range increase does not yield significantly higher mission performance once a certain threshold is achieved.

7.4.3 Effect of Simultaneously Varying the Performance Parameters

In the studies presented so far, the performance parameters were varied one at a time. However, their impact on the mission performance is not independent of each other. DUADE can be used to assess the effect of varying multiple performance parameters at once.

Here, the analysis is restricted to two parameters at a time to allow a visual representation of the results through surface plots. The output variance and confidence intervals are omitted to increase the readability of the plots.

For this example, the payload mass and the UAV range have been selected as input parameters.

Figure 7-7 shows the simultaneous effect of the two input parameters on the average waiting time and the number of saved lives. The data points (blue dots) have been obtained using a 5x5 full factorial experiment; the surfaces displayed have been obtained through a cubic spline interpolation of the data points. The plot indicates that the impact of an increase of the payload mass depends on the value of range and vice versa. In particular, it can be observed that payload

mass higher than 2.5 kg does not improve the number of saved lives significantly if the aircraft range is 300 km. Analogously, it can be observed that increasing the aircraft range from 400 km to 500 km has a much greater impact on the number of saved lives if the aircraft is equipped with a heavy payload. It is worth noting that some data points corresponding to high range and payload mass values are missing in the plot. This is due to the fact that such performance requirements cannot be satisfied by the UAV (which is constrained to have a maximum dry mass of 20 kg and a maximum take-off and landing distance of 100 m).

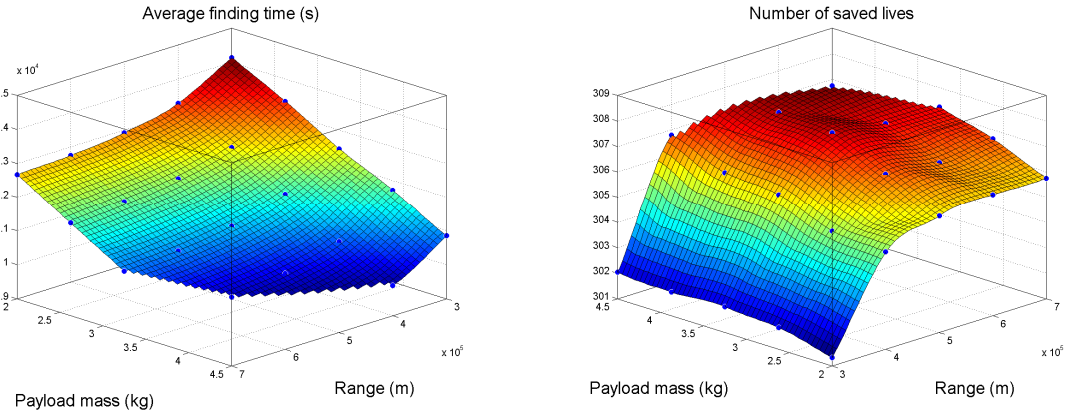

a. b.

Figure 7-7 – Effect of payload mass and UAV range on: **a**. Average finding time **b**. Number of saved lives. Note that input axes are rotated to enhance the picture readability.

Figure 7-8 shows the impact of payload mass and range on six mission performance metrics. Some of these have been defined in the previous paragraph (namely the UAV total flight time, the UAV fuel used and the UAV mishaps number); the others are:

- The **Total lifeboats utilization time** is the total time spent by all the lifeboats taking part to the SAR operation in the considered timespan.
- The **Number of take-offs** refers to the total number of UAV launches during the considered timespan.
- The **UAV total maintenance time** refers to the total time spent repairing faults to the UAV that did not cause an aircraft loss.

By comparing Figure 7-7a and Figure 7-8a it can be seen that the lifeboats utilization is strongly correlated with the average casualty finding time. This is not surprising because the less time required to spot the casualty the less time the SAR vessels have to spend looking for it. Data suggest that payload quality and range have both a positive impact.

It is perhaps counterintuitive that increasing the range, the UAV flight time (Figure 7-8b) increases while at the same time the average finding time decreases. This can be explained by the fact that the UAV can fly faster than the lifeboats can move. This means that the aircraft reaches the location of the incident and starts searching earlier. The higher the range, the more missions the UAV can fly. The incidents with the higher distance from the lifeboat stations are more likely to be identified by the UAV first.

Figure 7-8c shows that the fuel used by the UAV increases significantly with the increase of the range requirement, even though the flight time plot is relatively flat. It is because the aircraft has to carry the extra fuel load.

The number of take-offs (Figure 7-8d) decreases with range due to the fact that a UAV with short range has to go back to base and refuel more often. It also decreases with payload mass because the better the payload, the better the probability of detection; hence, the less the chance to have to come home and refuel.

Figure 7-8e and Figure 7-8b show that the UAV maintenance time is driven by the total UAV flight time. This is not surprising as the longer the UAV flies the higher the chance of some component failing. However, a closer examination of Figure 7-8e reveals that, for each value of the payload mass, there is a value of the UAV range requirement that maximises the maintenance time (and hence cost). This can be explained as follows: increasing range on one hand increases the UAV flight time but on the other hand decreases the number of UAV take-offs and landings which has an impact on the probability of some other components failing.

Also, the UAV mishaps number (Figure 7-8f) is influenced by the UAV total flight time and the number of the number of landings. However, there is a third variable that plays an important role: the kinetic energy at landing. As the range requirement increases, the aircraft mass at the moment of touch down increases because of the extra structural mass and the mass of unused fuel (in some missions). This increases the probability of a landing mishap. Similarly, payload mass has an effect on both increasing the aircraft kinetic energy upon landing and decreasing the UAV flight time. The general trend indicates that UAVs with a low range and a high-quality payload are likely to have fewer mishaps.

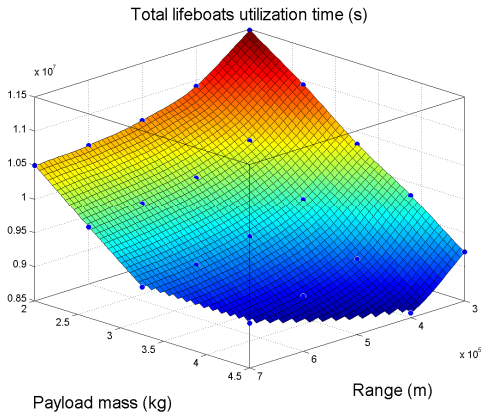

a.

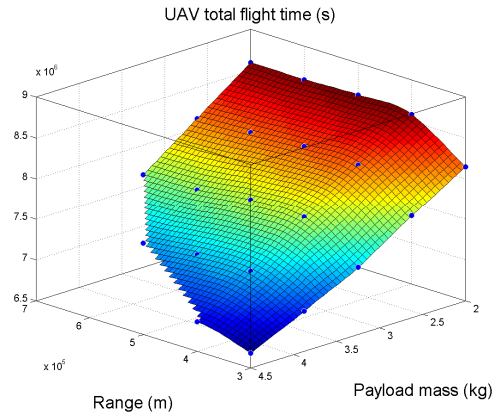

b.

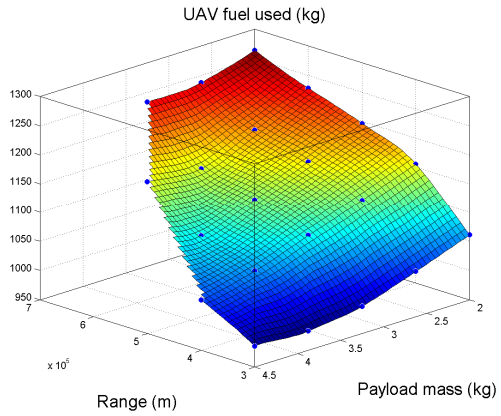

c.

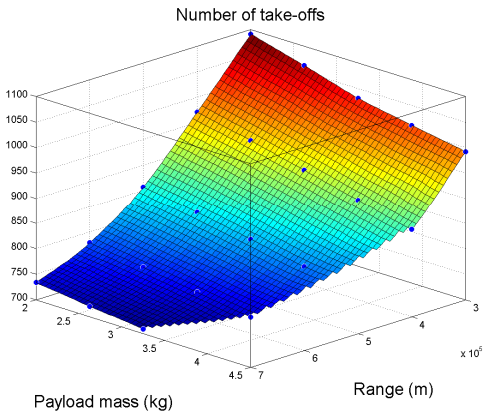

d.

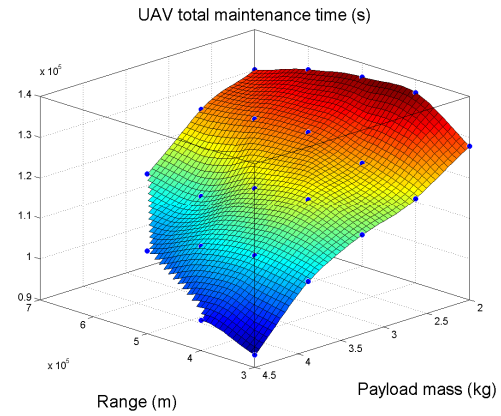

e.

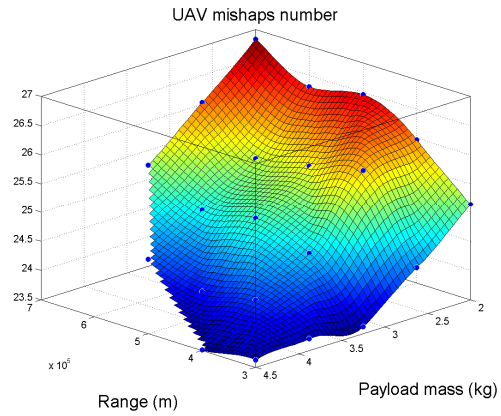

f.

Figure 7-8 – Effect of payload mass and UAV range on: **a**. Total lifeboats utilization time **b**. UAV total flight time **c**. UAV fuel used **d.** Number of take-offs **e.** UAV total maintenance time **f.** UAV mishaps number. Note that input axes are rotated to enhance the picture readability

7.4.4 Trade Space Exploration Using the Cost-Benefit Model

By using the output provided by the AST and the Operational Simulation, the range and payload mass can be linked to the SAR operational cost.

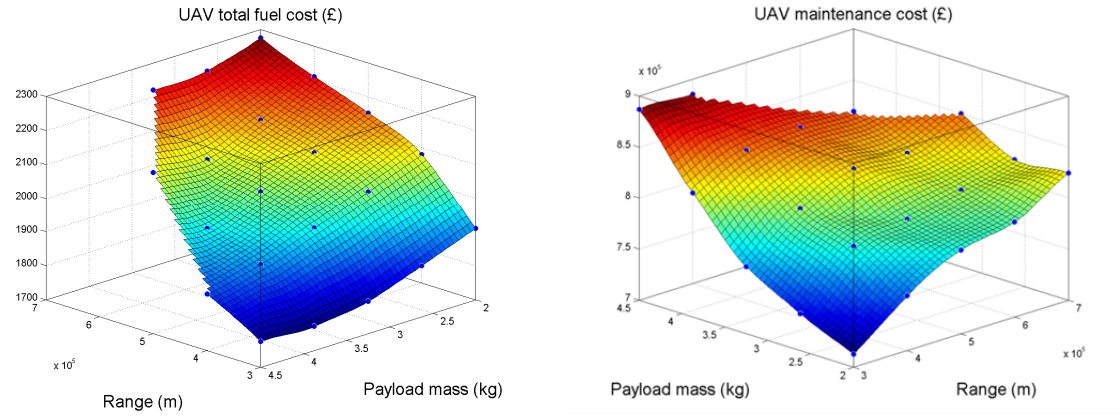

a. b.

Figure 7-9 – Effect of payload mass and UAV range on: **a**. UAV total fuel cost **b**. UAV maintenance cost. Note that input axes are rotated to enhance the picture readability.

Figure 7-9 shows the impact of the input parameters on two components of the total UAV operational cost: the total fuel cost and the maintenance cost[80]. By comparing the two, it can be seen that the fuel cost has a relatively small impact on the operational cost. Therefore, it could be argued that the designer should trade fuel efficiency for reliability.

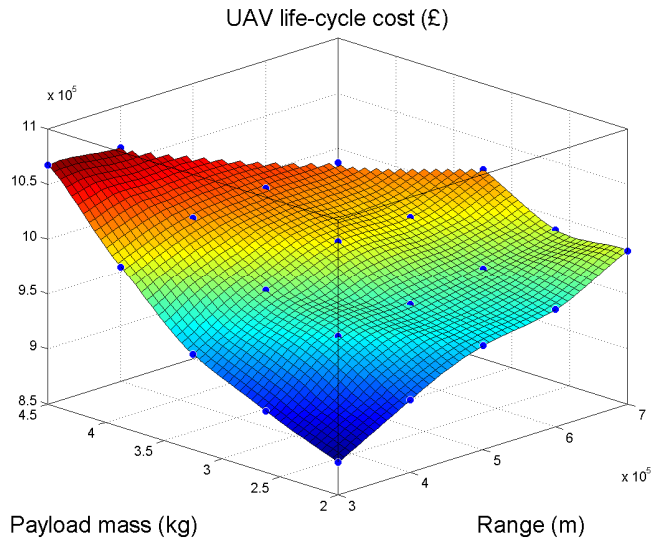

Figure 7-10 – Effect of payload mass and UAV range on the UAV life-cycle cost.

[80] The UAV maintenance cost `includes the cost of replacing the UAVs lost in service.

The design with the highest maintenance cost does not correspond to the one with the highest number of mishaps (Figure 7-9b and Figure 7-8f). This counterintuitive effect[81] is due to the impact of the UAV unit cost on the maintenance cost.

Figure 7-10 shows the effect of the two input parameters on the total cost of using the UAV for the SAR mission. By comparing Figure 7-10 and Figure 7-7b it can be seen that there is a clear trade-off between the number of saved lives and the life-cycle cost of the UAV.

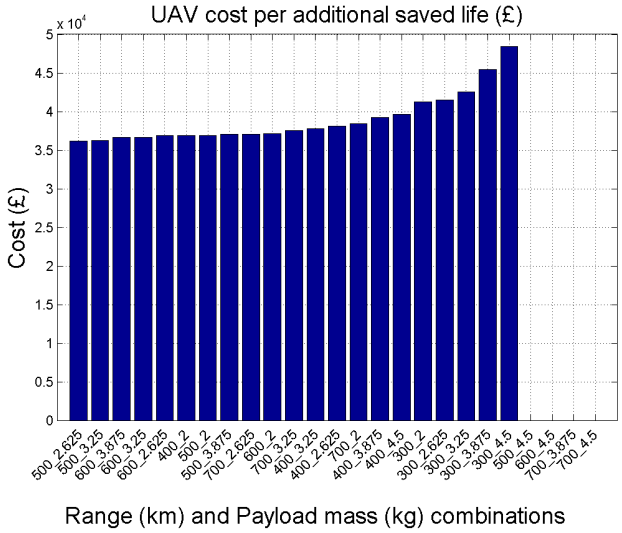

Figure 7-11 – UAV life-cycle cost per additional saved life; the labels on the x axis display the value of range (km) and payload mass (kg) separated by an underscore.

By comparing the performance of the SAR operation with the UAV and the baseline scenario (without the UAV) it is possible to calculate the additional saved lives, that are the lives that would have been saved due to the operation of the UAV. The bar-graph presented in Figure 7-11 shows the UAV cost per additional saved life. Each bar is labelled with a design name in the form *X_Y*, where *X* is UAV range (km) and *Y* is the payload mass (kg). If the designs are ranked according to this metric, the recommended optimal UAV has an intermediate value of range and payload capacity[82].

More information about the trade-off between saved lives and UAV life-cycle cost can be gained by examining the Pareto front plot in Figure 7-12. Four of the points on the front correspond to a range value of 500 km which appears to deliver good value irrespective of the payload mass.

[81] There are no planned maintenance operations. The UAV maintenance cost is entirely a consequence of subsystem failures or landing accidents.

[82] Some of the Range-Payload combination could not be achieved within the design space. Therefore the corresponding bars are missing.

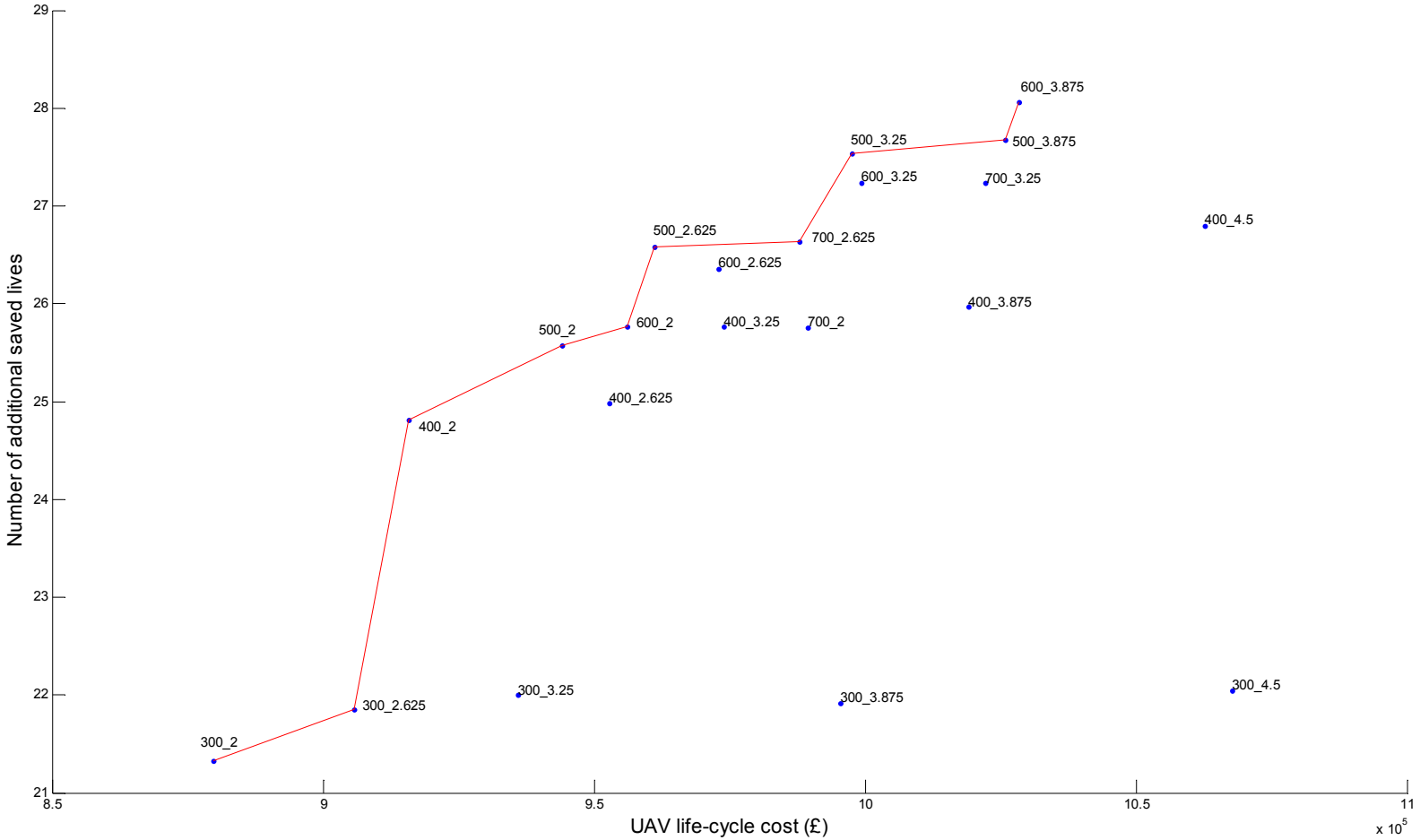

Figure 7-12 – Scatter plot of the number of additional saved lives and UAV life-cycle cost. The labels on the data points display the value of range (km) and payload mass (kg) separated by an underscore. The red line is the Pareto front.

Figure 7-12 also shows that a UAV with a higher life-cycle cost does not necessary provide better mission performance, but the increase in mission effectiveness depends on the correct balance between the range and payload performance.

Finally, it is worth noting that Figure 7-12 presents the decision maker with only a partial set of information regarding the design problem: it contains information about the SAR cost directly related to the use of the UAV, but neglects the secondary effects on the cost of the other assets participating to the mission.

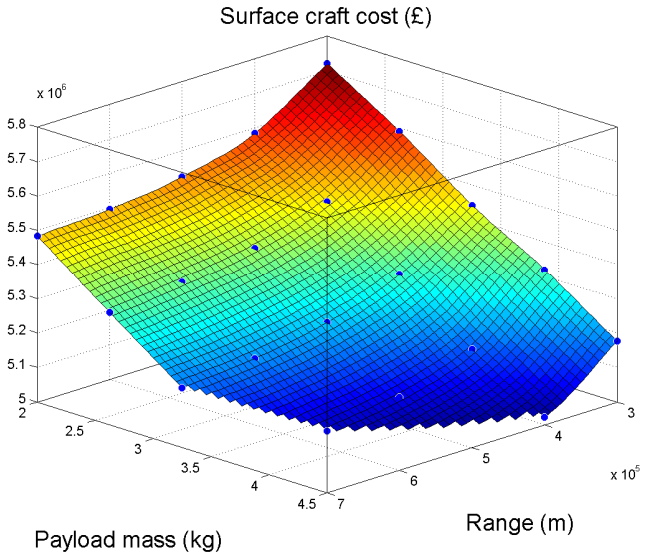

Figure 7-13 – Effect of payload mass and UAV range on the total Surface craft cost.

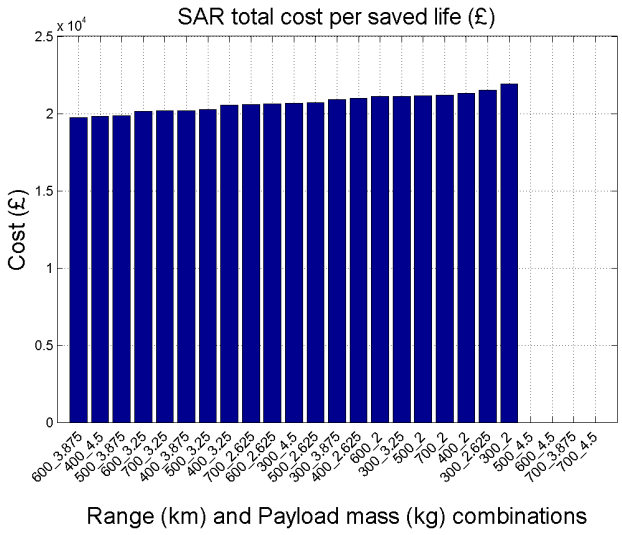

Figure 7-14 – SAR total cost per saved life; the labels on the x-axis display the value of range (km) and payload mass (kg)

Figure 7-13 shows the impact of the UAV design parameters on the surface craft cost, that is, the total cost of the operations of the lifeboats. It is strongly correlated with the total lifeboats utilization time (Figure 7-8a) and it is one of the largest factors contributing to the overall SAR mission cost: the hourly cost of a lifeboat is significantly higher than the one of the UAV; moreover, in the simulated scenario multiple lifeboats are present.

If the SAR total cost per saved life (Figure 7-14) is used as design ranking parameter, the model recommendation of the best system is different from the one provided by Figure 7-11. Note that in this case the total number of saved lives (i.e. including the saved lives in the baseline scenario) has been used. The SAR total cost includes the cost of the UAV and the surface craft.

The Pareto front of the overall SAR mission is shown in Figure 7-16. One design point dominates the set (600_3.875, in red). This point corresponds to the highest number of saved lives and the lowest overall cost of the SAR mission. Therefore, in this particular case, the identification of the best system can be performed without the need of an explicit aggregated value function.

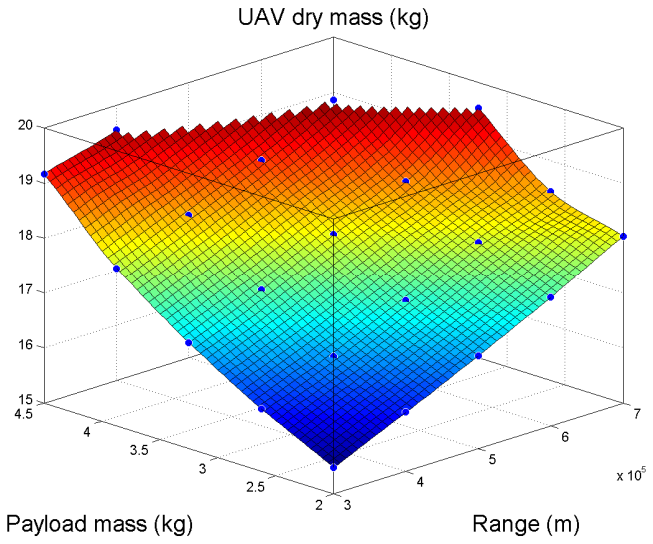

Figure 7-15 – Effect of payload mass and UAV range on the UAV dry mass.

By examining the surface plots in the previous figures, it can be seen that the point 600_3.875 is on the boundary of the feasible space. In particular, Figure 7-15 shows that the UAV dry mass limit of 20 kg is the limiting factor. The same applies to the points 400_4.5 and 700_3.25. These designs are subject to the risk that a small error in the estimate of the aircraft mass might result in surpassing the limit for the CAA SUA category and as a consequence incur in substantially higher regulatory costs. Therefore, the designer might decide to adopt a more conservative approach and select a design that provides a safety margin on the estimated mass.

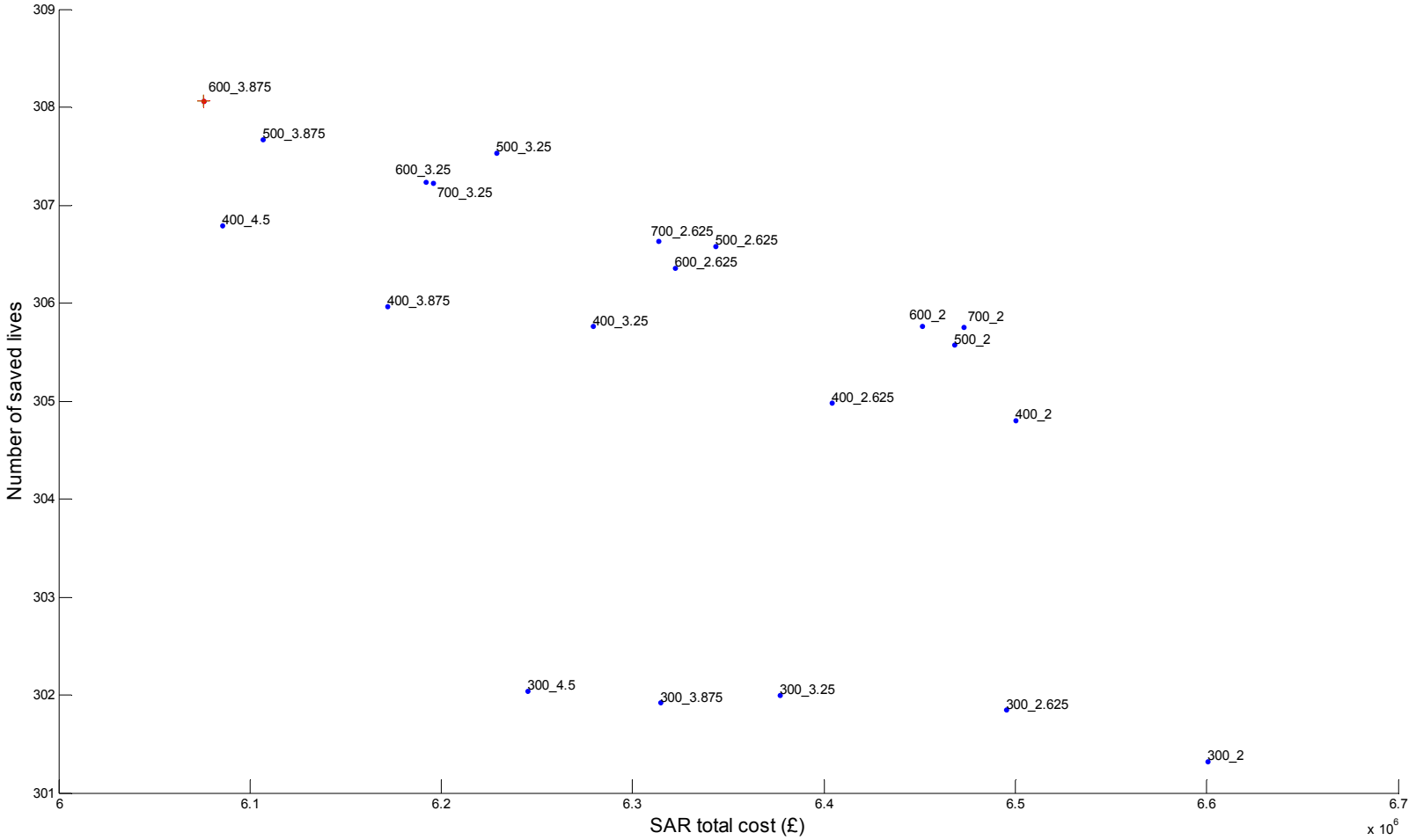

Figure 7-16 – Scatter plot of the total number of saved lives and SAR total cost. The labels on the data points display the value of range (km) and payload mass (kg) separated by an underscore. The red cross is the Pareto front.

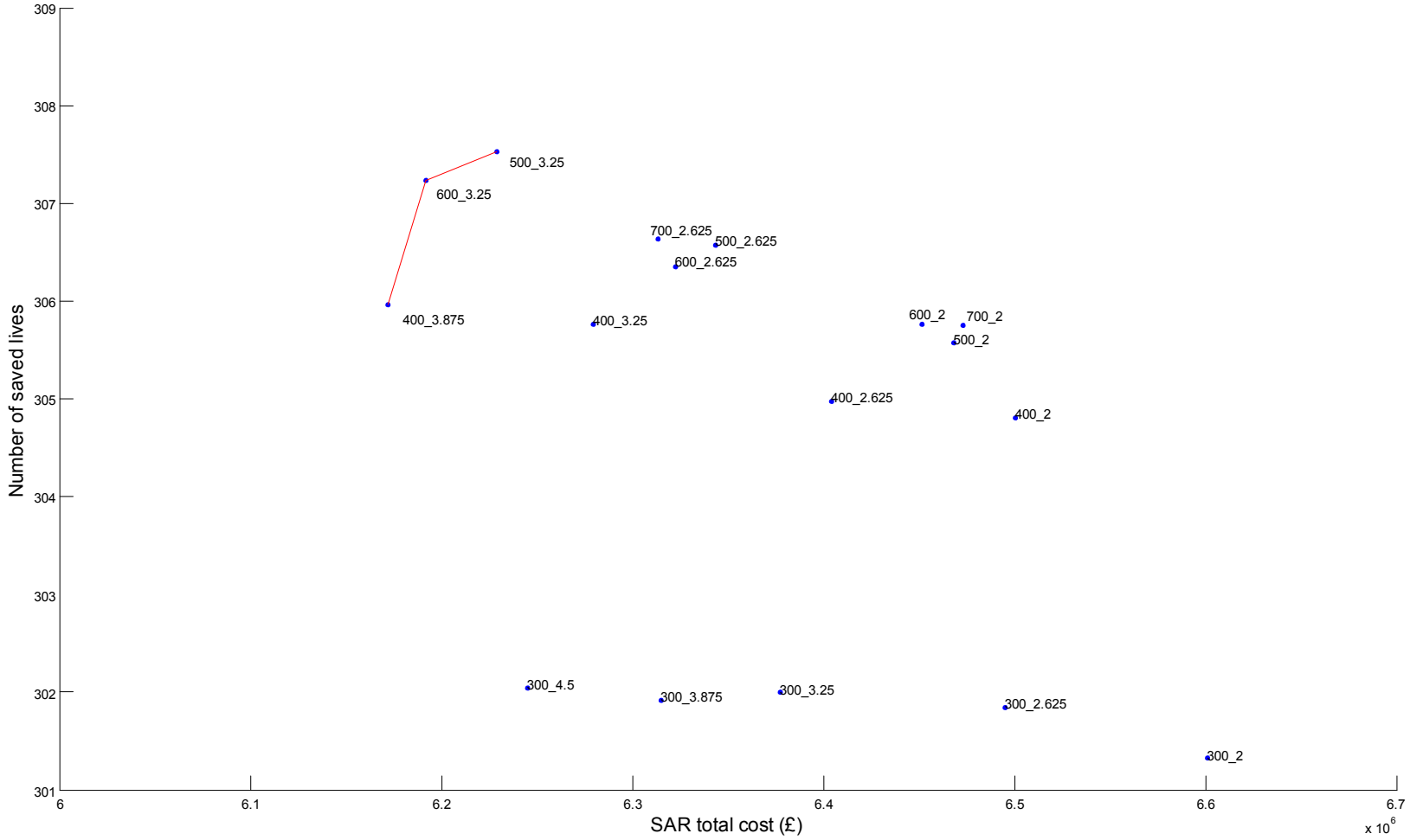

Figure 7-17 – Modified scatter plot of the total number of saved lives and SAR total cost: the designs with a dry mass higher than 19 kg have been excluded. The labels on the data points display the value of range (km) and payload mass (kg) separated by an underscore. The red line is the Pareto front.

Figure 7-17 was obtained by excluding the designs with a dry mass higher than 19 kg. This provides a 5% safety margin over the mass calculation. In this case, there are three points on the Pareto front and therefore the choice of the best system is not straightforward. The introduction of an aggregate value function can provide guidance in such a situation.

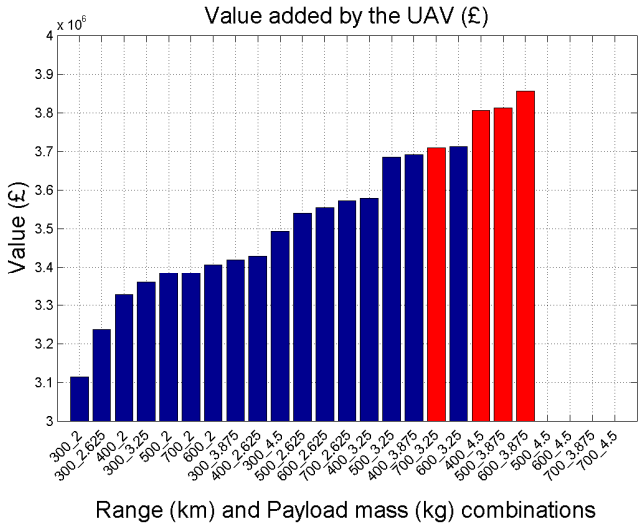

Figure 7-18 – Value added by the UAV to the SAR mission. The labels on the x-axis display the value of range (km) and payload mass (kg). The red bars correspond to UAVs with a dry mass higher than 19 kg.

In particular, if the worth model approach (Section 6.8.1.1) is used and risk neutrality is assumed, the value added by the UAV to the SAR mission can be obtained by adding the monetary benefit of the additional saved lives and subtracting the difference between the operational cost with and without the UAV. The bar plot in Figure 7-18 was obtained assuming the VSL equal to £32.2k[83]. Excluding the designs with a dry mass higher than 19 kg (corresponding to the red bars), the design with the highest value is 600_3.25. Additionally, Figure 7-18 shows that the other two points on the Pareto front (i.e. 400_3.875 and 500_3.25) have a similarly high value and could potentially be good design alternatives.

Figure 7-19 provides an additional piece of information: the value gradient. This can be used to identify robust design options. For example, the plot shows that the value gradient at point

[83] This value was obtained from the baseline SAR simulation as explained in Section 7.4.1. As already discussed in Section 6.8.1.1, the estimate of the VSL can vary massively; the effect on the model is to increase or decrease the relative importance of the number of saved lives. However, the main point is that, once agreed on a VSL, the aggregated value function provides the designer with a well-defined gradient that can be used to trade range and payload requirements.

400_3.875 is relatively steep, making it a high-risk design point[84]. Conversely, point 600_3.25 is a relatively robust design option with respect to range, but the value gradient with respect to the payload capacity is relatively high.

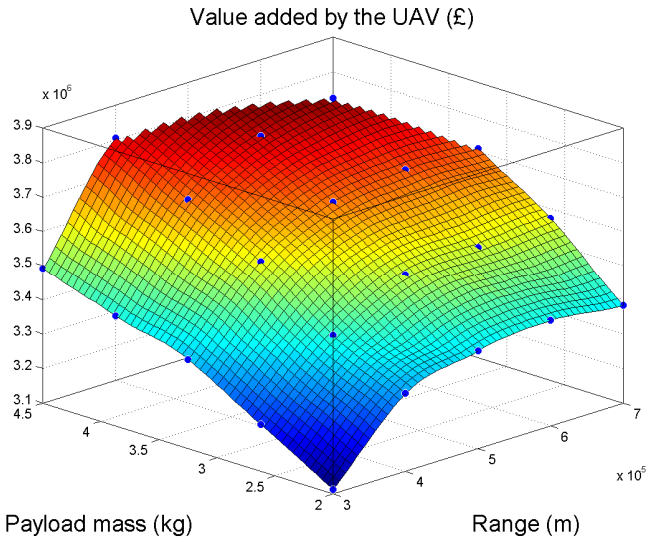

Figure 7-19 – Effect of payload mass and UAV range on the Value added by the UAV to the SAR mission.

7.4.5 The Impact of the Aircraft Configuration on the Value Metrics

DUADE can be used to compare different aircraft architectures. Figure 7-20 shows a comparison of five UAV configurations in terms of MTOM, unit cost, total SAR cost and number of saved lives. The design vector displayed in Table 9 was used for the comparison.

Figure 7-20a. and Figure 7-20b. indicate that configurations featuring a twin boom tail empennage achieve the design performance with lighter and cheaper aircraft: their engine is closer to the CoG of the aircraft and therefore they require shorter fuselages to ensure the correct stability margin. Comparing configuration 1 and 3 as well as 2 and 5, it can be seen that configurations featuring a "V" empennage are marginally lighter and cheaper than the ones featuring vertical and horizontal stabilisers. Configuration 4 is the heaviest and most expensive: the "canard" configuration is penalised by the rear engine position, the reduced flexibility of the position of the CoG, and the problems related to the use of flaps as high lift devices on the main wing (due to the associated pitching moment). These effects combined result in a larger, heavier and more expensive system for the same performance point.

[84] If the design requirements for range or payload capacity are not met, there is a high reduction of the system value.

Figure 7-20c. and Figure 7-20d. show the performance of the five configurations with respect to the mission value metrics. In particular, the UAV configuration has a small impact on the number of saved lives (Figure 7-20d.). This is not surprising because all the UAVs were designed to achieve the same mission capability.

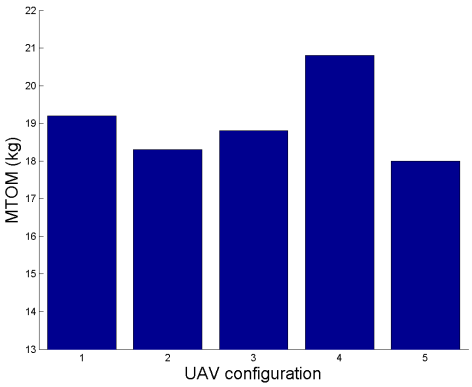

a.

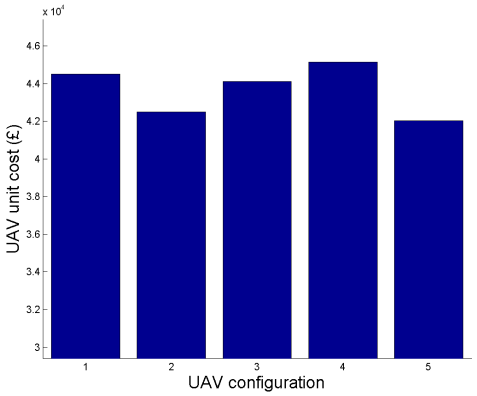

b.

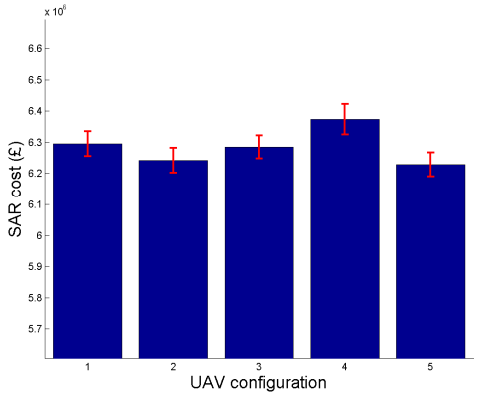

c.

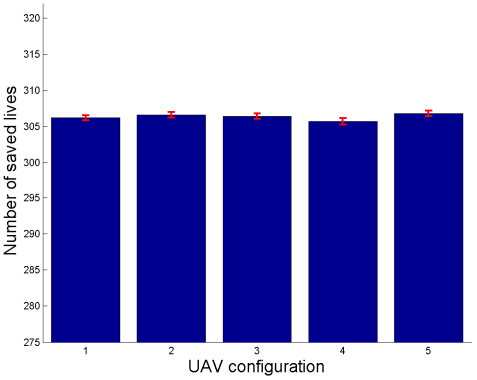

d.

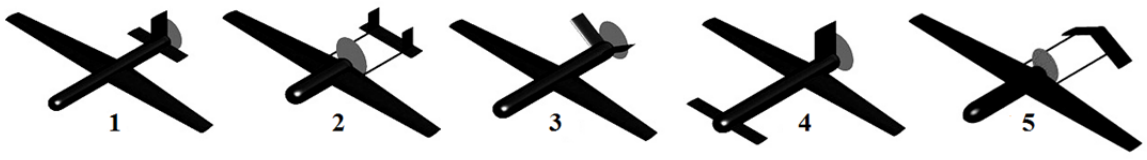

e.

Figure 7-20 – Comparison of five UAV configurations (displayed in **e.**) in terms of **a.** MTOM, **b.** UAV unit cost, **c.** total SAR cost, **d.** Number of saved lives. The red bars in **c.** and **d.** are the sample standard deviations.

The influence of the UAV configuration on the total SAR cost (Figure 7-20c.) is more evident, with configuration 2 and 5 performing better than the others. This is due to the fact that the lower mass offered by these configurations result in lower fuel burn and lower probability of landing mishaps. Configuration 2 and 5 are also cheaper than the others, thus the cost of replacing the airframe is lower when the mishaps do happen. The difference between the configuration 2 and 5 (as well as between 1 and 3) is very small; therefore, further higher-LOD analyses are required to select either configuration. Design consideration can also play a role in the decision (for example one can prefer the horizontal and vertical stabilizers solution because of their modularity even if they are marginally heavier).

Finally, it must be noted that the configuration ranking depends on the design point; different payload, range and speed requirements might result in a different optimal configuration.

7.5 Design Indications

The exploration of the design space provided the following indications.

High-performance aircraft generate higher value even if their life-cycle cost is higher. The value is generated by simultaneously increasing the number of saved lives and decreasing the surface vehicles' SAR cost. Range, search speed and payload mass are among the parameters with the highest impact on the mission effectiveness. The reduction in the operational cost of SAR surface vessels outweighs the life-cycle cost of the UAV support.

The configurations featuring a twin boom empennage can achieve the design performance with a lighter and less expensive airframe. The inverted "V" empennage results in a marginally better solution than the traditional configuration. However, the difference between the two is too small to be detected on the mission-level metrics.

The study showed that unreliability affects greatly the UAV life-cycle cost. Figure 7-21 shows the breakdown of the total cost of the UAV SAR support service for the design point 600_3.25. In this case, more than 80% of the total cost is due to maintenance (that includes the cost of repairing broken components and the cost of replacing the airframe in case of mishaps). The main contributor to this cost is the number of UAV mishaps, which are on average 24.7 for this design; 7.3 of which are inflight mishaps and 17.4 are landing mishaps[85]. By dividing the mishaps number by the total flight time in hours, it is possible to obtain an estimate of the mishap rate, which is

[85] The Operational Simulation provides two different outputs for mishaps due to landing crashes or to in-flight component failures. The data presented in this work refer to the sum of the two, unless otherwise stated.

1160 mishaps per 100,000 hours (817 mishaps per 100,000 hours if only inflight mishaps are considered). This value is comparable to the mishaps rate of military UAVs in their infancy: Figure 7-22 shows that the mishap rate of some of the military UAVs can be as high as 900 mishaps per 100,000 hours in their early service life[86]. Figure 7-22 also shows that the mishaps rate decreases as the cumulative flight hours increase, suggesting that iterative improvements to the system design have a very strong impact on the system reliability. However, in the case of bespoke rapid manufactured UAVs, the system life-cycle might be too short to offer the opportunity of substantial iterative improvements.

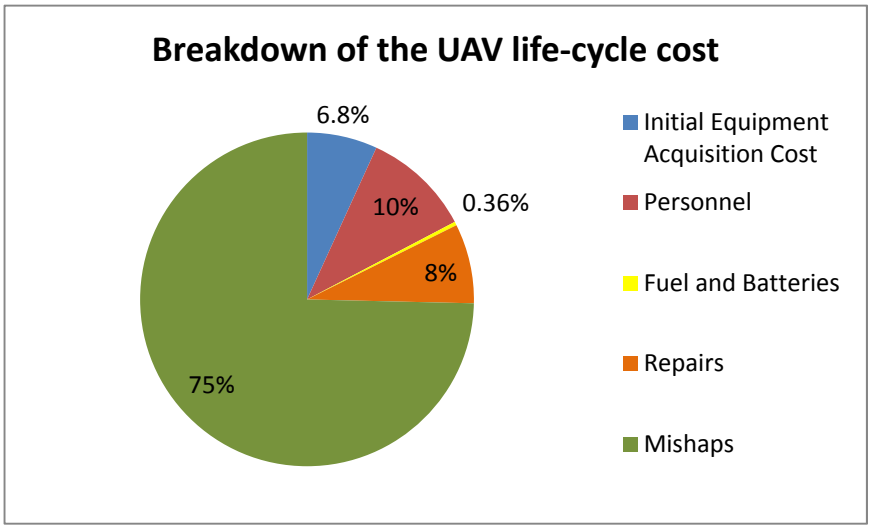

Figure 7-21 – Breakdown of the UAV life-cycle cost of the design 600_3.25.

The high maintenance cost suggests that there is an opportunity to increase the system value by investing more in reliability and exploring different strategies not accounted for in this study; such as increasing the number of redundant subsystems or introducing a planned maintenance schedule.

The number of UAV mishaps is influenced by the search speed and the payload mass (through the reduction of the UAV flight time) as well as the reliability of the components (through the RIR) and the landing speed (through the kinetic energy upon landing). Investing in a high-quality payload system can reduce the maintenance cost more than investing directly in more reliable components.

Overall, the study indicated that payload is among the subsystems with the highest impact on the mission performance and on the characteristics of the aircraft (cost, mass and size of the

[86] In the UAS Roadmap 2005-2030 [275], the Department of Defense of the United States of America defines a mishap as an accident resulting in significant damage or total loss of the aircrafts; class A and B identify the economical severity of the accident (accidents with loss of a UAV causing less than $1,000,000 are class B).

airframe). The quality of the payload affects heavily the value metrics, increasing the number of saved lives and decreasing the SAR mission cost. This information should lead the designers to invest time and effort to improve the payload model and validate the assumptions.

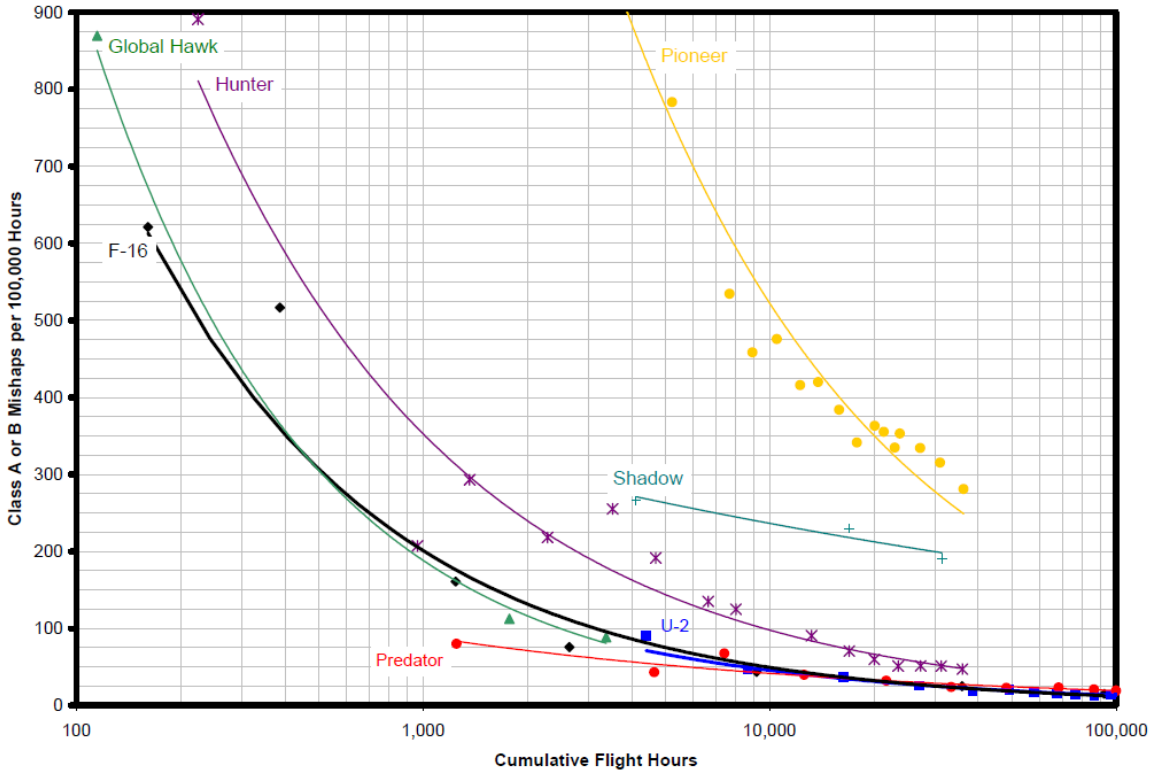

Figure 7-22 – Military UAV class A and B mishaps per 100,000 hours as a function of the cumulative flight hours [275].

Furthermore, this study highlighted the correlation between the impact on value of range and payload mass, allowing the designer to identify optimal range-payload combinations. Moreover, the integrated design environment enabled the assessment of the design trade-off over multiple system's attributes simultaneously. As a consequence, the designer could identify design options that offered both high value and an appropriate safety margin over the violation of design constraints. Additionally, it was possible to identify the more robust design options and to assess the sensitivity of the value function with respect to the input parameters.

Finally, the study highlighted that some of the factors that have the highest influence on the mission value are the ones that are normally neglected in concept design tools, such as the payload model, the subsystems' reliability, the landing mishaps, and so on.

7.6 Final Remarks

7.6.1 Benefits of DUADE System Design Loop

By integrating a value model and an operational simulation in the system design loop, DUADE introduces a number of improvements on traditional aircraft design tools.

- It facilitates the identification of quantitative relations between the engineering requirements and the mission level metrics (for example: the impact of the range requirement on the UAV maintenance cost).
- It enables the designer to assess the impact of design parameters on the overall mission scenario, thus capturing indirect effects of the UAV performance on mission metrics (for example: the impact of the range requirement on the surface craft maintenance cost).
- It unveils counterintuitive effects of the design parameters (For example: increasing the payload mass increases the hourly fuel consumption, but the total fuel burned decreases).
- It provides the designer with a tool to elicit optimal technical requirements from the concept of operations and the environmental model rather than relying on engineer's estimates.
- It provides a way to elicit the mutual value dependency of the performance attributes (For example: the impact of range given a certain payload capacity and vice versa).
- It provides the value gradient necessary to perform trade-offs between desirable characteristics.

7.6.2 Mutual Value Dependency of the Performance Parameters

One of the biggest advantages of the DUADE approach is that it provides a way to balance performance requirements by assessing their mutual value dependency. Most multi-objective value models are often based on the hypothesis of mutual utility independence (the MAUT is probably the best example). This is to say that the utility (or value) associated with the level of one of the attributes is independent of the value of the other attributes. Rigorously, the MAUT should be applied to the overall value attributes (in this case study, the number of saved lives and the SAR operational cost). However, in the absence of a detailed end-to-end simulation, performance attributes are often used as a proxy for the system value: the decision maker assigns weights and combines performance attributes as if they were independent value metrics. However, as demonstrated by the SAR case study, the value of the performance attributes is strongly dependent on their mutual value. In the end, while it is obvious that a very long endurance UAV is useless if it cannot carry any payload, the marginal value of range as a function

of the payload mass is difficult to estimate unless a quantitative analysis is performed. DUADE provides the ability to perform such analysis.

The impact of performance parameters can also be indirect by restricting the feasibility space: for example Figure 7-6 shows that reliability does not have a large impact on the number of saved lives. However, increasing the system reliability increases the UAV mass which consequently limits the maximum range and payload capacity achievable and therefore can negatively impact the number of saved lives.

7.6.3 Challenges of Modelling the Operational Simulation

The quality of the results produced by the DUADE trade space exploration strongly relies on the correct modelling of the Operational Simulation and Value Model. This represents at the same time the strength and the weakness of this design environment.

On one hand, modelling the interaction of the UAV with the other agents and the environment enhances the understanding of the operations and allows the designer to elicit the system characteristics that lead to the best value. The more details that are included in the model, the more secondary interactions can be unveiled and understood.

On the other hand, a detailed mission simulation requires models of the mission logic, agents and systems that are not the object of the design effort. These models have to be accurate enough to correctly capture the interaction with the UAV and output the overall mission performance. Gathering the information required to create these models can be very time-consuming, or the information can be simply not available to the designers. Moreover, each model implies the existence of assumptions and approximations that need to be understood and controlled. An aircraft designer might not have the necessary experience or skill to correctly model the behaviour of different vessels. Operational variables (for example the maximum time the lifeboat crew can spend in the mission before needing a replacement or the time it takes to launch a vessel) can have an even higher impact on the mission performance while being difficult to estimate accurately.

Increasing the complexity of the model implies a higher number of modelling parameters (for example the speed of the surface craft, the maintenance time and schedule, the casualty detection radius, the cost of fuel, and so on). The effect of uncertainty on the parameters of the value model downstream of the Operational Simulation can be assessed using Monte Carlo simulation or sensitivity analysis. Parameters that have an impact upstream or within the

Operational Simulation have a relatively high computational cost and such analysis can be extremely time-demanding.

7.6.4 The Role of the Intermediate Objective Function, Design Variables and Performance Parameters

The basic hypothesis that led to the introduction of the bi-level system design process was that an intermediate sizing optimisation was required to ensure the physical consistency of the model and to filter out suboptimal designs. However, the physical consistency of the model only requires the satisfaction of the equality constraints. This can be achieved without recurring to a performance-related intermediate objective function. Designs that do not satisfy inequality constraints can be filtered out by the algorithm before being fed to the Value Model. By using this approach, low-level design variables (for example, the wing span or the propeller size) can be linked directly to the mission level performance. However, the impact of low-level variables is strongly dependent on the mutual interaction with the other variables (i.e. increasing the wing span by a certain amount can lead to very different results on the mission performance depending on the size of the tailplane, fuselage, propeller, and so on). For small enough variations of the input parameters, the impact of the design variables can be considered approximatively independent. However, such small variations are also likely to generate small variations in the aircraft performance that are difficult to detect in the stochastic operational model because of the simulation noise. On the other hand, large variations of the input variables require adjustment of the other design variables in order to achieve a feasible design (a large increase in wing span requires an increase of the dimension of the vertical stabiliser, a more robust wing structure, a more powerful engine, and so on). Therefore, the impact of a particular design variable in isolation is very difficult to assess.

The simulation noise can be reduced by increasing the number of replications: the width of the confidence interval of the simulation outputs is inversely proportional to the square root of the number of replications; hence its reduction requires progressively increasing computational power. However, this has little practical sense for models based on relatively coarse approximations [87].

Another possible solution to “smooth” the model output is to create a surrogate model using response surfaces. However, if the aim is to link low-level design variables to the system value, such surrogate model has to include all these variables, which can be hundreds even in the

[87] Using a metaphor, it is like spending large resources to increase the precision of a measurement performed using an instrument with poor (unknown) accuracy.

concept and preliminary design phase. If, instead, the performance requirements are treated as input, the surrogate model can be built around a few key performance parameters. However, in this case, the design variables must be controlled by the sizing tool.

The intermediate sizing optimisation loop filters out suboptimal designs, thus reducing the overall computational time required to explore the design space. It also allows the designer to generate large changes in the performance parameters while ensuring that the aircraft meets the feasibility constraints. The impact of large performance changes can be more easily measured by the Value Model.

The intermediate sizing optimisation also increases the intelligibility of the value model results: it is easier for the designer to understand why range and/or cruise speed have a particular impact on the mission performance rather than explaining why the size of the horizontal stabiliser changes the number of saved lives. This is important because the model of a complex operational scenario cannot be exactly replicated in reality and therefore it is not possible to validate the model experimentally. Wrong assumptions and mistakes in the ConOps model have to be identified using the user judgment and experience. Therefore, it is paramount that the designer can explain the outputs of the Operational Simulation and Value Model, even when these seem counterintuitive.

However, the introduction of an intermediate sizing optimisation is not a straightforward process.

First of all, the choice of the intermediate objective function proved to be a more complex problem than anticipated. In Section 7.3.1 it was shown that optimising the aircraft for cost, mass or cruise efficiency can result in very different solutions. The three attributes were chosen because of their anticipated influence on the mission value metrics; however the interaction between the parameters of the aircraft model and the Operational Simulation cannot be fully captured by only two or three metrics. For example, the “empty mass” attribute was not used in the trade space exploration, even though the aircraft mass has a direct influence on some of the Operational Simulation output (for example the probability of landing mishaps). Similarly, the value of the fuel burn rate at cruise refers to a specific mass, flying speed and altitude of the aircraft. However, in the Operational Simulation, the UAV lifetime fuel consumption is obtained through a more complex calculation that accounts for different flight segments, current mass and several other parameters (drag polar coefficients, propeller efficiency, BSFC, and so on).

The impact of different UAV designs on the mission performance is directly influenced only by the parameters that define the aircraft model in the Operational Simulation (Section 6.8.2.1). It could be argued that they all should be included in the aggregated intermediate objective function; in

which case, even using a simple weighted sum of these parameters, a variable (the scaling factor) needs to be introduced for each of the aircraft parameters. These would increase the number of variables of the value trade space exploration beyond practicality.

Alternatively, only a subset of these parameters with the highest impact on mission value could be used. However, this requires a sensitivity analysis of the mission value with respect to the parameters of the aircraft model; but these parameters cannot be changed in isolation without compromising the consistency of the model (For example: if the mass is increased without changing the engine size and the wing area, the resulting UAV might not have enough power or lift to take-off).

Finally, the use of an additive aggregate objective function can result in a chaotic behaviour of the AST: it is possible that for a specific value of the scaling factors, multiple equivalent solutions can be found. In this case, small perturbations on the model parameters can result in radically different "optimal" aircraft indicated by the AST[88]. This can generate confusion in the interpretation of the value model results and therefore prevent the designer from using the model to guide design decisions.

The problem described above can also occur if only one attribute is used as the intermediate objective function. The aircraft empty unit cost is indeed an example of non-convex design space; for a particular design performance, there might be multiple geometries that minimise the objective function (the empty cost being the sum of several components).

Figure 7-23 shows a comparison between surface plots of MTOM, maximum engine power and overall SAR value obtained varying the UAV range and landing speed and optimising either for empty cost (a, c, and e) or fuel burn rate at cruise (b, d, and f). Surface plots displayed on the right-hand side appear "smooth", hence indicating that gradual changes in the performance requirements generate gradual changes in the design characteristics of the optimal aircraft. Instead, plots obtained by optimising the UAV for the empty unit cost (on the left-hand side of Figure 7-23) appear less regular. Moreover, the impact of design requirements on the system value seems to be dependent on the choice of the intermediate objective function: both Figure 7-23e and Figure 7-23f indicate that a low landing speed and a long range are associated with high value, but, if the range is fixed to 300 km, landing speed has a different impact in the two cases.

[88] For example, if the intermediate objective function is obtained as the weighted sum of fuel efficiency and airframe cost, two different designs – one with high efficiency and cost and the other with low efficiency and cost – can generate equivalent values of the intermediate objective function.

Optimised for empty unit cost | **Optimised for fuel burn rate at cruise**

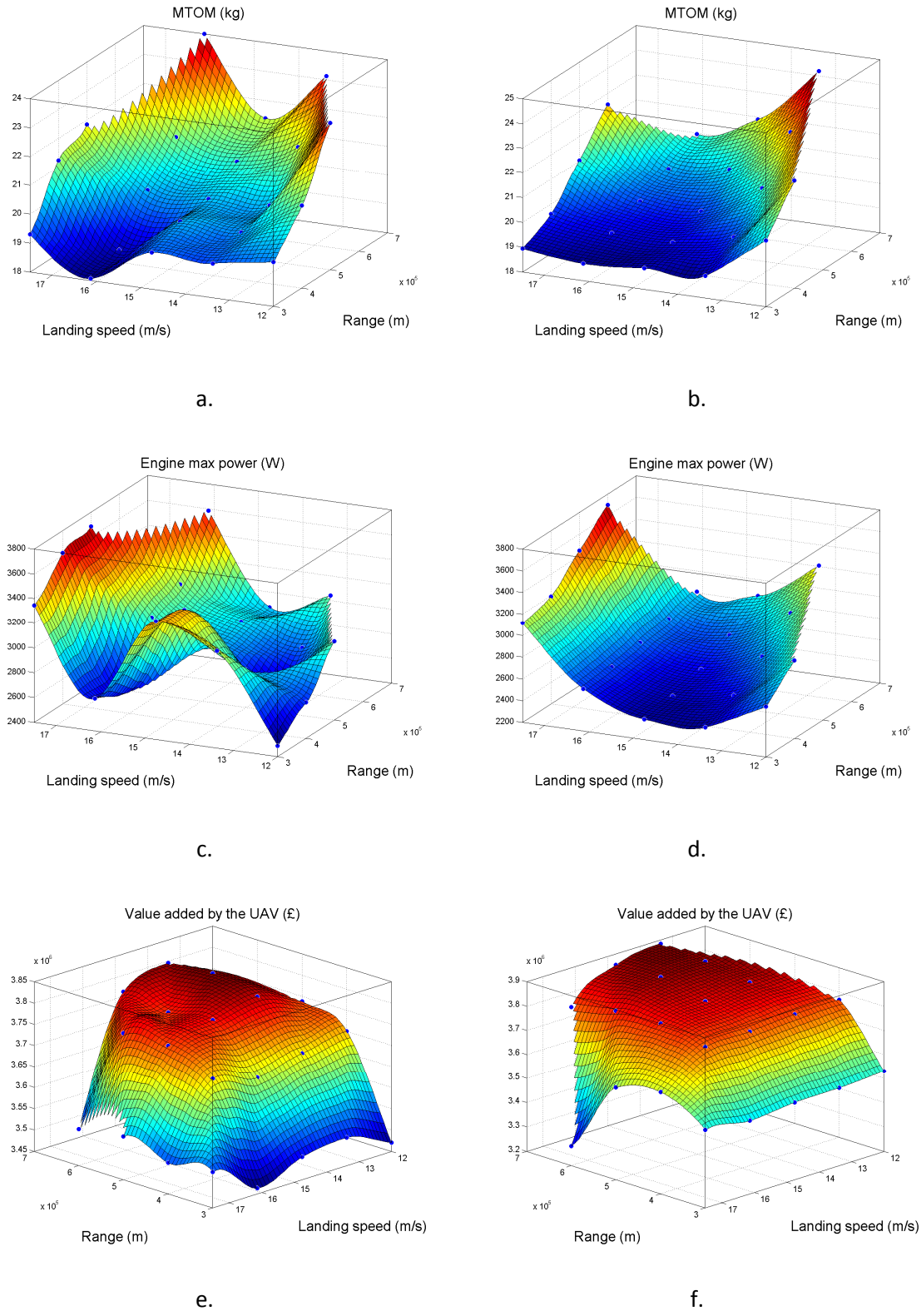

Figure 7-23 – Side-by-side comparison of UAV optimised for empty unit cost (left column) and fuel burn rate (right column). Effect of UAV landing speed and range on: **a**. and **b**.Maximum take-off mass **c**. and **d.** Engine max power.**e**.and **f.** Value added by the UAV. Note that input axes are rotated to enhance the picture readability.

In the case study presented in this chapter, optimising the aircraft for fuel efficiency generally leads to superior results. However, it is possible that the model of different missions will lead to the opposite result. In such cases, the author's opinion is that the designer would benefit most by choosing an intermediate objective function that leads to an easy understanding of the value trends. Once an optimal performance point has been identified, the impact of the intermediate objective function can be studied independently.

7.6.5 Supporting Value Driven Design After the Concept Phase

The DUADE System Design Loop was intended to support design in a spiral refinement development cycle. The value model and the Operational Simulation provide guidance in the selection of the system performance requirements in the concept design phase. Preliminary design calculations are performed concurrently during the design space exploration phase. As the design progresses toward the detailed phase, more accurate information is obtained regarding the UAV subsystems characteristics and attributes. For example, selected COTS parts become available and the estimation of their mass and cost can be updated with the actual values; the geometry of the airframe is refined and a more accurate aerodynamic and mass calculation can be performed.

During the progressive development of the system, designers have to deal with trade-off decisions on a smaller and smaller scale. For example, designing the empennage the engineers have to compromise between its mass, cost and aerodynamic efficiency. Having multiple design options, they can in principle rank them according to their value by updating the aircraft model and re-running the value model. Unfortunately, this process is not as straightforward as it appears.

Small deviations from the values calculated in the concept/preliminary design phase are likely to be undetectable for the value model due to the simulation noise. On the other hand, large deviations might require updating the design of other subsystems.

Moreover, designers rarely complete discrete design options before comparing them, particularly in the context of rapid system development where time pressure is very high. Instead, they rather concentrate their effort on achieving the desired characteristics focusing on the attributes they reckon more important. Providing a value gradient as a function of the subsystem's attributes would greatly help designers in the preliminary and detail phase.

This can be achieved through the decomposition and linearization of the system value as a function of its extensive attributes. This approach requires that the impact on value of the

extensive attributes can be measured independently at the system level. One way to achieve this is the introduction of scaling factors to be applied to the calculation of the extensive attributes. These Extensive Attribute Scaling Factors (EASFs) would act similarly to the RIR used in the study presented in this chapter. However, in order to isolate their contribution to the system value, no secondary effect should be linked to them. That is, each EASF should proportionally increase or decrease its extensive attribute without affecting the others. A similar idea is exploited by the Unified Trade-Off Environment [100,135,276] with the aim of capturing the effect of the infusion of an immature technology, but the impact of the EASFs is not propagated to the system value.

One interesting question is whether the EASFs should be applied to the model before or after the sizing optimisation. In the first case, they will influence the outcome of the sizing operation (for example, scaling the mass up or down will have an impact on the optimal aircraft geometry). In the second case, the aircraft design will be considered fixed and the impact of the EASF will be seen only on the value model and Operational Simulation output. In practice, the choice depends on the level of design freedom that is left at the moment of the study. If the aim is to guide low-level design decisions as in the case of detailed design, the second option should probably be preferred. However, in this case, there is no guarantee that the resultant aircraft would not violate the design constraints (for example requiring more power than the engine can provide) and hence generate errors in the system value assessment.

A sensitivity analysis can be used to evaluate the contribution of each subsystem to each of the overall system attributes. The impact of a particular subsystem's extensive attribute on the overall system value can then be obtained by propagating its contribution bottom-top (for example a 10% increase of the empennage mass might cause a 2% increase of the UAV mass and 0.5% decrease of the system value). A component/subsystem scorecard can be used to guide design decisions by providing the relative importance of the local extensive attributes (value gradients) [30,154].

This approach is based on the assumption that the value model is able to correctly capture the effects of small variations of the system extensive attributes. Figure 7-24 shows a simplistic representation of the problem. It is assumed that the modellers have been able to produce a relatively good model (blue curve) representing the impact of a generic attribute x on the true system value (red curve). The model correctly captures the general trend (decreasing x, the value increases). However, it neglects some second order effects, for example because of the approximations introduced or because some piece of information was not available.

During detail design, the engineers are provided with the value model (or its linearized form) and can only produce small changes of the attribute x. In the example of Figure 7-24, if the baseline

design is represented by point A, the value model will drive their design decisions in the direction of decreasing *x* (i.e. toward point C). By doing that, they will effectively decrease the real system value (point B)[89].

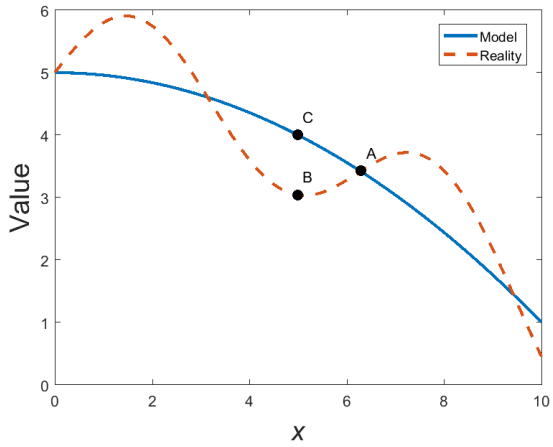

Figure 7-24 – Value model versus reality.

As shown by this simple example, the use of a high-level value model to guide detail design decisions can be misleading if the fidelity of the value model is not high enough to provide the correct value gradient in response to very small "perturbations" of the system attributes. The achievement of this level of fidelity is practically not possible due to the high complexity and the high number of unknowns that are involved in the creation of such a comprehensive model. For example, Section 7.6.3 has highlighted some of the issues related to the modelling of a non-physics based simulation. Analogous difficulties are encountered when modelling manufacturing, maintenance, and other activities involving human interaction and decision making[90].

The author's opinion is that VDD philosophy and the idea of value scorecards can still be applied to detail design but it requires dedicated local value models that account both for the indications provided by the top-level value model and the specific problems encountered during development of the subsystems.

7.7 Summary

This chapter has presented the application of DUADE to the design space exploration of a SAR UAV. The study has demonstrated the advantages of a design environment in which technical

[89] For example, the designer might decide to eliminate an inspection hatch from the fuselage to decrease its manufacturing and assembly cost. However, this decision might generate a higher life cycle cost as a consequence of an increased maintenance time.

[90] It is worth noting that the low level of fidelity of these models is generally related to the ignorance/absence of an accurate theoretical model rather than to the lack of computational power.

requirements, mission level performance and life-cycle cost can be evaluated simultaneously. The importance of creating a comprehensive multidisciplinary design environment has been demonstrated by the impact that disciplines traditionally overlooked in concept design studies have on the system value.

The UAV performance requirements have been treated as the input of the design space exploration. Their impact on some of the aircraft extensive attributes (mass, cost and fuel efficiency) has been studied first. Then, the impact of performance requirements has been propagated to the mission level metrics through the use of the agent-based operational simulation. Finally, the Cost-Benefit model has been used to identify the designs that provide the best overall value and the most robust design solution. The impact of different design configurations has been studied, too.

The study has demonstrated how some counterintuitive effects can arise from the operation of the UAV in a complex environment featuring multiple agents cooperating for the same mission. This has also highlighted the importance of providing the decision maker with a comprehensive set of simulation outputs in order to facilitate the understanding of the factors and dynamics that contribute to the value generation. Moreover, the intermediate outputs generated by DUADE can be used to scrutinise the models and provide explanations for possible emergent behaviours.

Finally, some of challenges posed by the use of a stochastic operational simulation, the use of a bi-level sizing strategy and the use of VDD during detail design have been discussed.

8 Conclusion

8.1 Introduction

This chapter presents a summary of the novel contribution of this research. It also presents the answers to the research questions formulated in Chapter 1 and a review of the research hypotheses.

8.2 Novel Contribution

The original contribution to knowledge of this work can be summarised in the following points:

- The design, construction and flight test of largely 3D printed unmanned aircraft – among which is the world's first entirely 3D printed aircraft – has demonstrated that the use of Additive Manufacturing technology and materials is a viable option for the production of structural components of airframes with a maximum take-off mass up to 35 kg.
- The use of 3D printed structural components has allowed the author to highlight the merits and limitations of AM for UAV design. In particular, the short development time, the adaptability and the opportunity for continuous development have been identified as the main advantages; the process accuracy, the size limitation imposed on the parts and the unavailability of low-cost high-performance materials are currently the main drawbacks.
- Confined complexity – a design principle based on a simple manufacturing complexity measure, engineering judgment and a basic network analysis of the system physical architecture – has been proposed as a method to guide engineers during the design of partly 3D printed airframes.

- The development of a design framework for mission-specific rapid-manufactured aircraft, named DUADE, where an aircraft sizing tool, an agent-based operational simulation, and a value model are used concurrently to make design decisions about the system characteristics.
- The study has demonstrated the benefits of using a detailed life-cycle simulation from the concept design stage: the impact of the aircraft and payload performance, the reliability of its components, and the interaction with the environment (geography

and other agents) can be evaluated simultaneously in order to estimate the total life-cycle cost and mission effectiveness providing a superior understanding of the design space.

- The study has also highlighted the importance of providing the decision maker with a comprehensive set of simulation outputs in order to facilitate the understanding of the factors and dynamics that contribute to the value generation. Moreover, the intermediate outputs generated by DUADE can be used to scrutinise the models and provide explanations for possible emergent behaviours.

8.3 Review of Research Hypotheses

8.3.1 Design for Additive Manufacturing of UAV Airframes

Hypothesis 1 – The extensive use of additive manufacturing can improve the design process of small low-cost unmanned aircraft by increasing its flexibility and reducing the development time and cost.

The design, construction and test of the rapid-manufactured UAVs described in this work have proven that AM can be considered as a viable technology for the production of small unmanned aircraft. The short development time and the possibility of iteratively improving the design proved to be two of the most valuable advantages introduced by AM. Moreover, complex features can be confined to 3D printed parts while the geometry of the non-printed parts can be simplified, hence reducing the overall manufacturing and assembly cost, reducing the overall mass, and allowing the exploitation of mechanically superior materials.

Hence, this hypothesis is verified.

8.3.1.1 Answers to the Research Questions

1 - Is it possible to produce an entire UAV by using only 3D printed components and COTS avionics systems?

The world's first entirely 3D printed aircraft was designed, built and tested in the early phases of this research project. All the structural components were obtained through SLS of Nylon plastic. The motor, the servo actuators, the autopilot and the other electronics components were COTS components. The first prototype was designed to be assembled without the need for fasteners and featured 3D printed control mechanisms.

2 - Are the available materials suitable for the use in UAV structural components?

This research focused on SLS because it is the AM technology that offers the best compromise between cost, process accuracy, and structural performance. In particular, the study was restricted to the use of Nylon 12, which is the most commonly used material in SLS. Nylon 12 proved to be a suitable material for structural components for small UAV with a MTOM that spans from 3 kg to 35 kg. The relatively poor mechanical properties are compensated by the flexibility of SLS that enables the creation of efficient structures by exploiting advanced geometrical design and feature integration. No significant deterioration of the material properties was noticed during normal operation of the UAVs tested at the University of Southampton (some parts have been used for more than three years and 100 flight hours). However, a dedicated study on the long-term stability of Nylon 12 is recommended.

3 - What is the development time of a 3D printed airframe?

This depends on the scale and complexity of the system. The first prototype of SULSA was developed within two weeks; from concept design to flight test. Larger and more complex systems, such as DECODE-2 and SPOTTER, required a few months of design work[91]. In all the cases, the manufacture of the structure was completed in less than two weeks, including the final assembly. The design, prototype, and testing of bespoke avionics systems is currently the limiting factor that prevents even further reduction of the development time of rapid-manufactured UAV. Finally, in the current regulatory framework for the LUAS, the time required to obtain the CAA authorisation to perform the flight test campaign of a novel system can exceed the time required to design and build the system.

4 - What are the major advantages and disadvantages of 3D printed structures?

The main advantages of 3D printed structures derive from the flexibility and rapidity of the AM process. The first can be exploited to create structurally, aerodynamically and cost efficient parts by making full use of the almost complete absence of geometrical constraints. The latter can be used to reduce the product development time and to postpone any cost commitment to the very late phases of the design cycle. Overall, flexibility and rapidity increase the adaptability and customisability of the product and incentivise a process of continuous development.

[91] SPOTTER has been undergoing a process of iterative development for the last three years. However, the design team adopts an agile product development approach where each design iteration is completed within few months from the start of the design activity.

The main disadvantages of 3D printed structures derive from the limitations of the current technology. In particular, the process accuracy and the surface finish can be limiting factors in some applications. The parts produced with AM of plastic, although relatively inexpensive, are sub-optimal for the applications that involve high levels of mechanical stress. On the other hand, AM of metals is expensive and subject to stricter size and geometrical constraints. The main cost driver of 3D printed parts is their physical size, therefore AM is not the most economical way to produce large parts with relatively simple geometry.

5 - Should 3D printed airframes be designed differently to conventional ones? If a partly 3D printed airframe is designed, what parts are best produced using AM?

3D printing removes the penalty traditionally associated with the production of complex structures. As a consequence, the design of multifunctional parts becomes attractive because it can generate mass savings by merging functional and structural features. Moreover, the integration of multiple features into a single structure allows the designer to simplify the assembly operation hence creating the opportunity for an overall cost reduction.

However, multi-functionality and structural integration do not necessary imply the sacrifice of the system physical modularity. In partly 3D printed aircraft, the designer should aim at maximising the advantages of AM by confining complexity to 3D printed components while simplifying the geometry of non-printed components. These 3D printed hubs can be used to provide flexible one-to-one interfaces for multiple parts. Consequently, the overall structure can benefit from the economical and mechanical advantages of non-printed components while retaining a high adaptability. Network analysis can be used to identify parts that would benefit the most from the adoption of AM as well as highlight the opportunity for components integration and modularisation of the assembly.

8.3.2 Development of a Value Driven Design Framework for the Design of Search and Rescue Unmanned Aerial Vehicles

Hypothesis 2 – *A Value Driven Design framework based on a holistic system model and a life-cycle operational simulation can improve the understanding of the problem, support design decision making and guide the system design toward the highest value for the stakeholders.*

This work has demonstrated how a design environment based on a holistic system description and a life-cycle simulation can facilitate the identification of quantitative relations between the engineering requirements and the mission level metrics. Moreover, it can unveil indirect effects of

the design parameters on the overall mission scenario identifying the counterintuitive effects that can arise from the operation of the UAV in a complex environment featuring multiple agents cooperating for the same mission.

The use of an explicit value model provides the designer with a tool to elicit optimal technical requirements from the concept of operations and the environmental model rather than relying on engineer's estimates. Moreover, it provides a value gradient necessary to perform trade-offs between desirable characteristics and assess the mutual value dependency of the performance attributes.

Despite the difficulty of modelling the several aspects of the system life-cycle, the VDD approach has the merit to force the designers to think systematically about all the aspects of the product development, identify the areas of poor or incomplete knowledge and express their assumptions in an explicit quantitative form. The importance of creating a comprehensive multidisciplinary design environment has been demonstrated by showing that disciplines traditionally overlooked in concept design studies can have a large impact on the system value.

Therefore, this hypothesis is verified.

8.3.2.1 Answers to the Research Questions

1 - What process should be used to design mission-specific UAVs?

The design process should start with the creation of a detailed ConOps. This should include a model of the aircraft operations, the geographical environment and the other agents interacting with the system during its mission. The objective of the system should be clearly stated and linked to measureable mission level performance parameters. It is also important that a life-cycle cost model of the UAV and a cost model for the entire mission are part of the design environment. The technical requirements of the UAV should be identified through a phase of design space exploration during which the mission level performance parameters are evaluated concurrently with the overall cost.

2 - How should the system value of mission-specific UAVs be measured?

There are many possible choices of system value models that can lead to different recommendations of the best UAV. The author's opinion is that the designer should prioritise the simplicity and transparency of the model. Whenever possible, the model should be based on measurable attributes and/or performance parameters of the system. The life-cycle cost of the system, as well as any other outputs that can be directly measured in monetary units, should be explicit. For mission-specific systems, a quantitative measure of the mission effectiveness should

be presented as well. By doing so, cost and benefit of the system can be compared quantitatively using graphs or tables.

However, it is also important to define a common value function that aggregates cost, benefits and any other measurable attributes important to the stakeholders. The value function can be used to guide multi-attribute decisions and identify optimal and robust design solutions. Worth is the simplest and most direct way to express value, therefore it is advised that benefits and the other relevant systems attributes are converted to equivalent worth.

Defining a value function *a priori* (i.e. before performing the analysis and design space exploration) can be beneficial because the stakeholders don't have to be interviewed multiple times. However, the use of an *a priori* value function during the design exploration performed through automatic algorithms can prevent the full exploration of the design space. Conversely, an *a posteriori* definition of the value function can exploit the more accurate information about the system capability and cost-benefit trade-offs. In any case, it is important that the individual components of the final value are always available to the decision maker so that the value model can be used not only to identify the systems with the highest value but also to understand the reason behind this.

3 - Is it possible to link technical system requirements to mission level performance and ultimately to the system value? Is it possible to link low-level (detail design) variables to the system value?

The analysis of the quantitative relationships between the system requirements and the mission level performance requires the integration of an operational simulation into the design loop. This is particularly important for systems that operate in complex environments because the effect of technical parameters on the mission level performance is difficult to estimate *a priori* and counterintuitive second order effects can arise from the interaction between the system and the other agents. A holistic design environment can be used to propagate the effect of system requirements on the system's characteristics, its life-cycle cost and the mission effectiveness. These can be integrated *a posteriori* into a single value measure that can be used to establish the ideal system requirements and the sensitivity of value with respect to them.

The use of system requirements as the input of the trade space exploration is justified by the fact that relatively large variations of such requirements can be analysed independently of each other while still retaining the physical consistency of the UAV model. Moreover, large variations of technical requirements are likely to generate large variations of mission performance, cost and

ultimately value. This is important if a stochastic operational simulation is used because the noise of the simulation can hide the effect of small variations of the UAV performance.

On the other hand, even large variations of the low-level design variables are likely to generate relatively small variations of the UAV performance and thus of value. Moreover, the low-level design variables cannot be controlled independently of each other without compromising the physical consistency of the UAV model. Finally, it is practically impossible for any high-level value model to have sufficient LOD and fidelity to offer meaningful recommendations in response to small perturbations of detail design variables.

4 - What are the practical obstacles preventing the adoption of a VDD approach for the design of rapid-manufactured UAVs?

The major obstacle to the adoption of VDD is related to the difficulty of creating a holistic system model that accounts for all the aspects of the system life-cycle. In some cases, the designer is forced to integrate the evidence-based analysis tools with intuition-based models. In a holistic model, the effect of the propagation of wrong assumptions can be very difficult to predict because of the complexity of the interactions between modules. As a result, the fidelity of the overall system model is difficult to estimate.

The use of a detailed life-cycle operational model increases the complexity of the design problem. On one hand, this has the potential to increase the user's understanding of the design space by capturing and quantifying counterintuitive interactions. On the other hand, it increases the number of models, parameters and the sources of epistemic uncertainty. Gathering the data required for such models can be difficult and time-consuming.

Overall, the workload required for the creation of a VDD environment is substantially higher than for more traditional design approaches. This can discourage the use of VDD, especially in the context of rapid development.

8.4 Further Research

This section provides suggestions for further research.

8.4.1 Additive Manufacturing of Airframes

One of the biggest obstacles to the widespread adoption of AM for the production of aircraft structural components is the lack of data about some of the mechanical properties of 3D printed materials. In the case of AM of plastic, there are very few data on the long-term stability of

materials (such as the Polyamide 12) and on the effect that prolonged exposure to environmental agents (such as sun radiation, oxygen and air moisture, engine oil, fuel and other chemical agents) can have on their mechanical properties. In the case of AM of metal, there are a lack material testing standards and of computationally efficient methods to characterise the mechanical properties of the materials. The problem is particularly challenging for the fatigue and fracture properties of the material, which depend on the processing defects (such as surface roughness, micro-porosity, residual stress, and so on). Structurally critical components of large UAVs will likely require certification, but the current process is very expensive and time-consuming [189]. These challenges need to be addressed by academic, industrial, and government institutions though an integrated research approach that involves various science and engineering disciplines [188].

DFM principles are intended to be adapted to the changes and evolution of the manufacturing technology. It is to be expected that accuracy and resolution of the AM processes, the material range and their mechanical properties will improve over time, while their cost and geometrical limitations will decrease. Design for AM principles, including the principle of confined complexity, will have to be continuously updated to account for the new opportunities and constraints.

While this thesis was focused on the AM of plastic aircraft components, further research is needed to explore the use of metal and/or composite AM for the production of airframes.

Finally, research focusing on the AM of electronic components [277,278] might lead to the possibility of 3D printing the fully-functioning avionics and power systems as part of the airframe.

8.4.2 Value Driven Design Framework for the Design of Unmanned Aerial Vehicles

Due to the limited research time scale, several assumptions were made during the development of DUADE. The following suggestions may be used to increase the accuracy of this design methodology.

- A model to account for the uncertainties of the aircraft properties and performance, as well as the uncertainty of the cost parameters, will help the decision maker to assess their implication on the final system value and the risk associated with them.
- Some of the disciplinary modules require more advanced models and a verification of the underlying hypothesis. These include the landing mishap model, the payload model, the communication model, the reliability and maintenance model.

- The Value Model could be used to assess operational strategies concurrently with the system performance. For example, the planned maintenance intervals of the UAV could be optimised, or the use of multiple UAVs with different characteristics could be explored.
- The effect of weather (such as, wind, precipitation and the sea state) on the operational performance of the UAVs and the other vessels might be modelled to assess the value of the weather-resistance of each design.
- A more detailed Value Model and a deeper analysis of the stakeholders' value drivers may account for the mission outputs that are not directly measured by the mission effectiveness and its cost. For example, UAV mishaps could generate negative value by increasing the risk of injuring people or damaging properties. This would generate direct and indirect costs (due to negative publicity). Similarly, by reducing the operational time of manned vessels, the use of UAVs can decrease the life hazard for the crew members and therefore generate positive value.
- Finally, further research is required to establish the optimal LOD of the disciplinary modules, particularly for the operational simulation. The trade-off is between very detailed models, which can provide a superior understanding of the problem but require many inputs and a high pre-processing effort, and low LOD models, which provide a coarser solution with minimal effort. In addition to the obvious dependency on the design phase, intuition suggests that the optimal LOD of the models is influenced by the impact of the modelled characteristics on the system value. That is, a system characteristic that does not significantly impact the system value does not require a very detailed model. Instead, the analysis effort should be focused on the system attributes that have a large impact on the value generation.

Appendix A. Mechanical Properties of Direct Metal Laser Sintering Materials

Material	Density	Tensile Modulus (XY)	Tensile Modulus (Z)	Yield Strength (XY)	Yield Strength (Z)	Tensile Strength (XY)	Tensile Strength (Z)	Elongation at Break (XY)	Elongation at Break (Z)
Aluminium AlSi10Mg	2670 kg/m³	65 ± 10 GPa	60 ± 10 GPa	170 ± 40 MPa	150 ± 40 MPa	265 ± 35 MPa	265 ± 35 MPa	4 ± 2%	4 ± 2%
Cobalt-Chrome Alloy Co28Cr6Mo	8300 kg/m³	200 ± 20 GPa	200 ± 20 GPa	600 ± 100 MPa	600 ± 100 MPa	1100 ± 100 MPa	1100 ± 100 MPa	min. 20%	min. 20%
Nickel Alloy In718	8150 kg/m³	170 ± 20 GPa	170 ± 20 GPa	1150 ± 100 MPa	1150 ± 100 MPa	1400 ± 100 MPa	1400 ± 100 MPa	15 ± 3%	15 ± 3%
Maraging Steel 1.270	8100 kg/m³	180 ± 20 GPa	180 ± 20 GPa	1990 ± 100 MPa	1990 ± 100 MPa	2050 ± 100 MPa	2050 ± 100 MPa	4 ± 2%	4 ± 2%
Stainless Steel 316L	7900 kg/m³	185 ± 20 GPa	180 ± 20 GPa	530 ± 60 MPa	470 ± 90 MPa	650 ± 50 MPa	540 ± 55 MPa	40 ± 15%	50 ± 20%
Stainless Steel 15-5PH	7800 kg/m³	Data not available	Data not available	1300 ± 100 MPa	1300 ± 100 MPa	1450 ± 100 MPa	1451 ± 100 MPa	12 ± 2%	12 ± 2%
Titanium Alloy Ti6Al4V	4410 kg/m³	116 ± 10 GPa	114 ± 10 GPa	1000 ± 20 MPa	1000 ± 20 MPa	1050 ± 20 MPa	1060 ± 20 MPa	14 ± 1%	15 ± 1%
Commercially Pure Titanium TiCP	4500 kg/m³	98 ± 15 GPa	98 ± 15 GPa	384 ± 20 MPa	384 ± 20 MPa	460 ± 20 MPa	460 ± 200 MPa	19.2 ± 1%	19.2 ± 1%

Table 10 – Mechanical properties of DMSL materials in the horizontal (XY) and vertical (Z) direction with respect to the building plane (source 3T-RPD [279]).

Appendix B. Examples of Rapid Manufactured UAVs

B.1 Introduction

Throughout the duration of this research project several unmanned aircraft have been designed, built and tested. All of them have been produced using the RM techniques described in Chapter 4. This appendix presents two examples focusing on the lessons learned during their development.

B.2 DECODE-2

DECODE-2 is a research UAV developed as part of the DECODE project. Its configuration was optimised for the maritime SAR mission presented in Chapter 7. Following the indication of Section 7.4.4, the design point 600_3.25[92] was selected because of the high mission value, the safety margin on the mass calculation and the robustness of the value function with respect to the range requirement.

The twin boom configuration was selected following the indication of Section 7.4.5. The inverted V-tail configuration was selected because it provides pitch and yaw control redundancy with a minimum number of control surfaces and servo actuators. That is, if one of the four ruddevators' actuators fails commanding the control surface full deflection in the worst possible position, the aircraft will retain half of its control authority.

The design team was given the task of completing the detail design, system construction and the initial flight test campaign within ten weeks from the end of the concept design[93]. The team included three design engineers, one aerodynamics specialist and two avionics engineers. The detail design activities are summarised in Figure A 1: after the value trade-space exploration that resulted in the preliminary design of the aircraft, the aerodynamic optimisation of the fuselage and the detail design of the avionics systems proceeded in parallel with the creation of a parametric high-LOD geometry model. Frequent communication between the design specialists was maintained and the AST was updated with the increasingly accurate estimate of the mass and geometry of the components. The final design of the geometry was obtained by progressively integrating the outputs of these activities. The design iteration was planned in order to correct

[92] The aircraft was designed to carry a 3.25 kg payload and have a range of 600 km at the cruise speed of 25 m/s.
[93] The project timeline is presented in Appendix E.

possible design mistakes that could have become evident after the flight test of the first prototype.

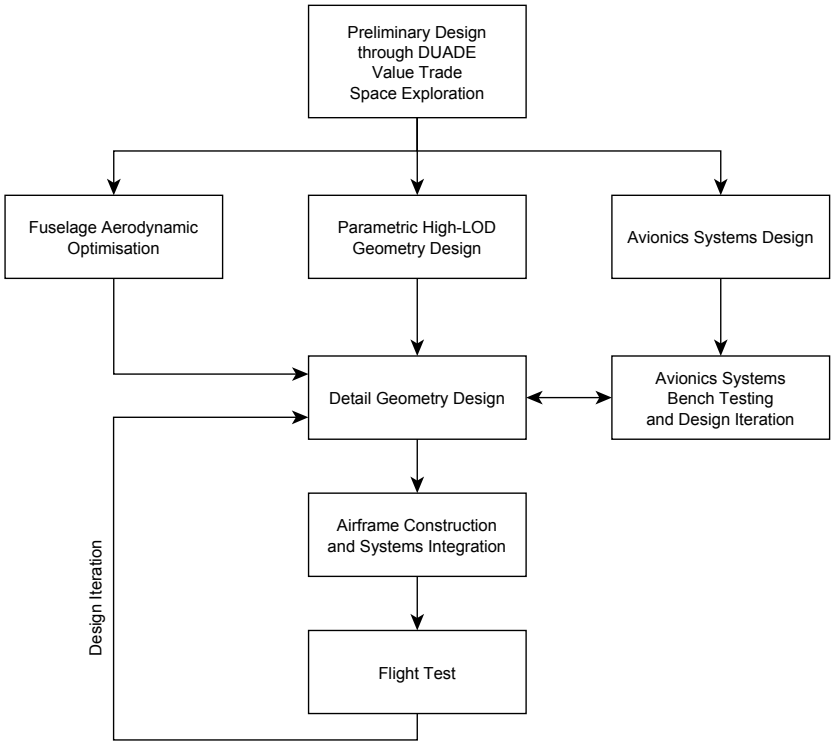

Figure A 1 – DECODE-2 detail design activities.

B.2.1 The Aerodynamic Optimisation of DECODE-2 Fuselage

The shape of the fuselage of DECODE-2 is the result of a two-level aerodynamic optimisation process which is only briefly described here[94]. The study demonstrates the integration of high-LOD tools in the DUADE system design loop.

The baseline design was the result of the low-LOD optimisation loop and featured a cylindrical fuselage connected to the wing without fairings. This initial shape was sized to meet the payload, avionics and fuel volume requirements (Figure A 3a.). For the aerodynamic optimisation of the fuselage, a more complex geometry was defined using the parameters in Appendix F.

The strategy employed for the aerodynamic optimisation is described in Figure A 2: the top-level optimisation loop was coupled with a low-level aerodynamic optimisation of the fuselage. The

[94] The algorithm used for the aerodynamic optimization of the fuselage of DECODE-2 was created by Dr. Erika Quaranta. The author contributed to the definition of the two-level optimization strategy and by managing the top-level optimization loop. More details about the design optimization of the DECODE-2 fuselage can be found in Quaranta *et al.* [300].

estimate of the aerodynamic coefficients[95] was performed using a commercial CFD code based on Reynolds Averaged Navier-Stokes[96]. The top level optimisation loop was performed using the CDT; the IOF was the one described in Equation 7-2 with $w_{EUC} = 0$. The aerodynamic coefficients were kept constant during the top-level optimisation. The updated geometry was then passed to the low-level optimisation loop, where the fuselage geometrical parameters were optimised to maximise the aircraft efficiency in cruise condition. The aerodynamic coefficients were then updated and the loop was iterated until convergence[97].

Figure A 3 and Table 11 show the comparison between the baseline geometry and the result of the optimisation process featuring a blended wing-body (BWB). The aerodynamic efficiency was improved by 16.3% over the baseline design. However, the mass and cost of the airframe increased as well. These effects were due to the additional lift provided by the blended wing-body which impacted negatively on the vehicle stability. As a consequence, a larger tailplane and a longer fuselage were required to satisfy the stability and control requirements.

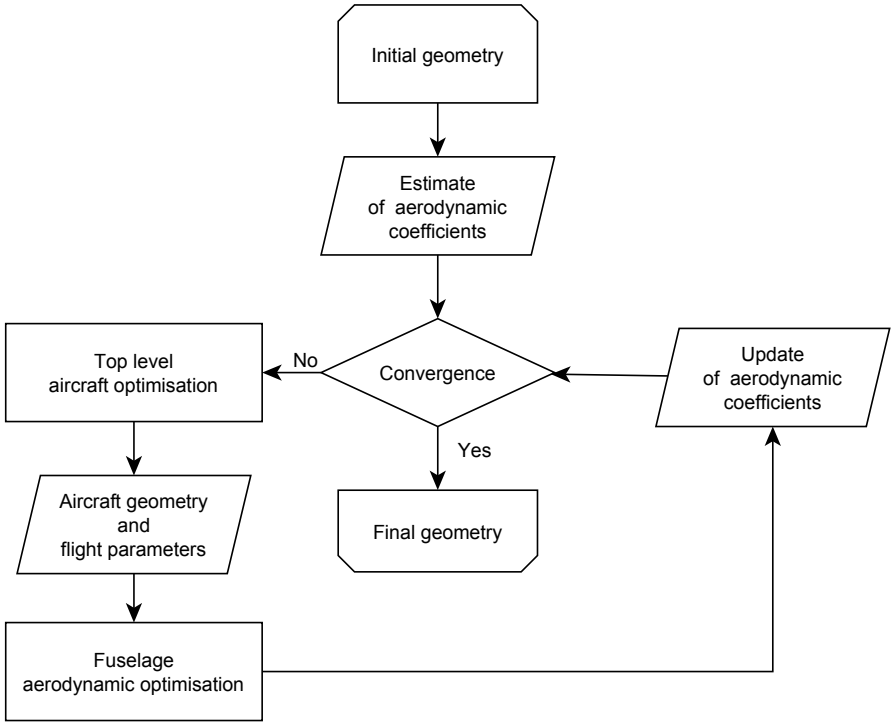

Figure A 2 – DECODE-2 aerodynamic optimisation loop.

[95] The drag polar coefficients defined in Equation 6-1, the slope of the coefficient of lift, drag and moment with respect to the angle of attack, and the position of the neutral point of the aircraft.
[96] ANSYS Fluent® software [235].
[97] The optimization loop was considered complete when the difference between the aerodynamic efficiency at cruise calculated at two consecutive steps was lower than 1% and the minimum static margin constraint was satisfied.

The resultant geometry was automatically imported in a CAD tool, where the main structural elements and design features were added. Like in the case of SULSA, the CAD model was parametric and governed by updating the fuselage sections obtained through the optimisation (Figure A 4). This allowed for a high degree of flexibility in the initial phase of the detail design, when the final sizing of the aircraft was not yet complete. The parametric model also provided a more accurate components' weight estimation that was fed back to the AST.

Design variable	**Baseline**	**BWB**	**Unit**
Wing area	1.53	1.49	m^2
Wing aspect ratio	10.2	11.0	-
Wing taper ratio	0.543	0.512	-
Fuselage front bulkhead position	0.588	0.698	m
Horizontal tail longitudinal position	-1.105	-1.304	m
Equivalent horizontal tailplane area	0.217	0.276	m^2
Equivalent horizontal tailplane aspect ratio	4.33	4.12	-
Equivalent vertical tailplane volume coefficient	0.024	0.031	-
Maximum engine power	3.21	2.93	kW
Percentage of engine power at cruise	31.7	25.9	%
Fuel mass	4.34	3.85	kg
Maximum take-off mass	22.7	23.0	kg
Maximum load factor	6.75	6.45	g
Output values			
Empty UAV cost	15400	16200	£
Dry mass	18.4	19.2	kg
Fuel burn rate at cruise	621	546	g/h
Cruise efficiency (L/D)	8.99	10.5	-

Table 11 – Design variables and objective functions for the DECODE-2 UAV.

.

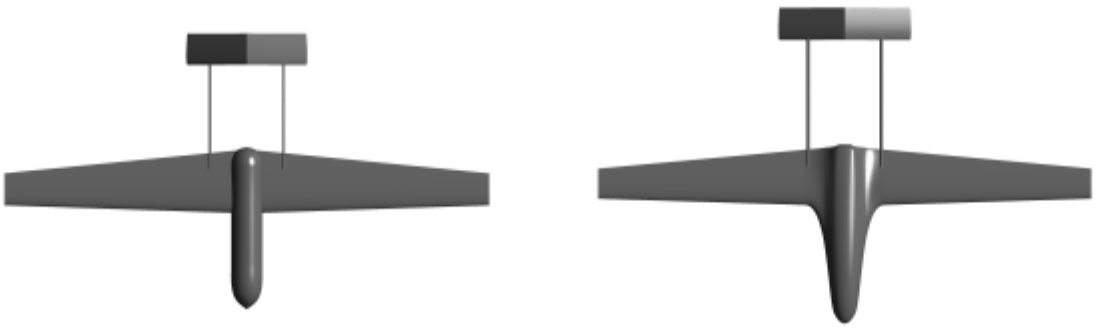

a. b.

Figure A 3 – Size and shape comparison between: **a.** DECODE-2 baseline geometry **b.** Aerodynamically optimised blended wing-body geometry.

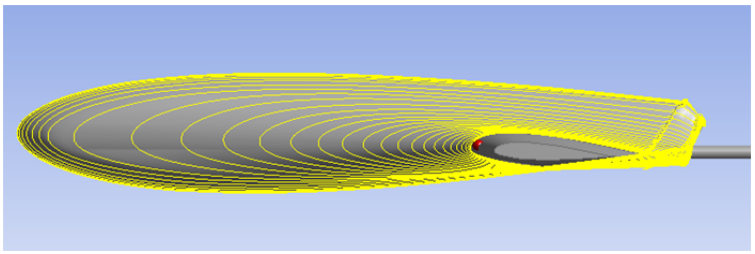

Figure A 4 – Detail of the curves used to control the parametric geometry of the fuselage.

B.2.1.1 The Value-Driven Design Point of View

The aerodynamic optimisation of the 3D printed blended wing-body was an academic exercise performed to demonstrate the flexibility of the rapid design and manufacturing process and to explore the consequent aerodynamic benefits. However, the assessment of the result should have been evaluated considering also the other factors contributing to the value of the aircraft. Was the aerodynamic optimisation of the body a good VDD decision?

Despite the significant improvement of the aerodynamic efficiency and consequently of the fuel burn rate at cruise, the impact on the overall value of the aircraft was negative, as shown in Figure A 5.

The BWB design uses 12% less fuel that correspond to a life-cycle saving in fuel cost of £249[98]. On the other hand, the UAV life-cycle cost increases by 3.33%, corresponding to £33.2k. This effect is due to the fact that the UAV life-cycle cost is dominated by the maintenance and mishaps cost. The increase in mass and cost of the airframe increases the likelihood and financial severity of landing mishaps. Overall, the impact of the design modification results in a 0.48% increase in the SAR total cost and a 0.74% decrease of the value added by the UAV. The small impact on the mission level metrics is explained by the fact that the performance parameters of the two designs (range, search speed, and payload capacity) were kept constant and therefore the number of saved lives and the cost of the other SAR vehicles were not affected significantly.

The use of an IOF with a higher relative importance of the UAV empty cost might have resulted in a cheaper airframe while still benefiting from the advanced aerodynamic shape of the BWB. The exploration of this approach is recommended for future iterations of the DECODE-2 design.

[98] The estimated fuel price is 1.8 £/kg and it is based on the average price of petrol in UK between 2010 and 2016, published by the RAC Foundation (http://www.racfoundation.org/data/uk-pump-prices-over-time). A 40:1 mix with engine oil is assumed.

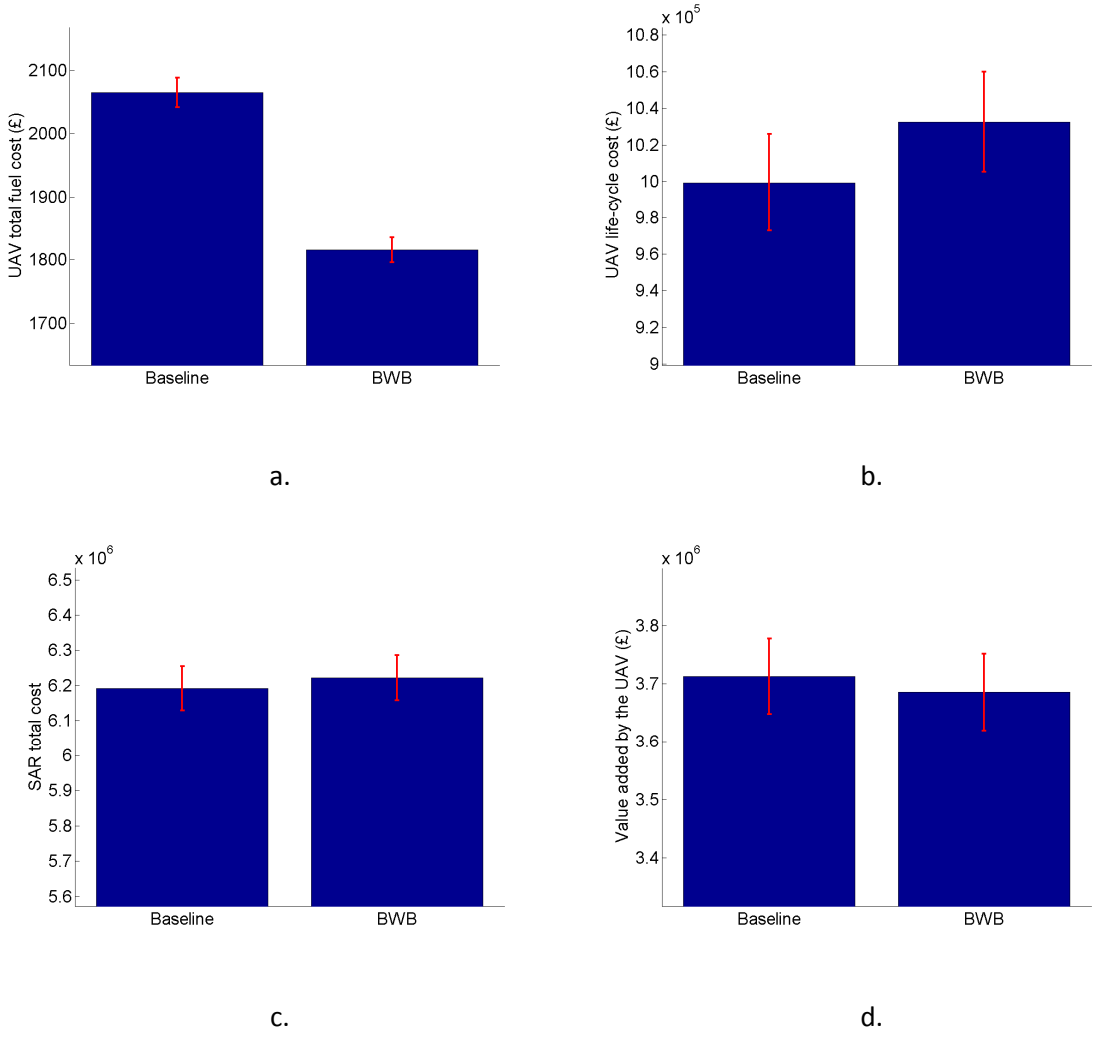

Figure A 5 – Life-cycle cost and value comparison between the DECODE-2 baseline design and aerodynamically optimised blended wing-body geometry. The red bars are the sample standard deviations.

B.2.2 Manufacture and Flight Tests

DECODE-2 was designed for RM using a combination of the techniques described in Section 6.6.1. The wing and control surfaces skin were obtained using a composite of CNC-cut Styrofoam and fiberglass cloth. Carbon fibre composite tubes were used for the main spar and tail booms. 3D printed Nylon ribs were used in the wings and tailplanes to provide servo mounting points and hinges for the control surfaces (Figure A 6a). The fuselage is an entirely 3D printed body that was produced in three chunks because its size was exceeding the dimension of the SLS machine printing chamber used for the production (Figure A 6b)

The first flight of the DEOCDE-2 prototype was performed within fifty days of the beginning of the detail design. The manufacture of the structure, including the integration of the avionics components took only two weeks. The flight tests were performed within line of sight of the

vehicle and were intended to prove the general handling quality of the vehicle and to measure its flying performance through the post-flight analysis of the telemetry data [99]. Overall, the tests demonstrated that the aircraft performance and flight characteristics were in line with the prediction of the AST (Table 12).

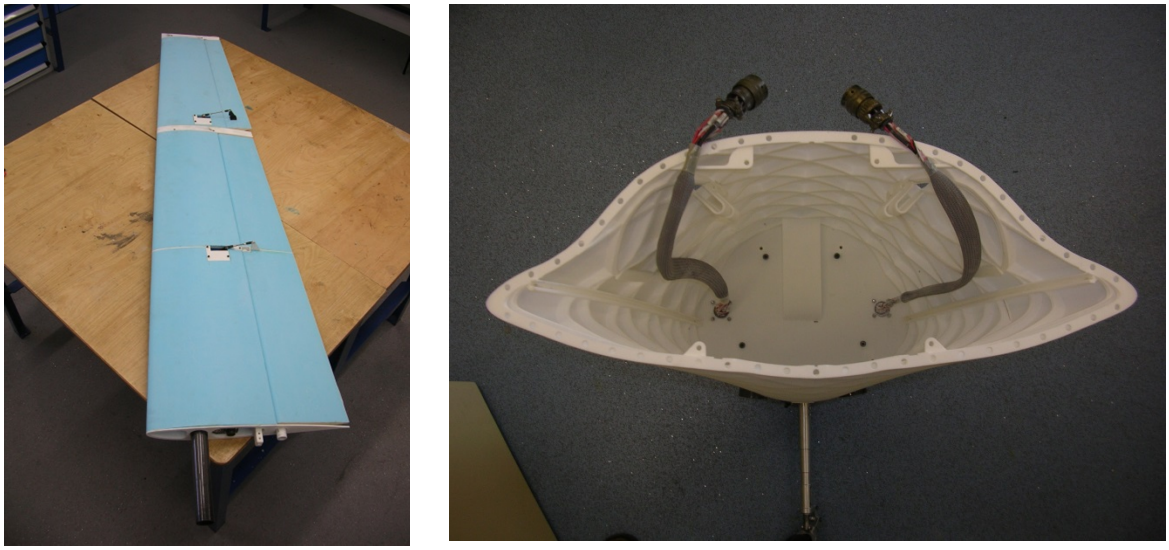

a. b.

Figure A 6 – **a.** Port wing of DECODE-2 showing the Styrofoam skin, 3D printed Nylon ribs, and the carbon fibre main spar. **b.** Central fuselage of DECODE-2 showing the GISM structure.

a. b.

Figure A 7 – **a.** DECODE-2 during the pre-flight checks. **b.** iFlyer in flight with the BBC colour scheme.

During the development of the first iteration of DECODE-2, the design team was presented with the opportunity of building a low-cost aerial vehicle to be used by the British Broadcasting Corporation (BBC) for the aerial filming of the 2012 Olympics torch relay. Given the short time

[99] A description of the tests performed during a typical flight test campaign is given in the Appendix G.

available for the completion of the project, it was decided to adapt DECODE-2 to the new payload requirements[100] with minimal design changes.

The design and construction of the second iteration of DECODE-2 – which was renamed iFlyer – was completed within one month. It introduced a major design modification to the power management system that became necessary in consequence of the adaptation of the design to the BBC requirements. In particular, a generator was introduced in order to meet the power requirements of the payload[101]. The generator was composed of an alternator unit that was mounted on the engine shaft – in between the engine and the propeller – and a power management unit and voltage regulator unit mounted in the fuselage. The introduction of these components required minor changes to the structural components in order to accommodate them and ensure the correct mass balancing (for example, Figure A 8 shows the modification to the geometry of the fuselage). This resulted in a 1.5 kg increase in the dry mass of the aircraft. Moreover, the power drawn from the alternator reduced the propulsive power available by 23%. As a consequence, the MTOM had to be limited to 23 kg and the take-off distance requirement had to be relaxed. The more stringent mass limitation was met by limiting the fuel mass, which resulted in a substantial reduction of the estimated maximum range.

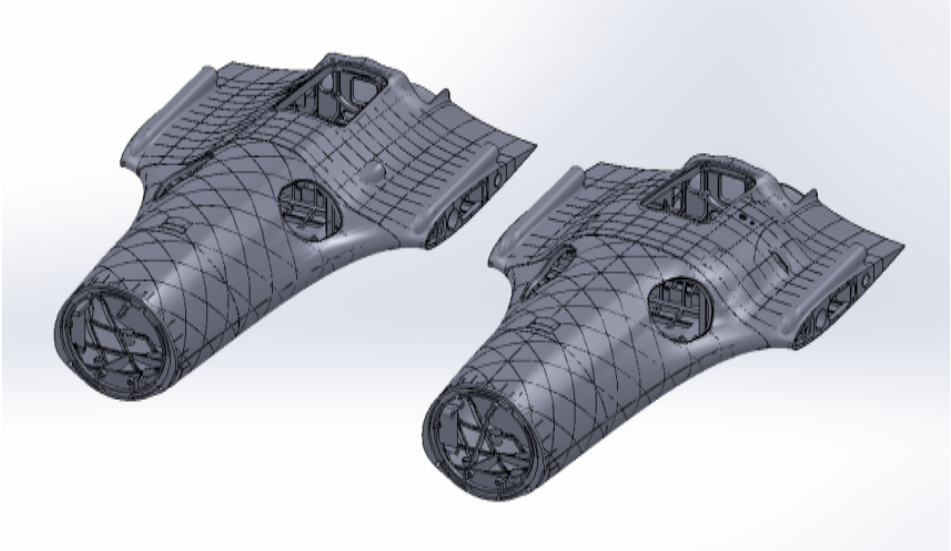

Figure A 8 – Side-by-side comparison of the fuselage of DECODE-2 (on the left) and iFlyer (on the right).

[100] The payload provided by the BBC consisted of a camera (Sony CX700VE full HD flash memory camcorder) with the associated gimbal system and a camera transmitter (Cobham SOLO4 Bodywire transmitter with amplifier). The scope and the technical details of this payload were different than the one assumed in the DUADE analysis. However, the size and weight of the BBC system, as well as the position requirements, were similar to the original design specifications.

[101] The generator was a Sullivan S676-500U-01.

		Preliminary design	Detail design	DECODE-2	iFlyer	Unit
Specifications	Length	2.35	2.66	2.66	2.64	m
	Wing span	3.81	4.05	4.05	4.18	m
	Wing area	1.42	1.49	1.49	1.51	m^2
	Aspect ratio	10.2	11.0	11.0	11.6	-
	Payload mass	3.25	3.25	3.5	3.5	kg
	Dry mass	18.3	19.2	19.8	21.3	kg
	Fuel mass	4.36	3.85	3.85	1.70	kg
	MTOM	22.7	23.0	23.7	23.0	kg
	Engine	52 cc 4-stroke petrol engine	53 cc 4-stroke petrol engine	Saito FG-57T	Saito FG-57T with Sullivan S676-500U-01	-
	Maximum engine power	3.86	3.96	4.00	3.07	hp
	Propeller	Three-bladed pusher 20x10	Three-bladed pusher 20x10	Fiala 20x10	Fiala 20x10	inch
Performance at MTOW with full fuel	Maximum speed	41.2	42.6	40.5 (.27)	37.3 (.34)	m/s
	Stall speed (landing configuration)	13.2	13.2	12.3 (.37)	12.1 (.21)	m/s
	Minimum runway length (semi prepared grass field)	100	100	100	130	m
	Cruise efficiency (L/D)	8.99	10.5	9.91 (.82)	9.53 (.79)	-
	Fuel burn rate at cruise	621	546	573 (31)	712 (44)	g/h
	Estimated range at cruise speed	600	600	570	180	km

Table 12 – DECODE-2 specifications and performance[102].

The characteristics and performance of DECODE-2 and iFlyer are displayed in Table 12 together with the estimate of these values provided by the AST during preliminary and detail design. The DECODE-2 parameters were obtained by direct measurement (such as in the case of the physical dimensions and mass) or calculated from the results of the flight test campaign. The performance parameters of the first iteration of DECODE-2 are in good agreement with the AST detail design calculations: the maximum speed and the stall speed in landing configuration (i.e. with the flaps fully deployed) were overestimated by 5% and 7% respectively. The estimate of the structural

[102] Data displayed in parentis show the standard error of the mean of the values measured during the flight tests.

weight of the UAV obtained through the high-LOD Mass module was accurate within a 5% error. This level of accuracy was possible thanks to the iterative refinement of the predictions of the Mass module that was progressively updated with the measured mass of the completed components[103].

As expected, the performance of iFlyer was worse than the one of the DECODE-2 because of the decreased available power and the increased structural mass. However, they were sufficient to meet the BBC requirements. The main disadvantage of iFlyer was a legal one: the aircraft mass exceeded the limit of the SUA CAA category. Therefore, the aircraft flight tests with the full payload weight could only be performed after the permission was obtained from the CAA[104]. This introduced costs and time delays that were not initially accounted for. Nevertheless, the experience and the data obtained by flight testing DECODE-2 proved to be important for the preparation and approval of the Safety Case document. In the end, the risk associated to the intended commercial operations of iFlyer was judged too high by the CAA and the vehicle was only used as a research platform by the University of Southampton.

B.2.2.1 Mishaps

The iFlyer airframe was heavily damaged as a consequence of an engine failure during the final approach at the end of its fourth flight test. The pilot was forced to an emergency landing in a crop field, 10 m away from the beginning of the runway. The fuselage was damaged at the front and rear undercarriage mounting points and the camera mount dome was destroyed.

Investigations carried out to determine the cause of the mishap concluded that the wrong tuning of the air-fuel mixture caused the engine to fail during the approach manoeuvre.

In order to continue the flight test campaign, a new fuselage was printed featuring additional reinforcements to the undercarriage mounting points.

[103] The progressive update of components' mass was particularly important for the avionics components whose mass was underestimated by 34% during preliminary design. This error was partly due to the discrete nature of avionics components and partly to the modification of some of components during the detail avionics design. The residual error on the mass estimate is due to the difficulty of predicting the mass of fasteners and other minor components (such as the cable ties used for the wiring installation, the glue used for the wing assembly, and so on).

[104] iFlyer was one of the first civil LUAS to obtain the authorisation for flight testing from the CAA in the UK.

a. b.

Figure A 9 – **a.** Damage to the rear undercarriage mount. **b.** Damage to the camera mount dome.

B.2.3 Lessons Learned

The experience gained by the author during the development of DECODE-2 led to the following considerations.

- **Aircraft configuration**. The nose mounted payload configuration has several practical disadvantages. The payload – which is often the most valuable part of the system – is in one of the most vulnerable positions in case of mishaps or bird strike. The aircraft cannot fly without payload (or an equivalent amount of ballast). This prevents the testing of the aircraft in low mass configuration, which is a useful way to reduce the risk in the early flight tests. Moreover, the adaptability of the aircraft is greatly reduced. Scenarios in which a heavier payload is treaded for a lower fuel load are not possible. Finally, this configuration increases the impact of design errors in the calculation of the CoG.

  The nature of the inverted V-tail and twin booms is such that there is a coupling between the empennage geometry, its vertical position and the distance between the booms. This implies that an error in the calculation of the required empennage size is difficult to correct without impacting the design of the fuselage and/or undercarriage.

  The rear mounted pusher engine configuration requires a long forward fuselage for mass balancing and therefore incurs a mass penalty.
- **Engine reliability.** Engines available on the radio controlled aircraft hobbyists' market are unreliable in their early service life because they require precise tuning of the carburettor and other minor adjustments. Moreover, they require frequent maintenance as a consequence of the high level of wear they experience (tappets adjustment is required as frequently as every ten flight hours). According to the author's experience, an inflight engine failure is not unlikely during the first two or three flight hours, while the engine's

life can be estimated in few tens of hours[105]. An inflight engine failure can have catastrophic consequences; therefore it is advisable to explore the option of multi-engine configurations in future designs.

- **Legal requirements for the operation of UAVs.** Despite the fact that a CAA certification is required for any UAV used for commercial operation operating beyond visual line of sight, there is still a large technical advantage in keeping the system mass below 20 kg so that the airframe can be tested before any permission is required. By doing so, the designers can run the flight test campaign in parallel with the preparation of the documentation required for the CAA permission. Incremental improvements to the aircraft design can be introduced and documented and successful flights can be used as evidence of the safety of the system.
- **Value Driven Design.** The example presented in Section B.2.1 has demonstrated the importance of applying the VDD thinking throughout the development cycle showing that performance improvements do not necessary lead to system value improvements. It has also shown the importance of presenting the designer with the intermediate results of the life-cycle simulation.

B.3 SPOTTER

After the end of the DECODE project, the author became a UAV designer at the University of Southampton primarily working at the iterative development of SPOTTER[106], a versatile, long-endurance UAV designed to perform a variety of missions in coastal and maritime environments.

SPOTTER was initially developed as part of the 2SEAS-3i project, a European Interreg project aimed at facilitating the development of UAV-based services[107]. The fifteen project partners included universities, specialist organizations, public sector entities and commercial companies based in three different countries (UK, Netherlands and France).

The system development was divided into four parts, each led by one of the partner organizations. In particular, the University of Southampton had the task of developing the

[105] There are no data available in the literature about the MTBF of engines used in the model aircraft market. This consideration is based on the author's experience – that is limited to the vehicles designed and tested at the University of Southampton – and supported by the opinion of Paul Heckles (http://www.paulhecklesrc.co.uk/), the contracted test pilot with over twenty years of experience as a professional model aircraft pilot.

[106] SPOTTER is the acronym of Southampton Platform for Observation, Tracking, Telecommunications and Environmental Reconnaissance.

[107] http://www.2seas-uav.com/

unnamed aircraft, while the development of the payload, the ground station and the human-machine interface were assigned to different organizations.

SPOTTER was designed using some of the tools and principles developed during the DECODE project. In particular, the structural design was inspired by the DECODE-2 airframe, making extensive use of 3D printed components and the other RM techniques described in this work (Figure A 10). A derivation of the AST was used for the airframe sizing and preliminary design calculations.

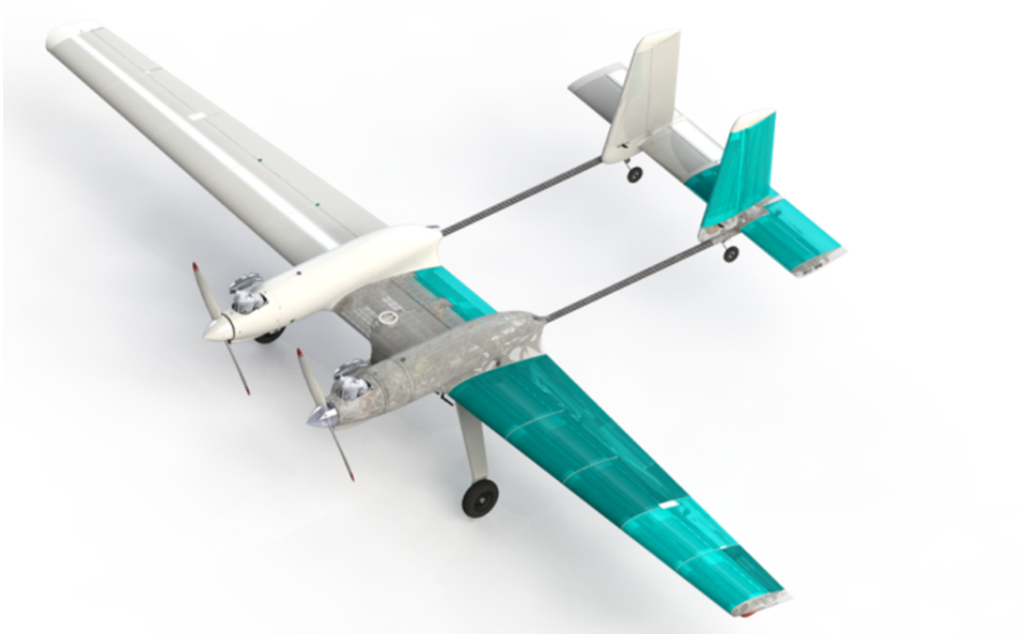

a.

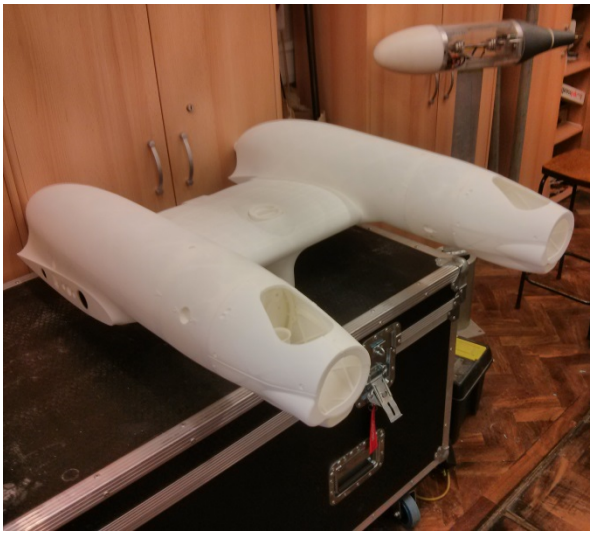

b.

c.

Figure A 10 – a. Transparent view of SPOTTER showing the aircraft structural design. b. Subassembly of the 3D printed fuselage. c. Phase of the assembly of the composite wing.

SPOTTER's configuration is shown in Figure A 11. It is a twin-fuselage, twin-boom aircraft propelled by two petrol engines arranged in a tractor configuration. The payload is accommodated in a modular pod located at the CoG of the aircraft. The study of this configuration required an adaptation of the AST but it was justified by the following considerations based on the experience gained during the development of DECODE-2 and on the result of the customer needs analysis.

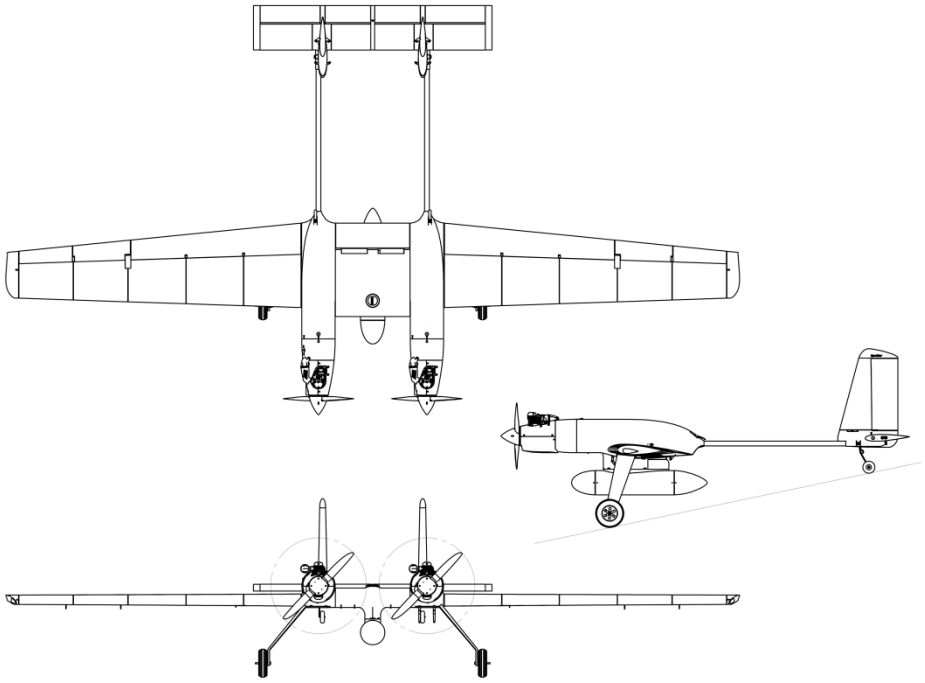

Figure A 11 – Three-view drawings of SPOTTER.

- The UAV features two engines as well as redundant components for each of the flight critical systems, following a fail-safe design philosophy[108]. This choice was driven by the importance of safety of the aircraft operation for the stakeholders. The risk was considered particularly high for mishaps happening in large commercial harbours, where the presence of dangerous chemicals could result in catastrophic consequences. The missions performed over the sea and far from populated areas were considered less hazardous. However, even in this case, there was a clear desire for a system that could reliably bring back the expensive sensors used to perform the mission. Finally, the aircraft

[108] Multiple mechanically and electronically independent control surfaces per each axis guarantee a sufficient control authority even in the event of a control surface jamming in the worst possible position. Each engine is connected to a power generator, each providing power to backup batteries and to half of the systems. The aircraft is designed to be able to fly back to the base in case of failure of one of the power systems.

had to demonstrate a high safety standard in order to obtain the permission to fly from the CAA.

- The fail-safe design together with the use of redundant low-cost components was preferred to the use of single highly-reliable and expensive components. This choice was based on two considerations: firstly, the achievement of a low mishaps rate requires tests and iterations, as demonstrated by Figure 7-22. This implies that a high number of subsystem failures have to be expected in the early development stages. A fault-tolerant design decreases the chances of a total loss of the airframe as a consequence of the failure of one of its subsystems. Secondly, the use of low-cost components resulted in a relatively low-cost airframe, hence decreasing the financial risk of accidents during flight tests.
- The engines positioned at the front of the fuselages allows for a better mass balancing of the aircraft. The fuselages can be more compact and this reduces the structural mass and the cost of 3D printed parts.
- Both the fuel tank and the payload pod are positioned at the CoG. This provides the system with great versatility: the aircraft can fly at its MTOM or at its empty mass with minimal impact on the flight characteristics. As a consequence, minimal time is required for the flight controller tuning. Moreover, the user has the possibility to trade fuel mass for additional payload equipment if beneficial for the particular mission. Finally, the payload modularity enabled the partners to decouple the aircraft design from the payload development.
- In the case of a minor accident, the payload is protected in all directions by the airframe structure and main undercarriage.

The development of the SPOTTER was divided into two phases. Initially, a prototype of the aircraft with a dry mass lower than 20 kg – named 2SEAS-20 – was designed, built and tested. This allowed the team to perform the initial flight test campaign under simplified air regulations at the cost of some compromises of the performance and payload capability of the system. The full-scale version of SPOTTER was designed in the second phase by using the information obtained from the 2SEAS-20 flight tests and the study of the operational scenarios. SPOTTER features a number of enhancements over 2SEAS-20: it is equipped with quieter, more powerful and fuel efficient 4-stroke engines, a larger capacity fuel tank, ruggedised avionics and an increased level of redundancy of the control surfaces, actuators, and the system health monitoring sensors. Table 13 lists some of the specifications and flight performance parameters of the two aircraft.

		2SEAS-20	SPOTTER	Unit
Specifications	Length	2.12	2.18	m
	Wing span	3.74	3.92	m
	Wing area	1.4	1.46	m^2
	Aspect ratio	10	10.5	-
	Empty mass	19.2	23.5	kg
	Fuel mass	4.5	6	kg
	MTOW	24.5	34.5	kg
	Engines	2x 2-stroke 28cc	2x 4-stroke 40cc	-
	Payload mass	0.8	5	kg
Performance	Maximum speed	41	41	m/s
	Cruise speed	26	30	m/s
	Stall speed clean	15	17.5	m/s
	Stall speed take off flaps	14.5	16.5	m/s
	Stall speed landing flaps	13.5	15.5	m/s
	Maximum flap extended speed	20	20	m/s
	Take-off distance	55	105	m
	Distance to clear 10 m obstacle	85	140	m
	Endurance (standard operating conditions)	2.5	>5	h

Table 13 – Comparison between the specification and performance at maximum take-off mass of 2SEAS-20 and SPOTTER.

B.3.1 Manufacture and Flight Tests

2SEAS-20 had its maiden flight within seven months of the beginning of the project[109]. Excluding the time required to adapt the AST to the twin-engine configuration, the design and construction of the airframe was completed within ten weeks. The design, construction, and integration of the avionics and wiring required four months of work by two avionics engineers.

The flight tests were designed to record the flight performance and to prove the effectiveness of the redundant design in several failure scenarios. They were performed following an incremental risk approach: the first flights were aimed at assessing the general handling characteristics and were performed under the control of a human pilot. During this phase, the entire flight envelope was explored and the flight performance recorded. The second phase was dedicated to the automatic flights performed using the on-board autopilot. During this stage, completely automated flights including automatic take-offs and landings were accomplished. The results are

[109] The 2SEAS-3i project timeline is displayed in Appendix H.

illustrated in Figure A 12, which shows the trails and the landing touch down points of 23 completely automated flights performed at the port of Ramsgate in February 2014. Finally, the team dedicated particular attention to the tests simulating sub-system failures, including: single engine failure; the failure of the engine throttle servo actuator in a position that commanded full power; the jamming of one of elevator, aileron or rudder in the worst possible position; the failure of one of the two independent power buses causing complete loss of power to half of the control surfaces. In all the cases the UAV was able to retain sufficient power and control authority to land undamaged. By the end of the flight test campaign, 2SEAS-20 had accumulated 135 take-offs and more than 12 flight hours[110].

a. b.

Figure A 12 – **a.** Trails of 23 automatic flights at Ramsgate port. **b.** Automatic landing touch-down points [21].

SPOTTER design was largely based on 2SEAS-20: the two aircraft share the same configuration and overall dimensions, although SPOTTER has a 40% higher MTOM. The increased mass is due to additional payload and fuel capacity as well as the introduction of structural reinforcements and enhancements of the avionics systems. SPOTTER has a dry mass of 23.5 kg and therefore required the CAA approval for flight testing which was obtained in a relatively short time thanks to the data and experience obtained through the flight tests of 2SEAS-20.

SPOTTER had its maiden flight in April 2014. The design and construction of the airframe were completed within three months. The avionics systems design and integration required multiple iterations before a satisfactory result was achieved (Table 18) because of the manifestation of unforeseen technical problems. The flight tests confirmed that the aircraft performances are in good agreement with the prediction of the AST.

SPOTTER has accumulated more than 50 flight hours and its iterative development is still ongoing.

[110] At the end of the flight test campaign, 2SEAS-20 was donated to the Delft University of Technology, a partner of the 2SEAS-3i project.

B.3.2 Mishaps

Alongside the many successful flights, there were two major accidents that resulted in damage of the airframe.

The first of these accidents was due to the failure of a flap during a remotely piloted flight; the aircraft exceeded the maximum speed in the full-flap configuration causing one of the flap servo protection fuses to blow. The ground crew failed to promptly recognise the cause of the resulting rolling moment and although the pilot was initially able to regain some control by fully deflecting the ailerons, there was not enough control authority left on approach to allow an emergency landing. The aircraft impacted the runway at a 40° bank angle causing it to cartwheel resulting in damage to the structure. A number of changes were implemented in the airframe and procedure to avoid the repetition of the accident. These included more powerful flap servos to provide a larger safety factor on the maximum torque and a stricter policy concerning flap deployment. Also, the two flap servos were connected electronically so that the input power is cut to both of them simultaneously if an anomaly is detected. This mishap also provided an opportunity to validate one of the design features: despite the damage to the fuselages, wings and empennage, the payload pod and the fuel tank were protected by the airframe configuration and survived the crash undamaged (Figure A 13).

a. b.

Figure A 13 – **a.** Moment of the crash landing. **b.** The payload pod and the fuel tank survived the crash undamaged.

The second accident was caused by the use of an experimental version of the autopilot software which contained a code error. The problem manifested itself during an automatic landing trial. The aircraft experienced an un-commanded roll on final approach to landing which inverted the aircraft at a height of approximately 12 m. The test pilot was unable to correct the resulting nosedive and the aircraft impacted the ground. As a consequence of the crash, a stricter policy

concerning the introduction of autopilot software upgrades was adopted. Also in this case the fuel tank and the payload attachment point were protected by the aircraft configuration (Figure A 14).

a.

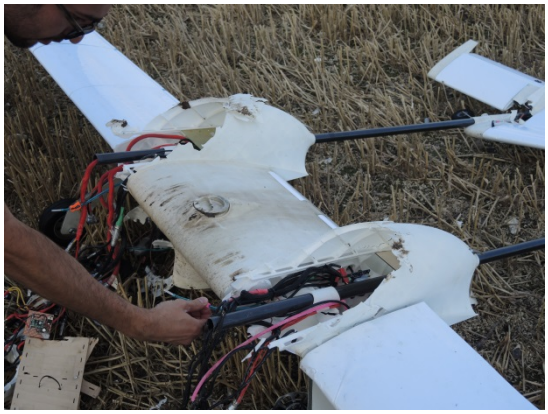

b.

Figure A 14 – Damage resulting from the automatic landing mishap.

B.3.3 SPOTTER and the DUADE Workflow

The development of SPOTTER was not part of the DECODE research project and therefore the study of the application of the VDD approach was not a priority during the system design. Despite using some of the DUADE analysis tools, SPOTTER design did not follow the DUADE workflow and in particular, the value trade space exploration based on the system life-cycle simulation was not used to decide the target performance parameters. The analysis of the motivations for this choice can help understanding the practical obstacles to the adoption of the VDD approach for future projects.

SPOTTER was designed shortly after the end of the DECODE-2 project. That experience played an important role in the choice of the aircraft configuration and the sizing of the first prototype. The overall dimensions and performance of SPOTTER and DECODE-2 are similar and the two aircraft share several structural design characteristics. This allowed the team to exploit the knowledge obtained in the previous project and focus on improving aspects such as the reliability and modularity of the system.

Moreover, SPOTTER was conceived to be a versatile remote sensor platform. The decision of developing a versatile UAV as opposed to a mission-specific system was partly due to the limitations imposed by the current regulatory framework and partly to the fact that the University of Southampton was responsible for the development of the airframe only. Moreover, the project's stakeholders did not have a clear view on the ConOps of the UAV at the start of the project. As a consequence, the definition of a detailed life-cycle operational simulation was not initially required.

Nevertheless, an academic study presenting the CB analysis of the operation of the UAV was performed for two scenarios which were detailed with the assistance of the Kent Police, the Port of Rotterdam and the Dutch National Police, which were partners of the 2SEAS-3i project. In the first one, the UAV was used for supporting the coastal monitoring and emergency response operations of the Kent Police in the South East region of England. In the second, the UAV was used by the Port of Rotterdam Authority to perform harbour monitoring activities. A detailed description of these scenarios and the result of the system life-cycle simulation were presented in a different publication [22]. On one hand, the study highlighted the usefulness of the VDD and the operational simulation in supporting design decisions. On the other hand, the study had to rely on several unverified assumptions because of the difficulty of obtaining reliable data for the modelling of the life-cycle operational simulation and VM.

Finally, the preparation of the mission scenarios and the adaptation of the various modules of DUADE required several months of work because the logic and assumptions embedded into the various analysis tools had to be reviewed and modified. By the time the life-cycle simulation of the two scenarios was starting to produce the first results, the 2SEAS-20 had already started the flight test campaign and the focus of the design team had shifted toward the phase of testing and troubleshooting of the first prototype.

B.3.4 Lessons Learned

The experience gained during the development of SPOTTER led to the following considerations.

- **Avionics.** For both SPOTTER and 2SEAS-20, the construction of the avionics systems exceeded the time required for the manufacture of the airframe by a factor of two or more. This was partly due to the fact that, given the complexity of the redundant systems design, the avionics could not rely only on COTS components. The time required for the production of bespoke avionics system is currently one of the main factors limiting to the further reduction of the development time of rapid manufacture aircraft. Moreover, the aircraft required a relatively complex wiring loom that was produced relying on the manual labour of technicians. This introduced a source of manufacturing errors which caused various problems during system development. In the future, the use of multi-material 3D printers could lead to the concurrent manufacture of the structure and electronics mitigating some of these problems.
- **Versatility.** Despite the fact that rapid manufactured UAVs can be developed in a relatively short time, the versatility of the system remains a great advantage. Most of the improvements introduced on SPOTTER over the years have been motivated by problems that manifested themselves during the system integration phase or during the flight

tests[111]. The test and troubleshooting phase of the development can require substantial time and resources.

- **Rapid manufacturing.** The use of RM was a great advantage for the iterative development approach adopted for SPOTTER. The absence of fixed cost made the creation of a sub-20 kg prototype affordable. Design improvements were progressively introduced and the designers were able to quickly react to unforeseen technical problems and accidents.
- **Life-cycle simulation and VDD.** Despite the use of a life-cycle simulation is very useful to provide the quantitative analysis required for VDD, the task of information gathering can become overwhelming for a small design team in the context of rapid system development. If on one hand, the use of detailed models can generate a superior understanding of the value trade-offs, on the other hand they require the initial investment of significant amount of time and effort.

B.4 Summary

This appendix has presented two examples of rapid-manufactured aircraft designed using some of the design and manufacturing techniques described in this work.

In the first case, the results of the value trade space exploration presented in Chapter 7 were used to design a SAR UAV, named DECODE-2. The end-product proved that DUADE and RM enable engineers to design and test a relatively complex aircraft in a very short time. The AST was also used to drive the aerodynamic optimisation of DECODE-2 airframe during the detail design phase. A later study based on the VM demonstrated that, although improving the efficiency of the aircraft, the new aerodynamic design decreased the life-cycle value of the system. This proved the importance of applying the VDD thinking throughout the development cycle.

The second example described the development of SPOTTER, a versatile, long-endurance UAV designed for maritime patrol missions. SPOTTER derived many of its design characteristics from the practical experience of the DECODE-2 project. The use of RM allowed the team to adopt an iterative development approach where the capabilities of the system were progressively increased. The construction and tests of the prototypes highlighted that, as the complexity of the aircraft design increases, the avionics systems manufacture and integration become the most time consuming activities of the production phase. The project also highlighted how the time and

[111] For example, multiple design modifications had to be introduced on SPOTTER in order to eliminate a problem related to the effect of the engine-induced vibrations on the flight controller. The problem was not present on 2SEAS-20, despite the similarity of the structural configuration and the use of the same autopilot.

effort required to obtain the information necessary for a detailed life-cycle simulation of the UAV can discourage the use of VDD.

Appendix C. Adjacency Matrices

This Appendix presents the Adjacency Matrices used for the network analysis of the empennage assemblies of DECODE-2 and SPOTTER.

Nodes	1	2	3	4	5	6	7	8	9	10	11	12	13	Centrality
1	0	1	1	0	0	1	0	0	0	0	0	0	0	**3**
2	1	0	1	0	0	0	1	0	0	0	0	0	0	**3**
3	1	1	0	1	0	1	1	0	0	0	0	0	0	**5**
4	0	0	1	0	1	0	0	0	0	0	0	0	0	**2**
5	0	0	0	1	0	0	0	0	0	0	0	0	0	**1**
6	1	0	1	0	0	0	1	0	0	1	0	0	1	**5**
7	0	1	1	0	0	1	0	1	1	1	0	0	0	**6**
8	0	0	0	0	0	0	1	0	0	0	0	0	0	**1**
9	0	0	0	0	0	0	1	0	0	1	0	0	1	**3**
10	0	0	0	0	0	1	1	0	1	0	1	0	1	**5**
11	0	0	0	0	0	0	0	0	0	1	0	1	0	**2**
12	0	0	0	0	0	0	0	0	0	0	1	0	0	**1**
13	0	0	0	0	0	1	0	0	1	1	0	0	0	**3**

Table 14 – Adjacency Matrix of the tail assembly of DECODE-2.

Nodes	1	2	3	4	5	6	7	8	9	10	11	12	13	14	15	16	17	Centrality
1	0	1	1	1	1	0	0	0	0	0	0	0	0	0	0	0	0	**4**
2	1	0	0	0	1	0	0	0	0	0	0	1	0	0	0	1	1	**5**
3	1	0	0	1	0	0	0	0	0	0	0	1	0	0	1	0	1	**5**
4	1	0	1	0	1	0	0	0	0	0	0	1	0	0	0	0	0	**4**
5	1	1	0	1	0	0	0	0	0	0	0	1	0	0	0	0	0	**4**
6	0	0	0	0	0	0	0	0	0	0	0	1	0	0	0	0	0	**1**
7	0	0	0	0	0	0	0	1	0	0	1	0	1	0	0	0	0	**3**
8	0	0	0	0	0	0	1	0	0	0	0	1	1	0	0	0	0	**3**
9	0	0	0	0	0	0	0	0	0	0	0	1	0	0	0	0	0	**1**
10	0	0	0	0	0	0	0	0	0	0	0	1	0	0	0	0	0	**1**
11	0	0	0	0	0	0	1	0	0	0	0	1	1	0	0	0	0	**3**
12	0	1	1	1	1	1	0	1	1	1	1	0	1	1	1	1	0	**13**
13	0	0	0	0	0	0	1	1	0	0	1	1	0	0	0	0	0	**4**
14	0	0	0	0	0	0	0	0	0	0	0	1	0	0	0	0	0	**1**
15	0	0	1	0	0	0	0	0	0	0	0	1	0	0	0	1	1	**4**
16	0	1	0	0	0	0	0	0	0	0	0	1	0	0	1	0	1	**4**
17	0	1	1	0	0	0	0	0	0	0	0	0	0	0	1	1	0	**4**

Table 15 – Adjacency Matrix of the tail assembly of SPOTTER.

Nodes	1	2	3	4	5	6	7	8	9	10	11	12	13	Centrality
1	0	1	1	0	0	1	0	0	0	0	0	0	0	**3**
2	1	0	1	0	0	0	1	0	0	0	0	0	0	**3**
3	1	1	0	0	0	1	1	0	0	0	0	0	0	**4**
4	0	0	0	0	0	0	0	0	0	0	0	0	0	**0**
5	0	0	0	0	0	0	1	0	0	0	0	0	0	**1**
6	1	0	1	0	0	0	1	0	0	1	0	0	1	**5**
7	0	1	1	0	1	1	0	1	1	1	0	1	0	**8**
8	0	0	0	0	0	0	1	0	0	0	0	0	0	**1**
9	0	0	0	0	0	0	1	0	0	1	0	0	1	**3**
10	0	0	0	0	0	1	1	0	1	0	0	0	1	**4**
11	0	0	0	0	0	0	0	0	0	0	0	0	0	**0**
12	0	0	0	0	0	0	1	0	0	0	0	0	0	**1**
13	0	0	0	0	0	1	0	0	1	1	0	0	0	**3**

Table 16 – Adjacency Matrix of the re-designed tail assembly of DECODE-2.

Appendix D. Spreadsheet Interface of the Concept Design Tool

The spreadsheet is subdivided into several worksheets, each of which performs a series of computations for a particular discipline and/or for a particular component of the aircraft. These sheets have been provided with a clear arrangement to identify the inputs and outputs and to isolate them from the cells used for the calculations. All the inputs and outputs of the various worksheets are linked to the main control sheet which is called “sizing” worksheet (Figure A 15). The sizing worksheet is where the user can define the value of the parameters and decide which are the variables, constraints and the objective function of the aircraft optimisation process. A screenshot of the sizing sheet is provided in Figure A 15 in order to highlight the code structure: the parameters are organised following a column-based scheme. This structure is optimised to exploit the filtering function of Microsoft Excel® and allows the designer to easily manage a large number of parameters. Moreover, this structure is particularly convenient to transfer the information into databases used in other codes.

	A	B	C	D	E	F	G	H
1	Group	Name	Value	Units	Description	Tag	min value	max value
33	geometry.wing	c_mean	0.319	m	mean geometric chord	o		
34	geometry.wing	c_root	0.415	m	wing root chord	o		
35	geometry.wing	c_tip	0.224	m	wing tip chord	o		
36	geometry.wing	c_ell_eq	0.407	m	root chord of the equivalent elliptic wing	o		
37	geometry.wing	x_main_spar	0.000	m	long position of main spar	o		
38	geometry.wing	thickness_mean	0.146	-	airfoil max thickness on chord ratio t/c (average of the three sections)	o		
39	geometry.wing	taper_av	0.539	-	average taper raito (=c_tip_equivalent/c_root)	x	0.300	1.000
40	geometry.wing	taper_1	0.686	-	taper raito=c_mid/c_root	o	0.300	1.000
41	geometry.wing	taper_2	0.785	-	taper raito=c_tip/c_mid	o	0.300	1.000
42	geometry.wing	actual_thick	0.047	m	wing mean thickness	c	0.048	
43	geometry.wing	twist	2.000	deg	washout at wingtip positive nose down	o	0.000	4.000
44	geometry.wing	midsec_pos	0.680	-	position of the mid section (0.5=50%, 1=tip)	o	0.100	0.900
45	geometry.wing	twist_mid	1.360	deg	washout at mid airfoil positive nose down	o		
46	geometry.wing	a_o_i_r	2.000	deg	angle of incidence of the root chord	o		
47	geometry.wing	a_o_i_m	0.640	deg	angle of incidence of the mid chord	o		
48	geometry.wing	a_o_i_t	0.000	deg	angle of incidence of the tip chord	o		
49	geometry.wing	c_mid	0.285	m	wing mid section chord	o		
50	geometry.wing	naca_r	23013	-	naca airfoil at the root chord	o		
51	geometry.wing	naca_t	23017	-	naca airfoil at the tip chord	o		
52	geometry.wing	naca_m	23015	-	naca airfoil at the mid section chord	o		
53	geometry.wing	wing_spar_diam	0.033	m	diameter of the wing main spar	o		
54	geometry.wing	aileron_chord_ratio	0.250	-	aileron chord ratio	o		
55	geometry.wing	flap_chord_ratio	0.300	-	flap chord ratio	o		
56	geometry.wing	flap_area_ratio	0.520	-	fraction of the wing area that has flaps	o		
57						o		
58	geometry.fuselage	x_fnt_bkhd	0.702	m	long position of front bulkhead	x	0.458	2.000
59	geometry.fuselage	depth_fuse	0.311	m	fuselage depth (vertical dimension)	o	0.120	
60	geometry.fuselage	width_fuse	0.311	m	fuselage width (horizontal dimension)	o	0.120	

Figure A 15 – Concept Design Tool Excel interface.

Each parameter is identified by a group name and a proper name. The group name identifies the “kind” of parameter: examples include the “design” group, in which some general sizing requirements and performance can be specified (like the payload size and mass or the range at cruise speed) and the “geometry” group which is used to describe the geometrical parameters of the aircraft and is divided into subgroups that correspond to the main components of the aircraft.

The proper name is used to distinguish the parameters within the same group. The user is also provided with a brief description for each of these parameters. The numerical value and unit are shown next to the parameter name. A conditional text-formatting function is used to identify the cells that contain numerical value and hence are independent parameters (text in red), and the cells that contain formulas (text in black). A “tag” column is used to identify the “role” of the parameter in the optimisation process, where the variables are identified by “x”, the constraints by “C”, the inactive parameters by “o” and the target function by “T”. The values for the constraints and variable bounds are provided following the same approach. Colour codes are used to increase the readability of the code; for example cells in purple indicate a formula or value that depends on the configuration of the aircraft or on the LOD of the aerodynamic computation, while cells in light blue indicate that a surrogate variable coupled with an equality constraint is used to break the information loop in multidisciplinary calculations.

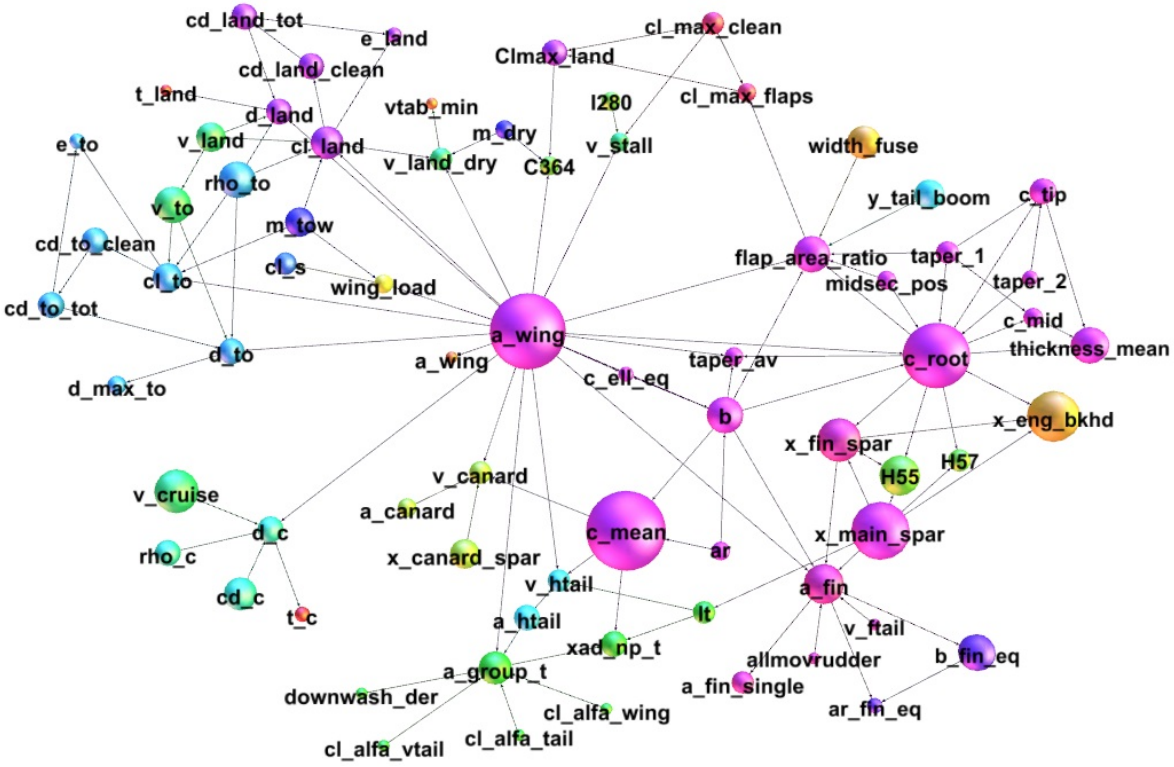

Figure A 16 – Wing area (a_wing) variables network map. The colours indicate the parameter group; the size of the nodes indicates the number of relations with other nodes.

The sizing worksheet contains approximately 400 parameters. A part of these are just outputs of disciplinary calculations that converge into the central worksheet. The rest are parameters that control the aircraft design. Of these, only a relatively small fraction can be independently controlled by the designer, depending on the number of relations that the user decides to consider (for example, the propeller diameter can be scaled with the engine size or the two can be considered independent). The filtering function allows the designers to visualise only the

parameters they are interested in. For example, one can isolate only the parameters defining the wing geometry or the parameters that are variables or constraints in the design optimisation. In order to help the user understand the relations between the design parameters, the CDT can be automatically exported to Gephi®, an open-source network visualisation software. Figure A 16 shows an example of the network maps that can be generated: in this case, the nodes that are connected to the wing area parameter (a_wing) are displayed up to the second degree of connection. The colour of the nodes identifies the parameters group name while their size the number of connections they share with other nodes.

The CDT can support the design also during the later phases of the product development. The spreadsheet interface allows the designer to access and modify the design parameters and the equations used for the sizing operation. In this way the initial model can be progressively refined as new and more accurate information are available (for example the mass of the components already built can be measured and fed back to the CDT, and the optimisation algorithm can be used to modify accordingly the yet-to-built components).

Appendix E. DECODE-2 Project Timeline

	Task	02/02/2012	09/02/2012	16/02/2012	23/02/2012	01/03/2012	08/03/2012	15/03/2012	22/03/2012	29/03/2012	05/04/2012	12/04/2012	19/04/2012	26/04/2012	03/05/2012	10/05/2012	17/05/2012	24/05/2012	31/05/2012	07/06/2012	14/06/2012	21/06/2012
DECODE-2	Aerodynamic Optimization of the Fuselage																					
	Parametric High-LOD Geometry Design																					
	Avionics Detail Design																					
	Avionics Systems Bench Testing and Design Iteration																					
	Final Detail Design																					
	Airframe Construction and Systems Integration																					
	Flight Tests																					
iFlyer	Avionics Design Iteration																					
	Geometry Design Iteration																					
	Airframe Construction and Systems Integration																					
	Preparation of Technical Documentation																					
	Safety Case Assessment by the CAA																					
	Flight Tests																					

Table 17 – DECODE-2 project timeline.

Appendix F. Geometrical Parameters of the Fuselage of DECODE-2

This Appendix introduces the parameters used for the aerodynamic optimisation of DECODE-2 fuselage. The high-LOD aerodynamic optimisation, as well as the automatic pre and post processing operations were created by Dr. Erika Quaranta[112].

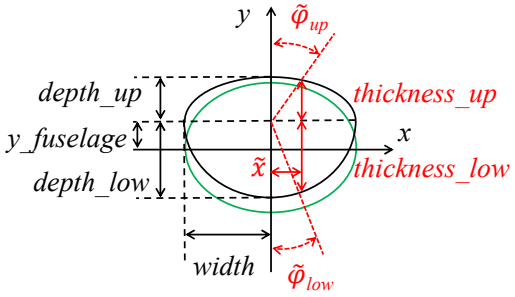

a.

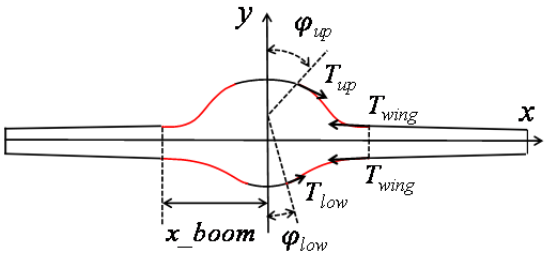

b.

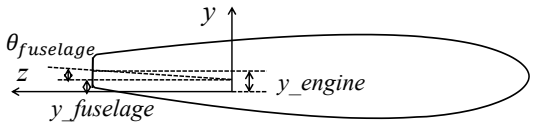

c.

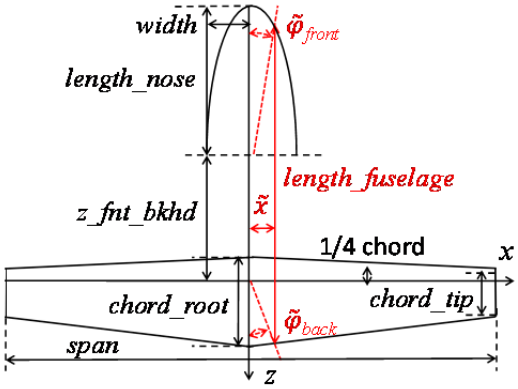

d.

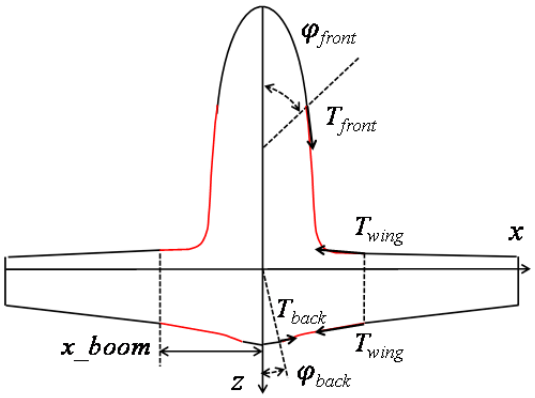

e.

Figure A 17 – Geometric parameters used for the aerodynamic optimisation of the fuselage of DECODE-2

[112] Former member of DECODE research team at the University of Southampton.

The parameters indicated with φ are polar coordinates, the parameters indicated with T are tensions (magnitude of the tangents) of the Fergusson's spline used for the blending between the fuselage and the wing (displayed in Figure A 17b. and Figure A 17d.). The variables used for the optimisation are: φ_{up}, T_{up}, φ_{front}, T_{front}, T_{back} and T_{low}.

Appendix G. Performance Flight Tests

This Appendix briefly describes the standard tests performed to assess the performance of the vehicles designed by the University of Southampton. The preliminary airworthiness and shake-down tests are not described.

G.1 Measuring and Recording Data

All the aircraft described in this work have been equipped with a commercial autopilot[113]. The autopilot has various sensors including GPS antenna, magnetometer, accelerometers, gyroscopes and pressure sensors that are used to estimate the position, speed, and orientation of the aircraft. These data are recorded on board and streamed to the ground control station via a telemetry link. Pressure Altitude, True Air Speed[114], and the position of the UAV with respect to the ground are always recorded. Other parameters are recorded depending on the needs of the particular test.

The aircraft take-off mass, the position of the CoG as well as the wind speed and direction at the take-off and landing site are recorded before each test.

The performance estimates are obtained by averaging the values obtained in at least three consecutive measures. The Cruise L/D is obtained from glide tests. The range at cruise speed is extrapolated from hourly fuel consumption measures. The minimum runway distance is calculated by adapting the measured take-off run to the worst case scenario (45 ° wind at 7 m/s).

G.2 Take-Off and Landing Distance

The take-off distance test is performed by recording airspeed, ground distance from the starting point and the UAV height with respect to the runway level (measured through pressure altitude). The take-off is considered complete when the UAV has reached a height of 10 m from ground level. The flaps are set to the take-off position and the manoeuvre is performed using manual control.

The landing distance is measured using the same parameters plus the acceleration in the vertical axis used to detect the exact point of touch-down. The landing distance is measured from the touch-down point to full stop.

[113] SkyCircuit SC2.
[114] True Air Speed is indicated simply as Speed in the rest of this Appendix.

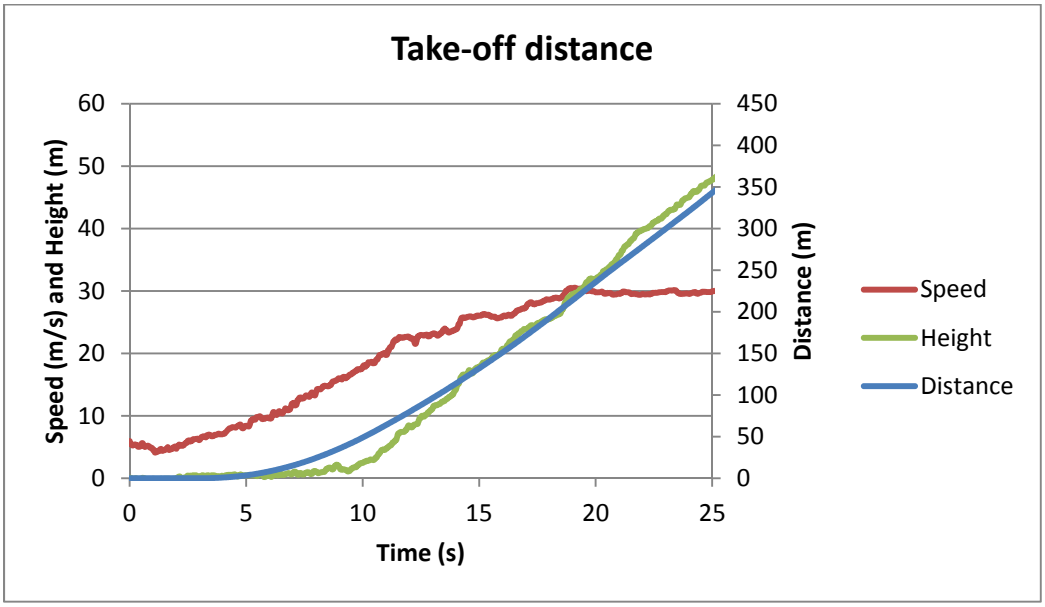

Figure A 18 – Telemetry data recorded during a take-off test of SPOTTER on 30/04/2014.

G.3 Maximum Speed

The maximum flight speed is measured by performing a series of straight flight segments at full throttle and constant altitude. The flight speed is measured by averaging the instantaneous reading of airspeed during a period of five seconds where there is no significant acceleration or altitude change.

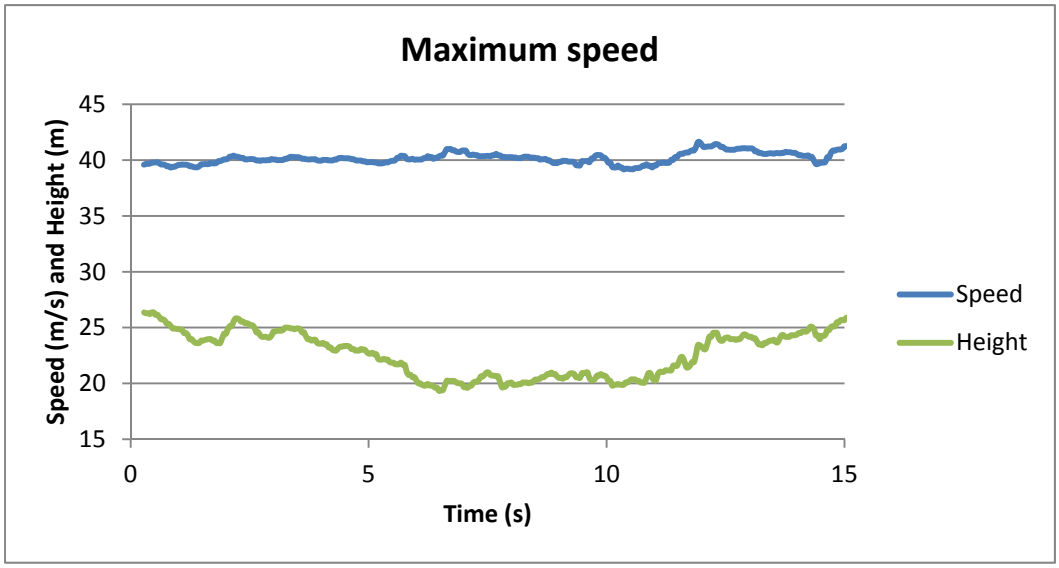

Figure A 19 – Telemetry data recorded during a maximum speed test of SPOTTER on 30/04/2014.

G.4 Stall Speed

The stall speed is measured for the clean (i.e. with flaps completely retracted), take-off and landing configuration. Airspeed, height, pitch and bank angle are recorded during the tests. The stall is detected by monitoring the change in pitch and bank angle.

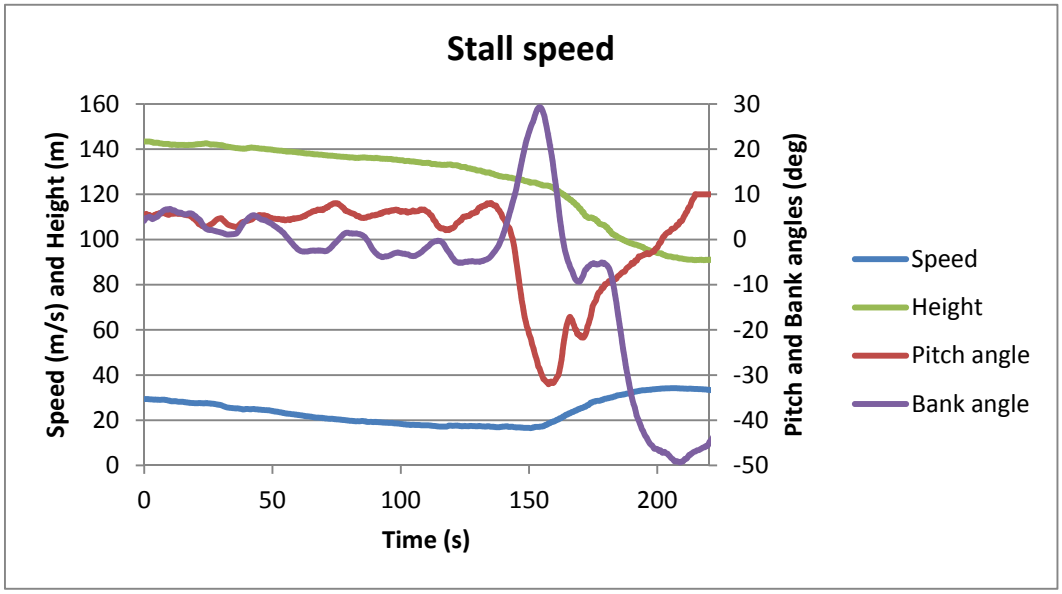

Figure A 20 – Telemetry data recorded during a stall speed test of SPOTTER on 30/04/2014.

G.5 Climb Rate

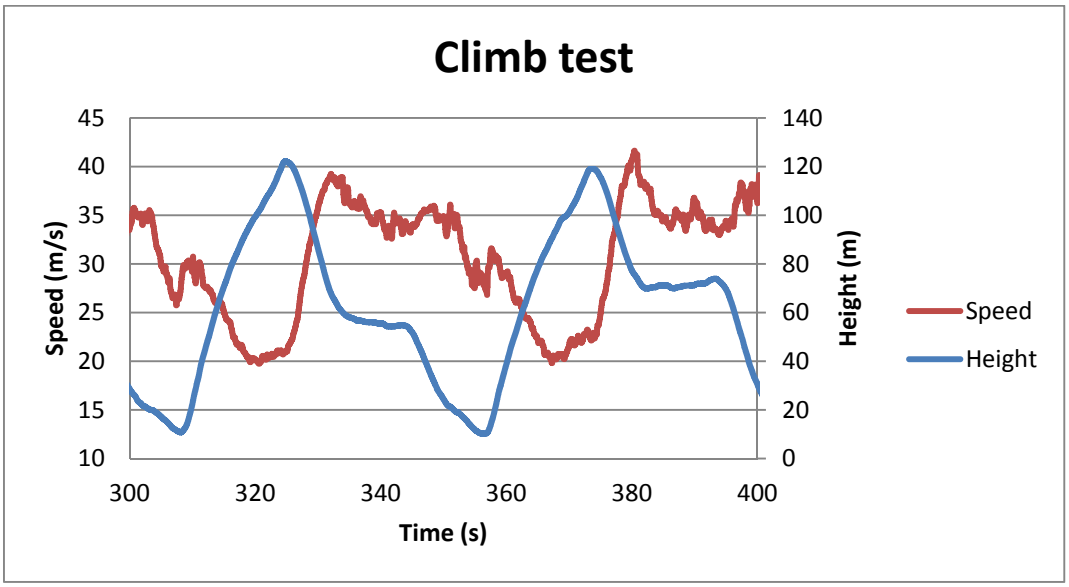

Figure A 21 – Telemetry data recorded during a climb test of SPOTTER on 04/03/2015.

The maximum climb rate is obtained by measuring the airspeed and altitude of the aircraft during a climb manoeuvre at full throttle and at the calculated ideal climb speed. The maximum climb rate is calculated by identifying a chunk of data for which the airspeed is approximately constant

and close to the ideal climb speed; then the difference between the height at the beginning and at the end of the data chunk is divided by the time span of the chunk.

G.6 Glide Ratio

The glide ratio is obtained by measuring the airspeed and altitude of the aircraft that is flying with engines at idle and at a constant flying speed corresponding to the calculated maximum efficiency speed. The average glide ratio is equal to the ratio between the average forward speed and the average rate of descent.

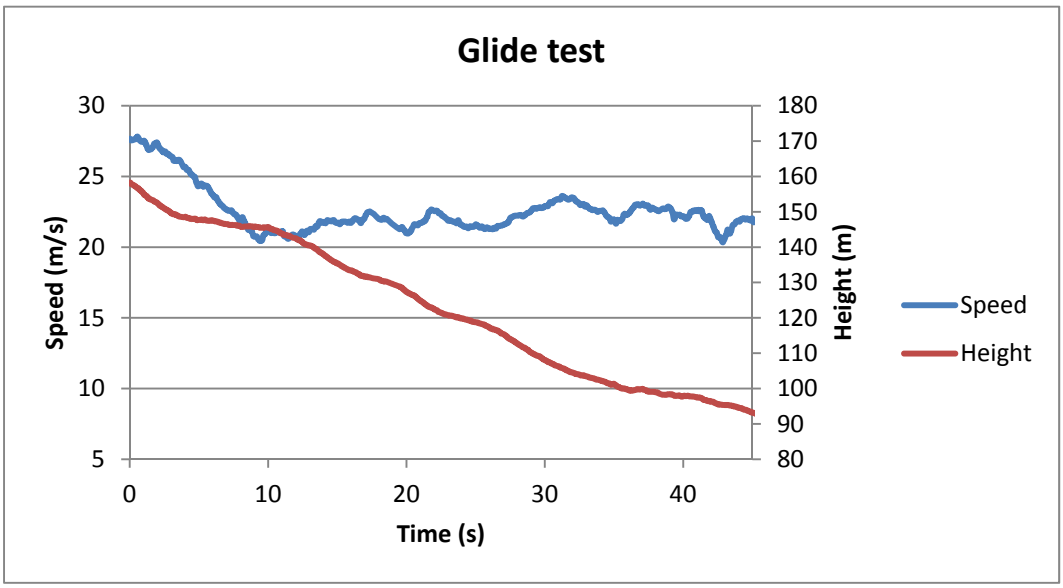

Figure A 22 – Telemetry data recorded during a glide test of SPOTTER on 30/04/2014.

G.7 Fuel Consumption

The hourly fuel consumption is estimated by measuring the amount of fuel burned during long endurance tests flown at the design cruise speed. The duration of the test is as long as practically possible (typically one hour) to minimise the impact of the fuel burned during taxi, take-off, and landing. Endurance tests are generally carried out with the autopilot in control of the aircraft.

Appendix H. 2SEAS-3i Project Timeline

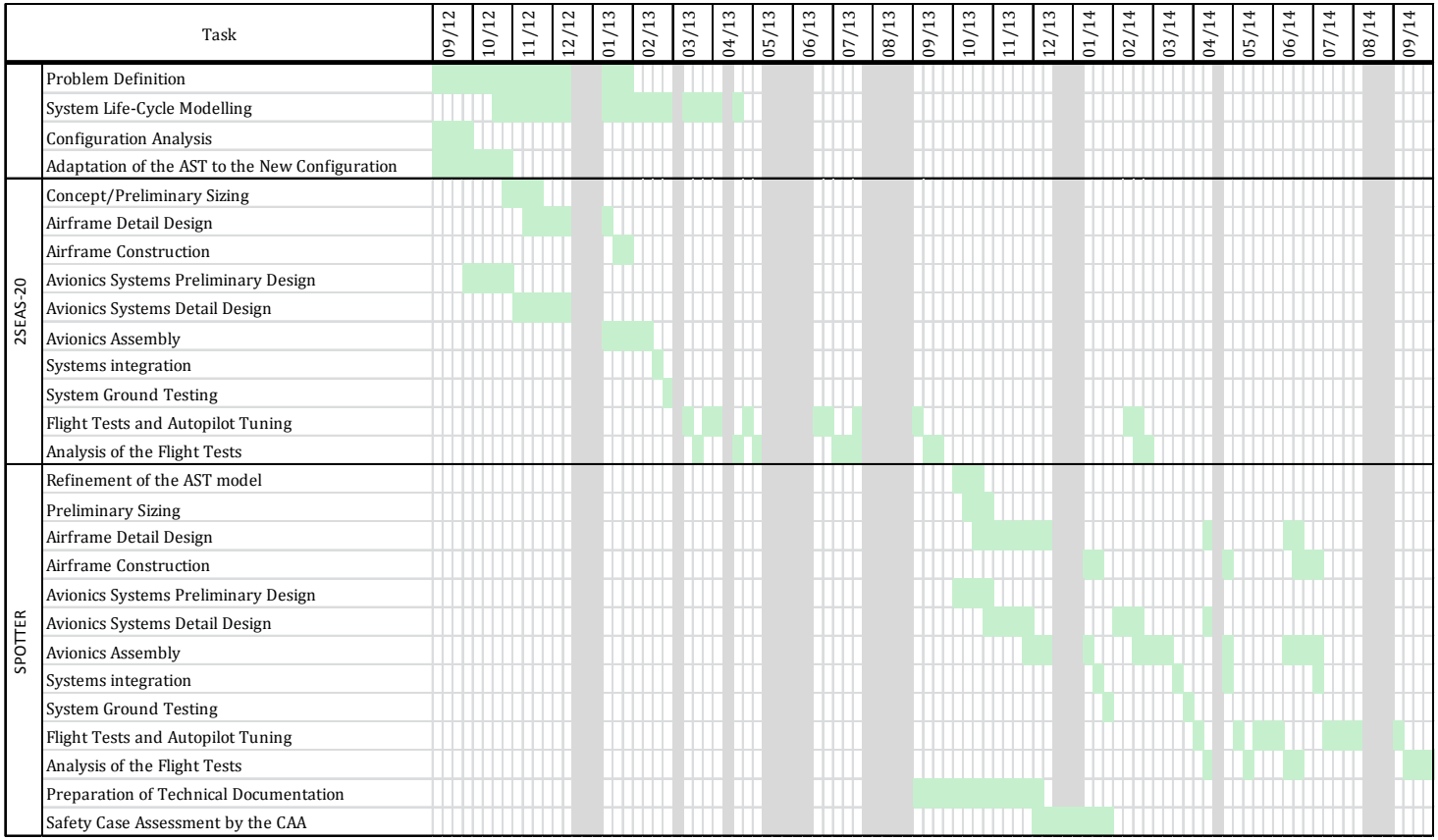

Table 18 – 2SEAS-3i project timeline.

List of References

1. Civil Aviation Authority. "*CAP 722 - Unmanned Aircraft System Operations in UK Airspace – Guidance*". (CAA, 2015).

2. Marks, P. "3D printing: The world's first printed plane". *New Scientist* pp. 30–33, Issue 2823 (2011).

3. Campbell, I., Bourell, D. & Gibson, I. "Additive manufacturing: rapid prototyping comes of age". *Rapid Prototyping Journal* 18 (4), pp. 255–258 (2012).

4. Wohlers, T. "Tracking Global Growth in Industrial-Scale Additive Manufacturing". *3D Printing and Additive Manufacturing* 4 (1), pp. 2–3 (2014).

5. Yeh, C. C. "Trend Analysis for the Market and Application Development of 3D Printing". *International Journal of Automation and Smart Technology* 4 (1), pp. 1–3 (2014).

6. Bak, D. "Rapid prototyping or rapid production? 3D printing processes move industry towards the latter". *Assembly Automation* 23 (4), pp. 340–345 (2003).

7. Berman, B. "3-D printing: The new industrial revolution". *Business Horizons* 55 (2), pp. 155–162 (2012).

8. Atzeni, E. & Salmi, A. "Economics of additive manufacturing for end-usable metal parts". *The International Journal of Advanced Manufacturing Technology* 62 (9), pp. 1147–1155 (2012).

9. Petrovic, V., Haro Gonzalez, J. V., Jordá Ferrando, O., Delgado Gordillo, J., Blasco Puchades, J. R. & Portolés Griñan, L. "Additive layered manufacturing: sectors of industrial application shown through case studies". *International Journal of Production Research* 49 (4), pp. 1061–1079 (2011).

10. Gasser, A., Backes, G., Kelbassa, I. & Wissenbach, K. "Laser Additive Manufacturing: Laser Metal Deposition (LMD) and Selective Laser Melting (SLM) in Turbo-Engine Applications". *Laser Technik Journal* 7 (2), pp. 58–63 (2010).

11. Simmons, D. "Airbus had 1,000 parts 3D printed to meet deadline". *BBC News* (6th May 2015).

12. The AirbusVoice Team. "How 3D Printing Is Delivering Airplane Parts On Demand". *Forbes* (15th July 2014).

13. BAE Systems. "3D printed metal part flown for first time on UK fighter jet". *BAE Systems Newsroom* (5th January 2014).

14. Golson, J. "A Military-Grade Drone That Can Be Printed Anywhere". *Wired* (16th September 2014).

15. The University of Sheffield. "3D printing trials of unmanned aircraft at the University of Sheffield

broaden the possibilities for this emergent technology". *News releases - The University of Sheffield* (2014). Available at: http://www.sheffield.ac.uk/news/nr/3d-printing-trials-of-unmanned-aircraft-1.364084. (Accessed: 20th September 2014)

16. Muir, M. J., Kolb, E. J., Parkinson, A. T., Robertson, G. A., Muldal, C. L., Querin, O., Hewson, R. W. & Toropov, V. "The use of MDO and Advanced Manufacturing to Demonstrate Rapid , Agile Construction of a Mission Optimized UAV". in *54th AIAA/ASME/ASCE/AHS/ASC Structures, Structural Dynamics, and Materials Conference* pp. 1–21 (Boston, MA, 2013).

17. Stark, B., Stevenson, B., Stow-Parker, K. & Chen, Y. "Embedded sensors for the health monitoring of 3D printed unmanned aerial systems". in *ICUAS 2014 - International Conference on Unmanned Aircraft Systems* pp. 175–180 (Orlando, FL, 2014).

18. Ferraro, M., Gorissen, D., Scanlan, J., Keane, A., Quaranta, E., Schumann, B., van Schaik, J. & Bolinches i Gisbert, M. "Toward Value-Driven Design of a Small, Low-Cost UAV". in *53rd AIAA/ASME/ASCE/AHS/ASC Structures, Structural Dynamics and Materials Conference* pp. 1–9 (Honolulu, HI, 2012).

19. Gorissen, D., Quaranta, E., Ferraro, M., Schumann, B., Schaik, J. Van, Gisbert, M. B. I., Keane, A. & Scanlan, J. "Value-Based Decision Environment: Vision and Application". *Journal of Aircraft* 51 (5), pp. 1360–1372 (2014).

20. Surendra, A., Ferraro, M., Schumann, B., van Schaik, J., Daniels, J. J., Gorissen, D., Scanlan, J. P. & Keane, A. J. "The Challenges of using Value-Driven Design for practical design of UAVs". *Journal of Aerospace Operations* 1 (4), pp. 377–386 (2012).

21. Ferraro, M., Lock, A., Scanlan, J. & Keane, A. "Design and flight test of a civil unmanned aerial vehicle for maritime patrol: the use of 3D-printed structural components". in *4th Aircraft Structural Design Conference - Royal Aeronautical Society* pp. 1–14 (Belfast, 2014).

22. Schumann, B., Ferraro, M., Surendra, A., Scanlan, J. P. & Fangohr, H. "Better Design Decisions Through Operational Modeling During the Early Design Phases". *Journal of Aerospace Information Systems* 11 (4), pp. 195–210 (2014).

23. Mavris, D. N., DeLaurentis, D. A., Bandte, O. & Hale, M. A. "A Stochastic Approach to Multi-disciplinary Aircraft Analysis and Design". in *AIAA 36th Aerospace Sciences Meeting & Exhibit* pp. 1–17 (AIAA, Reno, NV, 1998).

24. Asiedu, Y. & Gu, P. "Product life cycle cost analysis: state of the art review". *International Journal of Production Research* 36 (4), pp. 883–908 (1998).

25. Price, M., Raghunathan, S. & Curran, R. "An integrated systems engineering approach to aircraft design". *Progress in Aerospace Sciences* 42 (4), pp. 331–376 (2006).

26. Newnes, L. B., Mileham, a. R., Cheung, W. M., Marsh, R., Lanham, J. D., Saravi, M. E. & Bradbery, R. W. "Predicting the whole-life cost of a product at the conceptual design stage". *Journal of Engineering Design* 19 (2), pp. 99–112 (2008).

27. Goh, Y. M., Newnes, L. B., Mileham, A. R., McMahon, C. a. & Saravi, M. E. "Uncertainty in Through-Life Costing – Review and Perspectives". *IEEE Transactions on Engineering Management* 57 (4), pp. 689–701 (2010).

28. Kirby, M. "A methodology for technology identification, evaluation, and selection in conceptual and preliminary aircraft design". (PhD Thesis, Georgia Institute of Technology, 2001).

29. Collopy, P. D. "Economic-based distributed optimal design". in *AIAA Space 2001 Conference and Exposition* pp. 1–9 (Albuquerque, NM, 2001).

30. Collopy, P. D. & Hollingsworth, P. M. "Value-Driven Design". *Journal of Aircraft* 48 (3), pp. 749–759 (2011).

31. Soban, D., Price, M. & Hollingsworth, P. "Defining a research agenda in Value Driven Design: Questions that need to be asked". *Journal of Aerospace Operations* 1 (4), pp. 329–342 (2012).

32. Howe, D. "*Aircraft conceptual design synthesis*". (Professional Engineering Publishing, 2000).

33. Kossiakoff, A., Sweet, W., Seymour, S. & Biemer, S. "*Systems engineering principles and practice*". (Wiley, 2011).

34. Johnson, C. & Smith, M. "*Kelly: more than my share of it all*". (Smithsonian Institution, 1985).

35. Ahmed, S., Blessing, L. & Wallace, K. "The relationships between data, information and knowledge based on a preliminary study of engineering designers". in *ASME Design Theory and Methodology* pp. 1–10 (Las Vegas, NV, 1999).

36. Hansen, C. & Ahmed, S. "An analysis of design decision-making in industrial practice". in *DESIGN 2002, the 7th International Design Conference* pp. 1–6 (Dubrovnik, 2002).

37. Raymer, D. P. "*Aircraft Design: A Conceptual Approach – Fourth Edition*". (AIAA Education Series, 2006).

38. Jayaram, S., Myklebust, A. & Gelhausen, P. "ACSYNT—A standards-based system for parametric computer aided conceptual design of aircraft". in *Aerospace Design Conference* pp. 1–14 (Irvine,CA, 1992).

39. McCullers, L. A. "FLOPS - Flight Optimization System - Release 7.40 - User's Guide". (2008).

40. Von Kaenel, R., Rizzi, A., Oppelstrup, J., Goetzendorf-Grabowski, T., Ghoreyshi, M., Cavagna, L. & Bérard, A. "CEASIOM: Simulating stability & control with cfd/csm in aircraft conceptual design". in *26th International Congress of the Aeronautical Sciences* pp. 1–14 (Anchorage, AK, 2008).

41. Da Ronch, A., McFarlane, C., Beaverstock, C., Oppelstrup, J., Zhang, M. & Rizzi, A. "Benchmarking CEASIOM software to predict flight control and flying qualities of the B-747". in *27th International Congress of the Aeronautical Sciences* 5, pp. 1–21 (Nice - France, 2010).

42. Optimal Aircraft Design. "ADS - Aircraft Design Software v3.20". (2013).

43. Roskam, J., Malaek, S. M. & Anemaat, W. "AAA (Advanced Aircraft Analysis): A User-Friendly Approach to Preliminary Aircraft Design". in *17th International Council of Aeronautical Sciences Congress* pp. 90–92 (Stockholm, 1990).

44. DARcorporation. "Advanced Aircraft Analysis v3.5". (2013).

45. Hahn, A. & Langley, N. "Vehicle Sketch Pad : A Parametric Geometry Modeler for Conceptual Aircraft Design". in *48th AIAA Aerospace Sciences Meeting* pp. 1–11 (Orlando, FL, 2010).

46. Chaput, A., Akay, E. & Rizo-Patron, S. "Vehicle Sketch Pad (VSP) Structural Layout Tool". in *49th AIAA Aerospace Sciences Meeting Including The New Horizons Forum And Aerospace Exposition* pp. 1–13 (Orlando, FL, 2011).

47. Gonzalez, L., Whitney, E., Srinivas, K. & Periaux, J. "Multidisciplinary Aircraft Design and Optimisation Using a Robust Evolutionary Technique with Variable Fidelity Models". in *10th AIAA/ISSMO Multidisciplinary Analysis and Optimization Conference* pp. 1–42 (Albany, NY, 2004).

48. Lee, D., Periaux, J., Gonzalez, L., Srinivas, K. & Onate, E. "Robust multidisciplinary UAS design optimisation". *Structural and Multidisciplinary Optimization* 45 (3), pp. 433–450 (2012).

49. Ghoman, S. S., Kapania, R. K., Chen, P. C., Sarhaddi, D. & Lee, D. H. "Multifidelity, Multistrategy, and Multidisciplinary Design Optimization Environmen". *Journal of Aircraft* 49 (5), pp. 1255–1270 (2012).

50. Nguyen, N. Van, Maxim, T., Park, H., Kim, S. & Lee, J. "A Multidisciplinary Robust Optimization Framework for UAV Conceptual Design". *Aeronautical Journal* 118 (1200), pp. 123–142 (2014).

51. Rajagopal, S. & Ganguli, R. "Conceptual design of UAV using Kriging based multi-objective genetic algorithm". *Aeronautical Journal* 112 (1137), pp. 653–662 (2008).

52. Cooper, C., Alderliesten, R., La Rocca, G. & Benedictus, R. "In Search of a Knowledge Based Preliminary Design Method of Complex Aircraft Wings". in *7th Annual Conference on System Engineering Research* pp. 1–7 (Loughborough, 2009).

53. La Rocca, G. & van Tooren, M. J. L. "Knowledge-based engineering to support aircraft multidisciplinary design and optimization". *Proceedings of the Institution of Mechanical Engineers, Part G: Journal of Aerospace Engineering* 224 (9), pp. 1041–1055 (2010).

54. Amadori, K. "A Framework for Aerodynamic and Structural Optimization in Conceptual Design". in *25th AIAA Applied Aerodynamics Conference* pp. 1–10 (Miami, FL, 2007).

55. Amadori, K. "On Aircraft Conceptual Design: A Framework for Knowledge Based Engineering and Design Optimization". (PhD Thesis, Linkoping University Institute of Technology, 2008).

56. Bohnke, D., Nagel, B. & Gollnick, V. "An approach to multi-fidelity in conceptual aircraft design in distributed design environments". in *2011 IEEE Aerospace Conference* pp. 1–10 (IEEE, Big Sky, MT, 2011).

57. Wicks, M. N. & Dewar, R. G. "A new research agenda for tool integration". *Journal of Systems and Software* 80 (9), pp. 1569–1585 (2007).

58. Ziemer, S., Glas, M. & Stenz, G. "A conceptual design tool for multi-disciplinary aircraft design". in *2011 IEEE Aerospace Conference* (Big Sky, MT, 2011).

59. Azamatov, A., Lee, J.-W. & Byun, Y.-H. "Comprehensive aircraft configuration design tool for Integrated Product and Process Development". *Advances in Engineering Software* 42 (1–2), pp. 35–49 (2011).

60. Sobieszczanski-Sobieski, J., Agte, J. S. & Sandusky, R. R. "Bilevel integrated system synthesis". *AIAA Journal* 38 (1), pp. 164–172 (2000).

61. Sobieszczanski-sobieski, J., Altus, T. D., Phillips, M. & Sandusky, R. "Bilevel integrated system synthesis for concurrent and distributed processing". *AIAA Journal* 41 (10), pp. 1996–2003 (2003).

62. Roth, B. & Kroo, I. "Enhanced Collaborative Optimization : Application to an Analytic Test Problem and Aircraft Design". in *12th AIAA/ISSMO Multidisciplinary Analysis and Optimization Conference* pp. 1–14 (Victoria, BC, 2008).

63. Allison, J. T., Walsh, D., Kokkolaras, M., Papalambros, P. & Cartmell, M. "Analytical Target Cascading in Aircraft Design". in *44th AIAA Aerospace Sciences Meeting and Exhibit* pp. 1–9 (Reno, NV, 2006).

64. Zhang, K. "*Chapter 9: Concurrent Subspace Optimization for Aircraft System Design*". *Aeronautics and Astronautics* (InTech, 2011).

65. Schumann, B. "Aeronautical Life-Cycle Mission Modelling Framework for Conceptual Design". (PhD Thesis, University of Southampton, 2014).

66. Faulconbridge, R. I. & Ryan, M. J. "*Systems Engineering Practice*". (ArgosPress, 2014).

67. NASA. "*Systems Engineering Handbook*". (National Aeronautics and Space Administration, 2010).

68. INCOSE. "*Systems Engineering Handbook: A Guide for System Life Cycle Processes and Activities*". (Wiley, 2015).

69. Department of Defense. "*Systems Engineering Fundamentals*". (Defense Acquisition University Press, 1999).

70. Suh, N. P. "*The Principles of Design*". (Oxford University Press, 1990).

71. Suh, N. P. "Axiomatic Design Theory for Systems". *Research in Engineering Design - Theory, Applications, and Concurrent Engineering* 10 (4), pp. 189–209 (1998).

72. Suh, N. P. "*Axiomatic Design: Advances and Applications*". (Oxford University Press, 2001).

73. Gumus, B. "Axiomatic Product Development Lifecycle". (PhD Thesis, Texas Tech University, 2005).

74. Malmqvist, J. "A Classification of Matrix-based Methods for Product Modeling". in *DESIGN 2002, the 7th International Design Conference* pp. 203–210 (Dubrovnik, 2002).

75. Govers, C. P. M. "What and how about quality function deployment (QFD)". *International Journal of Production Economics* 46–47 (95), pp. 575–585 (1996).

76. Chan, L.-K. & Wu, M.-L. "*Quality function deployment: A literature review*". *European Journal of Operational Research* 143 (3), (2002).

77. Steward, D. V. "Design Structure System: A Method for Managing the Design of Complex Systems". *IEEE Transactions on Engineering Management* EM-28 (3), pp. 71–74 (1981).

78. Browning, T. R. "Applying the Design Structure Matrix to System Decomposition and Integration Problems: a Review and New Directions". *Engineering Management, IEEE Transactions on* 48 (3), pp. 292–306 (2001).

79. Ramos, A. L., Ferreira, J. V. & Barceló, J. "Model-Based Systems Engineering: An Emerging Approach for Modern Systems". *IEEE Transactions on Systems, Man, and Cybernetics, Part C (Applications and Reviews)* 42 (1), pp. 101–111 (2012).

80. International Council on Systems Engineering. "Systems Engineering Vision 2020". *INCOSE-TP-2004-004-02* 1 (2.03), pp. 1–32 (2007).

81. Royce, W. W. "Managing the Development of Large Software Systems". *Proceedings of IEEE WESCON* 26 (8), pp. 328–338 (1970).

82. Boehm, B. "Spiral Development : Experience, Principles, and Refinements". *Spiral Development Workshop* (Carnegie Mellon University Software Engineering Institute, 2000).

83. Darrin, M. A. G. & Barth, J. L. "*Systems Engineering for Microscale and Nanoscale Technologies*". (CRC Press, 2011).

84. Haberfellner, R. & Weck, O. "Agile SYSTEMS ENGINEERING versus AGILE SYSTEMS engineering". in *15th Annual International Symposium of the International Council On Systems Engineering (INCOSE)* pp. 1–17 (Rochester, NY, 2005).

85. Takeuchi, H., Nonaka, I. & Takeuchi, H. "The new new product development game". *Harvard Business Review* 64 (1), pp. 137–146 (1986).

86. Lage Junior, M. & Godinho Filho, M. "Variations of the kanban system: Literature review and classification". *International Journal of Production Economics* 125 (1), pp. 13–21 (2010).

87. Winner, R. I., Pennell, J. P., Bertrand, H. E. & Slusarczuk, M. M. "The role of concurrent engineering in weapons system acquisition". (Institute For Defense Analyses, 1988).

88. Marx, W. J., Mavris, D. N. & Schrage, D. P. "Integrating Design And Manufacturing For A High Speed Civil Transport Wing". in *19th ICAS/AIAA Aircraft Systems Conference* 53, pp. 1–10 (Anaheim, CA, 1994).

89. Kusiak, A. "Integrated product and process design: A modularity perspective". *Journal of Engineering Design* 13 (3), pp. 223–231 (2002).

90. Department of Defense. "*DoD Integrated Product and Process Development Handbook*". (Office Of The Under Secretary Of Defense, 1998).

91. Krammer, J., Sensburg, O., Vilsmeier, J. & Berchtold, G. "Concurrent engineering in design of aircraft structures". *Journal of Aircraft* 32 (2), pp. 423–430 (1995).

92. Mavris, D. N., Baker, A. P. & Schrage, D. P. "IPPD Through Robust Design Simulation for an Affordable Short Haul Civil Tiltrotor". in *American Helicopter Society 53rd Annual Forum* pp. 1615–1627 (Virginia Beach, VA, 1997).

93. Ardalan, S. . "DrawCraft: a spacecraft design tool for integrated concurrent engineering". in *2000 IEEE Aerospace Conference* pp. 501–510 (Big Sky, MT, 2000).

94. Avnet, M. S. & Weigel, A. L. "An application of the Design Structure Matrix to Integrated Concurrent Engineering". *Acta Astronautica* 66 (5–6), pp. 937–949 (2010).

95. European Space Agency. "The ESA Concurrent Design Facility". Available at: http://www.esa.int/Our_Activities/Space_Engineering_Technology/CDF. (Accessed: 6th June 2016)

96. DLR - German Aerospace Center. "Concurrent Engineering Facility (CEF)". Available at: http://www.dlr.de/irs/en/desktopdefault.aspx/tabid-11079. (Accessed: 2nd December 2015)

97. Ma, Y. S., Chen, G. & Thimm, G. "Paradigm shift: unified and associative feature-based concurrent and collaborative engineering". *Journal of Intelligent Manufacturing* 19 (6), pp. 625–641 (2008).

98. Eres, M. H., Bertoni, M., Kossmann, M. & Scanlan, J. "Mapping customer needs to engineering characteristics: an aerospace perspective for conceptual design". *Journal of Engineering Design* 25 (1–3), pp. 64–87 (2014).

99. Zhang, X., Auriol, G., Eres, H. & Baron, C. "A prescriptive approach to qualify and quantify customer value for value-based requirements engineering". *International Journal of Computer Integrated Manufacturing* 26 (4), pp. 327–345 (2013).

100. Mavris, D. N. & DeLaurentis, D. "Methodology for examining the simultaneous impact of requirements, vehicle characteristics, and technologies on military aircraft design". in *22nd Congress of the International Council on the Aeronautical Sciences (ICAS)* 145, pp. 1–10 (Harrogate, 2000).

101. Jayaram, S., Myklebust, A. & Gelhausen, P. "ACSYNT - A standards-based system for parametric, computer aided conceptual design of aircraft". in *Aerospace Design Conference* pp. 1–14 (Irvine,CA, 1992).

102. Conceptual Research Corporation. "RDS software". (2010).

103. Lyssis Ltd. "PIANO - Project Interactive Analysis and Optimisation software v5.3". (2014).

104. Krus, P. & Jouannet, C. "Whole Mission Simulation for Aircraft Preliminary Design". in *48th AIAA Aerospace Sciences Meeting Including the New Horizons Forum and Aerospace Exposition* pp. 1–11 (Orlando, FL, 2010).

105. Krus, P. "Whole Aircraft Simulation for System Design and Optimsation in Preliminary Design". in *3rd CEAS Air&Space Conference - 21st AIDAA Congress* (Venice, 2011).

106. Pace. "Pacelab Suite software". (2012).

107. Ternion Corporation. "FLAMES software". (2015).

108. AGI. "STK - System Tool Kit FLAMES software". (2015).

109. Duquette, M. "Effects-Level Models for UAV Simulation". in *AIAA Modeling and Simulation Technologies Conference* pp. 1–12 (Chicago, IL, 2009).

110. Wei, Y., Madey, G. & Blake, M. "Agent-based Simulation for UAV Swarm Mission Planning and Execution". in *Agent-directed Simulation Symposium* (San Diego, CA, 2013).

111. Soban, D. S. "A Methodology for the Probabilistic Assessment of System Effectiveness as Applied to Aircraft Survivability and Susceptibility". (PhD Thesis, Georgia Institute of Technology, 2001).

112. Evans, E. "A Simulation Optimization Approach to the Design of Unmanned Aerial Vehicles". (MSc Thesis, Air Force Institute of Technology, 2008).

113. Nilubol, L. O. "Development Operational Combat Aircraft of a Design Methodology". (PhD Thesis, Cranfield University, 2005).

114. Cassidy, P., Gatzke, T. & Vaporean, C. "Integrating Synthesis and Simulation for Conceptual Design". in *46th AIAA Aerospace Sciences Meeting and Exhibit* pp. 1–9 (Reno, NV, 2008).

115. Thokala, P. "Life cycle cost modelling as an aircraft design decision support tool". (PhD Thesis, University of Southampton, 2009).

116. Thokala, P., Scanlan, J. & Chipperfield, a. "Life cycle cost modelling as an aircraft design support tool". *Proceedings of the Institution of Mechanical Engineers, Part G: Journal of Aerospace Engineering* 224 (4), pp. 477–488 (2010).

117. Schumann, B., Scanlan, J. P. & Takeda, K. "A generic operational simulation for early design civil unmanned aerial vehicles". in *The Third International Conference on Advances in System Simulation* pp. 75–78 (Barcelona, 2011).

118. Yifeng, T., Hu, L. & Jun, H. "Design space exploration in aircraft conceptual design phase based on system-of-systems simulation". *International Journal of Aeronautical and Space Sciences* 16 (4), pp. 624–635 (2015).

119. Collopy, P. D. "Aerospace System Value Models: A Survey and Observations". in *AIAA SPACE 2009 Conference & Exposition* pp. 1–18 (Pasadena, CA, 2009).

120. Ross, A. M., O'Neill, M. G., Hastings, D. E. & Rhodes, D. H. "Aligning Perspectives and Methods for Value-Driven Design". in *AIAA SPACE 2010 Conference & Exposition* pp. 1–12 (Anaheim, CA, 2010).

121. Brown, O., Eremenko, P. & Collopy, P. "Value-centric design methodologies for fractionated spacecraft: Progress summary from phase 1 of the darpa system F6 program". in *AIAA SPACE 2009 Conference & Exposition* (Pasadena, CA, 2009).

122. Peoples, R. & Willcox, K. "Value-based multidisciplinary optimization for commercial aircraft design and business risk assessment". *Journal of Aircraft* 43 (4), pp. 913–921 (2006).

123. Value Driven Design Program Commitee of the American Institute of Aeronautics and Astronautics. "About Value-Driven Design". (2008). Available at: https://info.aiaa.org/tac/pc/VDDPC/Web Pages/About VDDPC.aspx. (Accessed: 12th December 2011)

124. Dahlgren, J. W. "Real Options and Value Driven Design in Spiral Development". in *INCOSE International Symposium 2006* pp. 1–12 (Orlando, FL, 2006).

125. Collopy, P. "Adverse impact of extensive attribute requirements on the design of complex systems". in *7th AIAA ATIO Conference, 2nd CEIAT International Conference on Innovation and Integration in Aero Sciences, 17th LTA Systems Tech Conference* pp. 1–7 (Belfast, 2007).

126. Lee, B. D., Binder, W. R. & Paredis, C. J. J. "A Systematic Method for Specifying Effective Value Models". *Procedia Computer Science* 28 (Cser), pp. 228–236 (2014).

127. Keeney, R. L. "The Foundations of Collaborative Group Decisions". *International Journal of Collaborative Engineering* 1 (4), pp. 4–18 (2009).

128. Lai, V. S., Wong, B. K. & Cheung, W. "Group decision making in a multiple criteria environment: A case using the AHP in software selection". *European Journal of Operational Research* 137 (1), pp. 134–144 (2002).

129. Matsatsinis, N. F., Grigoroudis, E. & Samaras, A. "Aggregation and disaggregation of preferences for collective decision-making". *Group Decision and Negotiation* 14 (3), pp. 217–232 (2005).

130. Papageorgiou, E., Eres, M. H. & Scanlan, J. "Value Modelling for MultiStakeholder MultiObjective Optimization in Engineering Design for Review". *Journal of Engineering Design* 27 (10), pp. 697–724 (2016).

131. Smith, A. "*An Inquiry into the Nature and Causes of the Wealth of Nations*". (T. Nelson and Sons, 1887).

132. Bouyssou, D., Dubois, D., Prade, H. & Pirlot, M. "*Decision Making Process: Concepts and Methods*". (Wiley, 2009).

133. Bernoulli, D. "Exposition of a new theory on the measurement of risk". *Econometrica* 22 (1), pp. 23–36 (1954).

134. Von Neumann, J. & Morgenstern, O. "*Theory of games and economic behavior*". (Princeton University Press, 1944).

135. Baker, A. & Mavris, D. "Assessing the simultaneous impacts of requirements, vehicle characteristics, and technologies during aircraft design". in *39th AIAA, Aerospace Sciences Meeting and Exhibit* pp. 1–11 (Reno, NV, 2001).

136. Mavris, D. N. & DeLaurentis, D. A. "A probabilistic approach for examining aircraft concept feasibility and viability". *Aircraft Design* 3 (2), pp. 79–101 (2000).

137. Kirby, M. & Mavris, D. "A method for technology selection based on benefit, available schedule and budget resources". in *2000 World Aviation Conference* pp. 1–17 (San Diego,CA, 2000).

138. Hollingsworth, P. "Requirements Controlled Design: A Method for Discovery of Discontinuous System Boundaries in the Requirements Hyperspace". (PhD Thesis, Georgia Institute of Technology, 2004).

139. Dufresne, S., Johnson, C. & Mavris, D. N. "Variable Fidelity Conceptual Design Environment for Revolutionary Unmanned Aerial Vehicles". *Journal of Aircraft* 45 (4), pp. 1405–1418 (2008).

140. Stump, G., Lego, S., Yukish, M., Simpson, T. W. & Donndelinger, J. a. "Visual Steering Commands for Trade Space Exploration: User-Guided Sampling With Example". *Journal of Computing and Information Science in Engineering* 9 (4), pp. 44–501 (2009).

141. Chiu, P. W., Naim, A. M., Lewis, K. E. & Bloebaum, C. L. "The hyper-radial visualisation method for multi-attribute decision-making under uncertainty". *International Journal of Product Development* 9 (1–3), pp. 4–31 (2009).

142. Hwang, C.-L. & Yoon, K. "*Multiple Attribute Decision Making Methods and Applications - A State-of-the-Art Survey*". (Springer Berlin Heidelberg, 1981).

143. Velasquez, M. & Hester, P. T. "An Analysis of Multi-Criteria Decision Making Methods". *International Journal of Operations Research* 10 (2), pp. 56–66 (2013).

144. Saaty, T. L. "How to make a decision: The analytic hierarchy process". *European Journal of Operational Research* 48 (1), pp. 9–26 (1990).

145. Keeney, R. & Raiffa, H. "*Decisions with multiple objectives: preferences and value trade-offs*". (Cambridge University Press, 1993).

146. Ross, A. "Multi-attribute tradespace exploration with concurrent design as a value-centric framework for space system architecture and design". (MSc Thesis, Massachusetts Institute of Technology, 2003).

147. Thurston, D. "Real and misconceived limitations to decision based design with utility analysis". *Journal of Mechanical Design* 123 (2), pp. 176–182 (2001).

148. Matheson, J. & Howard, R. "*An Introduction To Decision Analysis - The Principles of Decision*

Analysis". (Strategic Decisions Group: Menlo Park, California, 1968).

149. Matheson, J. & Abbas, A. "Utility transversality: a value-based approach". *Journal of Multi-Criteria Decision Analysis* 13 (5–6), pp. 229–238 (2005).

150. Keeney, R. & VonWinterfeldt, D. "*Chapter 13: Practical Value Models*". *Advances in Decision Analysis: from Foundations to Applications* (Cambridge University Press, 2007).

151. Collopy, P. "Value of the Probability of Success". in *AIAA SPACE 2008 Conference & Exposition* 7868, pp. 1–6 (San Diego, CA, 2008).

152. Agte, J., de Weck, O., Sobieszczanski-Sobieski, J., Arendsen, P., Morris, A. & Spieck, M. "MDO: Assessment and direction for advancement-an opinion of one international group". *Structural and Multidisciplinary Optimization* 40 (1–6), pp. 17–33 (2010).

153. Collopy, P. D. "Surplus value in propulsion system design optimization". in *33rd Joint Propulsion Conference and Exhibit* pp. 1–7 (Seattle,WA, 1997).

154. Cheung, J., Scanlan, J. P., Wong, J., Forrester, J., Eres, H., Collopy, P., Hollingsworth, P., Wiseall, S. & Briceno, S. "Application of Value-Driven Design to Commercial Aero-Engine Systems". *Journal of Aircraft* 49 (3), pp. 668–702 (2010).

155. Hollingsworth, P. "An Investigation of Value Modelling for Commercial Aircraft". in *2nd Air Transport and Operations Symposium* pp. 358–371 (Delft, NL, 2011).

156. Miller, B. & Clarke, J. "Application of Real Options to Evaluate the Development Process of New Aircraft Models". in *4th AIAA ATIO Forum* pp. 1–11 (Chicago, IL, 2004).

157. Selva, D., Cameron, B. & Crawley, E. F. "A rule-based method for scalable and traceable evaluation of system architectures". *Research in Engineering Design* 25 (4), pp. 325–349 (2014).

158. Markish, J. & Willcox, K. "A value-based approach for commercial aircraft conceptual design". in *ICAS 2002 23rd International Congress of Aeronautical Sciences* pp. 1–10 (Toronto, 2002).

159. Markish, J. & Willcox, K. "Value-Based multidisciplinary techniques for commercial aircraft system design". *AIAA Journal* 41 (10), pp. 2004–2012 (2003).

160. Ross, A. & Rhodes, D. "Using natural value-centric time scales for conceptualizing system timelines through epoch-era analysis". in *INCOSE International Symposium* 18 (1), pp. 1186–1201 (Utrecht, 2008).

161. Fitzgerald, M., Ross, A. & Rhodes, D. "A Method Using Epoch-Era Analysis to Identify Valuable Changeability in System Design". in *9th Conference on Systems Engineering Research* pp. 1–13 (Los Angeles, CA, 2011).

162. Fitzgerald, M. & Ross, A. "Sustaining lifecycle value: Valuable changeability analysis with era simulation". in *2012 IEEE International Systems Conference (SysCon),* pp. 1–7 (2012).

163. Castagne, S., Curran, R. & Collopy, P. "Implementation of Value-Driven Optimisation for the Design of Aircraft Fuselage Panels". *International Journal of Production Economics* 117 (2), pp. 381–388 (2009).

164. Vučina, D., Lozina, Ž. & Vlak, F. "NPV-based decision support in multi-objective design using evolutionary algorithms". *Engineering Applications of Artificial Intelligence* 23 (1), pp. 48–60 (2010).

165. Hollingsworth, P. & Patel, D. "Development of a surplus value parameter for use in initial aircraft conceptual design". *Journal of Aerospace Operations* 1 (4), pp. 343–358 (2012).

166. Keller, S. & Collopy, P. "Value Modeling for a Space Launch System". *Procedia Computer Science* 16, pp. 1152–1160 (2013).

167. Defense Advanced Research Projects Agency. "System F6". (2008). Available at: http://www.darpa.mil/Our_Work/TTO/Programs/System_F6.aspx. (Accessed: 12th December 2011)

168. Brown, O. & Eremenko, P. "Application of value-centric design to space architectures: the case of fractionated spacecraft". in *AIAA SPACE 2008 Conference & Exposition* 7869, pp. 1–31 (San Diego, CA, 2008).

169. O'Neill, M. G., Yue, H., Nag, S., Grogan, P. & de Weck, O. "Comparing and Optimizing the DARPA System F6 Program Value-Centric Design Methodologies". *AIAA SPACE 2010 Conference & Exposition* pp. 1–17 (2010).

170. Ferster, W. "DARPA Cancels Formation-flying Satellite Demo". *SpaceNews* (2013).

171. Bryden, D. "*CAD and Rapid Prototyping for Product Design*". (Laurence King Publishing, 2014).

172. Wong, K. V. & Hernandez, A. "A Review of Additive Manufacturing". *ISRN Mechanical Engineering* 2012, pp. 1–10 (2012).

173. Hopkinson, N. & Dicknes, P. "Analysis of rapid manufacturing - using layer manufacturing processes for production". *Proceedings of the Institution of Mechanical Engineers, Part C: Journal of Mechanical Engineering Science* 217 (1), pp. 31–39 (2003).

174. Kulkarni, P., Marsan, A. & Dutta, D. "A review of process planning techniques in layered manufacturing". *Rapid Prototyping Journal* 6 (1), pp. 18–35 (2000).

175. Groover, M. P. "*Fundamentals of modern manufacturing: materials processes, and systems*". (John Wiley & Sons, 2010).

176. Barnatt, C. "*3D Printing: The Next Industrial Revolution*". 6, (ExplainingTheFuture.com, 2013).

177. Hague, R., Campbell, I. & Dickens, P. "Implications on design of rapid manufacturing". *Proceedings of the Institution of Mechanical Engineers, Part C: Journal of Mechanical Engineering Science* 217 (1), pp. 25–30 (2003).

178. Hague, R., Mansour, S. & Saleh, N. "Design opportunities with rapid manufacturing". *Assembly*

Automation 23 (4), pp. 346–356 (2003).

179. Rosochowski, A. & Matuszak, A. "Rapid tooling: the state of the art". *Journal of Materials Processing Technology* 106 (1–3), pp. 191–198 (2000).

180. Levy, G. N., Schindel, R. & Kruth, J. P. "Rapid Manufacturing And Rapid Tooling With Layer Manufacturing (LM) Technologies, State Of The Art And Future Perspectives". *CIRP Annals - Manufacturing Technology* 52 (2), pp. 589–609 (2003).

181. Pham, D. T. & Dimov, S. S. "Rapid prototyping and rapid tooling - the key enablers for rapid manufacturing". *Proceedings of the Institution of Mechanical Engineers, Part C: Journal of Mechanical Engineering Science* 217 (1), pp. 1–23 (2003).

182. Ruffo, M., Tuck, C. & Hague, R. "Cost estimation for rapid manufacturing-laser sintering production for low to medium volumes". *Proceedings of the Institution of Mechanical Engineers, Part B: Journal of Engineering Manufacture* 220 (9), pp. 1417–1427 (2006).

183. Atzeni, E., Iuliano, L., Minetola, P. & Salmi, A. "Redesign and cost estimation of rapid manufactured plastic parts". *Rapid Prototyping Journal* 16 (5), pp. 308–317 (2010).

184. Amado-Becker, A., Ramos-Grez, J., Yañez, M. J., Vargas, Y. & Gaete, L. "Elastic tensor stiffness coefficients for SLS Nylon 12 under different degrees of densification as measured by ultrasonic technique". *Rapid Prototyping Journal* 14 (5), pp. 260–270 (2008).

185. 3T-RPD. "Plastic AM Materials". (2015). Available at: http://www.3trpd.co.uk/sls-materials.htm.

186. Seepersad, C. C., Govett, T., Kim, K., Lundin, M. & Pinero, D. "A Designer's Guide for Dimensioning and Tolerancing SLS parts". in *23rd Annual International Solid Freeform Fabrication Symposium* pp. 921–931 (Austin, TX, 2012).

187. Shapeways. "Design Rules and Detail Resolution for SLS 3D Printing". (2015). Available at: http://www.shapeways.com/tutorials/design_rules_for_3d_printing.

188. Lewandowski, J. J. & Seifi, M. "Metal Additive Manufacturing: A Review of Mechanical Properties". *Annual Review of Materials Research* 46 (1), pp. 151–186 (2016).

189. Frazier, W. E. "Metal Additive Manufacturing: A Review". *Journal of Materials Engineering and Performance* 23 (6), pp. 1917–1928 (2014).

190. Simmons, D. "Airbus had 1,000 parts 3D printed to meet deadline". *BBC News* (2015). Available at: http://www.bbc.co.uk/news/technology-32597809. (Accessed: 28th October 2015)

191. Tangmere Museum. "Supermarine Spitfire". (2007). Available at: http://www.tangmere-museum.org.uk/aircraft-month/supermarine-spitfire-prototype-k5054-mk5b-bl924-replicas.

192. Brooklands Museum. "Vickers 290 Wellington Mk1A". (2010). Available at: https://www.brooklandsmuseum.com/explore/our-collection/aircraft/vickers-290-wellington-mk1a.

193. Eschenauer, H. a & Olhoff, N. "Topology optimization of continuum structures: A review". *Applied Mechanics Reviews* 54 (4), pp. 331 (2001).

194. Tomlin, M. & Meyer, J. "Topology Optimization of an Additive Layer Manufactured (ALM) Aerospace Part". in *The 7th Altair CAE Technology Conference 2011* pp. 1–9 (Gaydon, 2011).

195. Kelly, L., Keane, A., Sóbester, A. & Toal, D. "Topology Optimisation : Increasing the Speed and Reliability of Design". in *15th AIAA/ISSMO Multidisciplinary Analysis and Optimization Conference* pp. 1–11 (Atlanta, GA, 2014).

196. Dassault Systèmes. "SolidWorks Versions 2010-2016". (2015).

197. Tornincasa, S. & Di Monaco, F. "the Future and the Evolution of Cad". in *14th International Research/Expert Conference "Trends in the Development of Machinery and Associated Technology"* pp. 1–18 (Mediterranean Cruise, 2010).

198. Keane, A., Scanlan, J., Lock, A., Ferraro, M., Spillane, P. & Breen, J. "Maritime Flight Trials of the Southampton University Laser Sintered Aircraft – Project Albatross". *Journal of Aircraft* (Submitted in 2016),

199. Cesaretti, G., Dini, E., De Kestelier, X., Colla, V. & Pambaguian, L. "Building components for an outpost on the Lunar soil by means of a novel 3D printing technology". *Acta Astronautica* 93, pp. 430–450 (2014).

200. Schmid, M., Woellecke, F. & Levy, G. N. "Long-term durability of SLS polymer components under automotive application environment". in *23rd Annual International Solid Freeform Fabrication Symposium - An Additive Manufacturing Conference* pp. 277–284 (Austin, TX, 2012).

201. Wudy, K., Drummer, D., Kühnlein, F. & Drexler, M. "Influence of degradation behavior of polyamide 12 powders in laser sintering process on produced parts". *AIP Conference Proceedings* 1593 (691), pp. 691–695 (2014).

202. McKeen, L. W. "*The Effects of UV Light and Weather on Plastics and Elastomers - Third Edition*". (William Andrew Pub., 2013).

203. Gijsman, P., Meijers, G. & Vitarelli, G. "Comparison of the UV-degradation chemistry of polypropylene, polyethylene, polyamide 6 and polybutylene terephthalate". *Polymer Degradation and Stability* 65, pp. 433–441 (1999).

204. Shamey, R. & Sinha, K. "A review of degradation of nylon 6.6 as a result of exposure to environmental conditions". *Review of Progress in Coloration and Related Topics* 33, pp. 93–107 (2003).

205. Ulrich, K. T. & Eppinger, S. D. "*Product Design and Development - Fifth Edition*". (McGraw-Hill Education, 2004).

206. Ulrich, K. "The role of product architecture in the manufacturing firm". *Research Policy* 24 (3), pp.

419–440 (1995).

207. Gu, P., Hashemian, M. & Nee, a. Y. C. "Adaptable Design". *CIRP Annals - Manufacturing Technology* 53 (2), pp. 539–557 (2004).

208. Crawley, E., Weck de, O., Eppinger, S., Magee, C., Moses, J., Seering, W., Schindall, J., Wallace, D., Whitney, D. & Weck, O. De. "*The Influence of Architecture in Engineering Systems*". *Engineering Systems Monograph* (The ESD Architecture Committee, 2004).

209. W. H. Elmaraghy, Hoda A. Elmaraghy, Tetsuo Tomiyama, L. M. "Complexity in engineering design and manufacturing". *CIRP Annals - Manufacturing Technology* 61, pp. 793–814 (2012).

210. ElMaraghy, W. H. & Urbanic, R. J. "Modelling of Manufacturing Systems Complexity". *CIRP Annals - Manufacturing Technology* 52, pp. 363–366 (2003).

211. Shannon, C. E. "*The Mathematical Theory of Communication*". (University of Illinois Press, 1949).

212. Newman, M. "*Networks: An Introduction*". (Oxford University Press, 2010).

213. Whitney, D. E. "*Chapter 17: Network Models of Mechanical Assemblies - in Unifying Themes in Complex Systems*". (Springer, 2010).

214. "Royal National Lifeboat Institution website". Available at: www.rnli.org.uk. (Accessed: 1st January 2011)

215. The MathWorks Inc. "MATLAB version R2014a". (2014).

216. CFS Engineering. "CEASIOM V2.0 - Computerised Environment for Aircraft Synthesis and Integrated Optimisation Methods". (2011).

217. Perkins, C. D. & Hage, R. E. "*Airplane Performance, Stability and Control*". (Wiley, 1967).

218. Roskam, J. "*Airplane Design*". (DAR Corporation, 1997).

219. Gundlach, J. "*Designing Unmanned Aircraft Systems: A Comprehensive Approach*". (AIAA Education Series, 2012).

220. Robinson, G. "A Spreadsheet Approach to Light Aircraft Design". in *Royal Aeronautical Society - Design Methods And Tools For Ligth Aircraft* pp. 1–76 (2009).

221. Raymer, D. "Modern Use of Spreadsheet Methods for Aircraft Design, Sizing, and Performance Analysis". in *42nd AIAA Aerospace Sciences Meeting and Exhibit* pp. 1–10 (Reno, NV, 2004).

222. Scanlan, J., Rao, A., Bru, C., Hale, P. & Marsh, R. "DATUM Project: Cost Estimating Environment for Support of Aerospace Design Decision Making". *Journal of Aircraft* 43 (4), pp. 1022–1028 (2006).

223. Microsoft Corporation. "Microsoft Excel 2010". (2010).

224. Lasdon, L. S., Fox, R. L. & Ratner, M. W. "Nonlinear optimization using the generalized reduced

gradient method". *RAIRO Operations Research* 8, pp. 73–103 (1974).

225. Kroshko, D. "OpenOpt version 0.5625 - A Python module for numerical optimization". (2008).

226. Eric Jones, Oliphant, T. & Peterson, P. "scipy.optimize.fmin_slsqp solver - SciPy: Open Source Scientific Tools for Python". (2001).

227. ANSYS Inc. "ANSYS version 14.0". (2011).

228. Nita, M. & Scholz, D. "Estimating the Oswald Factor from Basic Aircraft Geometrical Parameters". in *Deutscher Luft- und Raumfahrtkongress* pp. 1–19 (Berlin, 2012).

229. Torembeek, E. "*Synthesis of Subsonic Airplane Design*". (Delft University Press, 1982).

230. Abbott, I. H. & Von Doenhoff, A. E. "*Theory of Wing Sections*". (Dover Publications, 1958).

231. Roskam, J. "*Airplane Design: Airplane Design: Part VI - Preliminary Calculation of Aerodynamic, Thrust and Power Characteristics.*". (DAR Corporation, 1990).

232. Engineering Sciences Data Unit. "*Performance - Drag of Airframes*". (ESDU Engineering Data, 1997).

233. Engineering Sciencies Data Unit. "*Aerodynamics*". (ESDU Engineering Data, 1987).

234. Melin, T. "Tornado - A Vortex Lattice Method implemented in MATLAB". (2001).

235. ANSYS Inc. "Fluent version 14.0". (2011).

236. Phillips, J. D. "Approximate Neutral Point of a Subsonic Canard Aircraft". *NASA Technical Memorandum* 86694, pp. 1–14 (1985).

237. Joint Aviation Authorities. "*Joint Aviation Requirements Part-23. Normal, Utility, Aerobatic and Commuter Category Aeroplanes*". (JAA Headquarters, 1994).

238. Schrenk, O. "A Simple Approximation Method for Obtaining the Spanwise Lift Distribution". *NASA Technical Memorandum* 948, pp. 1–16 (1940).

239. Staton, R. "Statistical Weight Estimation Methods for Fighter/Attack Aircraft". *Vought Aircraft Report 2-59320/8R-50475* (1968).

240. Staton, R. "Cargo/Transport Statistical Weight Estimation Equations". *Vought Aircraft Report 2-59320/9R-50549* (1969).

241. Brandt, J. B., Deters, R. W., Ananda, G. K. & Selig, M. S. "UIUC Propeller Database". *University of Illinois at Urbana-Champaign* (2015). Available at: http://m-selig.ae.illinois.edu/props/propDB.html.

242. Brandt, J. B. & Selig, M. S. "Propeller Performance Data at Low Reynolds Numbers". in *49th AIAA Aerospace Sciences Meeting* pp. 1–18 (Orlando, FL, 2011).

243. Deters, R. W., Ananda, G. K. & Selig, M. S. "Reynolds Number Effects on the Performance of

Small-Scale Propellers". in *32nd AIAA Applied Aerodynamics Conference* pp. 1–8 (Atlanta, GA, 2014).

244. RCFAQ.com. "Model airplane engine propeller and rpm performance figures". Available at: http://www.rcfaq.com/RPMSTATS/RPMINDEX.ASP. (Accessed: 1st January 2012)

245. Top-Flite. "Propeller Chart". Available at: http://www.top-flite.com/accys/topq5000a.html. (Accessed: 1st January 2012)

246. Peckham, D. H. "Range Performance In Cruising Flight". *Royal Aircraft Establishment Technical Report No. 73164* (1974).

247. Johnson, V. "Minimizing life cycle cost for subsonic commercial aircraft". *Journal of Aircraft* 27 (2), pp. 139–145 (1990).

248. Khan, K. & Houston, G. "Design Optimization using Life Cycle Cost Analysis for Low Operating Costs". in *RTO AVT Design for Low Cost Operation and Support* pp. 1–9 (Ottawa, 1999).

249. Woodford, S. & Smith, H. "The Minimisation of Combat Aircraft Life Cycle Cost through Conceptual Design Optimisation". in *AIAA and SAE World Aviation Conference* pp. 1–9 (Anaheim, CA, 1998).

250. Curran, R., Price, M., Raghunathan, S., Benard, E., Crosby, S., Castagne, S. & Mawhinney, P. "Integrating Aircraft Cost Modeling into Conceptual Design". *Concurrent Engineering* 13 (4), pp. 321–330 (2005).

251. Curran, R., Raghunathan, S. & Price, M. "Review of aerospace engineering cost modelling: The genetic causal approach". *Progress in Aerospace Sciences* 40 (8), pp. 487–534 (2004).

252. Korpi, E. & Ala-Risku, T. "Life cycle costing: a review of published case studies". *Managerial Auditing Journal* 23 (3), pp. 240–261 (2008).

253. Niazi, A., Dai, J. S., Balabani, S. & Seneviratne, L. "Product Cost Estimation: Technique Classification and Methodology Review". *Journal of Manufacturing Science and Engineering* 128 (2), pp. 563–575 (2006).

254. Boren, H. E. "A Computer Model for Estimating Development and Procurement Costs of Aircraft (DAPCA-III)". *RAND Report* 1854, pp. 1–98 (1976).

255. Cherwonick, J. "Unmanned Aerial Vehicle System. Acquisition Cost Estimating Methodology". in *37th DoD Cost Analysis Symposium* pp. 1–26 (Williamsburg, VA, 2004).

256. Valerdi, R. "Cost Metrics for Unmanned Aerial Vehicles". in *Infotech@Aerospace* pp. 1–6 (Arlington, Virginia, 2005).

257. Chaput, A. J. "*Conceptual Design of UAV Systems*". (Lockheed Martin Aeronautics Company, 2003).

258. Vanguard Software Corporation. "Vanguard Studio version 5.2.0". (2012).

259. IEEE. "*IEEE Standard Glossary of Computer Networking Terminology*". (Institute of Electrical and Electronics Engineers, 1991).

260. Abernethy, R. "*Chapter 1: An Overview of Weibull Analysis - in The New Weibull Handbook: Reliability & Statistical Analysis for Predicting Life, Safety, Survivability, Risk, Cost and Warranty Claims*". (Gulf Pub. Co, 1996).

261. Williams, K. W. "A summary of unmanned aircraft accident/incident data: Human factors implications". *DOT/FAA/AM-04/24 Report of the Civil Aerospace Medical Institute* pp. 1–18 (2004).

262. Lee, D. a. & Long, E. A. "Estimating Cost and Schedule of Reliability Improvement". *Journal of Cost Analysis and Parametrics* 4 (2), pp. 93–105 (2011).

263. Long, E., Forbes, J., Hees, J. & Stouffer, V. "Empirical relationships between reliability investments and life-cycle support costs". *LMI Report SA701T1* pp. 1–90 (2007).

264. Forbes, J., Long, E., Lee, D., Esman, W. & Cross, L. "Developing a Reliability Investment Model". *LMI Report HPT80T1* pp. 1–108 (2008).

265. Forbes, J. A., Lee, D. A. & Long, E. A. "Predicting reliability investment to achieve given reliability improvement". *Reliability and Maintainability Symposium* pp. 1–6 (2009).

266. Department for Transport. "*Reported Road Casualties Great Britain: 2015 Annual Report*". (2016).

267. Bellavance, F., Dionne, G. & Lebeau, M. "The value of a statistical life: A meta-analysis with a mixed effects regression model". *Journal of Health Economics* 28 (2), pp. 444–464 (2009).

268. Viscusi, W. K. & Aldy, J. E. "The value of a statistical life: A critical review of market estimates throughout the world". *Journal of Risk and uncertainty* 27 (1), pp. 5–76 (2003).

269. Doucouliagos, C., Stanley, T. D. & Giles, M. "Are estimates of the value of a statistical life exaggerated?". *Journal of Health Economics* 31 (1), pp. 197–206 (2012).

270. Royal National Lifeboat Institution. "*RNLI Annual Report and Accounts 2011*". (2011).

271. The AnyLogic Company. "AnyLogic 6.9.1". (2013).

272. Wissler, E. H. "Probability of survival during accidental immersion in cold water". *Aviation, space, and environmental medicine* 74 (1), pp. 47–55 (2003).

273. Johnson, J. "Analysis of image forming systems". in *Image Intensifier Symposium* 513, pp. 244–273 (Warfare Electrical Engineering Department, U.S. Army Research and Development Laboratories, Ft. Belvoir, Va., 1958).

274. Robinson, S. "*Simulation: The Practice of Model*". (Wiley, 2004).

275. Department of Defense. "*Unmanned Aircrafts Systems Roadmap 2005-2030*". (Office of the Secretary of Defense, 2005).

276. Mavris, D. N., Baker, A. P. & Schrage, D. P. "Simultaneous assessment of requirements and technologies in rotorcraft design". in *56th Annual Forum of the American Helicopter Society* pp. 1–10 (Virginia Beach, VA, 2000).

277. Hoerber, J., Glasschroeder, J., Pfeffer, M., Schilp, J., Zaeh, M. & Franke, J. "Approaches for additive manufacturing of 3D electronic applications". *Procedia CIRP* 17, pp. 806–811 (2014).

278. Niese, B., Amend, P., Frick, T., Roth, S. & Schmidt, M. "Fast and Flexible Production of Mechatronic Integrated Devices by Means of Additive Manufacturing". in *12th International Congress Molded Interconnect Devices (MID)* pp. 1–6 (Wurzburg, 2016).

279. 3T-RPD. "Metal AM Materials". (2016). Available at: https://www.3trpd.co.uk/dmls/dmls-materials.htm.

280. Keane, A. J. & Prasanth, B. N. "*Computational Approaches for Aerospace Design*". (Wiley, 2005).

281. Keane, A. J. & Scanlan, J. P. "Design Search and Optimization in Aerospace Engineering". *Proceedings of the Royal Society A: Mathematical, Physical and Engineering Sciences* 365 (1859), pp. 2501–2529 (2007).

282. Sobieszczanski-Sobieski, J. & Haftka, R. T. "Multidisciplinary aerospace design optimization: survey of recent developments". *Structural Optimization* 14 (1), pp. 1–23 (1997).

283. Gross, D. C. "Report from the Fidelity Implementation Study Group". in *Simulation Interoperability Standards Organization - Simulation Interoperability Workshop* pp. 1–88 (Orlando, FL, 1999).

284. Howard, R. A. "Decision Analysis: Practice And Promise". *Management Science* 34 (6), pp. 679–695 (1988).

285. Walls, M. R. "Corporate risk-taking and performance: A 20 year look at the petroleum industry". *Journal of Petroleum Science and Engineering* 48 (3–4), pp. 127–140 (2005).

286. Shapeways. "3D Printing Materials". (2017). Available at: https://www.shapeways.com/materials.

287. Agnew, K. "The Spitfire: Legend or History? An argument for a new reserach culture in design". *Journal of Design History* 6 (2), pp. 121–130 (1993).

288. Huybrechts, S., Hahn, S. & Meink, T. "Grid stiffened structures: a survey of fabrication, analysis and design methods". in *12th International Conference on Composite Materials* pp. 1–10 (Paris, 1999).

289. Vasiliev, V. V. & Razin, a. F. "Anisogrid composite lattice structures for spacecraft and aircraft applications". *Composite Structures* 76 (1–2), pp. 182–189 (2006).

290. Vasiliev, V. V., Barynin, V. a. & Razin, a. F. "Anisogrid composite lattice structures – Development and aerospace applications". *Composite Structures* 94 (3), pp. 1117–1127 (2012).

291. Totaro, G. & Gürdal, Z. "Optimal design of composite lattice shell structures for aerospace applications". *Aerospace Science and Technology* 13 (4–5), pp. 157–164 (2009).

292. Morozov, E. V., Lopatin, a. V. & Nesterov, V. a. "Finite-element modelling and buckling analysis of anisogrid composite lattice cylindrical shells". *Composite Structures* 93 (2), pp. 308–323 (2011).

293. Vasiliev, V. V & Razin, a F. "Development of Geodesic Composite Aircraft Structures". in *28th International Congress of the Aeronautical Sciences* pp. 1–7 (Brisbane, 2012).

294. Hühne, C. "Advanced Lattice Structures for Composite Airframes". *Final Report of the ALaSCA FP7 Project* pp. 1–6 (2013).

295. De Fazio, T. L. & Whitney, D. E. "Simplified Generation of All Mechanical Assembly Sequences". *IEEE Journal on Robotics and Automation* 3 (6), pp. 640–658 (1987).

296. Mathew, A. T. & Rao, C. S. P. "A Novel Method of Using API to Generate Liaison Relationships from an Assembly". *Journal of Software Engineering and Applications* 3 (2), pp. 167–175 (2010).

297. Demoly, F., Yan, X. T., Eynard, B., Rivest, L. & Gomes, S. "An assembly oriented design framework for product structure engineering and assembly sequence planning". *Robotics and Computer-Integrated Manufacturing* 27 (1), pp. 33–46 (2011).

298. Li, B. M. & Xie, S. Q. "Module partition for 3D CAD assembly models: a hierarchical clustering method based on component dependencies". *International Journal of Production Research* 53 (17), pp. 5224–5240 (2015).

299. Badame, S. & Dig, D. "Refactoring meets spreadsheet formulas". in *IEEE International Conference on Software Maintenance, ICSM* pp. 399–408 (Niš, 2012).

300. Quaranta, E., van Schaik, J., Ferraro, M., Gorissen, D., Scanlan, J. P. & Keane, A. J. "Aerodynamic Optimization Integrated in Design of an Unmanned Aerial Vehicle". *Unpublished manuscript* pp. 1–23 (2014).

301. Stoliker, F. N. "*Introduction to Flight Test Engineering*". *AGARD Flight Test Techniques Series* Volume 14, (NATO Research and Technology Organisation, 1995).

302. Yao, W., Chen, X., Luo, W., van Tooren, M. & Guo, J. "Review of uncertainty-based multidisciplinary design optimization methods for aerospace vehicles". *Progress in Aerospace Sciences* 47 (6), pp. 450–479 (2011).

303. Civil Aviation Authority. "*The Air Navigation Order 2016*". (765), (CAA, 2016).

304. RNLI. "Mersey Technical Specification". Available at: http://rnli.org/aboutus/lifeboatsandstations/ lifeboats/Pages/Mersey.aspx. (Accessed: 15th May 2015)

305. RNLI. "Lifeboat Fleet Running Costs". Available at: http://rnli.org/aboutus/aboutthernli/ Pages/ Running-costs.aspx. (Accessed: 15th September 2014)

306. National Water Safety Forum. "*2015 Annual Fatal Incident Report*". (WAter Incident Database - WAID, 2015).